DESIGN, SYNTHESIS, AND STRUCTURE-PROPERTY RELATIONSHIP STUDY OF SHAPE-PERSISTENT PHENYLENE VINYLENE MACROCYCLES AND PORPHYRIN-BASED MOLECULAR CAGES THROUGH DYNAMIC COVALENT CHEMISTRY

by

Chenxi Zhang

B.S., Peking University, Beijing, China, 2009

A thesis submitted to the

Faculty of the Graduate School of the

University of Colorado in partial fulfillment

of the requirement for the degree of

Doctor of Philosophy

Department of Chemistry & Biochemistry

2014

This thesis entitled:

"Design, Synthesis, and Structure-Property Relationship Study of Shape-Persistent Phenylene Vinylene Macrocycles and Porphyrin-based Molecular Cages through Dynamic Covalent Chemistry"

written by Chenxi Zhang

has been approved for the Department of Chemistry & Biochemistry

_____

Wei Zhang, Ph. D.

_____

Douglas Gin, Ph. D.

Date: 04/17/2014

The final copy of this thesis has been examined by the signatories, and we Find that both the content and the form meet acceptable presentation standards Of scholarly work in the above mentioned discipline.

Thesis Abstract

Zhang, Chenxi
(Department of Chemistry & Biochemistry)

Design, Synthesis, and Structure-Property Relationship Study of Shape-Persistent Phenylene Vinylene Macrocycles and Porphyrin-based Molecular Cages through Dynamic Covalent Chemistry

Thesis directed by Dr. Wei Zhang

The objectives of the work described in this thesis are the design and synthesis of shape-persistent phenylene vinylene macrocycles (PVMs) and covalent organic polyhedrons (COPs) using dynamic covalent chemistry (DC_vC); and the study of their applications in host-guest chemistry, light harvesting, gas adsorption and separation. DC_vC has achieved tremendous progress during the past decade, and its application in constructing complex molecular architectures has attracted increasing attention. Conventional design and preparation of purely organic covalent architectures through irreversible bond formation usually requires multi-step synthesis and is very time consuming and low-yielding. DC_vC exhibits a significant advantage: the reversible nature of the bond formation in DC_vC ("self-correction"-enabled) allows the most thermodynamically stable product to be produced predominantly in one step from readily accessible precursors.

DC_vC has been applied in constructing macrocyclic compounds for decades. Moore and coworkers have applied alkyne metathesis in constructing shape-persistent arylene ethynylene

macrocycles. Such macrocyclic compounds showed interesting stacking properties for solid-state engineering.

Shape-persistent COPs with well-defined intrinsic cavities have been a research focus due to their unique structure features such as customizable geometry and isolated cavities. Moreover, constructed only through robust covalent bonds, the COPs usually have much higher chemical and thermal stability than their supramolecular analogues.

Further study beyond COPs involves incorporating COPs into frameworks to construct COFs. In this case, we can have individual well-defined built-in COPs in the frameworks, which are expected to be highly porous and be great candidate materials for gas adsorption, molecular separation, catalysis, chemical sensing and drug delivery.

Currently, there are still some limiting factors that impede the COP synthesis through DC_vC, and the most critical issue is that the dynamic covalent bonds formed are usually labile and cannot survive harsh conditions. Our research goals are to develop novel DC_vC methods utilizing more robust dynamic covalent bonds, and to construct shape-persistent molecular cages using such DC_vC methods.

In Chapter 1, an overview is given of the current (state-of-art) development and applications of covalent organic cage molecules. The advantages of the DC_vC approach will be highlighted.

In Chapter 2 the synthesis and aggregation study of shape-persistent phenylene vinylene macrocycles (PVMs) are described. With substitution groups varied, the PVMs exhibit very different aggregation behaviors, which help us to understand the structure-property relationship of this class of compounds.

In Chapter 3, a porphyrin-based molecular prism is described, which is the first shape-persistent organic molecular cage prepared via alkyne metathesis. More interestingly, the cage compound is able to selectively bind C_{70} over C_{60}, ($K_{C70}/K_{C60}>1000$), thus showing great potential for fullerene separation applications.

In Chapter 4, the formation of a ternary nanohybrid system consisting of the porphyrin-based molecular prism, fullerenes, and single-walled carbon nanotubes (SWCNTs) is described. A prototype device fabricated from this nanohybrid material gave decent photoconversion efficiency.

In Chapter 5, the synthesis of a porphyrin-based macrocycle is detailed. Unlike the 4-arm molecular cage reported in Chapter 4, this 2-arm macrocycle shows a highly adaptive cavity size and gives highest binding affinity for the larger fullerenes, *i.e.* C_{84}.

Chapter 6 focuses on perspectives and recommended future work based on current research progress. The construction of organic cage frameworks (OCFs) from covalent polyhedron molecules was pursued. Given the large intrinsic cavities of the molecular polyhedrons, the designed OCFs are anticipated to have large cavities and be highly porous. Moreover, since the COPs have shown very strong binding affinity for fullerenes, the designed OCFs can be used for capturing as well as separating fullerenes.

Acknowledgement

It is my great pleasure to have my doctoral program in University of Colorado at Boulder, with Professor Wei Zhang. I would like to express my great gratitude to Wei, for his guidance, support and encouragement throughout my graduate school. His commitment and enthusiastic for chemistry, along with his dedication to excellence are a model that I am always trying to achieve. His open mind and inspirations in chemistry can always brighten me with novel ideas. It has been an honor to work with and learn from him. I would also like to thank my thesis committee—Douglas Gin, David Walba, Gordana Dukovic, and Hai Long—for their helpful suggestions and valuable insight.

I am extremely grateful to all past and current members of the Zhang Group for their companionship over the past four and a half years. We discuss troubles, share ideas, and enjoy lab hours together. It has been a pleasant time to work in lab with them. All my experience in lab taught me to be a better chemist, and more importantly, to be a better man. I thank Alice Jin, Haishen Yang, Ya Du, Qi Wang, Ryan McCaffrey, Kenji Okochi, Chao Yu, Youlong Zhu, Philip Taynton, Guolong Lu, Setareh Azarnoush, Jyothish Kuthanapillil, Ryan Denman, Athena Jin, Aibo Zhang, and Kerry Betz.

I would also like to acknowledge the contributions of my collaborators. The collaborations are always an important part to success. I would like to thank Dr. Hai Long from National Renewable Energy Laboratory for his computational modeling. His collaboration gives me great insight into my research projects. I would also like to thank Dr. Shenqiang Ren from University of Kansas for the collaboration on the solar cell project. The corporation with his group gave the birth of the chapter 4.I would also like to thank our NMR coordinator, Dr. Richard Shoemaker, who is always very helpful in varies of NMR techniques. Moreover, I would also thank Nick Chisholm from Chemical Engineering for collaboration on the dye-sensitized solar cell project.

Most importantly, I would like to thank the people who have supported me during my pursuit of a Ph.D. Most importantly, my parents, Xiuwei Zhang and Lamei Hu. Their never-ending support and encouragement makes me persistent in pursuing my dreams. I would also like to thank my grandma, who is 97 years old, and always caring about my life in US. I would especially thank my wife Qi Wang. She is always behind me and supporting me on my research and daily life,

sharing my success and struggling. With her companion, life is much easier and more joyful. I dedicate this work for her.

Financial support was provided by National Science Foundation and University of Colorado at Boulder. I would also like to thank our Department of Chemistry and Biochemistry for providing such good research atmosphere and allow every person in it to chase his/her dreams.

Contents

CHAPTER 1

Overview of the Recent Progress in Molecular Cage Synthesis through Dynamic Covalent Chemistry

1.1 Introduction

The interest in three-dimensional (3-D) organic molecules has dramatically increased over the past few decades,[1-7] due to their structural novelty as well as their potential applications in catalysis, host-guest chemistry, molecular mechanics, *etc*.[7-10] Among all kinds of 3-D organic molecules, molecular cages with well-defined intrinsic cavity have attracted great attention in the past decade.[1,4,7,11,12]

The synthetic efforts toward molecular cage structures can date back to 1960s, where the cubane molecule was synthesized by Eaton and Cole.[13] The cubane molecule (Fig. 1.1) represents the simplest pure organic cage.

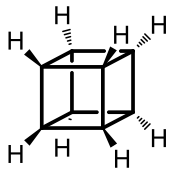

Figure 1.1 The structure of cubane.

Ever since then, a variety of molecular cages have been designed and synthesized in 1970s.[14,15] However, few applications have been developed from these compounds even with novel structures. In 1987, Losensky and coworkers synthesized one molecular cage and found it can encapsulate a variety of guest molecules (Fig. 1.2), thus indicating that it can be used for

molecular recognition.[8] This discovery opened many new possibilities of using cage molecules in host-guest chemistry.

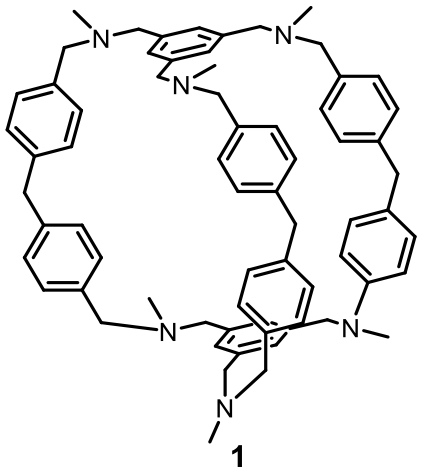

1

Figure 1.2. Molecular cage **1** with guest molecule binding capability.

To date, there are a large group of organic cage compounds that are built through supramolecular chemistry. The most prominent representative class of extended, highly ordered porous compounds today is metal–organic cages, which are usually constructed with metal ions and rigid organic ligands through metal-ligand coordination.[7,11,16-18] There is also another large group of molecular cages formed via other supramolecular interactions, such as hydrogen-bonding.[19,20]

Compared to supramolecular cage compounds that are usually formed via self-assembly of small precursors, organic cages based on purely covalent bonding are rare and still under exploration. The main reason for such slow progress is due to the irreversible nature of most covalent bond formation. Once the bonds are formed, they are hard to dissociate. Therefore, the self-correction process is prohibited, and large well-defined organic cage compounds cannot form predominantly (strong competition with oligomer and polymer side products). Previously, massive

synthetic efforts were required to make complex cage molecules, and usually they were obtained in very low overall yield.[21-23] This strongly impeded complex 3-D molecule preparation, until Lehn came up with a new idea of constitutional dynamic chemistry (CDC)[24], which allows dynamic combinatorial chemistry (DCC) applied to the synthesis route. Dynamic combinatorial chemistry exploits reversible chemistry to generate combinatorial libraries that are under thermodynamic control. Such a group of species containing reversible bonds constitute a dynamic combinatorial library (DCL). The dynamic and combinational feature of DCC enables self-correction, adaptability and response to external stimulants (heat, light, chemical additives, *etc*.). Under such circumstances, the thermodynamically most stable product will be produced predominantly. In general, DCC concerns both dynamic covalent chemistry (DC_vC) and dynamic noncovalent (supramolecular) chemistry, thus only dynamic covalent reactions are considered in DC_vC.

In the past decade, an increasing number of organic chemists have been focusing on the synthesis of covalent organic cage compounds using DC_vC. Recent research progress in this area is summarized in two review articles.[25,26] This chapter can be considered as an update of those reviews and is mainly focused on the most recent research efforts by using DCC, specifically DC_vC in which only reversible covalent reactions are utilized.

1.2 Dynamic covalent chemistry

Compared with the supramolecular chemistry that is commonly used in constructing non-covalent cages (*e.g.,* metal coordination, hydrogen-bonding), DC_vC always deals with more robust covalent bonds. There exists a large group of dynamic covalent bonds in DCL, which could be utilized to construct thermodynamically favored molecular architectures. In general, there are two types of dynamic covalent bonds: 1) bonds that can undergo exchange reactions, where the partners

can be swapped with the other (*e.g.,* olefin metathesis); 2) bonds that are formed through condensation (*e.g.,* imine condensation) or addition reaction (*e.g.,* aldol reaction).

1.2.1 Imine chemistry

The reversible condensation reaction of amino and carbonyl groups to form imine bonds is one of the most classic and unique reactions in chemistry. Such reaction products containing imine bond, which generally has the formula of $R^1R^2C{=}NR^3$, are called "Schiff's bases". They are named after Hugo Schiff, who discovered this reaction in 1864. Even after centuries, chemists' interests in such Schiff's Bases have not faded away, and they have guided this classic reaction into a brand new dynamic covalent chemistry field.

The reversible nature of the imine bond enables the synthesis of many complex molecules, and some examples are summarized in those two review articles by Stoddart.[27,28] The imine bond based structure has its great advantages not only in synthesis, but also in its unique properties:

1. The fast and highly reversible nature of imine bond formation enables highly efficient chemical synthesis[29-31]. Cooper and coworkers[31] have demonstrated that the reaction of 1,3,5-triformylbenzene (TFB) with a mixture of both 1,2-ethylenediamine (EDA) and (*1R,2R*)-1,2-cyclohexanediamine (CHDA) leads to a mixture of cages with a certain ratio. The reaction of CHDA with a pre-formed cage **2**, which is synthesized from only TFB and EDA, can also generate the mixture of cages with a similar ratio. Starting from the mixture of cage **2** and **3**, a comparable product ratio can also be obtained through the slow cage-cage interchange reactions. (Fig. 1.3) Moreover, the product distribution could be tuned by changing the ratio of two amines (EDA and

CHDA), which led to the reaction equilibriums having different cage distribution. Such demonstration indicates the highly active and reversible nature of imine bond formation.

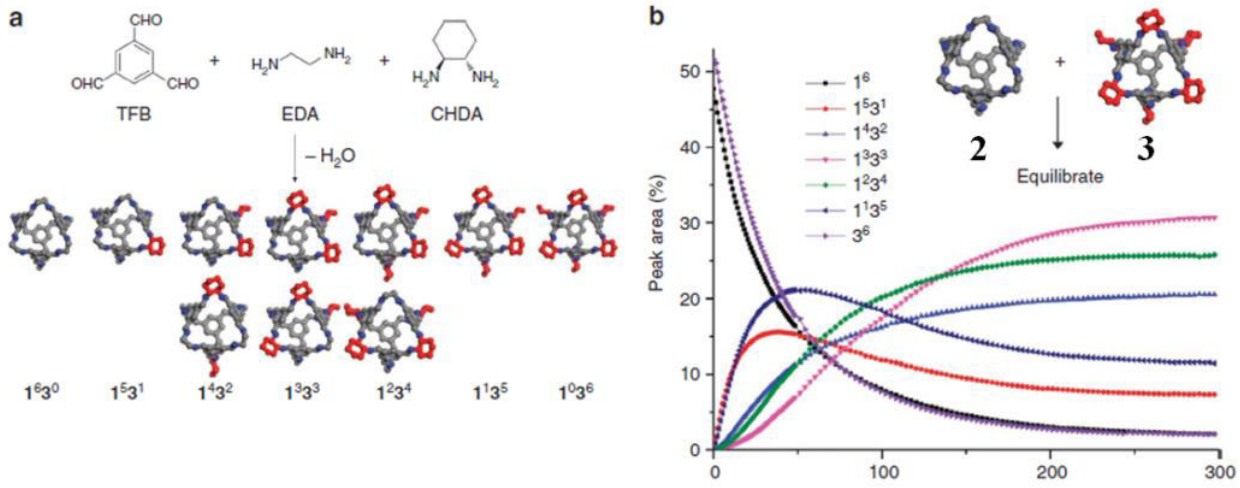

Figure 1.3. The kinetics of the cage dynamic scrambling process. (Reproduced from reference 31)

2. Rigid imine bond facilitated the formation of shape persistent molecular cages with large cavity as well as high surface area.[10,32,33] Mastalerz and coworkers have designed and synthesized an *exo*-functionalized [4+6] molecular cage **7** from readily accessible triptycene triamine **4** and resorcinol dialdehyde **5** in one step at 68% yield. Compared with previously designed *endo*-funcionalized cage **8**,[34,35] the *exo*-funcionalized cage **7** showed H-bonding directing effect. With the imine bond direction changed (Fig. 1.4), the size of the cavity was increased. The distance of two triptycene bridgehead protons was measured as 10.7 Å for *exo*-funcionalized cage **7**, which is larger than that of the *endo*-funcionalized cage **8** (9.6 Å). Such designed *exo*-functionalized cage exhibits a BET surface area of 1037 m^2/g. This represents the highest reported specific surface area among amorphous materials consisting of discrete organic molecules.[36]

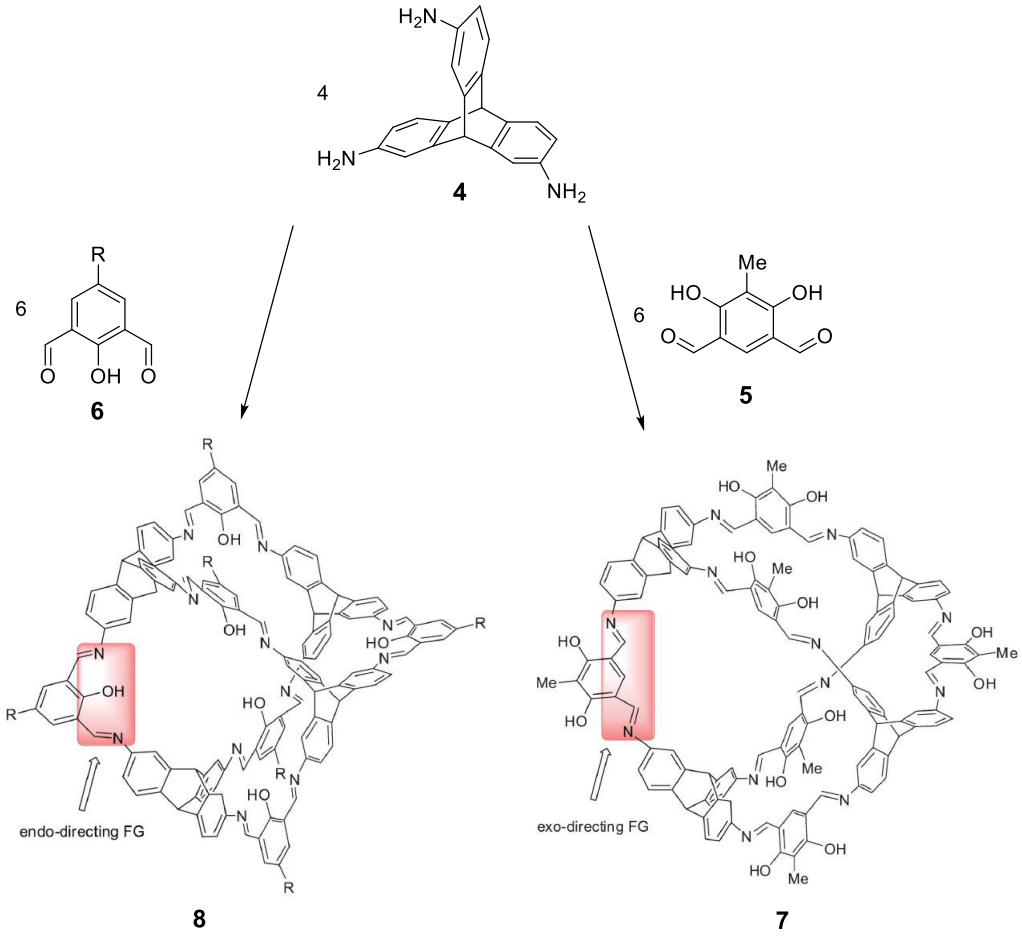

Figure 1.4. Molecular cages assembled from 10 subunits in one step. The cage has a BET surface area 1037 m^2/g.

3. The imine bond is polar and has certain degree of hydrophilicity, which enables water soluble cage synthesis. In this way, the application of such organic cage compound is broadened further. Warmuth and coworkers synthesized a series of water-soluble dynamic hemicarcerand cage **9** which was formed through the self-assembly of two cavitands **10** and 4 diamines **11** in water upon addition of template guest molecules (Fig. 1.5). Depending on the length of the diamine linker, the resulting cage compound showed selective binding with certain guest molecules of certain size and shape (*e.g.*, *p*-xylene over *o*-xylene and *m*-xylene).[37] Furthermore, it was demonstrated that the dynamic hemicarcerand cage **9** could serve as a molecular flask for the photochemical

generation of highly strained Bredt bridgehead olefin protoadamantene. This result shows the great potential of cage **9** in host-guest binding under hydrophilic conditions, such as in a drug-delivery bio-system.

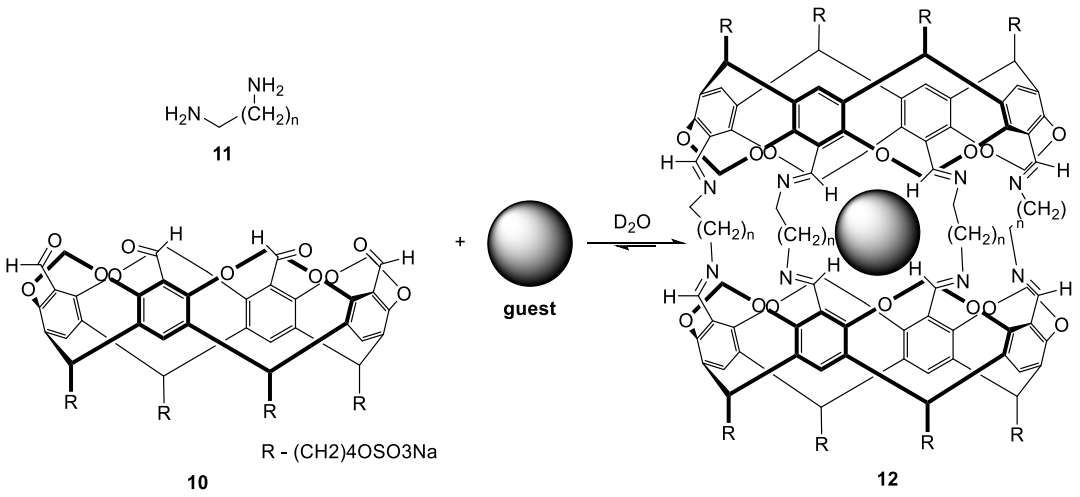

Figure 1.5. The water soluble cage with the reversible guest encapsulation.

4. The electron lone pair on N atom can coordinate with metal ions, which allows metal coordination and further structure tuning on the molecular level. Stoddart and coworkers have constructed a series of molecules with controlled topology. Molecular Borromean rings **12** and **13**[2] were designed and synthesized from 18 components through one-step self-assembly, forming 12 imines and 30 dative bonds (Fig. 1.6). With different metal coordination, a different topological structure Solomon link **14** was also obtained from the same building blocks (Fig. 1.6).[38] This work represents the scientist's great success in manipulating molecular structures.

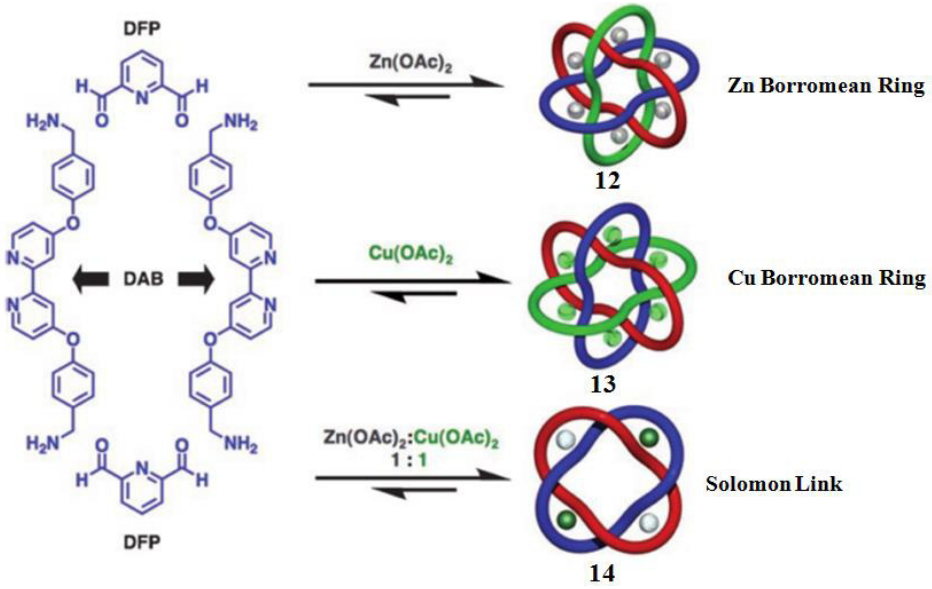

Figure 1.6. Construction of molecular Borromean rings and a Solomon link through imine condensation and metal-ligand coordination. (Reproduced from reference 38)

5. The imine groups can be easily reduced to amines, which lose their dynamic nature (*i.e.*, reversible formation), thus "locking" the structure in certain geometry. Zhang and coworkers synthesized a series of trigonal prismatic imine cages that were further subjected to the reduction condition.[10,32] With such treatment, the resulting amine-linked cage compounds exhibit significantly improved chemical and thermal stability, thus making the porous molecular cages easier to handle and more user-friendly toward their potential gas adsorption/separation application. The structure-property relationship study showed both the amino group density and the optimal cage pore size are important parameters in determining the gas adsorption selectivity. The obtained molecular cage **15** exhibited a very high ideal selectivity in adsorption of CO_2 over N_2 (up to 138/1, STP conditions), thus showing their great potential in carbon capture applications (Fig. 1.7).

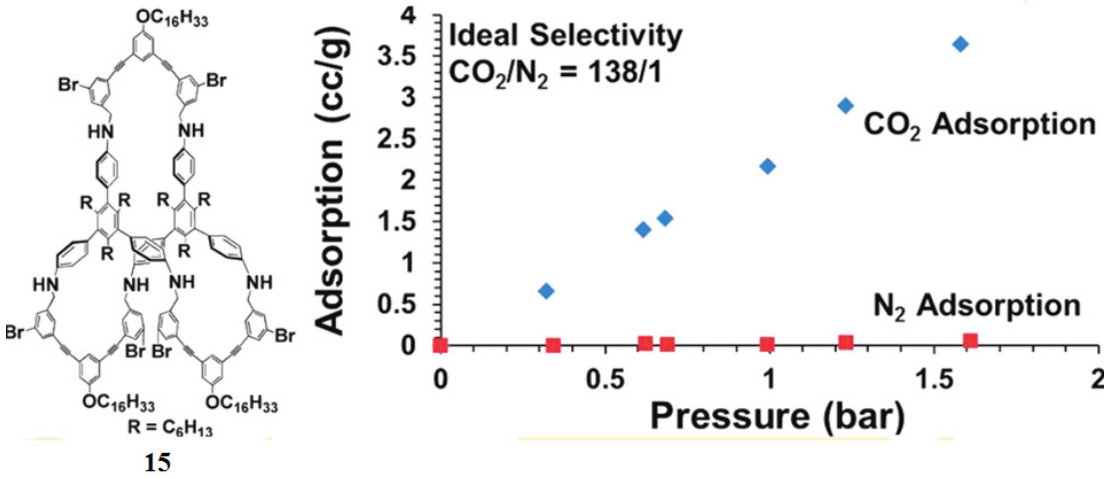

Figure 1.7. The amine cage **15** with an ideal selectivity of 138/1 in adsorption of CO_2 over N_2. (Reproduced from reference 32)

1.2.2 Boronic ester chemistry

The reversible B-O bond has been used for construction of 1-D polymer, 2-D and 3-D frameworks, and the research progress in this field has been reviewed by Fossy, Nishiyabu and coworkers.[39] But using such chemistry to synthesize 3-D molecular cages is much less explored, and the examples of constructing well-defined discrete molecular structures through boronic acid-diol condensation are still limited. Iwasawa and coworkers have accomplished the synthesis of four diastereomers out of five macrocyclic boronic esters (**16**-**20**) in high yield by utilizing the self-assembly of two chiral components with the proper choice of reaction conditions (Fig. 1.8)[40]. They also demonstrated that the formation of the macrocyclic compound is fully reversible: when *rac*-**16** was refluxed in MeOH/$CHCl_3$ (1:2) mixed solvent, *meso*-**20** was formed in 97% yield. This represents the very first time that people can achieve the construction of more than two enantiopure diastereomers of one discrete self-assembled structure with fine control.

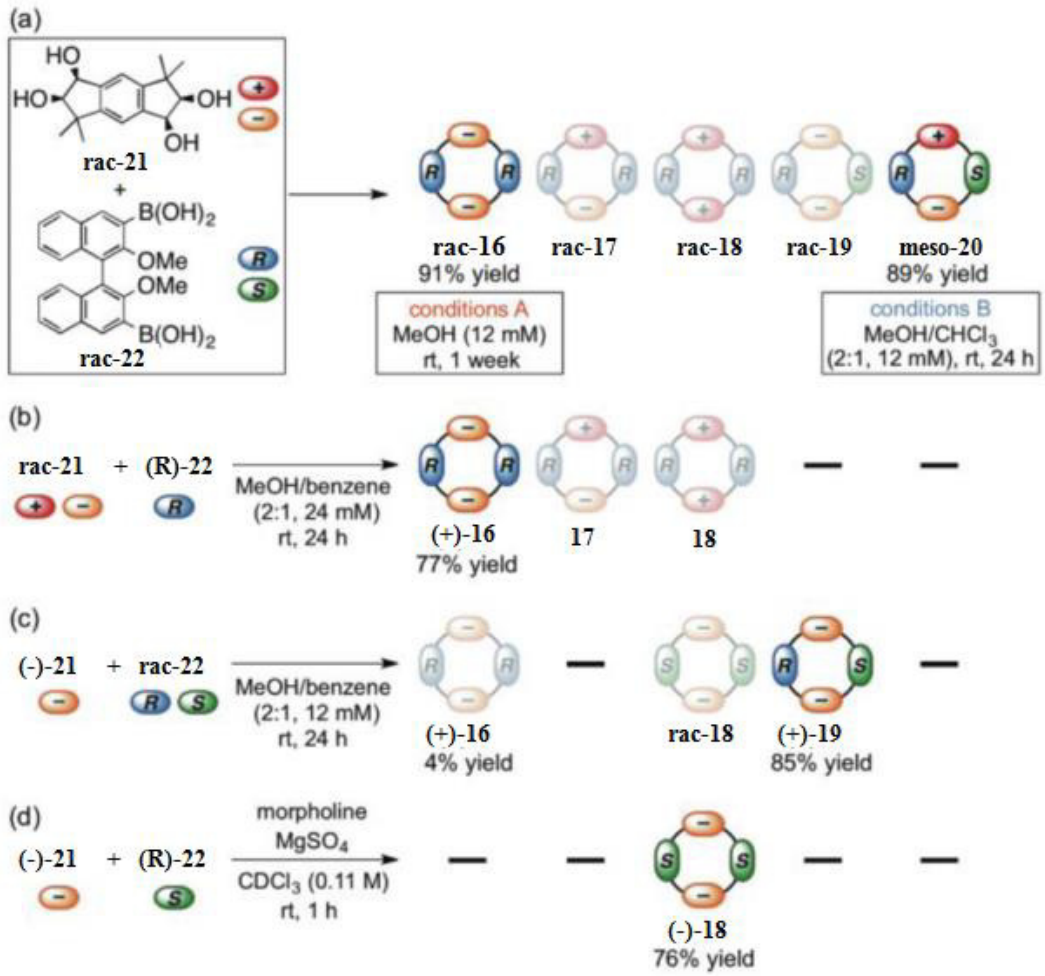

Figure 1.8. The controlled covalent-assembly of diols and boronic acids into diastereomeric macrocycles with the choice of the components and proper conditions (Reproduced from reference 40).

1.2.3 Alkene chemistry

Olefin metathesis, pioneered by Schrock and Grubbs,[41,42] is another type of well-known dynamic covalent chemistry. Olefin metathesis was initially been used in living ring-opening metathesis polymerization (ROMP) and has been well developed as a powerful synthetic tool. It has been widely used in the synthesis of flexible macrocyclic compounds.[43] Several examples were summarized in a previous review.[25] One recent example from Rissanen and coworkers[44] shows

that a porphyrin integrated cage **23** can be synthesized in moderate yield (56%) from half-cage precursors **24** through olefin metathesis, with 1,4-diazabicyclo[2.2.2]octane (DABCO) as the template. (Fig. 1.9) They also demonstrated that the template DABCO molecule can be removed by demetalation of the zinc porphyrins, in which a clean cage with free cavity was obtained. With the presence of two porphyrins and four pyridyl components in the cage molecule, the adjustment in the cavity size and shape with different kinds of external chemical signals was enabled. This opens different ways to tune the activity within the covalent cage. Another approach was used by Nolte to synthesize an interlocked porphyrin switch,[45] wherein ring-closing olefin metathesis was used to lock the catenanes structures. Although olefin metathesis has shown high efficiency in large flexible macrocycle synthesis, application of this method to the construction of shape-persistent macrocycles as well as 3-D molecular cages has rarely been reported, presumably due to the potential E/Z isomer issue and the significantly different reactivity between the internal double bonds versus the terminal olefins, which may limit the extent of their "self-correction" capability.

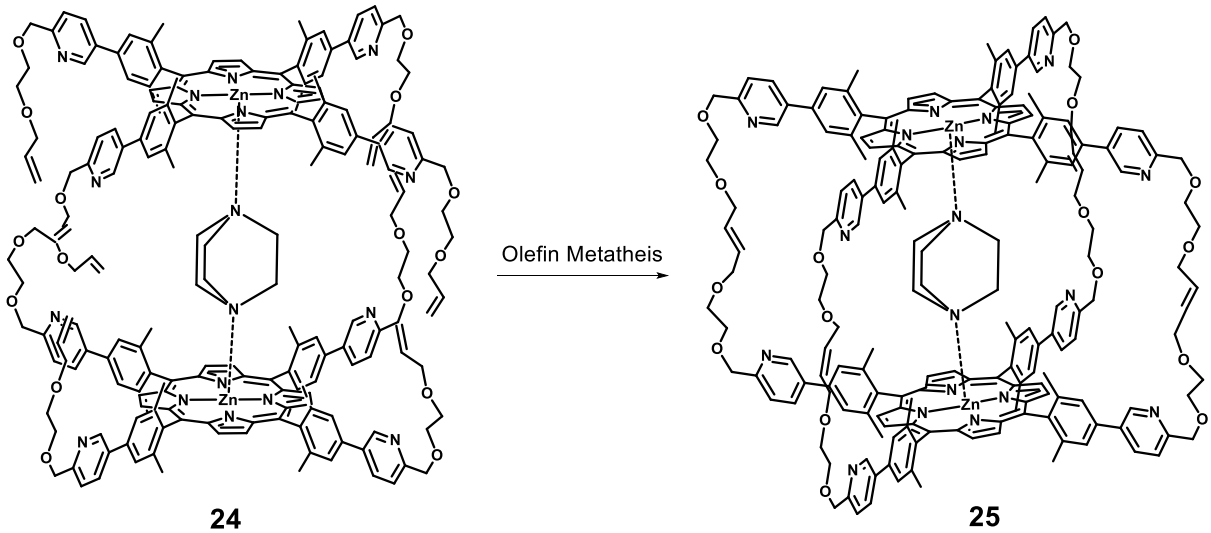

Figure 1.9. DABCO-templated cage synthesis via olefin metathesis.

1.2.4 Disulfide chemistry

Disulfide exchange is a classic dynamic covalent reaction and has been used frequently in the field of DCL. Nevertheless, disulfide linkage has rarely been used in 3-D molecular cage synthesis. One example was reported by Kuo and coworkers,[46] whereas they synthesized a cage compound **25** with disulfide linkage from small molecular precursors **26** and **27** in one step with very high yield (~90%). They also demonstrated that the obtained cage can be opened or closed to form the half cage **28** under controlled redox conditions. This cage is also capable of encapsulating small neutral molecules, such as DMF, which is supported by the single crystal structure of the resulting host-guest complex (Fig. 1.10).

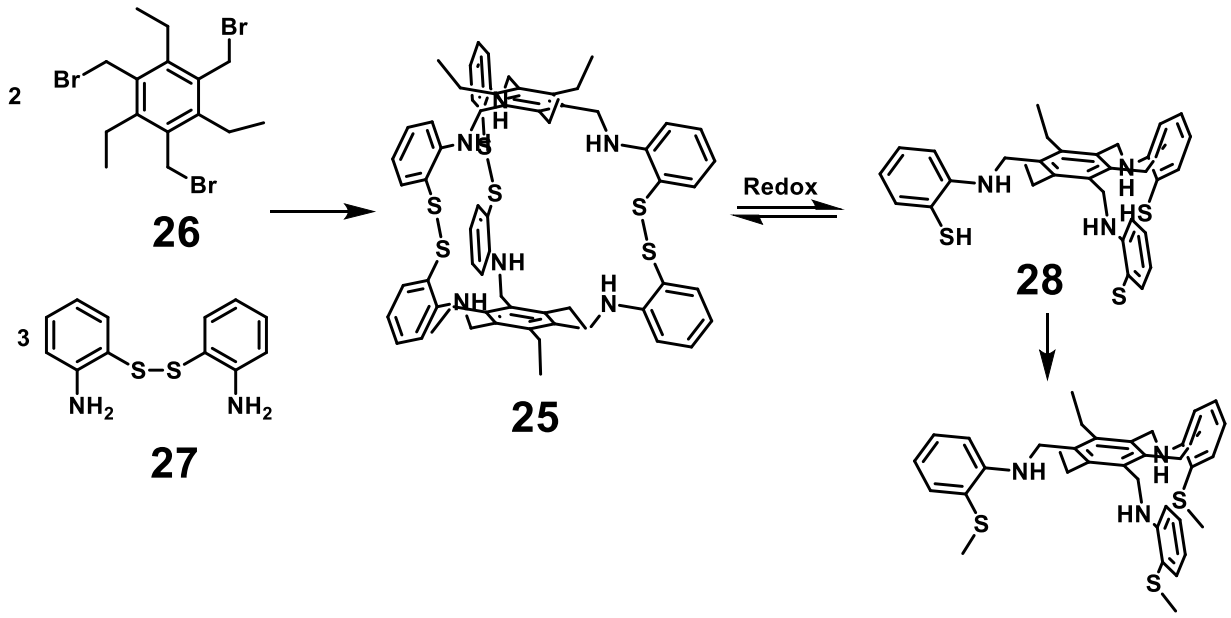

Figure 1.10. The synthesis of the disulfide cage **25** and demonstration of redox controlled cage opening/closing. Under reduction condition ($NaBH_4$, DMF), disulfide bond will dissociate to thiol and cage **25** was converted to half cage **28**. The half cage will turn back to cage **25** with the presence of oxidant (O_2 or I_2).

1.2.5 Alkyne chemistry

Alkyne metathesis was first discovered a few decades ago, but it has long been buried under the glory of its twin brother, olefin metathesis. The most important reasons for the slower development of alkyne metathesis are the instability of the catalysts employed in alkyne metathesis and the very rigorous oxygen and moisture-free conditions were required for the reactions. In order to achieve higher stability as well as higher catalytic activity, many research groups have been working hard on the catalyst development,[47-56] but this part will not be discussed here.

Alkyne metathesis was introduced as a synthetic tool for constructing shape-persistent macrocyclic compounds by Moore and coworkers.[57,58] With an active catalyst and an efficient precipitation-driven metathesis approach, the desired arylene ethynylene macrocycles (AEMs) **29** could be produced predominantly starting from simple diyne monomers. The reversible nature of the macrocycle formation was supported by the macrocycle scrambling experiment: when two different macrocycles **30** and **31** were subjected to the alkyne metathesis condition, a series of scrambled products could be observed at the end of the reaction (Fig. 1.11). This piece of work illustrated that alkyne metathesis represents an efficient chemical transformation that allows the dynamic process to achieve thermodynamic minimum. This opens many new possibilities of utilizing alkyne metathesis as a powerful synthetic tool to construct thermodynamically favored molecular architectures.

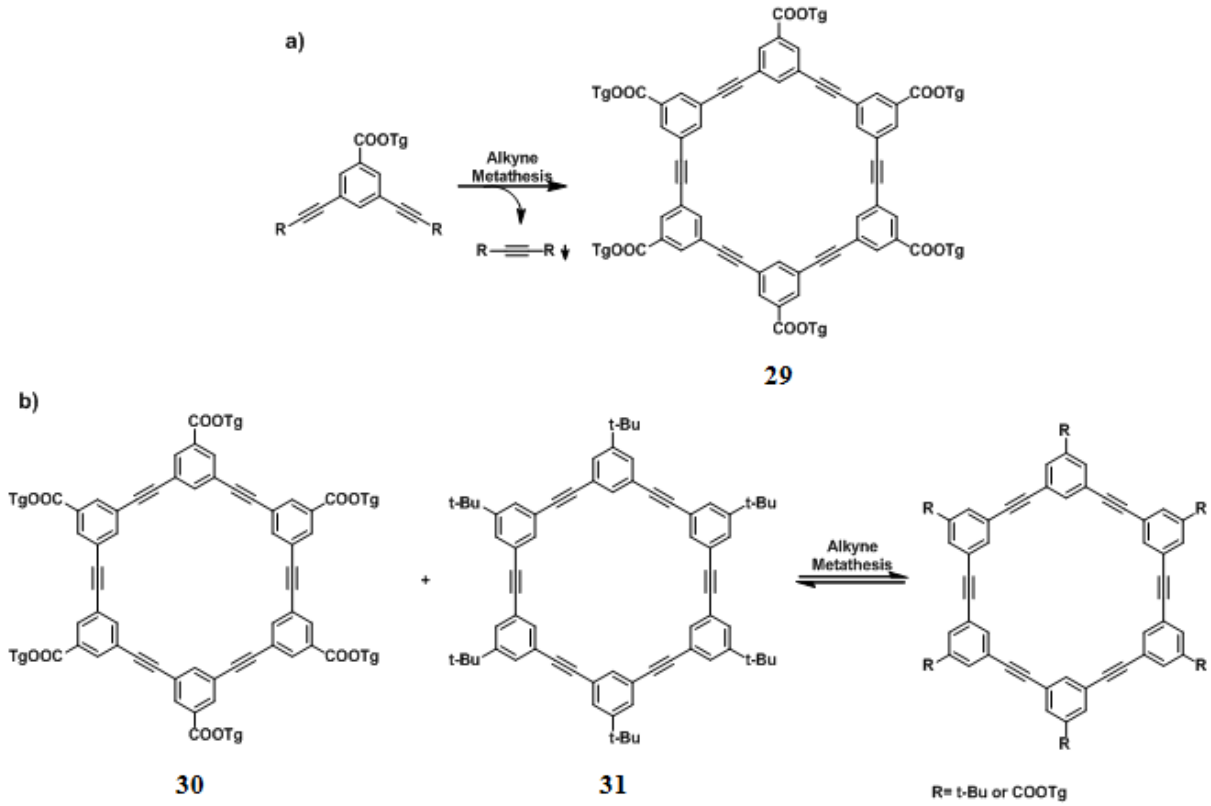

Figure 1.11. a) One-step synthesis of the hexameric macrocycle using alkyne metathesis. b) The scrambling experiment with two macrocycles. Starting from a mixture of macrocycle **30** and **31**, a series of scrambled macrocyclic products having different combinations of Tg and *t*-Bu substituted side chains were observed.

However, synthesis of 3-D molecular architectures through alkyne metathesis has never been reported before. Considering the rigid nature of triple bond as well as its stability, alkyne metathesis can serve as a powerful tool for construction of well-defined, discrete, 3-D molecular architectures in the future.

1.2.6 Combinations of two or more DC_vC reactions

Although DC_vC is a powerful tool for construction of complicated architectures, a combination of multiple different types of dynamic covalent bonds within one molecular structure

is rare. Nitschke *et al*[59] reported that imine and boronic acid-diol condensation can be utilized together to achieve efficient cage synthesis, in which three subcomponents (cyclotricatechylene **32** with *m*-xylylenediamine **33** and 2-formylphenylboronic **34**) in proper ratio reacted with one another and the target cage **35** was formed predominantly (Fig. 1.12). This synthesis is a beautiful illustration of the power of DC_vC.

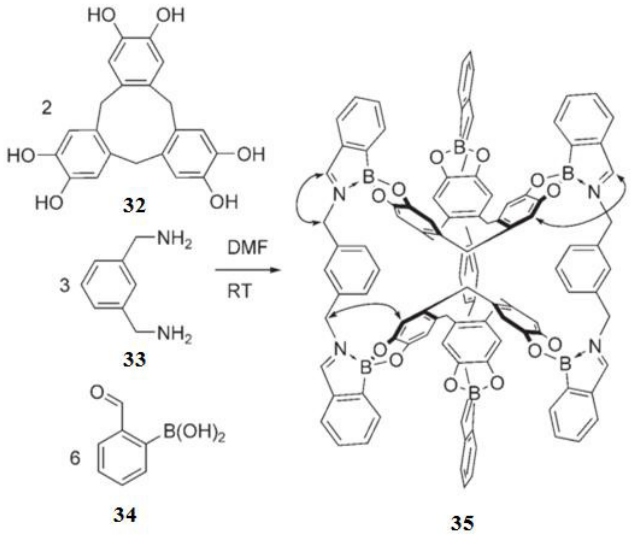

Figure 1.12. One step synthesis of cage **35** from three subcomponents.

Furlan and coworkers[60] demonstrated that different dynamic covalent chemistries can be applied sequentially in one system. (Fig. 1.13) Hydrazone condensation and metathesis was used first to construct the macrocycle backbone through the trimerization of building block **36**. Then followed by disulfide and thioester exchange in the presence of thioester **37**, the intra-crosslinked macrocycle **38** was formed. Such sequential application of DC_vC indicates the feasibility of controlling different DC_vC bonds on a complex molecular architecture.

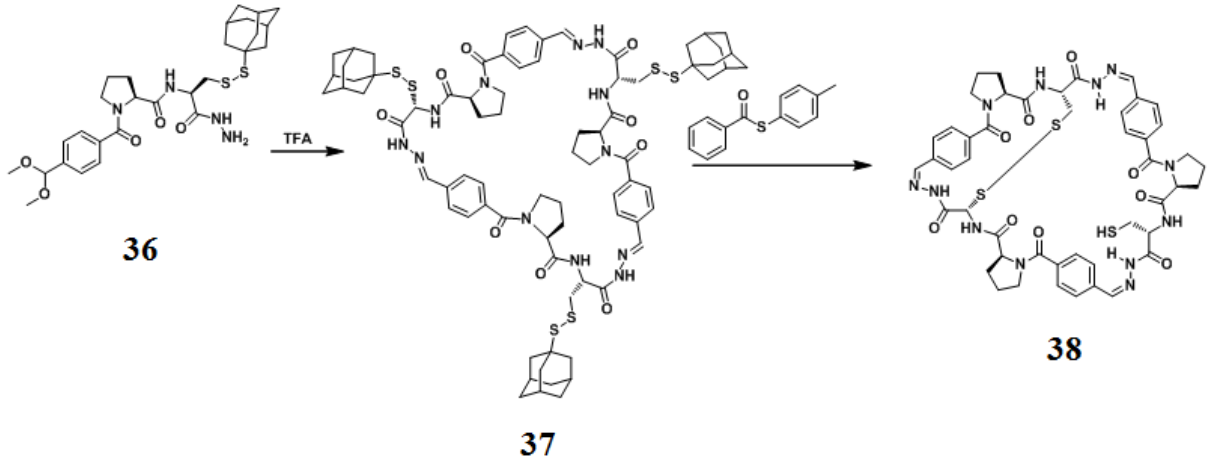

Figure 1.13. Macrocycle synthesis through sequential hydrazone condensation/metathesis and disulfide thioester exchange. Macrocycle **37** was obtained.

Zhang and coworkers[61,62] developed the idea of orthogonal dynamic covalent chemistry (ODCC). Combining olefin metathesis and imine condensation/metathesis in a one-pot fashion, a series of shape-persistent 2-D macrocycles and even a 3-D molecular cage **41** were successfully synthesized in good to excellent yields (Fig. 1.14). Such an approach allows incorporation of multiple different functional groups into a well-defined hetero-sequenced architecture. It also shows the possibility of functionalization of certain parts of a complex molecular structure.

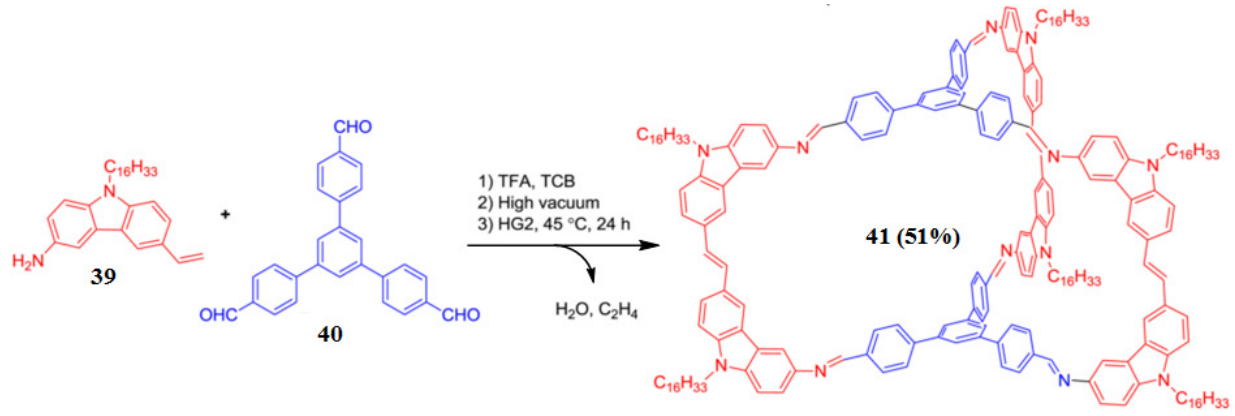

Figure 1.14. Synthesis of the molecular cage **41** using the ODCC method.

1.3 Conclusions and perspectives

The synthesis and study of molecular cage compounds with unique structural features and novel properties have become one important research focus. With the rapid development of DC_vC, a variety of molecular cages have been and will be synthesized and investigated in the future. Thus, more applications of the molecular cages will be explored, and even realized in the future, for example, catalysis, molecular separation, drug delivery for certain pharmaceutically active guest molecules, *etc*.

There are still many questions left open to the organic chemists. How well can we control the architecture on the molecular level? What kind of architectures could be designed and synthesized? How many different motifs and functional groups could be integrated in one system? Addressing these questions not only requires rational molecular design, but also needs further development of novel synthetic tools. Current molecular cage preparation mainly relies on dynamic imine chemistry and/or boronic acid-diol condensation reaction. Although, these two chemical transformations are usually highly efficient and can provide target structures in high yield, the formed imine or boronic ester linkage is labile and usually very sensitive to acids, water, or even moisture. Therefore, development of novel DC_vC tools that not only are kinetically fast (efficient "self-correction"), but also can provide robust linkage, are highly desired. This is particularly important for exploring certain materials that requires hash conditions (*e.g.*, humid environment, elevated temperature, high or low pH) in their applications.

1.4 References

1. Lehn, J. M. *Science* **2002**, *295*, 2400.

2. Chichak, K. S.; Cantrill, S. J.; Pease, A. R.; Chiu, S. H.; Cave, G. W. V.; Atwood, J. L.; Stoddart, J. F. *Science* **2004**, *304*, 1308.

3. Christinat, N.; Scopelliti, R.; Severin, K. *Angew. Chem. Int. Ed.* **2008**, *47*, 1848.

4. Tozawa, T.; Jones, J. T. A.; Swamy, S. I.; Jiang, S.; Adams, D. J.; Shakespeare, S.; Clowes, R.; Bradshaw, D.; Hasell, T.; Chong, S. Y.; Tang, C.; Thompson, S.; Parker, J.; Trewin, A.; Bacsa, J.; Slawin, A. M. Z.; Steiner, A.; Cooper, A. I. *Nat. Mater.* **2009**, *8*, 973.

5. Hasell, T.; Wu, X. F.; Jones, J. T. A.; Bacsa, J.; Steiner, A.; Mitra, T.; Trewin, A.; Adams, D. J.; Cooper, A. I. *Nat. Chem.* **2010**, *2*, 750.

6. Mitra, T.; Jelfs, K. E.; Schmidtmann, M.; Ahmed, A.; Chong, S. Y.; Adams, D. J.; Cooper, A. I. *Nat. Chem.* **2013**, *5*, 276.

7. Yoshizawa, M.; Tamura, M.; Fujita, M. *Science* **2006**, *312*, 251.

8. Vogtle, F.; Muller, W. M.; Werner, U.; Losensky, H. W. *Angew. Chem. Int. Ed.* **1987**, *26*, 901.

9. Koblenz, T. S.; Wassenaar, J.; Reek, J. N. H. *Chem. Soc. Rev.* **2008**, *37*, 247.

10. Jin, Y. H.; Voss, B. A.; Noble, R. D.; Zhang, W. *Angew. Chem. Int. Ed.* **2010**, *49*, 6348.

11. Olenyuk, B.; Whiteford, J. A.; Fechtenkotter, A.; Stang, P. J. *Nature* **1999**, *398*, 796.

12. Li, H.; Eddaoudi, M.; O'Keeffe, M.; Yaghi, O. M. *Nature* **1999**, *402*, 276.

13. Eaton, P. E.; Cole, T. W. *J. Am. Chem. Soc.* **1964**, *86*, 962.

14. Grimes, R. N.; Greene, P. T.; Bryan, R. F.; Rademake.W; Dennisto.M *J. Am. Chem. Soc.* **1972**, *94*, 1865.

15. Neely, S. C.; Vanderhelm, D.; Marchand, A. P.; Hayes, B. R. *Acta Cryst.* **1976**, *B32*, 561.

16. Klosterman, J. K.; Yamauchi, Y.; Fujita, M. *Chem. Soc. Rev.* **2009**, *38*, 1714.

17. Inokuma, Y.; Kawano, M.; Fujita, M. *Nat. Chem.* **2011**, *3*, 349.

18. Chakrabarty, R.; Mukherjee, P. S.; Stang, P. J. *Chem. Rev.* **2011**, *111*, 6810.

19. MacGillivray, L. R.; Atwood, J. L. *Nature* **1997**, *389*, 469.

20. Iyer, K. S.; Norret, M.; Dalgarno, S. J.; Atwood, J. L.; Raston, C. L. *Angew. Chem. Int. Ed.* **2008**, *47*, 6362.

21. Ashton, P. R.; Isaacs, N. S.; Kohnke, F. H.; Dalcontres, G. S.; Stoddart, J. F. *Angew. Chem. Int. Ed.* **1989**, *28*, 1261.

22. Ashton, P. R.; Girreser, U.; Giuffrida, D.; Kohnke, F. H.; Mathias, J. P.; Raymo, F. M.; Slawin, A. M. Z.; Stoddart, J. F.; Williams, D. J. *J. Am. Chem. Soc.* **1993**, *115*, 5422.

23. Lin, C. F.; Liu, Y. H.; Lai, C. C.; Peng, S. M.; Chiu, S. H. *Chem. Eur. J.* **2006**, *12*, 4594.

24. Lehn, J. M. *Chem. Soc. Rev.* **2007**, *36*, 151.

25. Mastalerz, M. *Angew. Chem. Int. Ed.* **2010**, *49*, 5042.

26. Jin, Y.; Yu, C.; Denman, R. J.; Zhang, W. *Chem. Soc. Rev.* **2013**, *42*, 6634.

27. Belowich, M. E.; Stoddart, J. F. *Chem. Soc. Rev.* **2012**, *41*, 2003.

28. Meyer, C. D.; Joiner, C. S.; Stoddart, J. F. *Chem. Soc. Rev.* **2007**, *36*, 1705.

29. Hasell, T.; Zhang, H. F.; Cooper, A. I. *Adv. Mater.* **2012**, *24*, 5732.

30. Hasell, T.; Chong, S. Y.; Jelfs, K. E.; Adams, D. J.; Cooper, A. I. *J. Am. Chem. Soc.* **2012**, *134*, 588.

31. Jiang, S.; Jones, J. T. A.; Hasell, T.; Blythe, C. E.; Adams, D. J.; Trewin, A.; Cooper, A. I. *Nat. Commun.* **2011**, *2*.

32. Jin, Y. H.; Voss, B. A.; Jin, A.; Long, H.; Noble, R. D.; Zhang, W. *J. Am. Chem. Soc.* **2011**, *133*, 6650.

33. Jiang, S.; Bacsa, J.; Wu, X. F.; Jones, J. T. A.; Dawson, R.; Trewin, A.; Adams, D. J.; Cooper, A. I. *Chem. Commun.* **2011**, *47*, 8919.

34. Mastalerz, M. *Chem. Commun.* **2008**, 4756.

35. Schneider, M. W.; Oppel, I. M.; Ott, H.; Lechner, L. G.; Hauswald, H. J. S.; Stoll, R.; Mastalerz, M. *Chem. Eur. J.* **2012**, *18*, 836.

36. Schneider, M. W.; Hauswald, H. J. S.; Stoll, R.; Mastalerz, M. *Chem. Commun.* **2012**, *48*, 9861.

37. Lin, Z. H.; Sun, J. L.; Efremovska, B.; Warmuth, R. *Chem. Eur. J.* **2012**, *18*, 12864.

38. Pentecost, C. D.; Chichak, K. S.; Peters, A. J.; Cave, G. W. V.; Cantrill, S. J.; Stoddart, J. F. *Angew. Chem. Int. Ed.* **2007**, *46*, 218.

39. Nishiyabu, R.; Kubo, Y.; James, T. D.; Fossey, J. S. *Chem. Commun.* **2011**, *47*, 1124.

40. Ito, S.; Ono, K.; Iwasawa, N. *J. Am. Chem. Soc.* **2012**, *134*, 13962.

41. Schrock, R. R. *Acc. Chem. Res.* **1990**, *23*, 158.

42. Novak, B. M.; Risse, W.; Grubbs, R. H. *Adv. Polym. Sci.* **1992**, *102*, 47.

43. Vougioukalakis, G. C.; Grubbs, R. H. *Chem. Rev.* **2010**, *110*, 1746.

44. Taesch, J.; Heitz, V.; Topic, F.; Rissanen, K. *Chem. Commun.* **2012**, *48*, 5118.

45. Coumans, R. G. E.; Elemans, J. A. A. W.; Rowan, A. E.; Nolte, R. J. M. *Chem. Eur. J.* **2013**, *19*, 7758.

46. Horng, Y. C.; Lin, T. L.; Tu, C. Y.; Sung, T. J.; Hsieh, C. C.; Hu, C. H.; Lee, H. M.; Kuo, T. S. *Eur. J. Org. Chem.* **2009**, 1511.

47. Furstner, A.; Davies, P. W. *Chem. Commun.* **2005**, 2307.

48. Mortreux, A.; Coutelier, O. *J. Mol. Catal. A: Chem.* **2006**, *254*, 96.

49. Weissman, H.; Plunkett, K. N.; Moore, J. S. *Angew. Chem. Int. Ed.* **2006**, *45*, 585.

50. Beer, S.; Hrib, C. G.; Jones, P. G.; Brandhorst, K.; Grunenberg, J.; Tamm, M. *Angew. Chem. Int. Ed.* **2007**, *46*, 8890.

51. Schrock, R. R.; Czekelius, C. *Adv. Synth. Catal.* **2007**, *349*, 55.

52. Zhang, W.; Moore, J. S. *Adv. Synth. Catal.* **2007**, *349*, 93.

53. Heppekausen, J.; Stade, R.; Goddard, R.; Furstner, A. *J. Am. Chem. Soc.* **2010**, *132*, 11045.

54. Jyothish, K.; Zhang, W. *Angew. Chem. Int. Ed.* **2011**, *50*, 3435.

55. Yang, H. S.; Liu, Z. N.; Zhang, W. *Adv. Synth. Catal.* **2013**, *355*, 885.

56. Furstner, A. *Angew. Chem. Int. Ed.* **2013**, *52*, 2794.

57. Zhang, W.; Moore, J. S. *J. Am. Chem. Soc.* **2005**, *127*, 11863.

58. Zhang, W.; Brombosz, S. M.; Mendoza, J. L.; Moore, J. S. *J. Org. Chem.* **2005**, *70*, 10198.

59. Hutin, M.; Bernardinelli, G.; Nitschke, J. R. *Chem. Eur. J.* **2008**, *14*, 4585.

60. Escalante, A. M.; Orrillo, A. G.; Cabezudo, I.; Furlan, R. L. E. *Org. Lett.* **2012**, *14*, 5816.

61. Okochi, K. D.; Jin, Y.; Zhang, W. *Chem. Commun.* **2013**, *49*, 4418.

62. Okochi, K. D.; Han, G. S.; Aldridge, I. M.; Liu, Y.; Zhang, W. *Org. Lett.* **2013**.

CHAPTER 2

Phenylene Vinylene Macrocycles (PVMs): Design, Synthesis, and Aggregation Study

2.1 Abstract

A series of shape-persistent phenylene vinylene macrocycles (PVMs) have been synthesized through one-step Acyclic Diene Metathesis Macrocyclization (ADMAC) from divinylbezene monomers in 47-74 % yield. The aggregation behavior of PVMs was investigated using 1H NMR, UV-Vis absorption and fluorescence. Interestingly, the PVMs with electron-rich substituents exhibit strong aggregation, which is in great contrast to their phenylene acetylene macrocycle (PAM) analogs substituted with electron-rich groups that barely show any aggregation. The structure-property relationship study by varying the length, polarity and bulkiness of PVM side chains clearly shows their tunable aggregation behavior, thus showing the great promise of utilizing this novel class of shape-persistent macrocycles in a variety of materials applications, such as ion channel, host-guest recognition and catalysis.

2.2 Introduction

Shape-persistent macrocycles (SPM) have attracted considerable attention due to their interesting self-aggregation behavior and unusual electronic and optoelectronic properties.[1-5] These molecules have rigid non-collapsible backbone structures and can be assembled into many interesting supramolecular systems, such as perforated monolayers and discotic liquid crystalline materials.[1-5] Among the numerous SPMs, arylene ethynylene macrocycles (AEMs) are the most widely studied and many interesting applications based on AEMs have emerged. Recent advances

in dynamic covalent chemistry, namely alkyne-metathesis, have enabled the facile access to AEMs in gram scale from simple precursors, and boosted the applications of these macrocycles toward materials development.[6,7] However, the analogous phenylene vinylene macrocycles (PVMs) are uncommon and their supramolecular properties have rarely been explored. Previously, we reported the efficient and high-yielding synthesis of PVMs via acyclic diene metathesis macrocyclization (ADMAC).[8] The macrocycles showed strong self-aggregation behavior and could be easily fabricated into nanofibrils. Herein, we report the syntheses of a series of hexameric PVMs through ADMAC approach. These macrocycles contain different side chains with their size and electronic nature varied. The self-aggregation behaviors of these macrocycles in solution were studied and compared to their ethynylene-linked analogs phenylene acetylene macrocycles (PAMs). Although PVMs are less rigid due to their possible conformational isomerism of vinylene moieties, in general, PVMs showed stronger self-association than the analogous PAMs bearing the same substituents. Our research reported herein represents a nice complement to the current structure design and synthetic approaches for shape-persistent macrocyclic compounds.

2.3 Results and discussion

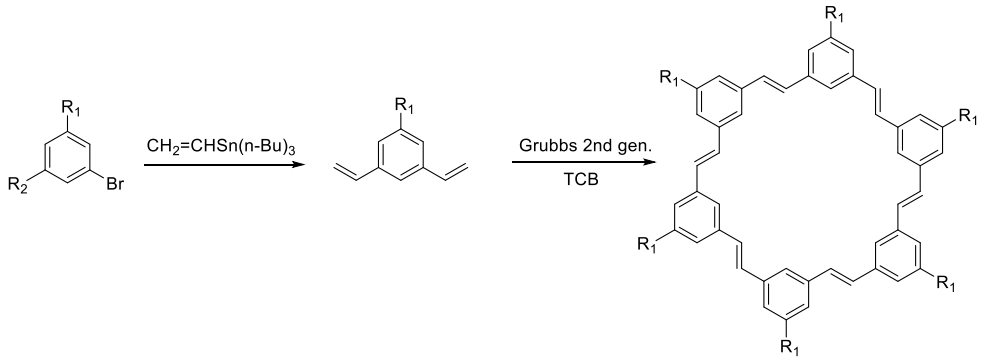

42: $R_1 = {}^{n}C_{10}H_{21}$; R_2 =Br
43: $R_1 = {}^{t}C_4H_9$; R_2 =Br
44: $R_1 = O^{n}C_{10}H_{21}$; R_2 =Br
45: $R_1 = O^{n}C_4H_9$ R_2=Br
46: $R_1 = OCO^{n}C_9H_{19}$; R_2 =Br
47: $R_1 = COO^{n}C_{10}H_{21}$; R_2 =I
48: $R_1 = COO^{n}C_4H_9$; R_2 =I
49: $R_1 = COO^{t}C_4H_9$; R_2 =I

50: $R_1 = {}^{n}C_{10}H_{21}$ (65 %)
51: $R_1 = {}^{t}C_4H_9$ (69 %)
52: $R_1 = O^{n}C_{10}H_{21}$ (59 %)
53: $R_1 = O^{n}C_4H_9$ (9 %)
53: $R_1 = OCO^{n}C_9H_{19}$ (84 %)
55: $R_1 = COO^{n}C_{10}H_{21}$ (57 %)
56: $R_1 = COO^{n}C_4H_9$ (47 %)
57: $R_1 = COO^{t}C_4H_9$ (72 %)

58: $R_1 = {}^{n}C_{10}H_{21}$ (54 %)
59: $R_1 = {}^{t}C_4H_9$ (65 %)
60: $R_1 = O^{n}C_{10}H_{21}$ (64 %)
61: $R_1 = O^{n}C_4H_9$ (59%)
62: $R_1 = OCO^{n}C_9H_{19}$ (61 %)
63: $R_1 = COO^{n}C_{10}H_{21}$ (45 %)
64: $R_1 = COO^{n}C_4H_9$ (74 %)
65: $R_1 = COO^{t}Bu$ (47 %)

Scheme 2.1. Synthesis of PVMs using ADMAC.

Divinylbenzene monomers (**50-57**) with various electronically and sterically different substituents were prepared from dihalogenbenzene (**42-49**, halogen = Br or I) via Stille coupling reactions. The crude yields of Stille coupling are generally above 90% based on the NMR analysis of the crude reaction mixture. However, considerably lower isolated yields (50-70%), were obtained mainly due to: (1) the low stability of the divinyl monomers. The monomers easily polymerize in solid states and in air within several hours to form waxy insoluble polymers. (2) Extensive purification process. The excess tributyl(vinyl)tin and tributyl-tin chloride byproduct oftentimes have similar polarities with products such as **50-53**, and their removal requires repetitive column chromatography purification. PVMs **58-65** were prepared through ADMAC using Grubb's second generation catalyst at 40 ^{o}C.

In all cases, cyclic hexamers were observed as the predominant species. The GPC traces of aliquots of reaction mixtures at different time intervals clearly showed the initial formation of higher molecular weight oligomers/polymers and their gradual conversion to the target cyclic hexamers (Fig. 2.1). We also observed various amounts of cyclic heptamer and cyclic pentamer in the MALDI-TOF MS spectra of crude product mixtures (Fig. 2.2). We found the metathesis reactions of monomers (**55-57**) bearing electron withdrawing groups produce more cyclic pentamers and heptamers compared to those of the monomers (**52-54**) with electron donating groups. Cyclic heptamers and pentamers were separated from the major cyclic hexamer through repetitive careful column chromatography. The cyclic hexamers (**58-65**) were obtained in decent isolated yields (49-74%) after careful purification. All PVMs were characterized by ^{1}H, and ^{13}C NMR, GPC and MALDI-TOF MS. We observed two sets of broad singlets that are corresponding to the protons on the phenyl ring. It is interesting to note that the vinyl protons of PVMs appear as

a singlet in the ^{1}H NMR spectra both at room temperature and at 0 °C. This chemical shift equivalence suggests the two seemingly different vinyl protons located inside and outside of the macrocyclic ring are interchangeable through the rapid rotational isomerization of the double bonds.

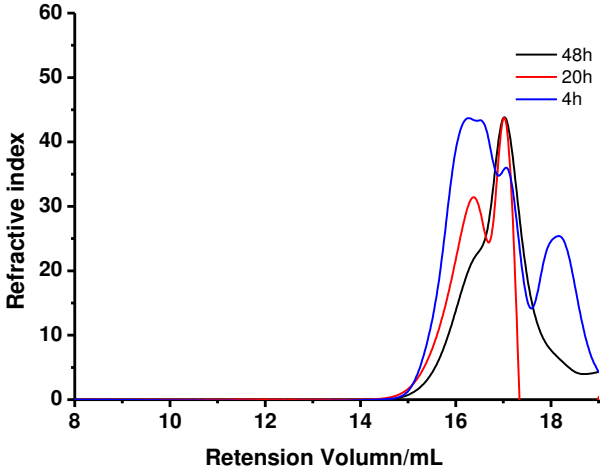

Figure 2.1. GPC traces of the crude ADMAC reaction product in the synthesis of PVM **63**.

2.3.1 Qualitative NMR observations

It has been reported that the self-association of PAMs is induced by face-to-face π-π interactions between aromatic rings, and is strongly influenced by the rigidity and pendant functional groups of the macrocycles: Electron withdrawing substituents promote self-aggregation of macrocycles compared to electron-donating functional groups; A planar and rigid framework enhances the aggregation while a flexible nonplanar geometry inhibits it.[9,10] In the previous communication, we briefly discussed the strong self-association of decyloxy substituted PVM **60**, which is in great contrast to the non-aggregation character of PVM substituted with $O^{n}C_4H_9$ in the same solvent ($CDCl_3$).[11] Our preliminary result suggests the significance of macrocyclic backbone

structure itself to the self-association property. We therefore investigated the self-association behaviors of various PVMs and compared them with those of the analogous PEMs. The concentration- and temperature-dependent aggregation of PVMs was studied with ^{1}H NMR spectroscopy. We observed the upfield shift of aromatic protons and vinyl protons with the increasing concentration of PVMs in $CDCl_3$. For example, at ambient temperature, the chemical shift of two anisochronous aromatic protons of PVM **62** changed from 7.49 ppm to 7.31 ppm and from 7.03 ppm to 6.89 ppm respectively as the concentration was increased from 0.39 to 6.2 mM. The changes in the chemical shift of both *exo*-annular (H^a) and the *endo*-annular (H^b) protons are similar in both trend and amplitude for the same PVM. The chemical shift of aliphatic protons remains unchanged over the same concentration range (Fig. 2.3). The aggregation behaviors of PVMs are also temperature dependent. When the temperature was raised, the chemical shift of both *exo*-annular protons and *endo*-annular protons of PVM **62** were shifted to the lower field, which indicates the dissociation occurs at elevated temperature. However, the amplitude of the chemical shift changes within the measured temperature range (22.7-59.2 ^oC) is much smaller than the chemical shift change when the concentrations are varied. The *endo*-annular and *exo*-annular protons in PVM **62** were shifted from 7.31 ppm to 7.36 ppm and from 6.89 ppm to 6.95 ppm respectively as the temperature was increased from 22.7 ^oC to 59.2 ^oC at the concentration of 6.2 mM in $CDCl_3$ (Fig. 2.4). We observed significant temperature and concentration dependent chemical shift changes in the NMR spectra of PVMs (**60**-**64**) with electron donating or withdrawing substituents. PVM **58** with decyl substituents show slight but gradient high field shifts of aromatic protons as the concentration is increased or the temperature is lowered. PVM **59** with bulky *t*-butyl groups does not show significant temperature or concentration-dependent chemical shifts changes. The significant shielding effects for aromatic and vinyl protons of PVMs with

increased concentration or decreased temperature suggest face-to-face aggregation geometry, similar to PAMs.

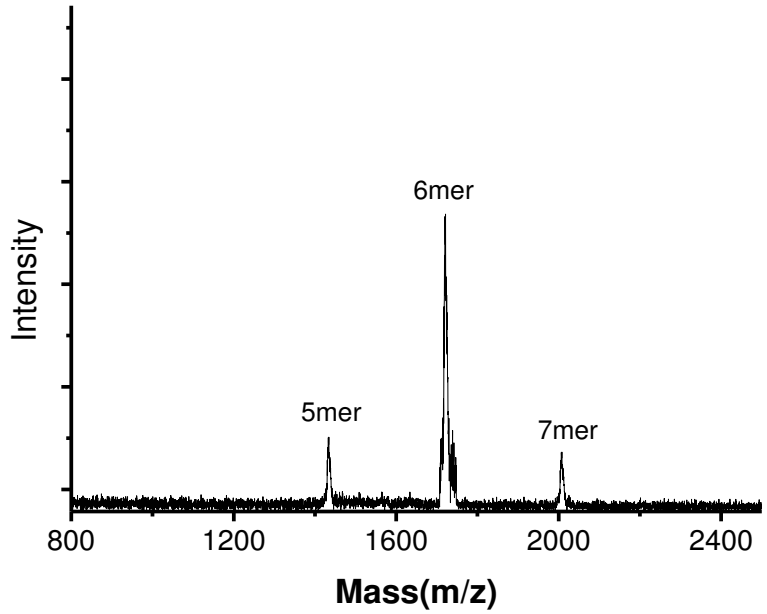

Figure 2.2 MALDI-TOF MS spectrum of the crude mixture of PVM **63**.

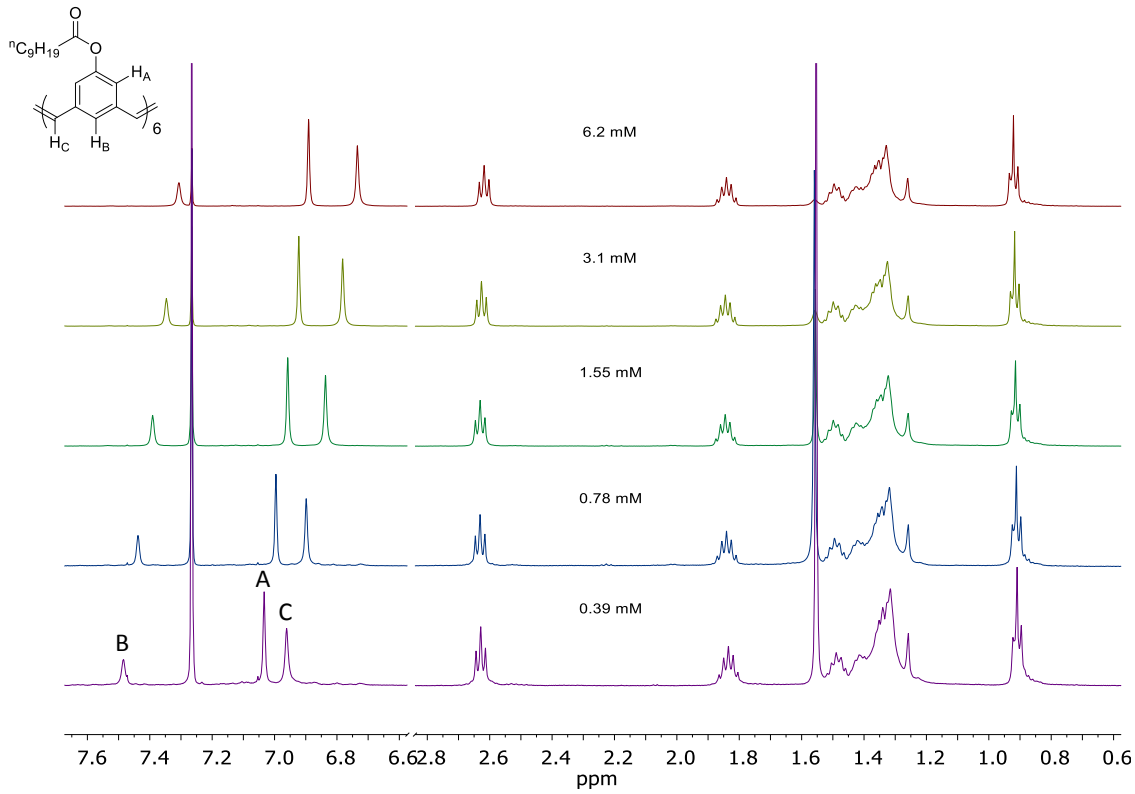

Figure 2.3. Concentration-dependent variation of ^{1}H-NMR chemical shifts of aromatic and vinyl protons of PVM **62** at 22.7 ºC.

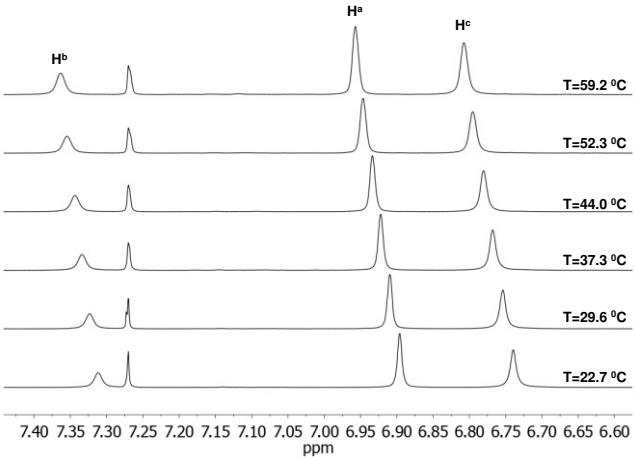

Figure 2.4. Temperature-dependent variation of ^{1}H-NMR chemical shifts of aromatic and vinyl protons of PVM **62** at 6.2 mM in $CDCl_3$.

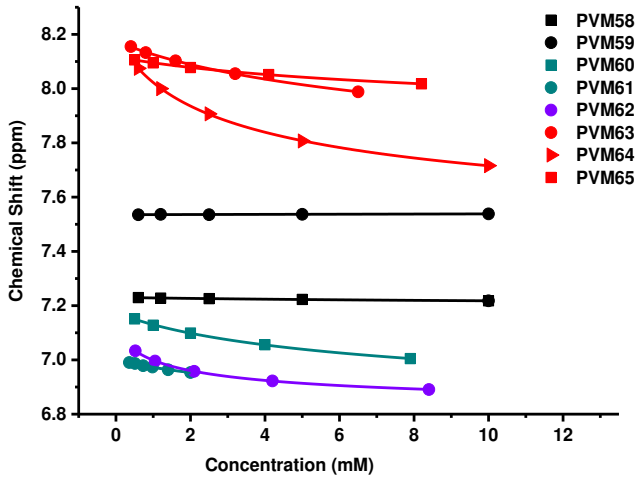

Figure 2.5. The concentration dependent chemical shifts of exo-annular protons of PVM **58-65**. ^{1}H NMR spectra was taken in CDCl3 at ambient temperature.

2.3.2 Diffusion ordered spectroscopy (DOSY) experiments

Next, we performed DOSY experiments in order to investigate the size of aggregates. The size of macrocycle aggregates can be estimated from the diffusion coefficient of the stacked species in Solution. We assumed macrocycle aggregates are spherical, and the particle densities (ρ) are the same. According to the Stokes-Einstein equation (Eq. 1), where r is the hydrodynamic radius of the aggregates, k is the Boltzmann constant (1.380×10^{-23} J·K^{-1}, T is the temperature, η is the viscosity of the solution, and D is the diffusion coefficient, and simple mass-volume-density equation (Eq. 2), the dependencies of particle radius (r) and diffusion coefficient (D) on the particle mass (M) can be obtained. It follows that the diffusion coefficient is inversely proportional to the radius of the aggregate and cube root of the mass of aggregates (M) (Eq. 3).

$$D = \frac{k_B T}{6\pi\eta r} \qquad \text{(Eq. 1)}$$

$$M = \frac{4}{3}\pi r^3 \rho \qquad \text{(Eq. 2)}$$

$$\frac{D_2}{D_1} = \frac{r_1}{r_2} = \sqrt[3]{\frac{M_1}{M_2}} \qquad \text{(Eq. 3)}$$

The diffusion coefficient is dependent on temperature and solvent viscosity. In order to minimize the inaccuracy caused by temperature fluctuation and the solution viscosity changes, we used $CDCl_3$ as the internal standard. The diffusion coefficients of macrocycle stacks are normalized by dividing them by the reference diffusion coefficients (D_{PVM}/D_{ref}). We assume that macrocycles exist mostly as monomers at a low concentration. The number of aggregates (N) at higher concentrations was then calculated based on the ratio of normalized diffusion coefficients of monomers and aggregates using Eq. 4.

$$N = \frac{M_{aggregates}}{M_{monomer}} = \left(\frac{D_{monomer}}{D_{aggregates}}\right)^3 \qquad \text{(Eq. 4)}$$

We used **PVM62** and **PVM64**, which show the strongest aggregation, as the representative examples to estimate the number of macrocycles per stacked species. Table 1 shows the summary of the DOSY experiments results. We assume that **PVM62** and **PVM64** are present as monomeric species at the lowest measured concentrations of 0.13 mM, and 0.66 mM, respectively. According to Eq. 4, the number of aggregates of both **PVM62** and **PVM64** at the highest measured concentrations (4.08 mM, and 10.5 mM respectively) were calculated to be around 2. These results indicate that it is mainly monomer-dimer aggregation and higher order aggregates beyond dimer is insignificant in the concentration range we studied for PVM **62** and **64**. We assumed that the aggregations of other PVMs (**60**, **61**, **63**, **65**), which show weaker self-association in $CDCl_3$ than **62** and **64**, are mainly limited to the dimerization.

Table 2.1. The diffusion coefficients of PVM **62** and **64** at different concentration at 295.85K.

PVMs	c(mM)	D ($10^{-10}m^2s^{-1}$)	D_{ref} ($10^{-10}m^2s^{-1}$)	D/D_{ref}	Number of Aggregates*
PVM **62**	4.08	3.15	23.93	0.132	2.19
PVM **62**	1.02	3.56	23.02	0.155	1.35
PVM **62**	0.13	3.85	22.53	0.171	1.00
PVM **64**	10.5	2.91	20.40	0.143	2.15
PVM **64**	2.63	3.46	21.31	0.162	1.46
PVM **64**	0.66	3.95	21.45	0.184	1.00

* The numbers of aggregates are calculated based on the lowest concentration data.

2.3.3 Quantitative NMR calculations

Since DOSY experiments support the monomer-dimer equilibrium is the major aggregation process, the concentration-dependent chemical shift data of *endo*- and *exo*- protons of PVMs were analyzed using the monomer-dimer model (Eq.5): [12]

$$\delta_{obs} = \delta_{monomer} - \Delta\left(1 + \frac{\left(1-\sqrt{8K_{assoc}c_t+1}\right)}{4K_{assoc}c_t}\right) \quad \text{(Eq. 5)}$$

Where δ_{obs} is the observed chemical shift, $P_{monomer}$ is the chemical shift of the monomer, K_{assoc} is the association constant, c_t is the molar concentration of the PVM, and Δ is the chemical shift difference between monomer and dimer. Based on the concentration-dependent chemical shifts of *exo*-annular (H^a) and the *endo*-annular (H^b) protons of PVMs at 20 °C, their self-association constants were extracted using non-linear least-squares regression method. We were able to identify the best values of association constants, which give the smallest standard deviations

in the curve fitting, for macrocycles showing significant aggregation. The self-association constants calculated from *endo*- and *exo*-annular protons of the PVMs are in good agreement within the experimental errors, and the averages are shown in Table 2.2. It is interesting to note that the aggregation properties of PVMs are strongly influenced by the polarity of substituents, and whether the functional groups can donate or withdraw the electron density from macrocyclic core appears less important. PVMs substituted with either electron donating alkoxy groups or electron withdrawing ester groups show increased aggregation tendencies compared to PVMs substituted with non-polar alkyl groups. It is in striking contrast to the analogous PAMs, which show considerable aggregation when functionalized with electron withdrawing groups (e.g. $COOC_4H_9$), and no obvious aggregation when functionalized with electron donating groups (e.g. OC_4H_9) (Table 2.2). It is unclear why more flexible PVMs have stronger aggregation tendencies compared to more rigid and shape-persistent PAMs. PVM **62** functionalized with reversed ester ($OCOC_9H_{19}$) shows the strongest self-association constants. It appears that the length of alkyl chains attached to the ether or ester groups negatively influence the aggregation of PVMs mainly due to the lager entropic loss upon aggregation. We observed much stronger aggregation of PVM **61** (R = $O^nC_4H_9$) and **64** (R = $COO^nC_4H_9$) compared to PVM **60** (R = $O^nC_{10}H_{21}$) and **63** (R = $COO^nC_{10}H_{21}$) respectively. It is surprising to notice that *t*-butyl ester substituted PVM **65** shows decent aggregation, although bulky substituents substantially reduce the PVM aggregation (four-fold decrease in K_{assoc} when *n*-butyl esters were replaced by *t*-butyl esters) due to the steric repulsion. The considerable aggregation of *t*-butyl ester functionalized PVM **65** suggests the off-set face-to-face dimerization of PVMs. Similar to the predicted PAM dimer geometry based on Hunter-Sanders model, 30° rotational off-set around the principle axis is likely preferred, which can minimize the steric repulsion between bulky substituents.

$$ln(K_{assoc}) = -\frac{\Delta H}{\mathrm{R}}\left(\frac{1}{T}\right) + \frac{\Delta S}{\mathrm{R}} \qquad \text{(Eq. 6)}$$

The thermodynamic parameters of the self-association of PVMs were further deduced by variant-temperature NMR experiments and subsequent Van't Hoff analyses applying Eq. 6, where ΔH is the enthalpy change, R is the gas constant, T is the absolute temperature and ΔS is the entropy change. The association constants (K_{assoc}) of PVMs **60-65** at six different temperatures were obtained as above using non-linear least-squares curve fitting and used to construct the Van't Hoff plots shown in Fig. 2.6. The plots of the natural logarithm of the association constants of PVMs against the inverse absolute temperatures provided straight lines for PVMs **60** and **63-65**, and the values of ΔH and ΔS of their aggregation process of PVMs are extracted from the slopes ($\frac{\Delta \mathrm{H}}{R}$) and the axis intercepts ($\frac{\Delta \mathrm{S}}{R}$) of the Van't Hoff plots. However, we could not obtain accurate values of ΔH and ΔS for PVM **61** and **62** dimerization due to the non-linear fitting of their temperature dependent aggregation data when subjected to the Van't Hoff analysis. The thermodynamic data indicates that the formation of aggregates is mainly attributed to the enthalpy gain, which is large enough to offset the entropic loss. The largest enthalpic contribution and entropy loss was observed for PVM **60**, which is substituted with decyloxy groups. Not surprisingly, longer alkyl chains on functional groups lead to greater entropy loss and diminish the tendency of aggregation. Our experimental data shows that the enthalpy gain (4.9 kcal·mol^{-1}) during the dimer formation of PVM **64** is comparable to the enthalpy contribution (5.0 kcal·mol^{-1}) in case of analogous PAM **25** dimerization. However, the dimerization of PVM is entropically more favored than PAM dimerization (ΔS = -6.1 cal·mol^{-1}·K^{-1} vs. -9.2 cal·mol^{-1}·K^{-1} for PVM **64** and COO^{n}C$_4$H$_9$ substituted PAM. At this stage, the driving force for the stronger aggregation of PVMs compared to the analogous PAMs bearing similar substituents remains unclear.

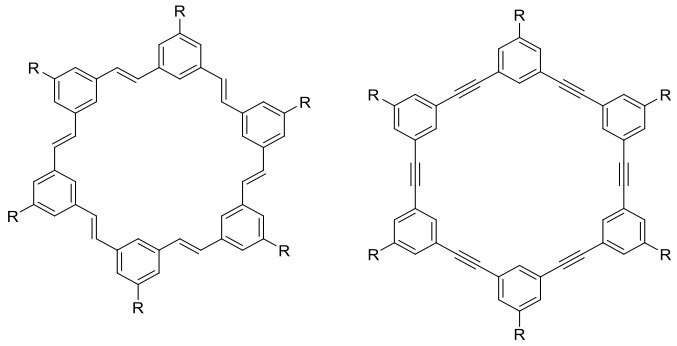

Table 2.2. The thermodynamic data of self-association of PVMs and PAMs in $CDCl_3$.

R (PVM)	K_{assoc} (M^{-1})	ΔH / (kcal·mol^{-1})	ΔS / (cal·mol^{-1}·K^{-1})	R (PAM[5a])	K_{assoc} (M^{-1})
$^{n}C_{10}H_{21}$(PVM **58**)	<5	N/A	N/A	$CH_2O^{n}C_4H_9$	~0
$^{t}C_4H_9$ (PVM **59**)	~0	N/A	N/A		
$O^{n}C_{10}H_{21}$ (PVM **60**)	60	-8.7±0.9	-21±3		
$O^{n}C_4H_9$ (PVM **61**)	99	N/A	N/A	$O^{n}C_4H_9$	~0
$OCO^{n}C_9H_{19}$ (PVM **62**)	628	N/A	N/A	$OCO^{n}C_4H_9$	~0
$COO^{n}C_{10}H_{21}$ (PVM **63**)	45	-4.9±0.2	-8.9±0.7		
$COO^{n}C_4H_9$ (PVM **64**)	168	-4.9±0.4	-6±1	$COO^{n}C_4H_9$	60
COO^{t}Bu (PVM **65**)	40	-5.8±0.7	-12±2	COO^{t}Bu	~0

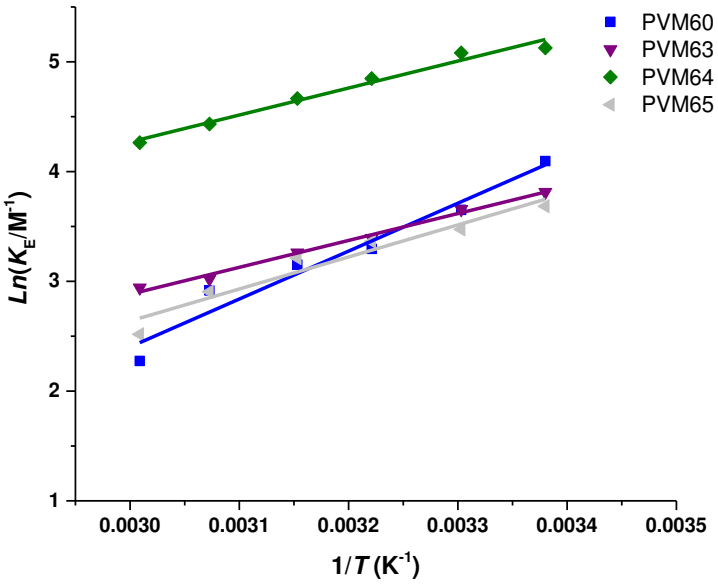

Figure 2.6. Van't Hoff's plots of PVMs.

Compared to the association coefficients of phenylene acetylene macrocycles (PAMs), the PVMs generally have larger association constants. The PVM **62** exhibits the highest binding affinity among all PVMs, while PVMs with alkyl chains show very weak aggregation. The PVMs with electron-donating groups have more negative enthalpy values, which means they are more enthalpically favored. The PVMs with longer or bulkier alkyl chains have smaller entropy changes, indicating that their aggregation is not entropically favored.

2.4 Conclusions

A series of phenylene vinylene macrocycles were successfully synthesized through one-step ADMAC from divinyl monomers. The aggregation behaviors of these PVMs were systematically studied. The ^{1}H NMR DOSY experiments support the predominant monomer-dimer equilibrium during the aggregation process rather than forming higher oligomers. Based on the "monomer-dimer" model, the thermodynamic parameters for the PVM aggregation process were

obtained based on the temperature and dependent NMR chemical shift data of the PVMs and Van't Hoff analyses. The aggregations of PVMs are enthalpy-favored process, and the entropy effects decrease the K_{assoc} of PVMs substituted with longer alkyl chains. Surprisingly, despite to their structural similarity, PVMs show much stronger aggregation tendency compared to the analogous PAMs. In great contrast to the non-aggregation character of PAMs functionalized with electron donating groups (OR, or OCOR) or bulky substituents (e.g. COO^{t}Bu), PVMs bearing those groups all show favorable aggregation. It appears that the polarity of substituents influences the aggregation of PVMs and whether the functional groups can donate or withdraw the electron density from macrocyclic core seems less important. Our study indicates the importance of macrocyclic backbone structure itself to the self-association property. Subtle differences in backbone structures, e.g. arylene-ethynylene backbones vs. arylene-vinylene backbone, can lead to major changes in their aggregation behavior. The sensitivity of macrocycle aggregation to the backbone structure would provide interesting insight into how their aggregation can be engineered by manipulating the backbone structures as well as side chain substituents.

2.5 Experimental section

2.5.1 Materials and general synthetic methods

Reagents and solvents were purchased from commercial suppliers and used without further purification, unless otherwise indicated. Tetrahydrofuran (THF), toluene, CH_2Cl_2 and dimethylformamide (DMF) are purified by the MBRAUN solvent purification systems.

All reactions were conducted under dry nitrogen in oven-dried glassware, unless otherwise specified. Solvents were evaporated using a rotary evaporator after workup. Unless otherwise

specified, the purity of the compounds was ≥95% based on ^{1}H NMR spectral integration.

Flash column chromatography was performed by using a 100-150 times weight excess of flash silica gel 32-63 μm from Dynamic Absorbants Inc. Fractions were analyzed by TLC using TLC silica gel F254 250 μm precoated-plates from Dynamic Absorbants Inc. Analytical gel permeation chromatography (GPC) was performed using a Viscotek GPCmaxTM, a Viscotek Model 3580 Differential Refractive Index (RI) Detector, a Viscotek Model 3210 UV/VIS Detector and a set of two Viscotek Viscogel columns (7.8 × 30 cm, l-MBLMW-3078, and l-MBMMW-3078 columns) with THF as the eluent at 30 °C. The analytical GPC was calibrated using monodisperse polystyrene standards. UV-vis absorption measurements were carried out with an Agilent 8453 spectrophotometer.

MALDI MS spectra were obtained using a Voyager-DE™ STR Biospectrometry Workstation using 2,5-dihydroxybenzoic acid (DHB) as the matrix. The high resolution Mass spectra were obtained on Waters SYNAPT G2 High Definition Mass Spectrometry System. Analyte molecules were diluted into ESI solvents, either methanol or acetonitrile/water mixture, for final concentrations of 10 ppm or lower. The solution was injected into the electrospray ionization (ESI) source at a rate of 5 μL/min. Either the ESI^{+} or ESI^{-} mode was used in reference to the molecular properties. Accurate mass analysis was performed by using the Lock Mass calibration feature with the instrument.

NMR spectra were taken using Inova 400 and Inova 500 spectrometers. $CHCl_3$ (7.27 ppm), toluene (2.09 ppm) were used as internal references in ^{1}H NMR, and $CHCl_3$ (77.23 ppm) for ^{13}C NMR. ^{1}H NMR data were reported in order: chemical shift, multiplicity (s, singlet; d, doublet; t, triplet; q, quartet; m, multiplet), coupling constants (*J*, Hz), number of protons.

2.5.2 Experimental procedures

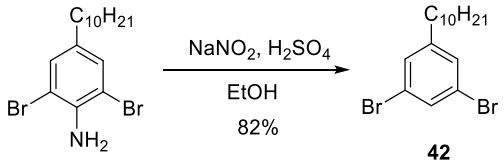

42

1,3-Dibromo-5-decyl benzene (42): To a solution of 2,6-dibromo-4-decylaniline (391 mg, 1.0 mmol) in ethanol (15 mL) was added concentrated H_2SO_4 (1.0 mL). The reaction mixture was heated to reflux, and $NaNO_2$ (690 mg, 10 mmol) was then slowly added. The reaction mixture was refluxed for another 3 h. Upon completion, the reaction mixture was neutralized with satd. $NaHCO_3$ (20 mL), and extracted with CH_2Cl_2 (3 x 30 mL). The combined organic extracts were dried with Na_2SO_4, and concentrated. The residue was purified by flash column chromatography using hexane as eluent to provide pure product as white solids (308 mg, 82%): ^{1}H NMR (400 MHz, $CDCl_3$) δ 7.48 (t, J = 1.8 Hz, 1H), 7.26 (d, J = 1.8 Hz, 2H), 2.53 (dd, J = 15.4, 7.4 Hz, 2H), 1.72-1.50 (m, 2H), 1.36-1.21 (m, 16H), 0.90 (t, J = 6.9 Hz, 3H); ^{13}C NMR (100 MHz, $CDCl_3$) δ 147.03, 131.46, 130.44, 122.88, 35.60, 32.13, 31.25, 29.82, 29.75, 29.62, 29.56, 29.37, 22.93, 14.37.

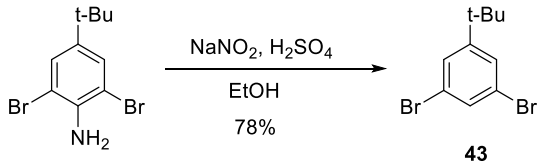

43

1,3-Dibromo-5-*tert*-butyl benzene (43): Typical procedure for deamination reaction from aniline described for compound **1** was followed. 2,6-dibromo-4-decylaniline (307 mg, 1.0 mmol) was converted to product (228 mg, 78 %). Physical data for compound **2**: ^{1}H NMR (400 MHz, $CDCl_3$) δ 7.38 (s, 2H), 4.41 (s, 2H), 1.26 (s, 9H); ^{13}C NMR (100 MHz, $CDCl_3$) δ 143.23, 139.66, 129.07,

108.94, 34.31, 31.48; $[M+H]^+$ calcd. for $C_{10}H_{13}Br_2N$, 307.9468; found, 307.9467.

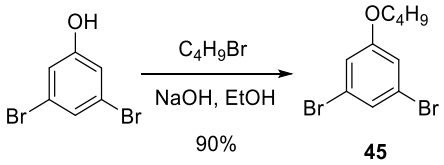

45

1,3-Dibromo-5-butoxyl-benzene (45): The procedure reported by Kandre et. al was followed. A mixture of 3,5-dibromophenol (1.0 g, 3.97 mmol) and 1-bromobutane (598 mg, 4.36 mmol), and NaOH (175 mg, 4.36 mmol) in EtOH (25 mL) was heated in a Schlenk tube at 95 ^oC for 18 h. It was then allowed to cool to room temperature. Water (50 mL) was added and the product was extracted with ethyl acetate (4 x 40 mL). The combined organic extracts were dried over anhydrous Na_2SO_4, concentrated, and purified by flash column chromatography using hexane as the eluent to provide the product as a colorless oil (1.10g , 90%): ^1H NMR (500 MHz, $CDCl_3$): δ 7.23 (t, J = 1.6 Hz, 1H), 6.99 (*d*, J = 1.7 Hz, 2H), 3.93 (t, J = 6.5 Hz, 2H), 1.82 – 1.69 (m, 2H), 1.53 – 1.42 (m, 2H), 0.98 (t, J = 7.4 Hz, 3H); ^{13}C NMR (100 MHz, $CDCl_3$): δ 160.55, 126.34, 123.25, 117.12, 68.51, 31.22, 19.34, 14.00. HRMS (m/z): $[M+H]^+$ calcd. for $C_{10}H_{12}Br_2O$,308.9313; found, 307.9318.

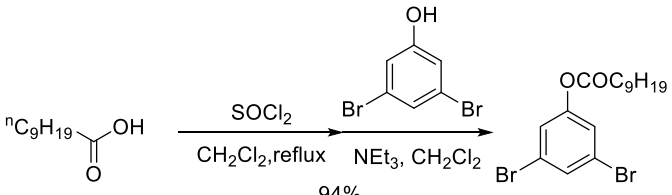

46

Decanoic acid 3,5-dibromo-phenyl ester (46): To a solution of decanoic acid (344 mg, 2.0 mmol) in CH_2Cl_2 (4 mL) was added $SOCl_2$ (571 mg, 4.0 mmol). The reaction was heated at 80 ^oC for 2 h. The excess $SOCl_2$ was removed by vacuum evaporation, and 3,5-dibromophenol (453 mg, 1.8 mmol) was added followed by triethyl amine (6.0 mL). After stirring at 50 ^oC for 4 h, the reaction

was quenched with satd. NH_4Cl solution. The product was extracted with CH_2Cl_2 (3 x 10 mL). The organic extracts were dried over Na_2SO_4, and concentrated. The residue was purified by flash column chromatography (CH_2Cl_2/hexane, 1/2, v/v) to give the product as a white solid (0.69 g, 94 %): ^{1}H NMR (400 MHz, $CDCl_3$): δ 7.53 (t, *J* = 1.7 Hz, 1H), 7.23 (d, *J* = 1.7 Hz, 2H), 2.53 (t, *J* = 7.5 Hz, 2H), 1.78 – 1.66 (m, 2H), 1.45 – 1.18 (m, 12H), 0.88 (t, *J* = 6.9 Hz, 3H); ^{13}C NMR (100 MHz, $CDCl_3$): δ 171.51, 151.75, 131.69, 124.34, 122.94, 34.40, 32.14, 29.68, 29.55, 29.51, 29.31, 25.02, 22.97, 14.43; HRMS (m/z): $[M+Li]^+$ calcd. for $C_{16}H_{22}Br_2O_2$, 411.0142; found, 411.0145.

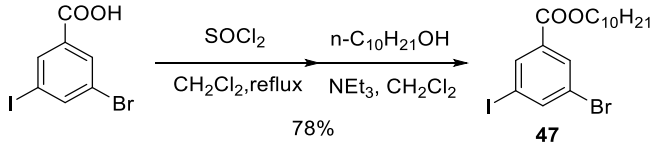

47

3-Bromo-5-iodo-benzoic acid decyl ester (47): Typical procedure for esterification reaction from acid and alcohol described for compound **45** was followed. Decanoic acid (344 mg, 2.0 mmol) and decyl alcohol (285 mg, 1.8 mmol) was converted to compound **47** (656 mg, 78 %) using $SOCl_2$ (571 mg, 4.0 mmol) and triethyl amine (6 mL). Physical data for compound **47**: ^{1}H NMR (400 MHz, $CDCl_3$) δ 8.27 (t, *J* = 1.5 Hz, 1H), 8.11 (t, *J* = 1.5 Hz, 1H), 8.02 (t, *J* = 1.7 Hz, 1H), 4.30 (t, *J* = 8.7 Hz, 2H), 1.87 – 1.67 (m, 2H), 1.47 – 1.07 (m, 14H), 0.88 (t, *J* = 7.0 Hz, 3H). ^{13}C NMR (100 MHz, $CDCl_3$) δ 164.11, 143.83, 137.29, 133.85, 132.10, 123.17, 94.23, 66.23, 32.10, 29.74, 29.70, 29.51, 29.45, 28.79, 26.14, 22.90, 14.35; HRMS (m/z): $[M+H]^+$ calcd. for $C_{17}H_{24}BrIO_2$, 467.0083; found, 467.0089.

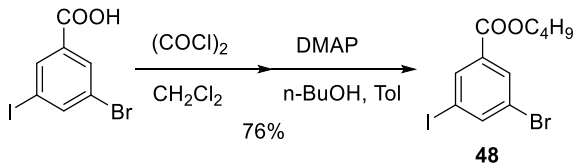

48

3-Bromo-5-iodo-benzoic acid butyl ester (48): Typical procedure for esterification reaction from acid and alcohol described for compound **45** was followed. Decanoic acid (344 mg, 2.0 mmol) and butyl alcohol (133 mg, 1.8 mmol) was converted to compound **48** (565 mg, 82 %) using $SOCl_2$ (571 mg, 4.0 mmol) and triethyl amine (6 mL). Physical data for compound **48**: ^{1}H NMR (400 MHz, $CDCl_3$) δ 8.29 (t, *J* = 1.5 Hz, 1H), 8.13 (t, *J* = 1.6 Hz, 1H), 8.04 (t, *J* = 1.7 Hz, 1H), 4.33 (t, *J* = 6.7 Hz, 2H), 1.86 – 1.67 (m, 2H), 1.53 – 1.41 (m, 2H), 0.99 (t, *J* = 7.4 Hz, 3H); ^{13}C NMR (100 MHz, $CDCl_3$) δ 164.16, 143.86, 137.31, 132.12, 123.19, 65.93, 30.85, 19.41, 13.96.; HRMS (m/z): $[M+H]^+$ calcd. for $C_{11}H_{12}BrIO_2$, 382.9144 ; found, 382.9149.

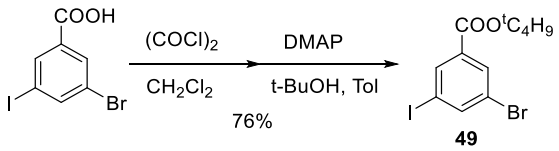

49

3-Bromo-5-iodo-benzoic acid *tert*-butyl ester (49): To a shlenk tube with 3-bromo-5-iodobenzoic acid (654 mg, 2.0 mmol) dissolved in 4 mL of CH_2Cl_2, oxalyl chloride (506 mg, 4.0 mmol) was added and the reaction was then heated at 50 ^{o}C for 2 h. Upon completion, the excess oxalyl chloride and solvent was removed by vacuum evaporation. *tert*-Butanol (163 mg, 2.2 mmol) was then added and followed by addition of 4-dimethylaminopyridine (489 mg ,4 mmol) in 10 mL of toluene. The reaction was stirred in 80 ^{o}C for 10 h. After completion, the reaction was quenched with saturated NH_4Cl aqueous solution, then extracted with CH_2Cl_2 (10 mL ×3) followed by vacuum removal of the solvent. Further purification by column chromatography (CH_2Cl_2/hexane, 1/2, v/v) gives product as white solids (0.582 g, 76%): ^{1}H NMR (400 MHz, $CDCl_3$) δ 8.20 (t, *J* = 1.5 Hz, 1H), 8.03 (t, *J* = 1.4 Hz, 1H), 7.97 – 7.96 (dd, *J* = 1.4 Hz, 1H), 1.57 (s, 9H); ^{13}C NMR (100 MHz, $CDCl_3$) δ 163.02, 143.42, 137.23, 135.36, 132.04, 123.06, 94.20, 82.62, 28.33. HRMS (m/z): $[M+Na]^+$ calcd. for $C_{11}H_{12}BrIO_2$, 404.8958; found, 404.8956.

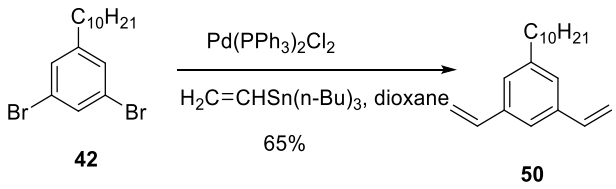

42 50

1-Decyl-3,5-divinyl-benzene (50): To a Schlenk tube were added $Pd(PPh_3)_4$ (41.4 mg, 0.036 mmol), lithium chloride (15.2 mg, 0.36 mmol), and tributylvinyltin (568.7 mg, 1.79 mmol), followed by a solution of **42** (270 mg, 0.72 mmol) in THF (6 mL). The mixture was stirred at 100 ^oC for 16 h, then cooled to rt. Saturated KF aqueous solution (10 mL) was then added and stirred for 30 min to remove excess tributyl tin salts. The mixture was extracted with diethyl ether (10 mL×4). The combined organic extracts were dried over Na_2SO_4, concentrated, and purified by flash column chromatography (CH_2Cl_2/hexane, 1/2, v/v) as eluent to yield pure product as a white solid (127 mg, 65 %). Physical data for compound **50**: ^1H NMR (400 MHz, $CDCl_3$) δ 7.28 (t, *J* =1.4Hz, 1H), 7.14 (d, *J* = 1.4 Hz, 2H), 6.71 (dd, *J* = 17.6, 10.9 Hz, 2H), 5.77 (dd, *J* = 17.6, 0.8 Hz, 2H), 5.25 (dd, *J* = 10.9, 0.8 Hz, 2H), 2.66-2.53 (m, 2H), 1.72-1.52 (m, 2H), 1.35-1.22 (m, 14H), 0.89 (t, *J* = 6.8 Hz, 3H); ^{13}C NMR (100 MHz, $CDCl_3$) δ 143.59, 137.88, 137.09, 126.08, 121.88, 113.99, 36.13, 32.14, 31.73, 29.86, 29.82, 29.75, 29.60, 29.57, 22.92, 14.36.

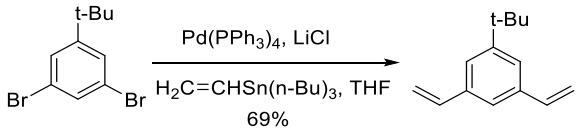

43 51

1-*tert*-Butyl-3,5-divinyl-benzene (51): Typical procedure for vinyllation via Stille coupling reaction described for compound **50** was followed. Compound **43** (210 mg, 0.72 mmol) was converted to the product (92 mg, 69 %) using $Pd(PPh_3)_4$ (41 mg, 0.036 mmol), lithium chloride (15 mg, 0.36 mmol), tributylvinyltin (569 mg, 1.79 mmol), and THF (6 mL). Physical data for compound **51**: ^1H NMR (400 MHz, $CDCl_3$) δ 7.33 (d, *J* = 1.5 Hz, 2H), 7.31 (d, *J* = 1.5 Hz, 1H),

6.74 (dd, *J* = 17.6, 10.9 Hz, 2H), 5.77 (dd, *J* = 17.6, 0.5 Hz, 2H), 5.25 (dd, *J* = 10.9, 0.5 Hz, 2H), 1.34 (s, 9H); ^{13}C NMR (100 MHz, $CDCl_3$) δ 151.77, 137.67, 137.39, 123.31, 121.34, 113.97, 34.88, 31.54.

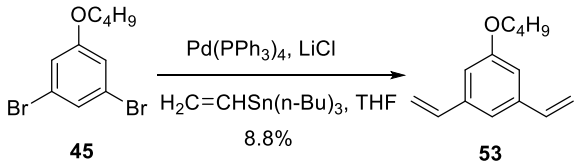

45 **53**

1,3-Divinyl-5-butoxy-benzene (53): Typical procedure for vinyllation via Stille coupling reaction described for compound **50** was followed. Using compound **45** (222 mg, 0.72 mmol), $Pd(PPh_3)_4$ (41 mg, 0.036 mmol), lithium chloride (15 mg, 0.36 mmol), tributylvinyltin (569 mg, 1.79 mmol), and THF (6 mL). The product was obtained as colorless oil. (12.8 mg, 8.8 %) Physical data for compound **53**: ^{1}H NMR (400 MHz, $CDCl_3$) δ 7.03 (t, *J* = 1.5 Hz, 1H), 6.88 (d, *J* = 1.5 Hz, 2H), 6.69 (dd, *J* = 17.6, 10.9 Hz, 2H), 5.76 (dd, *J* = 17.6, 0.9 Hz, 2H), 5.26 (dd, *J* = 10.7, 0.9 Hz, 2H), 4.00 (t, *J* = 6.5 Hz, 2H), 1.83 – 1.72 (m, 2H), 1.56 – 1.45 (m, 2H), 0.99 (t, *J* = 7.4 Hz, 3H); ^{13}C NMR (100 MHz, $CDCl_3$) δ 159.76, 139.19, 136.91, 117.42, 114.46, 111.78, 67.47, 31.21, 19.36, 14.01; HRMS (m/z): $[M+H]^+$ calcd. for $C_{14}H_{18}O$, 203.1436; found, 203.1433.

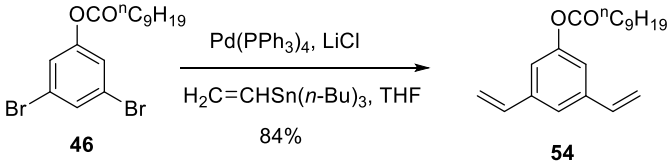

46 **54**

Decanoic acid 3,5-divinyl-phenyl ester (54): Typical procedure for vinyllation via Stille coupling reaction described for compound **50** was followed. Compound **46** (292 mg, 0.72 mmol) was converted to the product (182 mg, 84 %) using $Pd(PPh_3)_4$ (41 mg, 0.036 mmol), lithium chloride (15 mg, 0.36 mmol), tributylvinyltin (569 mg, 1.79 mmol), and THF (6 mL). Physical data for compound **54**: ^{1}H NMR (400 MHz, $CDCl_3$) δ 7.28 (t, *J* = 1.4 Hz, 1H), 7.03 (d, *J* = 1.5 Hz, 2H),

6.69 (dd, *J* = 17.6, 10.9 Hz, 2H), 5.76 (dd, *J* = 17.6, 0.5 Hz, 2H), 5.30 (dd, *J* = 10.9, 0.5 Hz, 2H), 2.57 (t, *J* = 7.5 Hz, 2H), 1.83-1.72 (m, 2H), 1.48-1.17 (m, 12H), 0.91-0.85 (m, 3H); ^{13}C NMR (100 MHz, $CDCl_3$) δ 172.51, 151.51, 139.44, 136.14, 122.21, 118.64, 115.28, 34.64, 32.13, 29.69, 29.68, 29.53, 29.37, 25.18, 22.94, 14.38; HRMS (m/z): $[M+Na]^+$ calcd. for $C_{20}H_{28}O_2$, 323.1982; found, 323.1980.

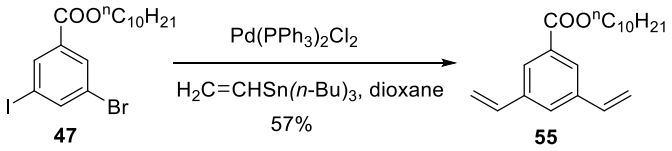

3,5-Divinyl-benzoic acid decyl ester (55): Typical procedure for vinyllation via Stille coupling reaction described for compound **50** was followed. Compound **47** (336 mg, 0.72 mmol) was converted to the product (129 mg, 57 %) using $Pd(PPh_3)_4$ (41 mg, 0.036 mmol), lithium chloride (15 mg, 0.36 mmol), tributylvinyltin (569 mg, 1.79 mmol), and THF (6 mL). Physical data for compound **55**: ^{1}H NMR (400 MHz, $CDCl_3$) δ 7.97 (d, *J* = 1.8 Hz, 2H), 7.60 (t, *J* = 1.7 Hz, 1H), 6.74 (dd, *J* = 17.4, 11.8 Hz, 2H), 5.84 (dd, *J* = 17.6, 2.0 Hz, 2H), 5.34 (dd, *J* = 11.8, 2.0 Hz, 2H), 4.33 (d, *J* = 6.4 Hz, 2H), 1.87-1.67 (m, 2H), 1.48-1.21 (m, 14H), 0.87 (d, *J* = 7.1 Hz, 3H). ^{13}C NMR (100 MHz, $CDCl_3$) δ 166.71, 138.24, 136.06, 131.34, 128.28, 126.74, 115.48, 65.54, 32.11, 29.75, 29.75, 29.53, 29.50, 28.92, 26.24, 22.90, 14.34; HRMS (m/z): $[M+H]^+$ calcd. for $C_{21}H_{30}O_2$, 315.2319; found, 315.2320.

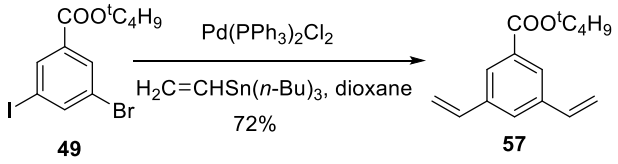

3,5-Divinyl-benzoic acid *tert*-butyl ester (57): Typical procedure for vinyllation via Stille coupling reaction described for compound **50** was followed. Compound **49**(276 mg, 0.72 mmol)

was converted to the product (119 mg, 72 %) using $Pd(PPh_3)_4$ (41 mg, 0.036 mmol), lithium chloride (15 mg, 0.36 mmol), tributylvinyltin (569 mg, 1.79 mmol), and THF (6 mL). Physical data for compound **57:** ^{1}H NMR (500 MHz, $CDCl_3$) δ 7.94 (d, *J* = 1.6 Hz, 2H), 7.57 (s, 1H), 6.75 (dd, *J* = 17.6, 10.9 Hz, 2H), 5.84 (d, *J* = 17.4 Hz, 2H), 5.32 (d, *J* = 8.4 Hz, 2H), 1.62 (s, 9H); ^{13}C NMR (100 MHz, $CDCl_3$) δ 165.77, 138.11, 136.20, 132.79, 127.97, 126.68, 115.30, 81.43, 28.40; HRMS (m/z): $[M+Na]^+$ calcd. for $C_{15}H_{18}O_2$, 253.1204; found, 253.1209.

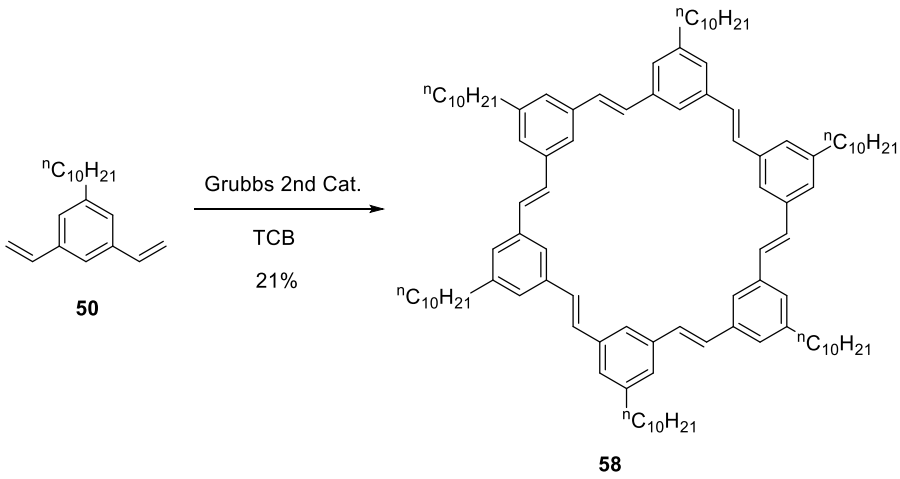

PVM 58: Typical **ADMAC** procedure for macrocycle formation using olefin metathesis is as following: To a Schlenk tube were added 1-decyl-3,5-divinyl-benzene (compound **50**, 100 mg, 0.37 mmol) and a solution of Grubb's 2nd generation catalyst (31 mg, 0.037 mmol) in 1,2,4-trichlorobenzene (10 mL). The reaction apparatus was evacuated and refilled with nitrogen, and this process was repeated three times. The red solution was heated at 40 °C under nitrogen for 18 h. Upon completion, all the solvent was removed and diethyl ether (10 mL) was added. The ethereal solution was washed with water (3 x 10 mL), dried over Na_2SO_4, and concentrated to give the crude product. Purification by flash column chromatography (CH_2Cl_2/hexane, 1/5, v/v) afforded **PVM 58** as a white solid (19 mg, 21 %): ^{1}H NMR (500 MHz, $CDCl_3$) δ 7.63 (s, 6H), 7.30 (s, 12H), 7.23 (s, 12H), 2.71-2.64 (m, 12H), 1.74-1.65 (m, 12H), 1.44-1.21 (m, 84H), 0.89 (t, *J* =

7.0 Hz, 18H); ^{13}C NMR (100 MHz, $CDCl_3$) δ 143.89, 138.47, 137.63, 128.21, 125.78, 35.94, 32.01, 31.84, 29.82, 29.79, 29.72, 29.57, 29.55, 22.90, 14.35; MALDI-TOF (m/z): $[M+H]^+$ calcd. for $C_{108}H_{156}$, 1455.23; found, 1455.45.

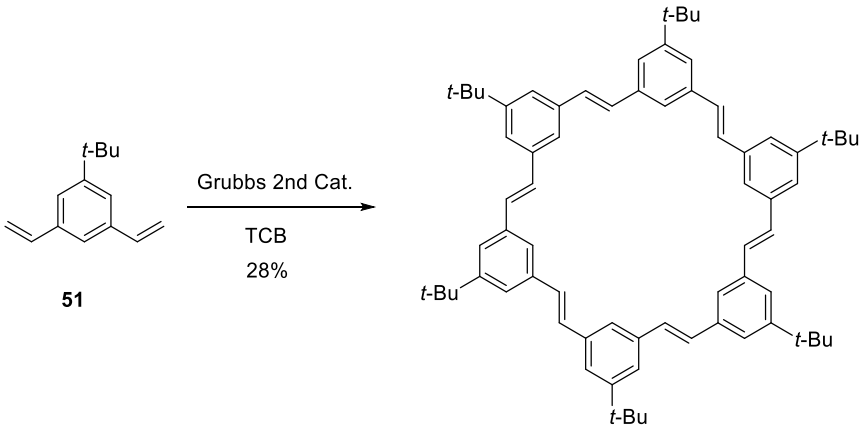

51 59

PVM 59: The typical **ADMAC** procedure described above was followed. 1-*tert*-Butyl-3,5-divinyl-benzene (compound **51**, 100 mg, 0.54 mmol) was converted to **PVM 59** (24 mg, 28 %) using Grubb's 2nd generation catalyst (45 mg, 0.054 mmol) and 1,2,4-trichlorobenzene (10 mL). Physical data for PVM **59**: ^{1}H NMR (500 MHz, $CDCl_3$) δ 7.65 (s, 6H), 7.54 (s, 12H), 7.27 (s, 12H), 1.45 (s, 54H); ^{13}C NMR (100 MHz, $CDCl_3$) δ 152.16, 137.40, 128.70, 123.19, 122.48, 35.10, 31.68; MALDI-TOF (m/z): $[M+H]^+$ calcd. for $C_{72}H_{84}$, 949.67; found, 949.72.

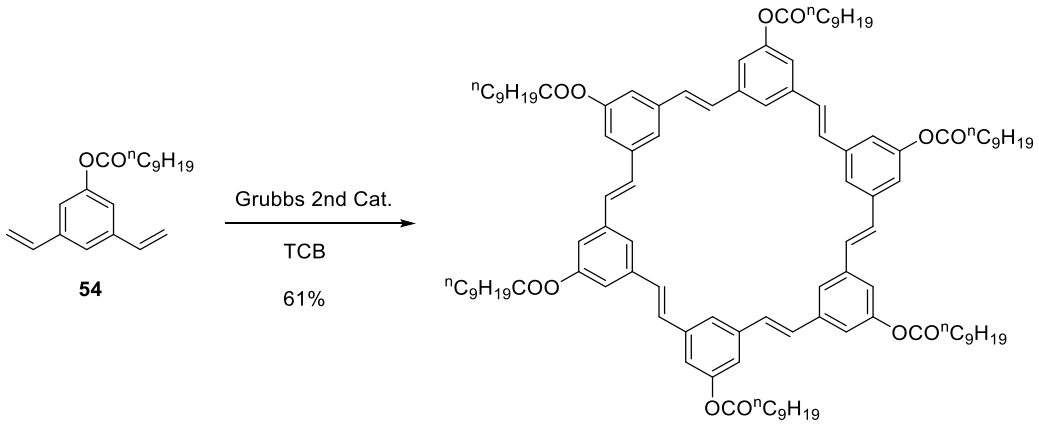

54 62

PVM 62: The typical **ADMAC** procedure described above was followed. Decanoic acid 3,5-divinyl-phenyl ester (compound **54**, 100 mg, 0.33 mmol) was converted to **PVM 62** (55 mg, 61 %) using Grubb's 2nd generation catalyst (27 mg, 0.033 mmol) and 1,2,4-trichlorobenzene (10 mL). Physical data for **PVM 62**: ^{1}H NMR (400 MHz, $CDCl_3$): δ 7.45 (s, 6H), 7.00 (s, 12H), 6.91 (s, 12H), 2.64 (t, *J* = 7.6 Hz, 12H), 1.90-1.79 (m, 12H), 1.54-1.46 (m, 12H), 1.46-1.20 (m, 60H), 0.96-0.89 (t, *J* = 7.0 Hz, 18H); ^{13}C NMR (100 MHz, $CDCl_3$) δ 172.92, 151.25, 139.43, 13.91, 128.25, 121.45, 34.53, 32.08, 29.66, 29.65, 29.51, 29.34, 25.16, 22.93, 14.37; MALDI-TOF (m/z): $[M+H]^+$ calcd. for $C_{108}H_{144}O_{12}$, 1635.08; found, 1635.21.

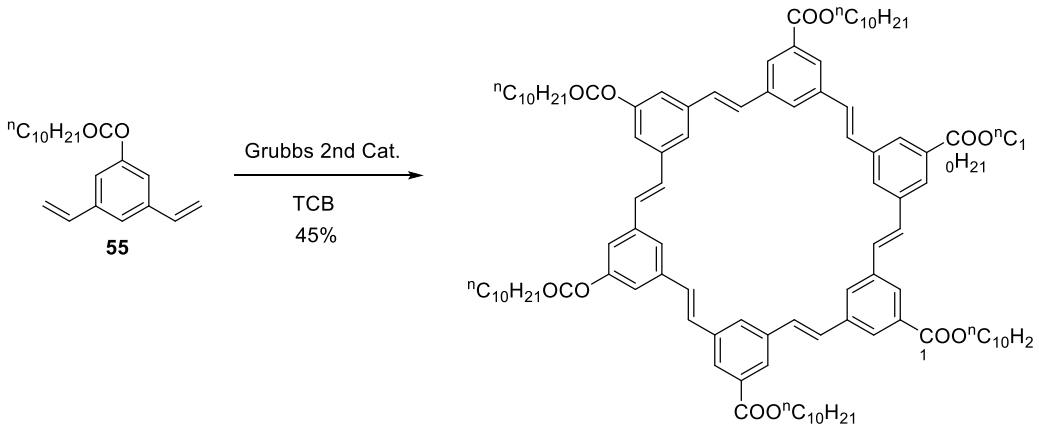

PVM 63: The typical **ADMAC** procedure described above was followed. 3,5-Divinyl-benzoic acid decyl ester: (compound **55**, 100 mg, 0.32 mmol) was converted to **PVM 63** (41 mg, 45 %) using Grubb's 2nd generation catalyst (27 mg, 0.032 mmol) and 1,2,4-trichlorobenzene (10 mL). Physical data for **PVM 63**: ^{1}H NMR (500 MHz, $CDCl_3$) δ 8.09 (s, 12H), 7.87 (s, 6H), 7.28 (s, 12H), 4.43 (t, *J* = 6.8 Hz, 18H), 1.89-1.70 (m, 12H), 1.46-1.21 (m, 84H), 0.88 (t, *J* = 7.1 Hz, 3H); ^{13}C NMR (100 MHz, $CDCl_3$) δ 166.13, 137.15, 131.73, 128.21, 128.05, 127.11, 65.75, 32.01, 29.69, 29.68, 29.64, 29.47, 28.89, 26.21, 22.78, 14.31; MALDI-TOF (m/z): $[M+H]^+$ calcd. for $C_{114}H_{156}O_{12}$, 1719.17; found, 1719.10.

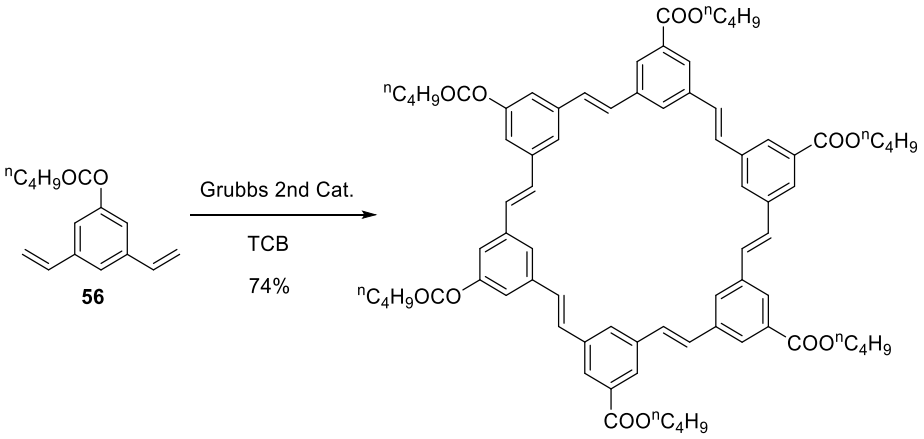

PVM 64: The typical **ADMAC** procedure described above was followed. 3,5-Divinyl-benzoic acid butyl ester: (compound **56**, 100 mg, 0.43 mmol) was converted to **PVM 64** (64 mg, 74 %) using Grubb's 2nd generation catalyst (33 mg, 0.039 mmol) and 1,2,4-trichlorobenzene (10 mL). Physical data for **PVM 64**: ^{1}H NMR (500 MHz, $CDCl_3$) δ 8.10 (s, 12H), 7.86 (s, 6H), 7.26 (s, 12H), 4.40 (t, J = 6.8 Hz, 18H), 1.98-1.73 (m, 12H), 1.51-1.15 (m, 36H), 1.02-0.85 (m, 18H); ^{13}C NMR (100 MHz, $CDCl_3$) δ 166.11, 137.17, 131.75, 128.22, 128.06, 127.12, 65.75, 31.79, 29.94, 28.93, 25.96, 22.85, 14.31; MALDI-TOF (m/z): $[M+H]^+$ calcd. for $C_{78}H_{84}O_{12}$, 1213.60; found, 1213.68.

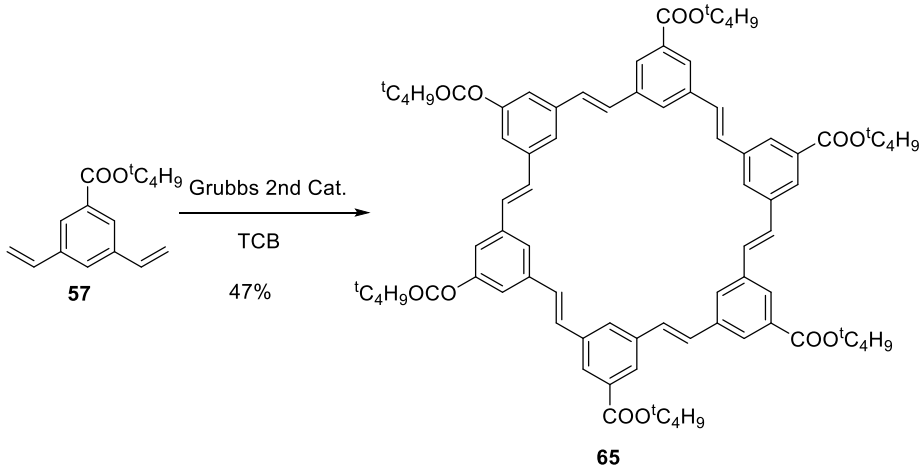

PVM 65: The typical **ADMAC** procedure described above was followed. 3,5-Divinyl-benzoic acid *tert*-butyl ester: (compound **57**, 100 mg, 0.43 mmol) was converted to **PVM 65** (41 mg, 47 %)

using Grubb's 2nd generation catalyst (36 mg, 0.043 mmol) and 1,2,4-trichlorobenzene (10 mL). Physical data for **PVM 65**: ^{1}H NMR (500 MHz, $CDCl_3$) δ 8.10 (s, 12H), 7.91 (s, 6H), 7.32 (s, 12H), 1.70 (s, 54H); ^{13}C NMR (100 MHz, $CDCl_3$) δ 166.17, 138.21, 132.79, 128.25, 127.97, 127.10, 82.56, 29.01; MALDI-TOF (m/z): $[M+H]^+$ calcd. for $C_{78}H_{84}O_{12}$, 1213.60; found, 1213.57.

DOSY NMR Experiments:

The DOSY experiment was carried out on Inova 500MHz spectrometers. The NMR was taken at 22.7 ºC after temperature calibration. Each data at certain concentration was obtained as an average of 3 repetitions. For macrocycles, the diffusion coefficients were estimated based on the aromatic peaks (proton As, Bs and Cs).The typical spectrum was shown in Fig. 2.7, and full data were shown as in Table 2.3.

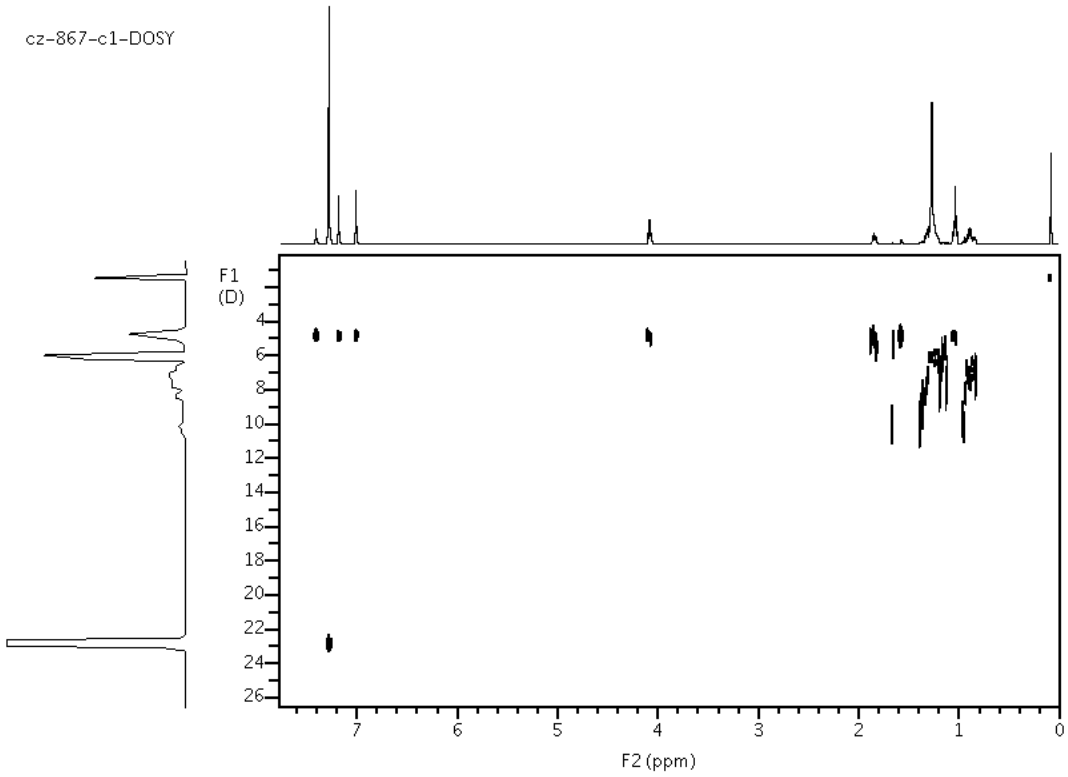

Figure 2.7. DOSY experiment on PVM **61** at 2.00 mM.

Table 2.3 The diffusion coefficients of PVMs and $CHCl_3$ at different conditions were listed.

PVMs	c/mM	D/ ($10^{-10}m^2s^{-1}$)			D_{ref}/ ($10^{-10}m^2s^{-1}$)		
PVM **62**	4.08	3.14	3.17	3.17	23.87	23.98	23.93
PVM **62**	1.02	3.56	3.53	3.61	23.00	23.05	23.97
PVM **62**	0.13	3.81	3.89	3.84	22.49	22.56	22.55
PVM **64**	10.5	2.92	2.90	2.90	20.42	20.45	20.33
PVM **64**	2.63	3.46	3.49	3.42	21.41	21.24	21.27
PVM **64**	0.66	3.93	3.95	3.99	21.41	21.39	21.54

2.6 References

1. Grave, C.; Schluter, A. D. *Eur. J. Org. Chem.* **2002**, 3075.

2. Hoger, S. *Chem. Eur. J.* **2004**, *10*, 1320.

3. MacLachlan, M. J. *Pure Appl. Chem.* **2006**, *78*, 873.

4. Zhang, W.; Moore, J. S. *Angew. Chem. Int. Ed.* **2006**, *45*, 4416.

5. Iyoda, M.; Yamakawa, J.; Rahman, M. J. *Angew. Chem. Int. Ed.* **2011**, *50*, 10522.

6. Zhang, W.; Brombosz, S. M.; Mendoza, J. L.; Moore, J. S. *J. Org. Chem.* **2005**, *70*, 10198.

7. Zhang, W.; Moore, J. S. *J. Am. Chem. Soc.* **2005**, *127*, 11863.

8. Jin, Y.; Zhang, A. B.; Huang, Y. S.; Zhang, W. *Chem. Commun.* **2010**, *46*, 8258.

9. Lahiri, S.; Thompson, J. L.; Moore, J. S. *J. Am. Chem. Soc.* **2000**, *122*, 11315.

10. Zhang, J. S.; Moore, J. S. *J. Am. Chem. Soc.* **1992**, *114*, 9701.

11. Shetty, A. S.; Zhang, J. S.; Moore, J. S. *J. Am. Chem. Soc.* **1996**, *118*, 1019.

12. Martin, R. B. *Chem. Rev.* **1996**, *96*, 3043.

CHAPTER 3

Synthesis of Porphyrin-Based Covalent Organic Polyhedrons through Alkyne Metathesis and Study of Their Fullerene Binding Behavior.[1]

3.1 Abstract

DC_vC provides an intriguing and highly efficient approach for building molecules that are usually thermodynamically favored. However, the DC_vC methods that are efficient enough to construct large, complex molecules, particularly those with three-dimensional (3-D) architectures, are still very limited. Here, for the first time, we have successfully utilized alkyne metathesis, a highly efficient DC_vC approach, to construct the novel 3-D rectangular prismatic molecular cage **COP-5** in one step from a readily accessible porphyrin-based precursor. **COP-5** consists of rigid, aromatic porphyrin and carbazole moieties as well as linear ethynylene linkers, rendering its shape-persistent nature. Interestingly, **COP-5** serves as an excellent receptor for fullerenes. It forms 1:1 complexes with C_{60}, C_{70} and C_{84} with association constants of $1.4\times10^5\ M^{-1}$ (C_{60}), $1.5\times10^8\ M^{-1}$ (C_{70}) and $2.4\times10^7\ M^{-1}$ (C_{84}) in toluene. This represents one of the highest binding affinities reported so far for purely organic fullerene receptors. **COP-5** shows an unprecedented high selectivity in binding C_{70} over C_{60} ($K_{C70}/K_{C60} > 1000$). Moreover, the binding between the cage and fullerene is fully reversible under the acid-base stimuli, thus allowing successful separation of C_{70} from a C_{60}-enriched fullerene mixture (C_{60}/C_{70}, 10/1, mol/mol) through the "selective complexation-decomplexation" strategy.

3.2 Introduction

Three-dimensional (3-D) molecular cages, particularly shape-persistent, covalent organic polyhedrons (COPs) with well-defined pore dimensions, have attracted considerable attention due to their numerous applications in host-guest chemistry,[2,3] chemical sensing,[4,5] catalysis,[6-9] gas adsorption,[10-12] etc. Current synthesis of rigid molecular cages is dominated by supramolecular chemistry, including metal coordination,[13-16] and hydrogen-bonding,[17,18] which usually provides the target species with high efficiency through the self-assembly process. The growing importance of supramolecular cages in the bottom-up design of novel functional materials has prompted the development of COPs, which usually possess high chemical and thermal stability, as promising candidates for those applications requiring harsh operating conditions (*e.g.*, in the presence of acid or base). While supramolecular cages have been extensively studied, purely organic covalent molecular cages are relatively rare and have only recently received increasing attention. Conventionally, COPs are constructed via irreversible chemical transformations, which usually require enormous synthetic and purification efforts with very low overall yields.[19,20] In great contrast, recent advances in DC_vC[21-24] offer convenient pathways to high-yielding synthesis of COPs.[25-27] To date, imine condensation/metathesis is the most widely used reversible DC_vC reaction that has been used in the construction of 3-D molecular architectures.[28-30] However, the potential drawbacks of imine groups are their sensitivity to acidic conditions and water. Further hydride reduction of imines provides more robust, but also flexible, amino groups, resulting in the loss of certain shape persistency of target structures.

Rigid, shape-persistent 3-D molecular cages[31] are attractive as hosts for selectively binding guest molecules of a certain size and shape. However, the construction of molecular cages with well-defined and large intrinsic cavities, which are not easily altered by the environmental stimuli,

still remains a grand challenge. To preserve such shape persistency, the molecules should consist of rigid, non-collapsible scaffolds. In the ocean of conformationally rigid building blocks exists a particularly interesting group of conjugated systems, porphyrins, which have attracted enormous research interest due to their intriguing applications in host-guest chemistry, artificial photosynthesis, and catalysis.

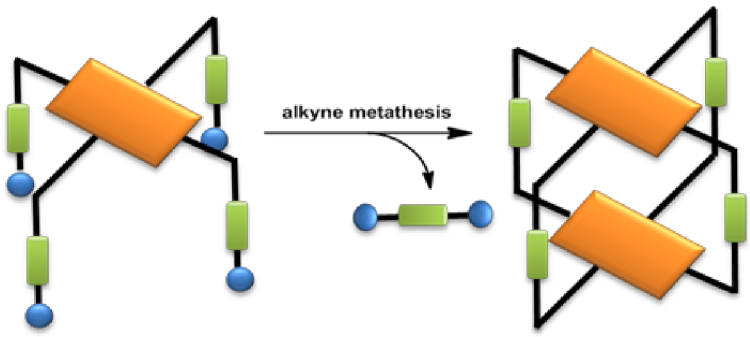

Figure 3.1. Schematic presentation of constructing a molecular cube from a tetra-armed precursor through alkyne metathesis.

Another important group of building blocks with inherent rigidity are arylene ethynylenes, and recent advances in shape-persistent 2-D macrocycles have taken advantage of their angular, rigid geometries and easy synthetic access.[32-34] In this context, alkyne metathesis,[35-37] a DC_vC approach, has emerged as a powerful synthetic tool for the efficient and versatile construction of shape persistent molecular architectures and has been elegantly applied to the one-step modular synthesis of a variety of 2-D macrocyclic compounds from simple arylene diacetylene monomers.[38,39] Such a synthetic approach is remarkable in that it can transform various undesired oligomeric and macrocyclic kinetic intermediates into the thermodynamically most stable product. Shape-persistent 3-D molecular architectures based on rigid arylene ethynylene backbones are synthetically more challenging than their 2-D analogues, and so far they have mainly been obtained

through multistep labor-intensive statistical or template-supported oxidative Glaser coupling.[40] Here we present, for the first time, a one-step synthesis of a shape-persistent organic rectangular prismatic cage consisting of only aromatic moieties in its backbone structure, via Mo(VI)-carbyne-catalyzed alkyne metathesis from tetra-substituted porphyrin monomers, in decent yield (Fig. 3.1). The unique combination of the conjugated system and the rigidity of this cage molecule render its rapid and selective binding of C_{70} over C_{60}; the cage exhibits a binding interaction with C_{70} compared to C_{60} that is stronger by 3 orders of magnitude. Moreover, the clean release of fullerenes (guest) and regeneration of the cage **COP-5** (host) was realized by simply tuning the pH of the media. Such a "selective complexation-decomplexation" strategy has been successfully applied to the isolation of C_{70} from a C_{60}-enriched fullerene mixture.

3.3 Results and discussion

Previously our group has demonstrated that various trigonal prismatic cage molecules can be constructed through the "panel-pillar-assembly" design strategy via a one-step imine condensation/metathesis reaction followed by further reduction of imines to more chemically robust amino groups.[41] However, these amine-linked molecular cages are semi shape-persistent and adopt a distorted-prismatic architecture due to the rotational freedom of the amine bond connections. Although COPs containing methylene, ether, amino, or similar saturated moieties could be shape-persistent to some extent, they are generally considered less conformationally rigid compared to those molecules constructed solely with aromatic fragments in their skeletons. Among functional groups capable of undergoing chemical transformations while retaining their conformational rigidity, the linear ethynylene group seems to be an appropriate robust rigid linker moiety. Given the fact that alkyne metathesis has been successfully utilized in the efficient synthesis of shape persistent 2-D arylene ethynylene macrocycles, we envisioned this dynamic

covalent transformation with a "self-correction" nature would be an ideal approach to construct the ethynylene-linked rigid molecular cage. The next challenge for the dynamic covalent construction of a molecular cage was then the identification of a rigid 90° corner piece that would yield a rectangular-prismatic structure with minimum angle strain. Careful examination of the geometrical parameters suggested that the C_4-symmetric carbazole-substituted porphyrin, in which the ethynyl groups are oriented approximately perpendicular to the porphyrin ring, could be a suitable monomer to yield **COP-5** (Scheme 3.1). Porphyrins are incorporated into the cage structure because of their interesting properties in fullerene binding, which would provide highly efficient donor-acceptor pairs for the photo-induced electron transfer (PET) process.[42,43] Precipitation driven alkyne metathesis was designed for the final cage synthesis. A large aryl group (called as PPT group) was involved in the molecular design. In the alkyne metathesis, di-aryl acetylene will be formed as a precipitate in the reaction, and thus can drive the reaction equilibrium to the product.

The monomer **71** was prepared from 3-iodo-6-formyl-9-hexadecylcarbazole (**66**) through the Lindsey method to form the 5,10,15,20-tetrakis(carbazolyl)porphyrin (**67**), followed by Sonogashira coupling to attach the benzoylbiphenyl acetylene group (Scheme 3.1). Benzoylbiphenyl (PPT group) was utilized as the end group so that insoluble byproduct diarylacetylenes would be formed along the reaction, thus driving the reversible alkyne metathesis to completion.[39] Our newly developed multidentate Mo(VI) carbyne was utilized as the metathesis catalyst, which has shown superior catalytic activity, broader substrate scope, and longer lifetime in comparison to its monodentate analogue.[44] Given the suitable geometrical shape, rigidity of the building block, and high activity of alkyne metathesis catalyst, the formation of the thermodynamically favored target molecular cage is expected. The reaction was performed at 75°C

under microwave irradiation in CCl_4. After 32 h, the predominant formation of cage **COP-5** was observed (56% isolated yield). The dynamic nature of alkyne metathesis offers the self-correction pathway toward the cage formation. The reaction progress monitored by gel permeation chromatography (GPC) showed the gradual conversion of initial high-molecular-weight oligomeric intermediates into the target cage **COP-5** (Fig. 3.2).

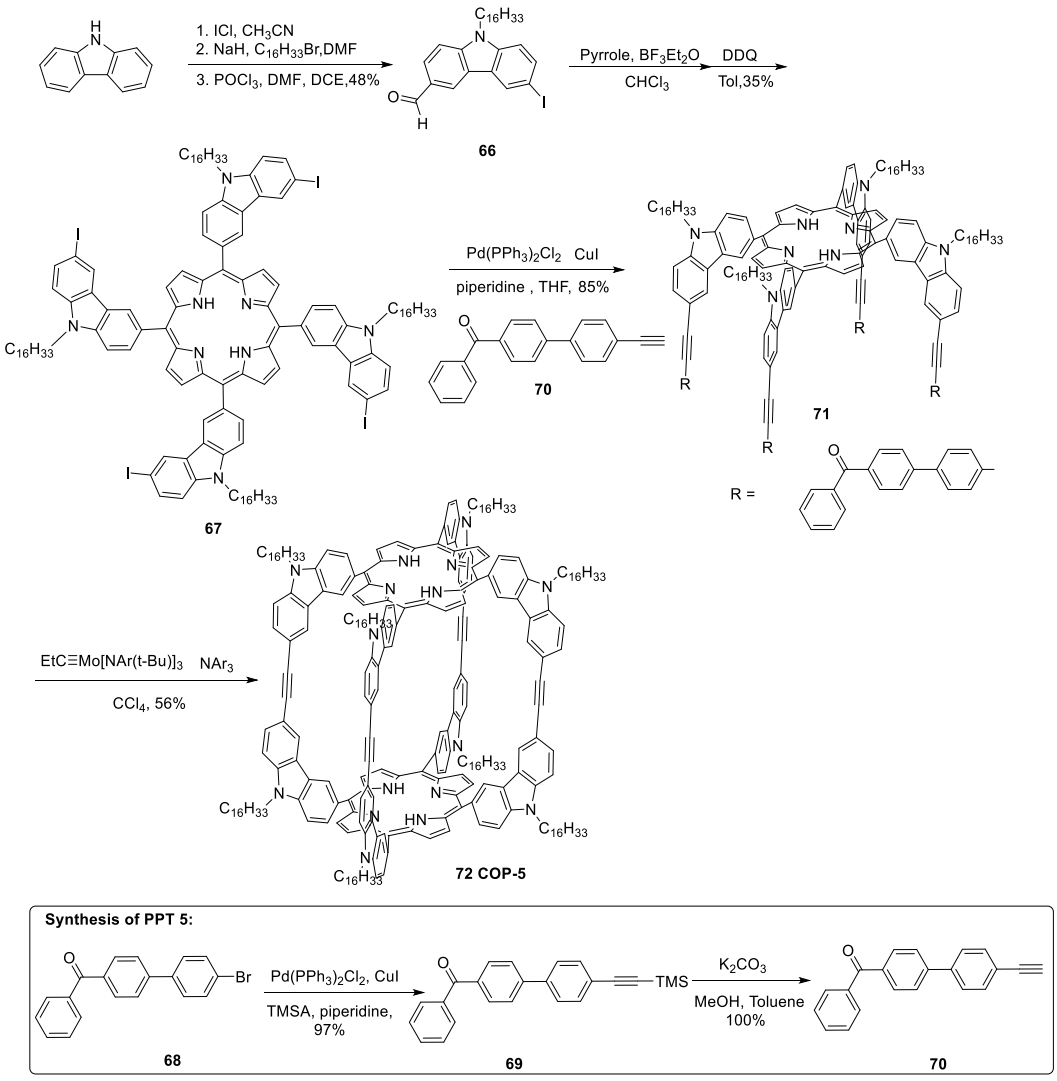

Scheme 3.1. The synthesis of **COP-5**.

Such a cage is enthalpy favored due to its minimal angle strain and also entropy-favored due to its consistent minimal number of building blocks (in comparison to larger oligomeric products). This cage synthesis represents the first time that alkyne metathesis has been used to construct a purely organic, shape-persistent molecular rectangular prism with high efficiency.

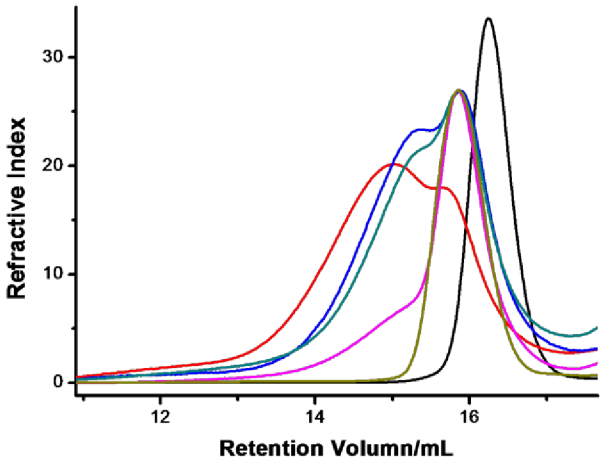

Figure 3.2. The GPC curves of the alkyne metathesis cage formation. The reaction start from monomer (black), and the reaction at 50 °C without microwave gives 20 h (red), 48 h (blue), 72h (green) reaction curves which showing the reaction kinetics pathway: Reaction start from monomer, the oligomers were formed quickly after a few hours and can go back to the dimeric cage slowly and form the new peak. The reaction continued under microwave at 70 °C for 16 h gives better conversion (pink), which can superimpose with the pure cage GPC curve (dark yellow) with only a small shoulder observed.

The cage **COP-5** was fully characterized by ^{1}H and ^{13}C NMR spectroscopy, UV-vis spectroscopy, GPC, and MALDI-TOF mass spectrometry. The ^{1}H NMR spectrum of **COP-5** in $CDCl_3$ shows only one set of singlets corresponding to the porphyrin protons at 8.73 ppm, indicating the high symmetry of the cage structure. The MALDI-TOF mass spectrum shows the desired molecular ion peaks at m/z 3825.80 ($[M+H]^+$ calcd. for $C_{272}H_{332}N_{16}$ 3825.66). Additional evidence supporting the rectangular-prismatic structure of **COP-5** was obtained through a

diffusion ordered spectroscopy (DOSY) experiment (Fig. 3.3). All the peaks assigned to **COP-5** have the same diffusion coefficients (D values) within the experimental errors ((4.1±0.4) $\times 10^{-10}$ $m^2\ s^{-1}$). From the Stokes-Einstein equation, the effective hydrodynamic radius r_H (9.2 ± 1.0 Å) is calculated, which is in good agreement with the calculated radius of gyration 9.7 Å based on the energy minimized structure in Fig. 3.4. The cage is thermally stable and also exhibits a very high chemical stability even with exposure to water and acids (*e.g.*, trifluoroacetic acid, TFA) for weeks, thus showing a great advantage over those supramolecular cages as well as imine-linked COPs.

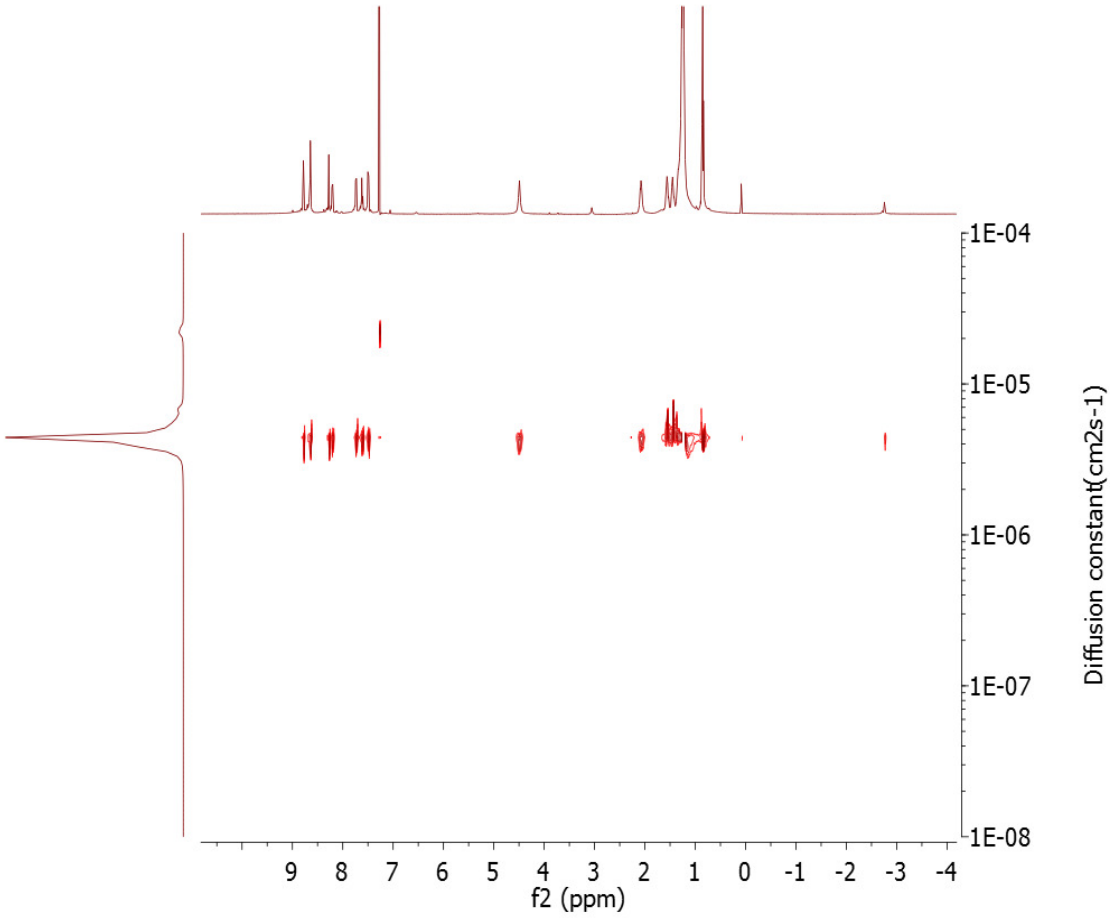

Figure 3.3. ^{1}H 2D-DOSY NMR spectrum of **COP-5** in $CDCl_3$. Diffusion cross-peaks for the solvent (7.27 ppm) are also present.

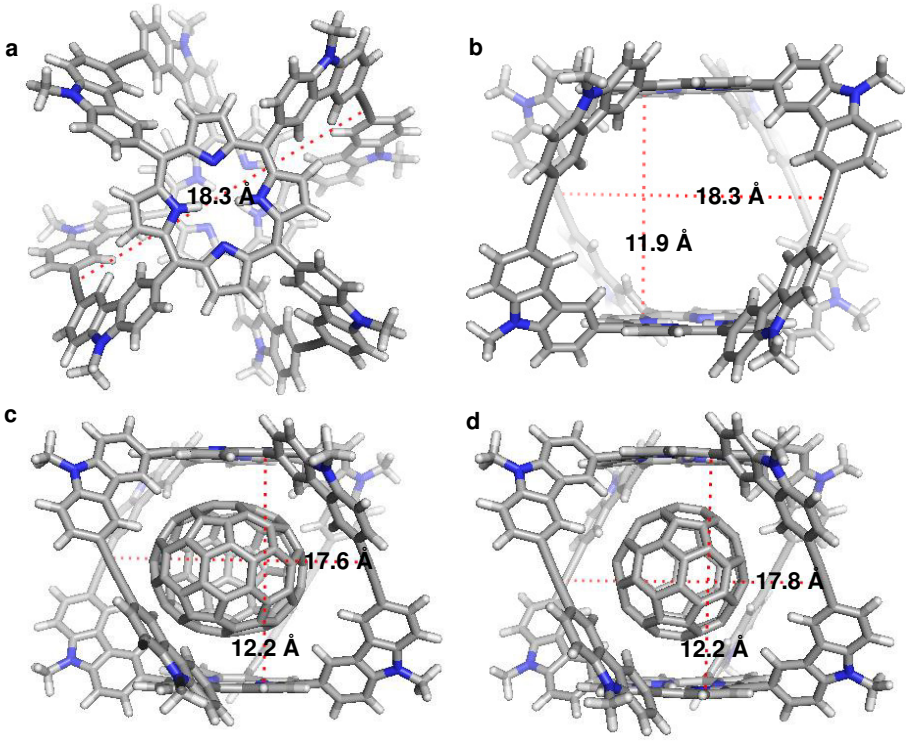

Figure 3.4. Energy-minimized structures of **COP-5** (a, top view; b, side view), C_{70}@**COP-5** (c), and C_{60}@**COP-5** (d). Methyl groups were used in the calculation instead of hexadecyl chains for simplicity. The height of **COP-5** was defined as the distance between the top and bottom porphyrin panels, and the diameter of the inside cavity of **COP-5** was defined as the distance between the two ethynylene groups in the diagonal edges.

One of our major motivations for constructing such rigid, porphyrin-containing molecular cages is to develop a novel class of organic fullerene receptors that could bind strongly and also selectively with a certain type of fullerene. Although covalent macrocycles[45,46] or supramolecular cages[47] containing porphyrin moieties have been reported to exhibit strong binding interactions with fullerenes, covalently bonded organic cages have rarely been reported as fullerene receptors. Porphyrin-fullerene binding is mainly driven by the electronic effect, i.e., the favored donor-acceptor interaction. With two porphyrin free base moieties as the top and bottom panels, the cage **COP-5** is expected to strongly bind fullerenes. The computational modeling study (Fig. 3.4)

reveals that **COP-5** has a cavity with a height (defined as the distance between the top and bottom porphyrin panels) of 11.9 Å, and a diameter of 18.3 Å (defined as the distance between the two ethynylene groups in the diagonal edges), in which a fullerene can be nicely accommodated.

The cage **COP-5** indeed showed a strong binding interaction with fullerenes. The binding of **COP-5** with C_{60}, C_{70} and C_{84} was characterized by UV-vis titration experiments in toluene (Figure 3.5 a-c). With a gradual addition of C_{70} to the cage solution (in toluene), the intensity of the absorption peak of **COP-5** at 428 nm decreases while a new signal at 437 nm arises. The cage-C_{70} complex (C_{70}@**COP-5**) formation is clearly signaled by the substantial intensity decrease (~55 %, with 1 equiv. of C_{70} added) at 428 nm and the red shift (9 nm) of the porphyrin Soret band compared to **COP-5** itself. The similar trend in the UV-vis titration curve was also observed when the solution of **COP-5** in toluene was titrated with C_{60} and C_{84}. According to the Job plot, both C_{60}, C_{70} and C_{84} formed a 1:1 host-guest complex with **COP-5** (Figure 3.6.). Consistent with this observation, when 0.25 equiv. C_{70} was added to the cage solution in toluene, the C_{70}@**COP-5** was formed instantaneously, and the ^{1}H NMR spectra (Fig. 3.5d) showed two sets of signals corresponding to the free **COP-5** and C_{70}@**COP-5** complex with the integration ratio of 3:1, further supporting the 1:1 binding mode between **COP-5** and C_{70}. MALDI-TOF spectra (Figure 3.7) of cage-fullerene complexes clearly showed peaks with mass-to-charge ratio of 4544.20 and 4664.74 corresponding to 1:1 host-guest complex, C_{60}@**COP-5** and C_{70}@**COP-5**, without any other complexes observed.

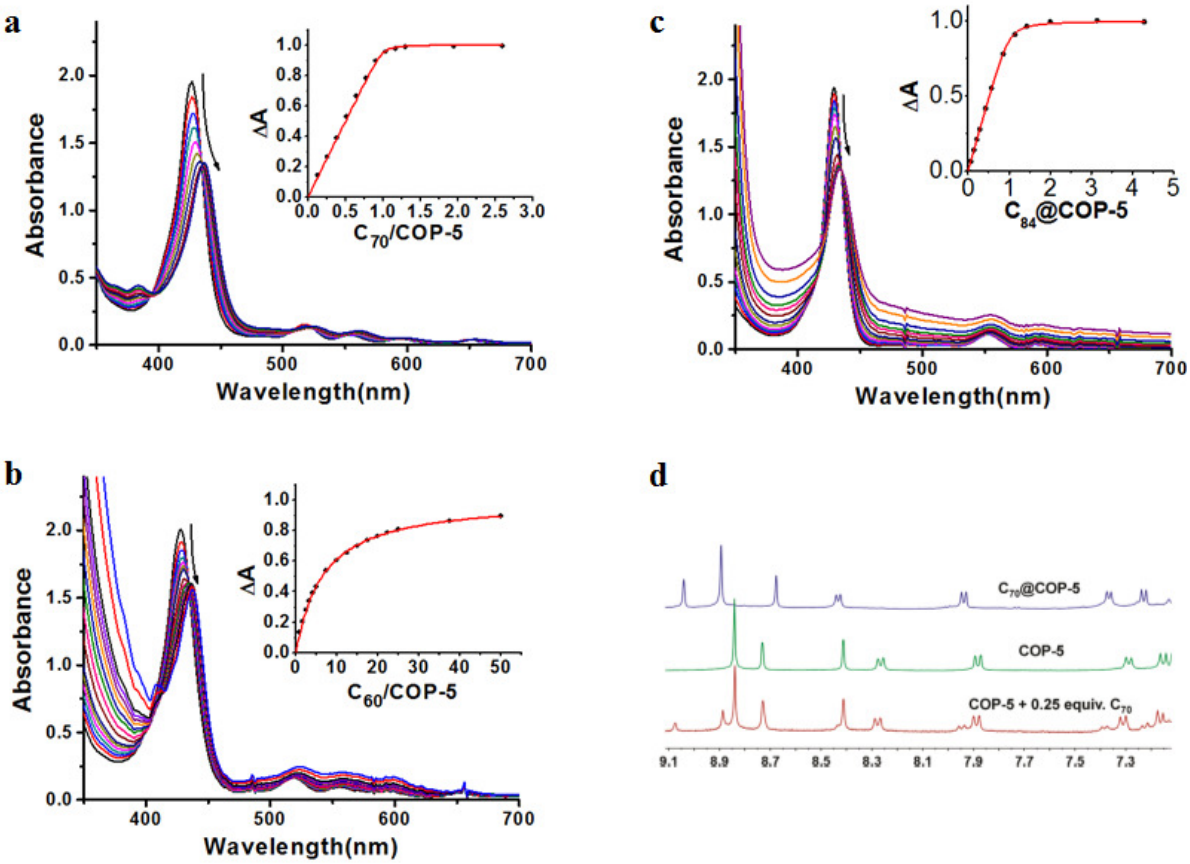

Figure 3.5. COP-5-fullerene (C_{70} and C_{60}) binding studies. (a) UV-vis absorption spectra of **COP-5** (2.0 μM) in toluene in the presence of various amounts of C_{70} (0 to 3 equiv.) at 23°C, while the concentration of **COP-5** was maintained constant. Inset: plot of ΔA_{428} nm vs equivalents of C_{70} added. (b) UV-vis absorption spectra of **COP-5** (2.0 μM) in toluene in the presence of various amounts of C_{60} (0 to 50 equiv.) at 23°C, while maintaining the concentration of **COP-5** constant. Inset: plot of ΔA_{428} nm vs equivalents of C_{60} added. (c) UV-vis absorption spectra of **COP-5** (2.0 μM) in toluene in the presence of various amounts of C_{84} (0 to 5 equiv.) at 23°C, while maintaining the concentration of **COP-5** constant. Inset: plot of ΔA_{428} nm vs equivalents of C_{84} added. The association constants modeled with a 1:1 equilibrium are $K_{C84@\textbf{COP-5}} = 2.4\times10^{7}$ M^{-1} (ΔG= -10.0 kcal/mol), $K_{C70@\textbf{COP-5}} = 1.5\times10^{8}$ M^{-1} (ΔG= -11.2 kcal/mol) for C_{70}@**COP-5** and $K_{C60@\textbf{COP-5}} = 1.4\times10^{5}$ M^{-1} (ΔG = -7.0 kcal/mol) for C_{60}@**COP-5**. (c) ^{1}H NMR spectra of C_{70}@**COP-5** (blue), **COP-5** (green), and a mixture of **COP-5** with 0.25 equiv. of C_{70} (red) in toluene-d_8.

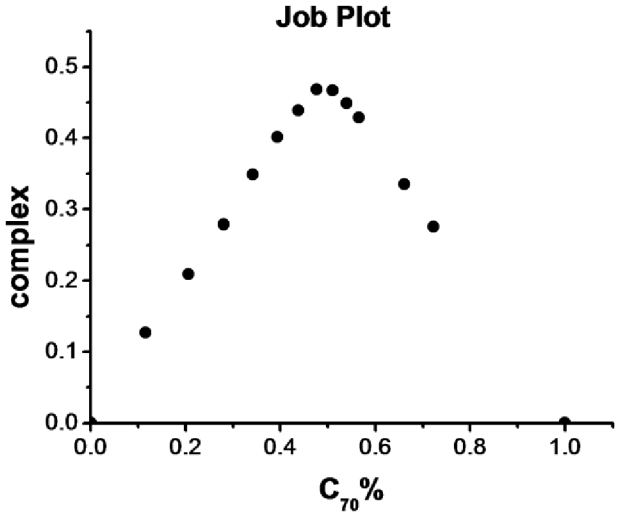

Figure 3.6. The Job plot of the **COP-5** and C_{70} binding (the absorption data at 428 nm was used for the plotting). The maximal amount of the cage-fullerene complex was found at the 50% of C_{70}, which indicates a 1:1 binding mode.

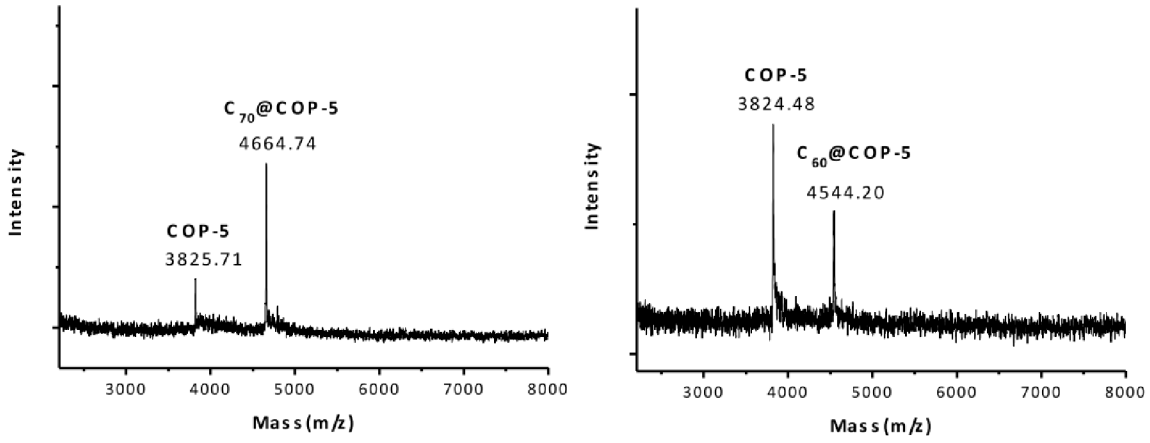

Figure 3.7. The MALDI-MS spectra of the C_{70}@**COP-5** (left) and C_{60}@**COP-5** (right). The peak for cage **COP-5** itself was observed presumably due to pre-mixing the complex solution with the matrix solution of sinapic acid, which could result in the cage-fullerene decomplexation.

Additional evidence in support of the fullerene encapsulation inside the cage comes from the analysis of ^{1}H NMR spectra of the cage-fullerene complexes. The chemical shifts of the protons at the 4,5-positions on the carbazole corner pieces, which are pointing to the inside cavity of the

cage, moved significantly downfield in both C_{60}@**COP-5** and C_{70}@**COP-5** while the other protons of the carbazole are not much affected (Fig. 3.8); such an observation indicates the fullerenes are located inside the cage. On the other hand, the internal N-H protons of the porphyrins at -1.97 ppm shifted significantly upfield by the influence of the fullerene ring current in C_{70}@**COP-5** (Fig. 3.8), which indicates a strong π-π interaction between C_{70} and the porphyrin panels of **COP-5**. The simplicity of the NMR signals of the C_{70}@**COP-5** and C_{60}@**COP-5** suggests a highly symmetrical structure for the complexes, further supporting the notion of fullerene binding inside the cage.

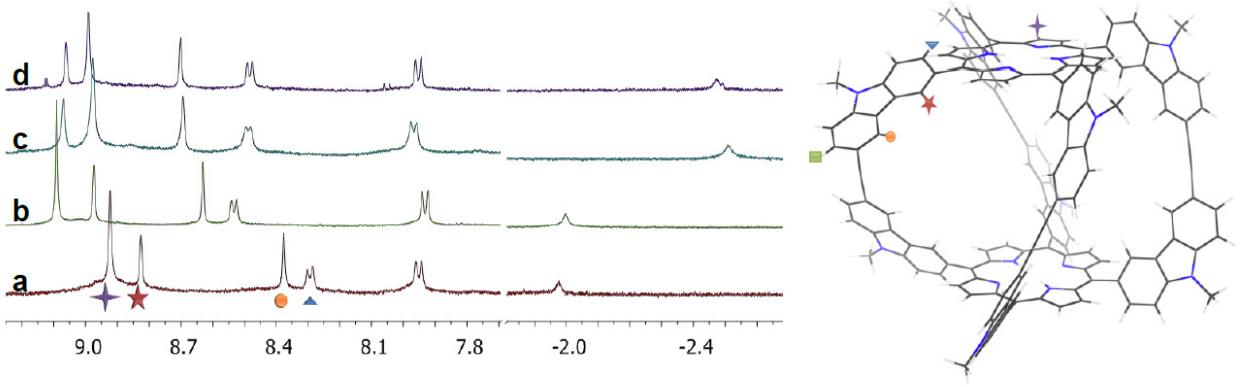

Figure 3.8. ^{1}H NMR spectra of **COP-5** and **COP-5**-fullerene complexes in C_6D_6: a) **COP-5**; b) C_{60}@**COP-5**; c) C_{70}@**COP-5**; d) a mixture of **COP-5** with 10.0 equiv. of C_{60} and 1.0 equiv. of C_{70}. C_{60}@**COP-5** and C_{70}@**COP-5** were prepared using 2 equiv. C_{60} and 2 equiv. C_{70} respectively.

On the basis of the 1:1 binding mode and fitting of the UV-vis adsorption changes at 428 nm under different fullerene concentrations, the association constants of C_{60}, C_{70} and C_{84} with **COP-5** were estimated to be 1.4×10^5 M^{-1} (C_{60}), 1.5×10^8 M^{-1} (C_{70}) and 2.4×10^7 M^{-1} (C_{84}) in toluene, which are comparable to those best-performing fullerene receptors reported thus far. It has been a great challenge to obtain host molecules that bind fullerenes with association constants higher than 10^5 M^{-1}. To the best of our knowledge, the highest fullerene binding affinity was observed in a

Ir(III) metalloporphyrin derivative reported by the Aida group, which showed $K_{assoc} = 1.3\times10^8$ M^{-1} in 1,2-dichlorobenzene and $K_{assoc} > 10^9$ M^{-1} in benzene for C_{60}.[48] The Anderson group also reported a cyclic porphyrin trimer with an impressive high affinity for fullerenes with $K_{assoc} = 2\times10^6$ for C_{60} and $K_{assoc} = 2\times10^8$ for C_{70} in toluene.[49] However, it should be noted that the previously reported best performers are all metalloporphyrins and release of the fullerene guest and regeneration of the valuable host would be difficult, thus making fullerene separation/purification based on these host molecules impractical.

It is noteworthy that the cage **COP-5**, containing nonmetalated porphyrin moieties, shows a high binding affinity with C_{70}, which is three orders of magnitude higher than that with C_{60}. Such a remarkable selectivity in the binding of C_{70} over C_{60} is unprecedented and is significantly higher than those of previously reported fullerene receptors, which are usually lower than 10, with highest being around 100, reported by the Anderson group.[49] And for the binding of C_{84} with **COP-5**, even though not as strong as for C_{70}, it is still much stronger than the binding of C_{60} (>100 selectivity). In order to further explore the potential of **COP-5** in fullerene separation, we used a mixture of two fullerene guests in a binding competition test. As expected, selective complexation of **COP-5** with C_{70} in a C_{60}-enriched fullerene mixture was observed. When **COP-5** was mixed with a solution of C_{60} (91 mol %) and C_{70} (9 mol %) in toluene, the **COP-5** selectively bound with C_{70} to form C_{70}@**COP-5**. The ^{1}H NMR spectrum clearly shows the major set of proton signals corresponding to C_{70}@**COP-5** (Fig. 3.5d).

Computational calculations on the energy-minimized structures of **COP-5** and **COP-5**-fullerene complexes provide further insight into the preferential binding of C_{70} versus C_{60}. The Amber 11.0 molecular dynamics program package[50] was used to optimize the structure of the fullerene, the cage, and the cage-fullerene binding complexes. The general Amber force field

(GAFF field)[51] was used with the charge parameters computed by the AM1-BCC method. The computational modeling study (Fig. 3.4) reveals that the heights of **COP-5** are slightly increased to 12.1 - 12.2 Å in C_{60}@**COP-5** and C_{70}@**COP-5** from the initial 11.9 Å in the unoccupied **COP-5**, while the diameters of the cavities are decreased slightly to 17.6 - 17.8 Å from 18.3 Å. Owing to the high degree of shape persistency of the cage **COP-5**, the size and geometry of the cage do not change much upon fullerene encapsulation. In both C_{60}@**COP-5** and C_{70}@**COP-5** complexes, the shortest atom-to-atom distances between porphyrin panels and fullerenes are similar and are close to 3.2 Å, which leads to an appreciable π-π interaction in both complexes. It is known that fullerenes also have CH-π interactions with host molecules, and the favored distance for CH-π interactions is around 2.9 Å.[52,53] This type of CH-π interactions also exists in fullerene-**COP-5** complexes. The average distances between fullerenes and those carbazole CH protons, which are pointing toward the inside cavity of the cage, in C_{60}@**COP-5** and C_{70}@**COP-5** are around 3.5 and 3.1 Å, respectively. Since the distance for CH-π interactions in C_{70}@**COP-5** (3.1 Å) is closer to the known favored distance 2.9 Å, the CH-π interactions are presumably stronger in C_{70}@**COP-5** compared to those in C_{60}@**COP-5**. Considering the rigid, noncollapsible nature of the cage **COP-5**, it would be difficult for the cage to adjust the distance between the top and bottom porphyrin panels to achieve stronger binding interactions with fullerene guests. The non-perfect match between the sizes of host and guest would result in a less favored binding interaction of **COP-5** with C_{60}. Given the conformational rigidity, the slight difference in the distance between the host and guest could lead to a large difference in their stabilization energy (4.2 kcal/mol, calculated from the binding constants of C_{70}@**COP-5** and C_{60}@**COP-5**) gained through the host-guest binding interaction and could be the origin of the remarkable binding selectivity. For C_{84}, the size of the fullerene increased slightly comparing with C_{70}. With the computer modeling of the

C_{84}@**COP-5**, the distance between porphyrin panels and fullerenes is 3.0 Å, which is much shorter than favored π-π stacking distance (3.6 Å), which result in the lower binding constant compared with that of C_{70}. The average distances between fullerenes and those carbazole CH protons are 2.9 Å, which is still a favored distance. And it fits well enough to generate such high binding affinity (2.4×10^7 M).

Intrigued by the impressive differentiating capability of cage **COP-5** in binding C_{60} and C_{70}, and to achieve a clean and efficient separation of C_{70} from fullerene mixtures, we then directed our efforts to the investigation of controlled release of fullerene guests and regeneration of host cage molecules. Since porphyrin-fullerene interactions are based on the attraction between electron-rich (porphyrin) and electron-poor (fullerene) moieties, their interactions could be tuned by changing the electronic properties of either one of them. Unlike the case for metalloporphyrins, the electron density of the porphyrin free base can be easily reduced by simple protonation, and thus the porphyrin-fullerene interactions could be weakened. We envisioned dissociation and release of the guest molecules, and regeneration of the **COP-5** can be realized by simply tuning the pH of the media. Trifluoroacetic acid (TFA) and triethylamine (TEA) were used as the acid and base stimuli. Upon addition of excess TFA (100 equiv.) to a solution of C_{70}@**COP-5** (or C_{60}@**COP-5**) in toluene, protonation of the porphyrin ring occurred, and consequently, complete release of the fullerene molecules was observed, as evidenced by the disappearance of the ^{1}H NMR signals corresponding to C_{70}@**COP-5** (or C_{60}@**COP-5**) and the appearance of a new set of signals corresponding to the protonated **COP-5** with an empty cavity. However, the subsequent addition of 100 equiv. of triethylamine (TEA) to the above mixture neutralized the porphyrin ring and restored the binding interaction between **COP-5** and fullerenes. As a result, the ^{1}H NMR spectrum of C_{70}@**COP-5** (or C_{60}@**COP-5**) was regenerated, indicating the reversibility of the

association/dissociation process. Such a reversible association/dissociation triggered by acid/base stimuli was also confirmed by monitoring the process with UV-vis absorption spectra (Fig. 3.9). In brief, we observed almost the identical UV-vis absorption spectra when we protonated **COP-5** and C_{70}@**COP-5** (or C_{60}@**COP-5**) with 100 equiv. of TFA, which indicates the complete dissociation of the cage-fullerene complex upon protonation of the porphyrin-free base center. The regeneration of C_{70}@**COP-5** (or C_{60}@**COP-5**) complex by the addition of 100 equiv. of TEA to the mixture of protonated **COP-5** and free C_{70} was evidenced by a UV-vis absorption almost identical with that of the pure C_{70}@**COP-5** (or C_{60}@**COP-5**). The association-dissociation process can be repeated in several cycles without leading to any noticeable change in the absorbance by the alternating addition of TFA and TEA (Fig. 3.9, inset), thus showing that the cage-C_{70} binding is a highly efficient, robust, and fully reversible process.

Fullerene purification has attracted great attention since the 1990s, and people are still actively pursuing a highly efficient and easy process for fullerene separations.[49,54-57] One of the most common methods aiming at the separation of fullerenes of specific size is based on selective complexation of a particular fullerene from an organic solution of fullerene mixtures. However, the difficult release of fullerenes and regeneration of hosts have greatly impeded the practical applications of this method.[57] Given the over 1000 times stronger binding interactions of **COP-5** with C_{70} over C_{60}, and the reversible nature of this host-guest binding triggered by pH, we envisioned that the separation of C_{70} from C_{60} can be achieved with a simple "selective complexation-decomplexation" process (Fig. 3.10). As a proof of concept, we used a C_{60}- enriched C_{60}/C_{70} mixture in the separation study. Carbon disulfide was chosen as the solvent for the encapsulation step, since both C_{60} and C_{70} have good solubility in CS_2. A mixture of **COP-5**

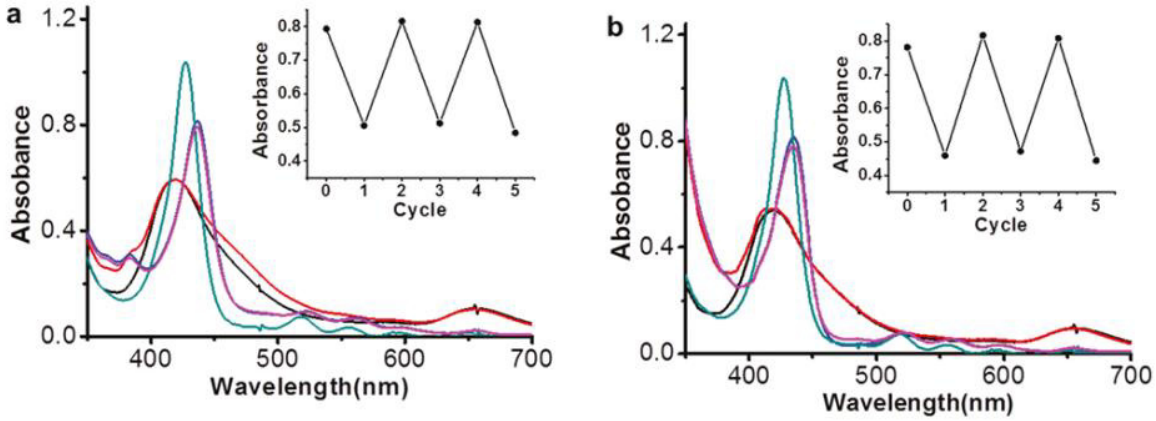

Figure 3.9. pH-Driven reversible **COP-5**-fullerene binding. **COP-5** concentration was 1.0×10^{-6} M in toluene. (a) UV-vis spectra of the free **COP-5** (cyan), of C_{70}@**COP-5** (magenta), after the addition of 100 equiv. of TFA to **COP-5** (black), after the addition of 100 equiv. of TFA to C_{70}@**COP-5** (red), and after the addition of 100 equiv. of TFA, followed by the subsequent addition of 100 equiv. of TEA to C_{70}@**COP-5** (blue). Inset: plot of absorption at 437 nm vs repetitive association-dissociation cycles. (b) UV-vis spectra of the free **COP-5** (cyan), of C_{60}@**COP-5** (magenta), after the addition of 100 equiv. of TFA to **COP-5** (black), after the addition of 100 equiv. of TFA to C_{60}@**COP-5** (red), and after the addition of 100 equiv. of TFA followed by the subsequent addition of 100 equiv. of TEA to C_{60}@**COP-5** (blue). Inset: plot of absorption at 436 nm vs repetitive association-dissociation cycles.

and C_{60}/C_{70}in CS_2 was sonicated for 30 s, and the solvent was evaporated. The residue was then dispersed in chloroform. Since fullerenes have very limited solubility in $CHCl_3$, free fullerenes remained as precipitates. The solution phase, which was composed of mostly C_{70}@**COP-5**, was separated from the insoluble fullerene mixtures by centrifugation. Further acidifying the C_{70}@**COP-5** complex with excess TFA followed by sonication (5 min) released C_{70} as a black precipitate, which allowed easy removal by centrifugation. The cage **COP-5** was then regenerated by neutralization with TEA and was recycled for the next round of fullerene separation. (Fig. 3.10) The UV-vis absorption showed that the C_{70} abundance of the fullerene mixture increased significantly (~9-fold increase) from the initial 9mol% to 79 mol% after only one cycle of

separation (Fig. 3.11). This result clearly demonstrates the simplicity and high efficiency of such a fullerene separation approach by using shape-persistent molecular cages as selective receptors. The "selective complexation-decomplexation" strategy presented here would greatly facilitate the purification of these intriguing graphitic materials and promote their wide application in organic photovoltaics, polymer electronics, and biopharmaceuticals.

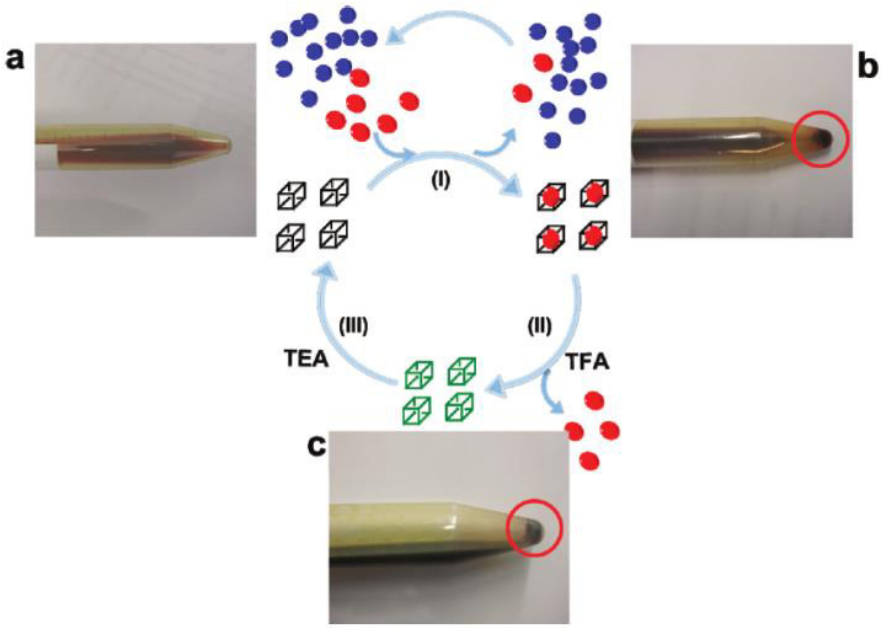

Figure 3.10. Schematic presentation of the C_{70} isolation process. Step I: to a solution of C_{60} and C_{70} mixture (C_{60}/C_{70} = 10/1, molar ratio) in CS_2 was added a small amount of **COP-5** (equal to or less than the stoichiometric amount of C_{70}), resulting in the favored formation of C_{70}@**COP-5**. After the unbound free fullerenes were separated by precipitation in $CHCl_3$ (precipitates shown in (b)), cage-fullerene complexes (mostly C_{70}@**COP-5**) were collected in the solution phase. Step II: upon the addition of 100 equiv. of TFA to the solution collected in step II, fullerene guest molecules (mostly C_{70}) were released as black precipitates and removed to complete one cycle of the isolation process (shown in (c)). Step III: regeneration of **COP-5** was accomplished by the addition of 100 equiv. of TEA to the above solution.

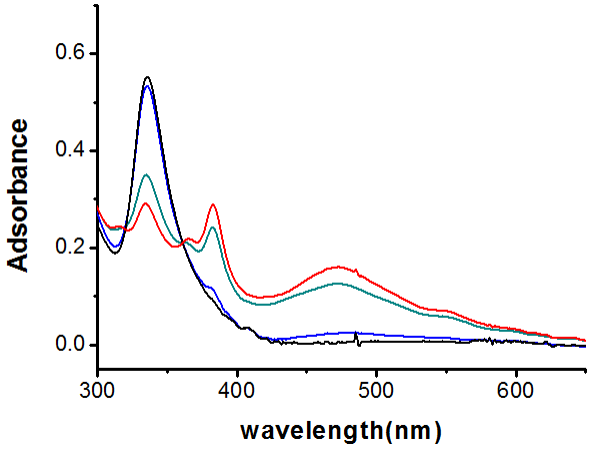

Figure 3.11. The UV-vis spectra of C_{60} (black), C_{70} (red), mixture of C_{60} and C_{70} in 10 :1 molar ratio (blue), fullerene mixtures after single extraction cycle (green). The solutions of C_{60} (black), C_{70} (red) are both in toluene with the concentrations of 8×10^{-6} M.

In summary, we have successfully synthesized a shape-persistent porphyrin-based molecular cage **COP-5** via highly efficient alkyne metathesis, which represents the first time of using such a reversible dynamic covalent approach to construct 3-D molecular cages. Such a DC_vC approach complements the existing dynamic assembly strategies for construction of large complex, molecular architectures, and would be particularly beneficial for the synthesis and study of non-collapsible, shape-persistent covalent cage molecules. The obtained cage **COP-5** shows an unprecedented high selectivity (>1000/1) in binding of C_{70} over C_{60}. The pH-driven reversible association and dissociation of fullerene-cage complexes enables an easy and efficient separation of C_{70} from a fullerene mixture. Currently the binding behavior of such porphyrin-based molecular cages with higher fullerenes and further assembly these cage-fullerene complexes into highly ordered 3-D architectures are being investigated.

3.4 Experimental section

3.4.1 Materials and general synthetic methods

Reagents and solvents were purchased from commercial suppliers and used without further purification, unless otherwise indicated. Tetrahydrofuran (THF), toluene, dichloromethane, and dimethylformamide (DMF) were purified by the MBRAUN solvent purification systems.

All reactions were conducted under dry nitrogen in oven-dried glassware, unless otherwise specified. Solvents were evaporated using a rotary evaporator after workup. Unless otherwise specified, the purity of the compounds was ≥ 95 % based on ^{1}H NMR spectral integration.

Flash column chromatography was performed by using a 100-150 times weight excess of flash silica gel 32-63 µm from Dynamic Absorbants Inc. Fractions were analyzed by TLC using TLC silica gel F254 250 µm precoated-plates from Dynamic Absorbants Inc. Analytical gel permeation chromatography (GPC) was performed using a Viscotek GPCmaxTM, a Viscotek Model 3580 Differential Refractive Index (RI) Detector, a Viscotek Model 3210 UV/VIS Detector and a set of two Viscotek Viscogel columns (7.8 × 30 cm, l- MBLMW-3078, and l- MBMMW-3078 columns) with THF as the eluent at 30 °C. The analytical GPC was calibrated using monodisperse polystyrene standards.

UV-vis absorption measurements were carried out with Agilent 8453 spectrophotometer and the emission measurements were obtained on a F-2500 Hitachi fluorescence spectrophotometer.

MALDI MS spectra were obtained on the Voyager-DE™ STR Biospectrometry Workstation using sinapic acid as the matrix. The high resolution Mass spectra were obtained on Waters SYNAPT G2 High Definition Mass Spectrometry System. Analyte molecules were diluted

into ESI solvents, either methanol or acetonitrile/water mixture, for final concentrations of 10 ppm orlower. The solution was injected into the electrospray ionization (ESI) source at a rate of 5 μL/min. Either the ESI^+ or ESI^- mode was used in reference to the molecular properties. Accurate mass analysis was performed by using the Lock Mass calibration feature with the instrument.

NMR spectra were taken using Inova 400 and Inova 500 spectrometers. $CHCl_3$ (7.27 ppm), benzene-d_6 (7.15 ppm) and toluene-d_8 (2.09 ppm) were used as internal references in ^1H NMR, and $CHCl_3$ (77.23 ppm) for ^{13}C NMR. ^1H NMR data were reported in order: chemical shift, multiplicity (s, singlet; d, doublet; t, triplet; q, quartet; m, multiplet), coupling constants (J, Hz), number of protons.

The Amber 11.0 molecular dynamics program package was used to optimize the structure of the fullerene, the cage and the cage/fullerene binding complexes. The force field used was the general Amber force field (GAFF field) with the charge parameters computed by AM1-BCC method. For each structure optimization run, the molecule was first minimized for 1000 steps using the conjugate gradient method, and then it was further optimized by simulated annealing method for 150 picosecond with a time-step of 1 femtosecond. During the simulated annealing, the system temperature was first raised up to 1000 K for 50 picosecond and then gradually cooled to 0 K for another 100 picosecond. Finally, the annealed structure was minimized again for another 1000 conjugate gradient steps and the final energy was recorded. The non-bonded interactions during the simulation were computed directly with a cutoff distance of 25 Å. A dielectric constant of 4.8 was assumed during the simulation, which is a typical value for organic solvents. By comparing the energies of the fullerene, the cage, and the binding complexes, the binding energy can be computed.

3.4.2 Synthetic procedures

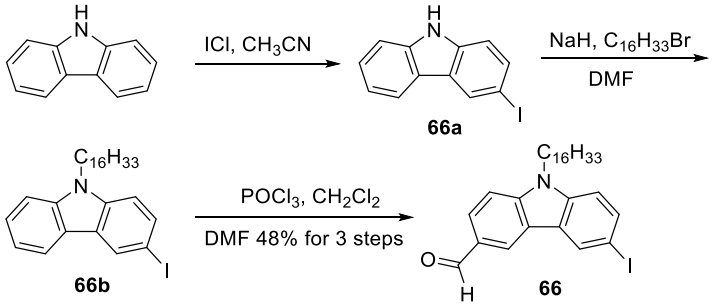

3-Formyl-N-hexadecyl-6-iodo-carbazole (66): To a solution of carbazole (5.00 g, 30.0 mmol) in CH_3CN (250 mL) was slowly added ICl (1.88 mL, 36 mmol) at 0 °C. The mixture was stirred at 0 °C for 2 h, then slowly warmed up to room temperature and was stirred for another 2 h. The reaction was quenched with saturated aqueous Na_2SO_3 solution. The product was extracted with CH_2Cl_2 (80 mL×3). The organic extracts were combined and the volatiles were removed. The crude product of 3-iodocarbazole (**66a**) was collected as a white solid. (~60 % yield was determined by crude ^1H NMR spectra analysis.) Without further purification, the crude 3-iodocarbazole (**66a**) was dissolved in DMF (100 mL). NaH (1.80 g, 45 mmol, 60% dispersion in mineral oil) was added to the above solution and stirred for 5 mins at room temperature. Then 1-bromohexadecane (13.74 g, 45 mmol) was added. After stirring for 4 h at room temperature, the solvent was removed. 1 M HCl (100 mL) was added to the residue, and the mixture was extracted with CH_2Cl_2 (3 x 100 mL). The combined organic extracts were washed with water (100 mL), and brine (100 mL), dried over anhydrous Na_2SO_4, and concentrated to give the crude product. Purification by flash column chromatography (CH_2Cl_2/hexane, 1/3, v/v) gave the product (**66b**) together with N-hexadecyl-3,6-diiodo-carbazole. To a mixture of DMF (47 mL, 600 mmol) and 1,2-dichloroethane (50 mL) was added $POCl_3$ (47.5 mL, 510 mmol) dropwise at 0 °C. The mixture was warmed up to 35 °C and N-hexadecyl-3-iodo-carbazole (**66b**) was added. After heating at 90 °C for 24 h, the mixture was cooled to ambient temperature and poured into water (500 mL). The product was extracted with

chloroform (150 mL × 3). The combined organic extracts were washed with water (200 mL) and brine (200 mL), dried over anhydrous $MgSO_4$ and concentrated. The residue was purified via flash column chromatography (CH_2Cl_2/hexane, 1/1 v/v) to provide pure product **66** as a white solid (7.85 g, 48 % in three steps): ^{1}H NMR (500 MHz, $CDCl_3$): δ 10.08 (s, 1H), 8.51 (d, *J* =1.5 Hz, 1H), 8.44 (d, *J* = 1.5 Hz, 1H), 8.03 (dd, J 1 = 8.5 Hz, J 2 = 1.5 Hz, 1H), 7.77 (dd, J 1= 8.5 Hz, J_2 = 1.5 Hz, 1H), 7.46 (d, *J* = 8.5 Hz, 1H), 7.22 (d, *J* = 8.5Hz, 1H), 4.29 (t, *J* = 7.0 Hz, 2H), 1.85 (m, 2H), 1.39-1.21 (m, 26H), 0.89 (t, *J* = 7.0 Hz, 3H); ^{13}C NMR (100 MHz, $CDCl_3$): δ 191.71, 144.02, 140.47, 135.10, 129.76, 129.06, 127.59, 125.53, 124.55, 121.87, 111.57, 109.40, 83.09, 43.71, 32.13, 29.90, 29.89, 29.87, 29.83, 29.78, 29.73, 29.64, 29.57, 29.51, 29.06, 27.39, 22.91, 14.35; HRMS (m/z): $[M+H]^+$ calcd. for $C_{29}H_{40}INO$, 546.2233; found, 546.2227.

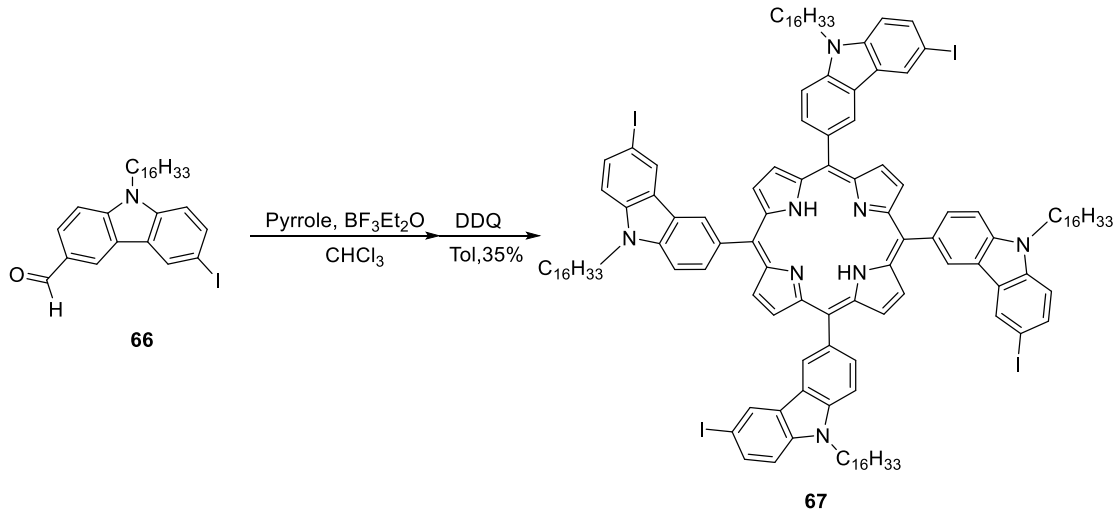

Compound 67: To a solution of compound **66** (2.18 g, 4.0 mmol) and pyrrole (0.28 mL, 4.0 mmol) in chloroform (200 mL) was added $BF_3 \cdot Et_2O$ (0.16 mL) dropwise at r.t.. The reaction mixture was stirred for 1 hour at rt. A solution of 2,3-dichloro-5,6-dicyanobenzoquinone (0.68 g, 3.0 mmol) in toluene (10 mL) was added slowly. After stirring 1 hour at r.t., the reaction mixture was filtered

through a silica gel pad. The volatiles were removed and the residue was purified by flash column chromatography (CH_2Cl_2/hexane, 1/1 v/v) to provide the product **67** as a purple solid (0.826 g, 35 %): ^{1}H NMR (500 MHz, $CDCl_3$): δ 8.95 (s, 4H), 8.91 (s, 8H), 8.54 (s, 4H), 8.41 (m, 4H), 7.81 (d, *J* = 8.8 Hz, 4H), 7.73 (m, 4H), 7.34 (d, *J* = 8.5 Hz, 4H), 4.47 (t, *J* = 7.0 Hz, 8H), 2.07 (m, 8H), 1.53 (m, 8H), 1.45 (m, 8H), 1.39-1.23 (m, 88H), 0.90 (t, *J* = 7.5 Hz, 12H), -2.41 (s, 2H); ^{13}C NMR (100 MHz, $CDCl_3$): δ 140.61, 140.18, 134.33, 133.74, 133.63, 133.55, 131.50, 129.75, 126.96, 125.66, 120.90, 120.53, 111.20, 107.01, 81.72, 43.78, 32.13, 29.92, 29.87, 29.81, 29.70, 29.58, 29.36, 27.66, 22.91, 14.37; MALDI-TOF (m/z): $[M+H]^+$ calcd. for $C_{132}H_{166}I_4N_8$, 2372.95; found: 2372.84.

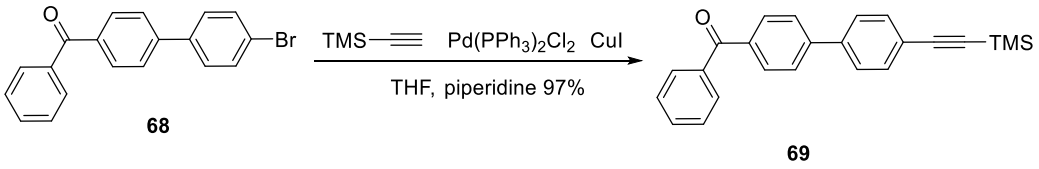

68 **69**

Compound 69: The general Sonogashira's procedure was followed. Using 4-benzoyl-4'-bromo-biphenyl (3.37 g, 10.0 mmol), trimethylsilylacetylene (1.47 g, 15.0 mmol), $Pd(PPh_3)_2Cl_2$ (0.210 g, 0.3 mmol), CuI (0.045 g, 0.25 mmol), piperidine (30 mL), and THF (30 mL), the product was obtained as a yellowish solid (3.45 g, 97 %): ^{1}H NMR (500 MHz, $CDCl_3$): δ 7.89 (d, *J* =7.6Hz, 2H), 7.83 (d, *J* =7.2Hz, 2H), 7.69 (d, *J* =7.6Hz, 2H), 7.59 (m, 5H), 7.50 (m, 2H), 0.29(s, 9H); ^{13}C NMR (100 MHz, $CDCl_3$) ; δ 196.3, 144.3, 139.9, 137.8, 136.6, 132.7, 132.6, 130.9, 130.1, 128.5, 127.2, 126.7, 123.2, 104.8, 95.8, 0.2; HRMS (m/z): $[M+H]^+$ calcd. for $C_{24}H_{22}OSi$, 355.1518; found, 355.1518.

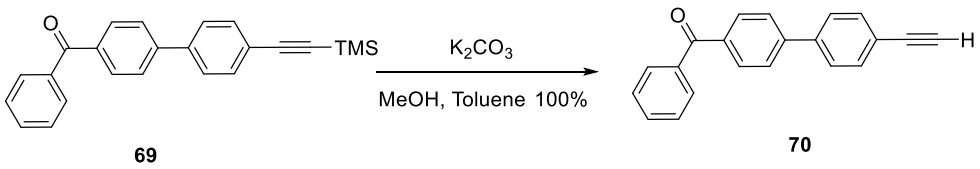

Compound 70: To a solution of **69** (3.45 g, 9.7 mmol) in MeOH (50 mL) and toluene (50 mL) was added K_2CO_3 (2.68 g, 19.4 mmol). The mixture was stirred at room temperature for 1 h. The solvents were removed and the residue was dissolved in CH_2Cl_2 (100 mL). The organic solution was washed with saturated NH_4Cl (50 mL), and brine (50 mL), dried over Na_2SO_4, and concentrated. Purification by flash column chromatography (CH_2Cl_2/hexane, 1/1, v/v) provided the product as a yellow solid (2.74 g, 100%): ^{1}H NMR (500 MHz, $CDCl_3$): δ 7.91 (d, *J* = 6.5 Hz, 2H), 7.85 (d, *J* = 8.0 Hz, 2H), 7.71 (d, *J* = 6.5 Hz, 2H), 7.61 (m, 5H), 7.52 (m, 2H), 3.18(s, 1H); ^{13}C NMR (100 MHz, $CDCl_3$): δ 196.3, 144.2, 140.3, 137.7, 136.7, 132.8, 132.6, 130.9, 130.1, 128.5, 127.3, 127.0, 122.1, 83.4, 78.6; HRMS (m/z): $[M+H]^+$ calcd. for $C_{21}H_{14}O$, 283.1123; found, 283.1125.

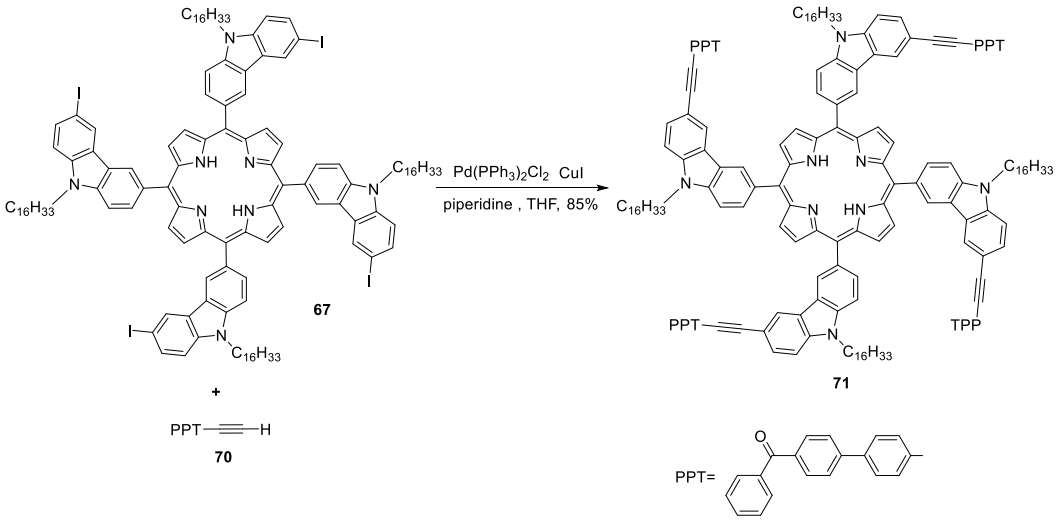

Compound 71: The general Sonogashira's procedure was followed. Compound **67** (500mg, 0.21 mmol) was converted to monomer **71** using acetylene **70** (593 mg, 2.1 mmol), $Pd(PPh_3)_2Cl_2$ (23.6 mg, 0.034 mmol), CuI (4.2 mg, 0.022 mmol), piperidine (10 mL), and THF (50 mL). The product **71** was obtained as a purple solid (536 mg, 85 %): ^{1}H NMR (500 MHz, $CDCl_3$): δ 9.01 (m, 4H), 8.94 (d, *J* = 3.6 Hz, 8H), 8.46 (m, 8H), 7.90-7.45 (m, 64H), 4.56 (t, *J* = 7.0 Hz, 8H), 2.11 (m, 8H), 1.59 (m, 8H), 1.48 (m, 8H), 1.41-1.22 (m, 88H), 0.86 (t, *J* = 7.5 Hz, 12H), -2.39 (s, 2H); ^{13}C NMR (100 MHz, $CDCl_3$, 59ºC*): δ 196.12, 144.58, 141.44, 140.86, 139.27, 138.16, 136.78, 134.11, 133.51, 132.44, 132.21, 131.54, 130.85, 130.15, 130.11, 129.93, 128.48, 127.27, 127.07, 126.90, 124.76, 124.32, 123.50, 121.67, 121.05, 114.01, 109.30, 107.16, 92.61, 87.82, 44.00, 32.12, 29.90, 29.88, 29.85, 29.71, 29.53, 29.46, 27.73, 22.86, 14.22; MALDI-TOF (m/z): $[M+H]^+$ calcd. for $C_{216}H_{218}N_8O_4$, 2990.72; found, 2991.30.

* The ^{13}C NMR at room temperature shows multiple signals for several peaks (δ = 196.12, 144.58, 138.16, 136.78, 130.85, 126.90) at r.t. ^{13}C NMR which is presumably due to the conformational inequivalence of the four 'arms' of **71**.

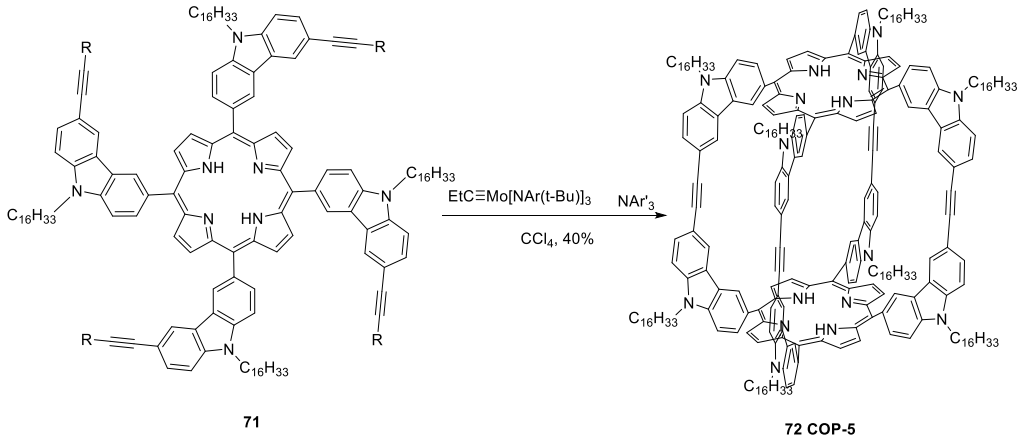

71 72 COP-5

Compound 72 (**COP-5**): The target cage compound was obtained by following the precipitation-driven alkyne metathesis procedures. The multidentate ligand (3.7 mg, 0.0078 mmol) and the

Mo(VI) carbyne precursor (5.0 mg, 0.0078 mmol) were premixed in dry carbon tetrachloride (7 mL) for 20 minutes to generate the catalyst in situ. Subsequently, the monomer **71** (150 mg, 0.050 mmol) was added and the stirring was continued for 16 h at 75 ^{o}C under microwave irradiation. Another 3 mL fresh catalyst solution was prepared as described above and added, and the reaction mixture was stirred for another 16 h at 75 ^{o}C, at which time the reaction was completed as monitored by GPC. Upon completion of the reaction, the reaction mixture was filtered to remove the byproduct and the filtrate was concentrated and subjected to flash column chromatography over alumina adsorption (CH_2Cl_2/hexane, 1/1 v/v). The pure **COP-5** was obtained as a purple solid (54 mg, 56 %): ^{1}H NMR (400 MHz, $CDCl_3$): δ 8.77 (s, 8H), 8.64 (s, 16H), 8.27 (s, 8H), 8.21 (d, *J* = 8.1 Hz, 8H), 7.74 (d, *J* = 8.6 Hz, 8H), 7.62 (d, *J* = 8.0 Hz, 8H), 7.50 (d, *J* = 8.7 Hz, 8H), 4.49 (s, 16H), 2.11 (s, 16H), 1.65-1.15 (m, 208H), 0.88 (t, 7.0Hz, 24H), -2.74 (s, 4H); ^{13}C NMR (100 MHz, $CDCl_3$): δ 140.80, 140.58, 133.59, 131.81, 130.96, 129.36, 125.71, 124.33, 123.09, 120.98, 120.61, 114.51, 109.03, 106.38, 89.19, 43.84, 32.14, 29.92, 29.88, 29.73, 29.59, 29.48, 27.75, 22.92, 14.36; MALDI-TOF (m/z): $[M+H]^+$ calcd. for $C_{272}H_{332}N_{16}$: 3825.66, Found: 3825.80.

The procedure for C_{70} purification: To a mixture of C_{70} (2.1 mg, 2.5 μmol) and C_{60} (18 mg, 25 μmol, C_{70}/C_{60}, 1/10, 9 mol % for C_{70}) in CS_2 (5 mL) was added **COP-5** (7.6 mg, 2.0 μmol). After sonication for 30 seconds, the solvent was evaporated and $CHCl_3$ (3 mL) was added. The undissolved solids were removed by centrifugation and the solution phase was treated with TFA (15 μL, 0.2 mmol). After sonication for 5 mins, dark solid precipitated, which were collected by centrifugation and washed with additional $CHCl_3$ (5 mL). The isolated fullerenes have a C_{70}/C_{60} ratio of 3.4:1 (79 mol % for C_{70}), which was determined by UV-vis absorption (Fig. 3.11). The C_{70}/C_{60} ratio in the fullerene mixtures were determined by the UV-vis absorbance at 335nm and 473nm respectively. The standard solutions of C_{60} (black), C_{70} (red) were prepared with the

concentrations of 8×10^{-6} M in toluene. The UV-vis absorption spectra were recorded for the standard C_{60} and C_{70} solutions with isosbestic point at 361 nm. The UV-vis absorption of the fullerene mixture was measured and normalized to have the same isosbestic point (361 nm) with the above standard fullerene solutions. Given the absorbance of C_{60}, and C_{70} standard solutions, the C_{70}/C_{60} ratio in the fullerene mixture can be determined from the following equation.

$$\frac{C_{70}}{C_{60}} = \frac{A_{mix} - A_{C60}}{A_{C70} - A_{mix}} \qquad \text{(Eq. 3.1)}$$

Table 3.1. The absorbance of C_{60}, C_{70} and the fullerene mixture solution at 335 nm and 473 nm.

Fullerene	A_{335nm}	A_{473nm}
C_{60}	0.55189	0.00602
C_{70}	0.29069	0.16063
Mixture after extraction	0.35043	0.12620

The ratios of C_{70}/C_{60} in the mixture after extraction that were calculated using the UV-vis absorption at 335 nm and 473 nm are 3.37 and 3.49 respectively. Therefore, the C_{70}/C_{60} ratio is estimated to be 3.4/1.

3.5 References

1. Zhang, C. X.; Wang, Q.; Long, H.; Zhang, W. *J. Am. Chem. Soc.* **2011**, *133*, 20995.

2. Meissner, R. S.; Rebek, J., Jr.; Demendoza, J. *Science* **1995**, *270*, 1485.

3. Rebek, J., Jr. *Angew. Chem. Int. Ed.* **2005**, *44*, 2068.

4. Ferrand, Y.; Crump, M. P.; Davis, A. P. *Science* **2007**, *318*, 619.

5. Bisson, A. P.; Lynch, V. M.; Monahan, M.-K. C.; Anslyn, E. V. *Angew. Chem. Int. Ed.* **1997**, *36*, 2340.

6. Thomas, J. M.; Raja, R.; Sankar, G.; Bell, R. G. *Acc. Chem. Res.* **2001**, *34*, 191.

7. Yoshizawa, M.; Tamura, M.; Fujita, M. *Science* **2006**, *312*, 251.

8. Inokuma, Y.; Kawano, M.; Fujita, M. *Nat. Chem.* **2011**, *3*, 349.

9. Koblenz, T. S.; Wassenaar, J.; Reek, J. N. H. *Chem. Soc. Rev.* **2008**, *37*, 247.

10. Tozawa, T.; Jones, J. T. A.; Swamy, S. I.; Jiang, S.; Adams, D. J.; Shakespeare, S.; Clowes, R.; Bradshaw, D.; Hasell, T.; Chong, S. Y.; Tang, C.; Thompson, S.; Parker, J.; Trewin, A.; Bacsa, J.; Slawin, A. M. Z.; Steiner, A.; Cooper, A. I. *Nat. Mater.* **2009**, *8*, 973.

11. Atwood, J. L.; Barbour, L. J.; Jerga, A. *Science* **2002**, *296*, 2367.

12. Jin, Y. H.; Voss, B. A.; Jin, A.; Long, H.; Noble, R. D.; Zhang, W. *J. Am. Chem. Soc.* **2011**, *133*, 6650.

13. Olenyuk, B.; Whiteford, J. A.; Fechtenkotter, A.; Stang, P. J. *Nature* **1999**, *398*, 796.

14. Olenyuk, B.; Whiteford, J. A.; Fechtenkotter, A.; Stang, P. J. *Nature* **1999**, *398*, 796.

15. Umemoto, K.; Yamaguchi, K.; Fujita, M. *J. Am. Chem. Soc.* **2000**, *122*, 7150.

16. Granzhan, A.; Schouwey, C.; Riis-Johannessen, T.; Scopelliti, R.; Severin, K. *J. Am. Chem. Soc.* **2011**, *133*, 7106.

17. Liu, Y.; Hu, C.; Comotti, A.; Ward, M. D. *Science* **2011**, *333*, 436.

18. MacGillivray, L. R.; Atwood, J. L. *Nature* **1997**, *389*, 469.

19. Ashton, P. R.; Isaacs, N. S.; Kohnke, F. H.; Dalcontres, G. S.; Stoddart, J. F. *Angew. Chem. Int. Ed.* **1989**, *28*, 1261.

20. Ashton, P. R.; Girreser, U.; Giuffrida, D.; Kohnke, F. H.; Mathias, J. P.; Raymo, F. M.; Slawin, A. M. Z.; Stoddart, J. F.; Williams, D. J. *J. Am. Chem. Soc.* **1993**, *115*, 5422.

21. Rowan, S. J.; Cantrill, S. J.; Cousins, G. R.; Sanders, J. K.; Stoddart, J. F. *Angew. Chem. Int. Ed.* **2002**, *41*, 898.

22. Corbett, P. T.; Leclaire, J.; Vial, L.; West, K. R.; Wietor, J. L.; Sanders, J. K. M.; Otto, S. *Chem. Rev.* **2006**, *106*, 3652.

23. Lehn, J. M. *Chem. Soc. Rev.* **2007**, *36*, 151.

24. Lehn, J. M. *Science* **2002**, *295*, 2400.

25. Liu, X.; Liu, Y.; Li, G.; Warmuth, R. *Angew. Chem. Int. Ed.* **2006**, *45*, 901.

26. Mastalerz, M. *Chem. Commun.* **2008**, 4756.

27. Christinat, N.; Scopelliti, R.; Severin, K. *Angew. Chem. Int. Ed.* **2008**, *47*, 1848.

28. Meyer, C. D.; Joiner, C. S.; Stoddart, J. F. *Chem. Soc. Rev.* **2007**, *36*, 1705.

29. Belowich, M. E.; Stoddart, J. F. *Chem. Soc. Rev.* **2012**, *41*, 2003.

30. Jin, Y. H.; Zhu, Y. L.; Zhang, W. *CrystEngComm* **2013**, *15*, 1484.

31. Mastalerz, M. *Angew. Chem. Int. Ed.* **2010**, *49*, 5042.

32. Eickmeier, C.; Junga, H.; Matzger, A. J.; Scherhag, F.; Shim, M.; Vollhardt, K. P. C. *Angew. Chem. Int. Ed.* **1997**, *36*, 2103.

33. Ge, P. H.; Fu, W.; Herrmann, W. A.; Herdtweck, E.; Campana, C.; Adams, R. D.; Bunz, U. H. F. *Angew. Chem. Int. Ed.* **2000**, *39*, 3607.

34. Shetty, A. S.; Zhang, J. S.; Moore, J. S. *J. Am. Chem. Soc.* **1996**, *118*, 1019.

35. Schrock, R. R. *Chem. Rev.* **2002**, *102*, 145.

36. Furstner, A.; Davies, P. W. *Chem. Commun.* **2005**, 2307.

37. Furstner, A. *Angew. Chem. Int. Ed.* **2013**, *52*, 2794.

38. Zhang, W.; Moore, J. S. *J. Am. Chem. Soc.* **2004**, *126*, 12796.

39. Zhang, W.; Moore, J. S. *J. Am. Chem. Soc.* **2005**, *127*, 11863.

40. Bunz, U. H. F.; Rubin, Y.; Tobe, Y. *Chem. Soc. Rev.* **1999**, *28*, 107.

41. Jin, Y. H.; Voss, B. A.; Noble, R. D.; Zhang, W. *Angew. Chem. Int. Ed.* **2010**, *49*, 6348.

42. Boyd, P. D. W.; Hodgson, M. C.; Rickard, C. E. F.; Oliver, A. G.; Chaker, L.; Brothers, P. J.; Bolskar, R. D.; Tham, F. S.; Reed, C. A. *J. Am. Chem. Soc.* **1999**, *121*, 10487.

43. Baskaran, D.; Mays, J. W.; Zhang, X. P.; Bratcher, M. S. *J. Am. Chem. Soc.* **2005**, *127*, 6916.

44. Jyothish, K.; Zhang, W. *Angew. Chem. Int. Ed.* **2011**, *50*, 3435.

45. Camps, C.; Iranzo, V.; Caballero, C.; Blasco, A.; Godes, M. J.; Safont, M. J.; Blasco, S.; Mengual, G.; Berrocal, A.; Sirera, R. *Clin. Transl. Oncol.* **2011**, *13*, 249.

46. Berrocal, V. J.; Gelfand, A. E.; Holland, D. M.; Burke, J.; Miranda, M. L. *Environmetrics* **2011**, *22*, 553.

47. Gramegna, N.; Della Corte, E.; Quaglia, G.; Lorente, F. G.; Loizaga, I.; Berrocal, S. *Metall Ital* **2011**, 19.

48. Yanagisawa, M.; Tashiro, K.; Yamasaki, M.; Aida, T. *J. Am. Chem. Soc.* **2007**, *129*, 11912.

49. Gil-Ramirez, G.; Karlen, S. D.; Shundo, A.; Porfyrakis, K.; Ito, Y.; Briggs, G. A. D.; Morton, J. J. L.; Anderson, H. L. *Org. Lett.* **2010**, *12*, 3544.

50. Case, D. A. e. a. *AMBER 11*; University of California, San Francisco.

51. Wang, J.; Wolf, R. M.; Caldwell, J. W.; Kollman, P. A.; Case, D. A. *J. Comput. Chem.* **2004**, *25*, 1157.

52. Umezawa, Y.; Tsuboyama, S.; Honda, K.; Uzawa, J.; Nishio, M. *Bull. Chem. Soc. Jpn.* **1998**, *71*, 1207.

53. Umezawa, Y.; Tsuboyama, S.; Takahashi, H.; Uzawa, J.; Nishio, M. *Tetrahedron* **1999**, *55*, 10047.

54. Sanchez-Molina, I.; Grimm, B.; Krick Calderon, R. M.; Claessens, C. G.; Guldi, D. M.; Torres, T. *J. Am. Chem. Soc.* **2013**, *135*, 10503.

55. Atwood, J. L.; Koutsantonis, G. A.; Raston, C. L. *Nature* **1994**, *368*, 229.

56. Huerta, E.; Metselaar, G. A.; Fragoso, A.; Santos, E.; Bo, C.; de, M. J. *Angew. Chem. Int. Ed.* **2007**, *46*, 202.

57. Komatsu, N. *J. Inclusion Phenom. Macrocycl. Chem.* **2008**, *61*, 195.

CHAPTER 4

Semi-conducting Carbon Nanotube and Covalent Organic Polyhedron–C_{60} Nanohybrids for Light Harvesting[1]

4.1 Abstract

We demonstrate noncovalent electrostatic and π-π interactions to assemble semiconducting single-wall carbon nanotube (SWCNT)-C_{60}@**COP-5** nanohybrids. The C_{60}@**COP-5** light harvesting complexes bind strongly to SWCNTs due to significant π-π stacking between C_{60}, the aromatic dicarbazolylacetylene moieties and the nanotube surfaces.

4.2 Introduction

Semi-conducting single-wall carbon nanotubes (SWCNTs) have unique electronic and optical properties for diverse optoelectronic applications, including photovoltaics, photo-detectors and photoswitches.[2-4] SWCNT–porphyrin molecular complexes are promising candidates for light harvesting applications, due to their long-lived charge separated states, and efficient charge-transport behavior of SWCNTs.[5,6] Sophisticated self-organization of the natural porphyrin photosystems serves as a model for artificial photosynthetic systems that require efficient energy and electron transfers.[7-9] Accordingly, the synthesis and supramolecular self-assembly of a variety of porphyrin pigments have been widely explored with the aim of constructing efficient photochemical and optoelectronic devices.[10] However, it is usually challenging and time-consuming to produce such complex supramolecules in reasonable yields.[11] The molecular-scale engineering of these materials also requires an understanding of their noncovalent interactions.[12] To overcome those challenges in the construction of complex nanohybrid light harvesting systems and to further explore the great potential of these intriguing nanomaterial assemblies in

photovoltaic applications, we report herein a novel strategy to form a new class of nanohybrids, namely the encapsulation of C_{60} into a shape-persistent covalent organic polyhedron (**COP-5**) to afford C_{60}@**COP-5** core–shell complexes, followed by their binding to the surface of SWCNTs in a ''side-to-face'' fashion through π–π stacking interactions. In the assembled C_{60}@**COP-5**/SWCNT nanohybrids, C_{60} and SWCNTs are positioned at close distance. A solar cell study revealed the great potential of such nanohybrid materials in photovoltaic applications.

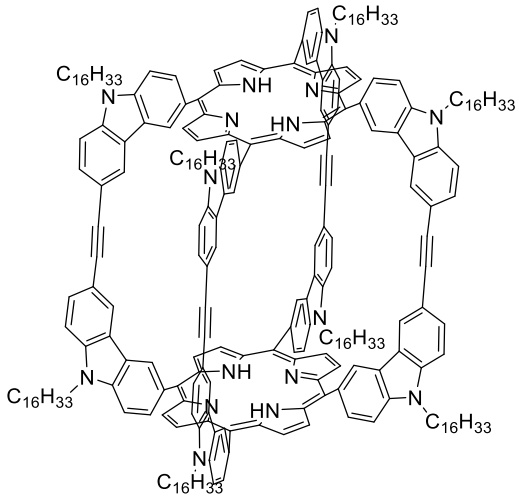

Figure 4.1. Structure of **COP-5**.

4.3 Results and discussion

Given the recent advances of DC_vC in highly efficient construction of well-defined, thermo-dynamically favored 2-D or 3-D molecular architectures,[13,14] A series of macrocyclic and cage compounds through imine or olefin metathesis were accomplished.[15,16] In Chapter 3 we have achieved the one-step synthesis of a shape-persistent porphyrin-based **COP-5** consisting of only aromatic moieties in its backbone structure utilizing alkyne metathesis. The **COP-5** (Fig. 4.1) was prepared from tetra-substituted porphyrin monomers, catalyzed by our newly developed multidentate Mo(VI) carbyne catalyst.[17] The unique combination of the conjugated system and the

rigidity of this **COP-5** molecule renders its rapid and strong binding with C_{60} to form the self-assembled C_{60}@**COP-5** complex. Stable suspensions of C_{60}@**COP-5**/SWCNT were generated by simply stirring a 1,2-dichlorobenzene solution of C_{60}@**COP-5** and SWCNTs under an argon atmosphere for 24 h. The π–π interaction between the C_{60}@**COP-5** complex and the SWCNTs results in the formation of three-component nanohybrids (Fig. 4.2a). The cage molecule we used consists of only rigid, aromatic building blocks, and it does not have too much conformational flexibility. But the four side arms indeed have some rotational freedom when they interact with SWCNTs. The corresponding highest occupied molecular orbital (HOMO) and lowest unoccupied molecular orbital (LUMO) energy levels were calculated using E_{ox} and E_{red} (onset) from the cyclic voltammetry measurements in solution of C_{60}@**COP-5.** Based on cyclic voltammetry results, the C_{60}@**COP-5** complex shows E_{HOMO} = -5.32 eV, E_{gap} = 1.2 eV and E_{LUMO} = -4.12 eV. Fig. 4.2b shows the band diagram with HOMO/LUMO levels of C_{60}@**COP-5** and SWCNT. Regarding to type-II heterojunction solar cells, these two materials can be used as a photoactive layer.

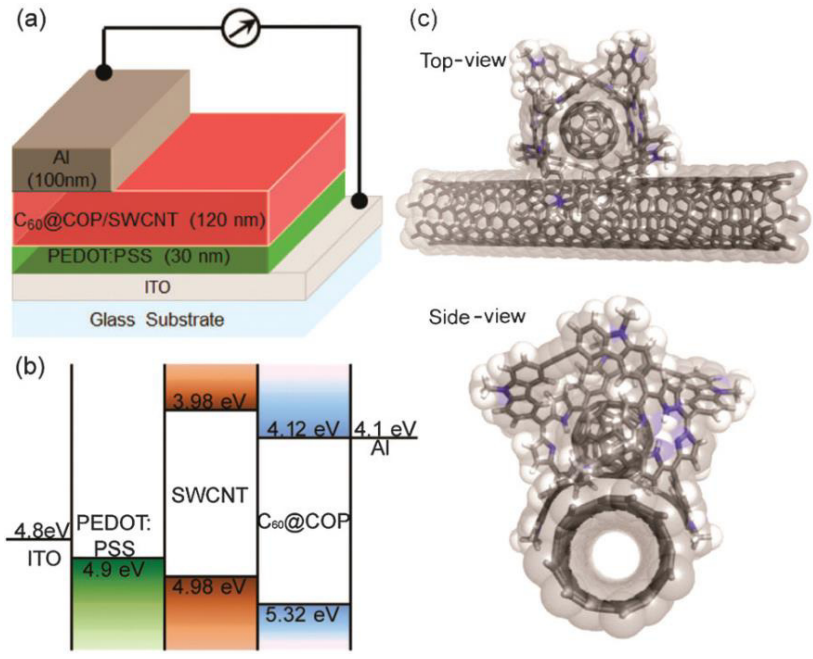

Figure 4.2. (a) Schematic of the C_{60}@**COP-5**/SWCNT nanohybrid solar cells. (b) Band alignment

diagram of solar cells, the semiconducting SWCNT as a donor and the C_{60}@**COP-5** complex as an acceptor. (c) Energy-minimized structures of the self-assembled SWCNT and the C_{60}@**COP-5** complex (top, top view; bottom, side view), semiconducting (7, 5) SWCNT is used in the calculation.

Valuable insights into structural features were obtained by transmission electron microscopy (TEM) and high-resolution transmission electron microscopy (HRTEM). Representative TEM images of the C_{60}@**COP-5**/SWCNT nanohybrids are shown in Fig. 4.3 and 4.4. Clearly, SWCNT debundling is far from quantitative, as SWCNT bundles with diameters ranging from 2 to 10 nm are present. Regardless of the presence of SWCNT bundles, there is clear evidence that individual C_{60}@**COP-5** (core–shell) complexes are immobilized on SWCNT surfaces. Importantly, there was no evidence for the formation of aggregated C_{60}@**COP-5** complexes. It has been widely accepted that porphyrins bind strongly to SWCNTs in a face-to-face fashion through π–π stacking interactions.[18]

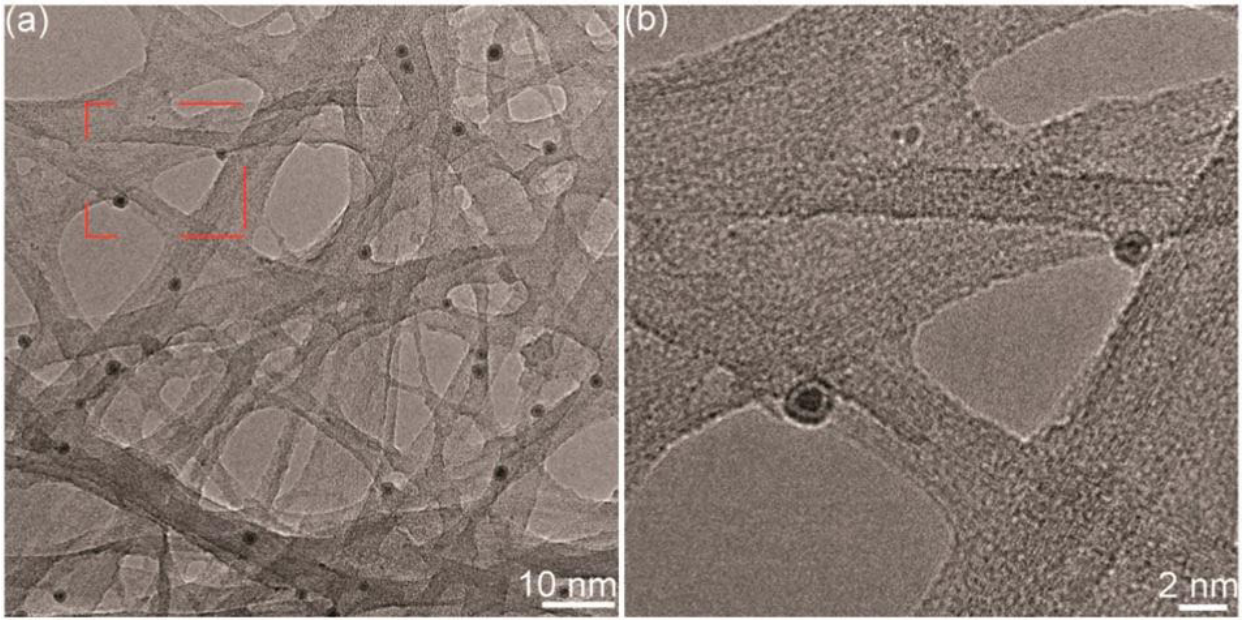

Figure 4.3. (a) The TEM image of C_{60}@**COP-5**/SWCNT (1 wt%) nanohybrids, which are diluted 10 times in comparison with the solution concentration of solar cell device fabrication; (b) the HRTEM image of the red dashed bar in (a).

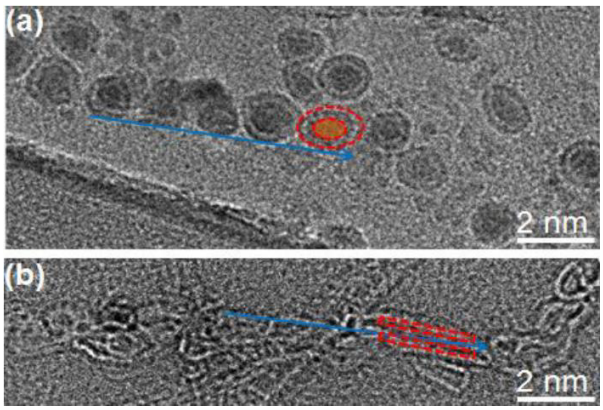

Figure 4.4. The TEM images of C_{60}@**COP-5**/SWCNT and C_{60}/**COP-5**/SWCNT, (a) and (b), respectively. The blue arrow indicates the direction of SWCNT, and red dashed line and orange shaded area represents the **COP-5** shell and C_{60} core in (a); and red dashed line shows the **COP-5** shell coating onto SWCNT in (b).

However, the computer modeling of the C_{60}@**COP-5**/SWCNT assembly shows that the C_{60}@**COP-5** binds the SWCNT through two bis(carbazolyl)acetylene side arms (Fig. 4.2c), instead of through the porphyrin panel. The simulated distance between the bottom of C_{60} and the SWCNT surface is 0.3 nm. This is consistent with the observed short distance (0.5 nm) between C_{60} and SWCNT from HRTEM investigation (Fig. 4.3b). This represents one of rare, if any, binding modes of porphyrin-containing molecules with SWCNTs. Such type of binding results in a close distance between the C_{60}@**COP-5** complex (particularly C_{60}) and the SWCNT, thus allowing efficient electron transfer to occur between the C_{60}@**COP-5** pigment complex and the attached SWCNT, as demonstrated below. Moreover, the flexible non-covalent interaction may allow the attached pigment complex to have considerable freedom in its orientation and thus facilitate interactions between pigments. The supramolecular assembly of the C_{60}@**COP-5** complex and the SWCNT creates a type-II heterojunction interface by forming the noncovalent bonding. As such, the SWCNTs will be particularly attractive scaffolds because of their highly

ordered carbon structures and well-defined interfacial band offset with the C_{60}@**COP-5** complex. The systematic preparation and characterization of both the individual building blocks and the nanohybrid in solution and thin film are ultimately beneficial for the understanding of optoelectronic interactions in solution-processed solar cells.

UV-vis and photoluminescence spectra are often used to quantify supramolecular interactions in the light-harvesting complex. Further evidence for the formation of C_{60}@**COP-5**/SWCNT nanohybrids was obtained from spectroscopic investigations of pure **COP-5**, C_{60}@**COP-5** complex, **COP-5**/SWCNT, and C_{60}@**COP-5**/SWCNT (Fig. 4.5). In line with the porphyrin, the absorption maxima of **COP-5**, which are ascribed to the electronic transition across the band gap, are clearly visible in the 300–700 nm range. A comparison of porphyrin led to continuously red-shifting maxima due to the increased conjugation length of **COP-5**. In Fig. 4.5a, absorption features of the porphyrin **COP-5** with an absorption maximum at 440 nm are depicted.

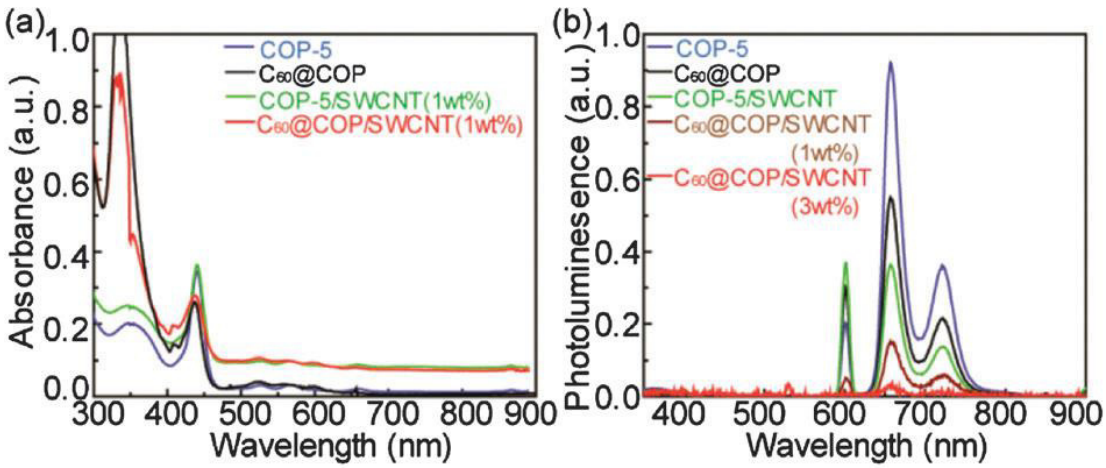

Figure 4.5. (a) The absorbance spectrum of **COP-5**, C_{60}@COP, **COP-5**/SWCNT (1 wt%) and C_{60}@**COP-5**/SWCNT (1 wt%) nanohybrids; (b) the photoluminescence quenching spectrum dependent on the photoactive complex phases and the SWCNT concentration (a).

In the absorption spectrum of **COP-5**/SWCNT, the signatures of the two constituents (i. e.,

the **COP-5** and SWCNT), are discernible. Importantly, the absorption in the region between 450 and 900 nm appeared as a result of the introduction of SWCNTs.[19] Coupling the C_{60}@**COP-5** complex to the SWCNT imposes, however, notable changes to the characteristic C_{60} band-gap transitions. In the absorption spectrum of the C_{60}@**COP-5**/SWCNT nanohybrids (Fig. 4.5a), C_{60}@**COP-5** transitions are registered in the ultraviolet and visible range, at 350, 440, 530, 565 and 600 nm. Transitions in the visible and in particular in the near-infrared range correspond to suspended and sufficiently debundled SWCNTs, as optical transitions between Van Hove singularities become discernible.[20] Notably, the characteristic C_{60}@**COP-5** band gap absorption is superimposed onto SWCNT transitions. Owing to the importance of the charge transfer in the light harvesting complex, we performed emission quenching experiments with **COP-5**, C_{60}@**COP-5** and C_{60}@**COP-5**/SWCNT with excitation at 350 nm (Fig. 4.5b). Excitation at 350 nm is preferential for $\pi-\pi^*$ transitions of **COP-5** and brings about fluorescence peaks at 600, 660, and 720 nm. All porphyrin **COP-5** samples display bright luminescence. The excitation spectra of the luminescence at 350 nm led to features that are in excellent agreement with ground-state absorption features including a band gap onset at 650 nm (see Fig. 4.5a). The underlying quenching mechanism is in line with the fact that now the charge transfer within the C_{60}@**COP-5**/SWCNT assembly, rather than that within the C_{60}@**COP-5** complex, dominates. Most significant is, however, nearly quantitative quenching of the band-gap luminescence by increasing the SWCNT loading (3 wt % vs. 1 wt %).

Table 4.1. Photovoltaic properties of solar cell devices with different photoactive nanohybrids and nanotube loading under AM 1.5 solar illumination (100 mW/cm^2).

Solar Cell Devices	J_{sc} (mA/cm^2)	V_{oc} (V)	FF (%)	Efficiency (%)
C_{60}@COP	0.0262	0.08	19	0.0004
C_{60}@**COP-5**/SWCNT (1 wt %)	1.4	0.47	24	0.16
C_{60}@**COP-5**/SWCNT (3 wt %)	2.34	0.49	14	0.16
C_{60}/**COP-5**/SWCNT (1 wt %)	0.0275	0.1	25	0.0007

Central to the understanding of the exciton and charge carrier dynamics in the C_{60}@**COP-5**/SWCNT nanohybrid active layer is the study of the electrical and optical properties of fabricated devices, so we next investigated the dependence of their performance on photoactive materials and SWCNT loading. Fig. 4.6a shows the operating characteristics of C_{60}@**COP-5** and C_{60}@**COP-5**/SWCNT hybrid devices at different nanotube concentrations; we report the complete set of results in Table 4.1.

The short-circuit current (J_{sc}) is observed to increase with nanotube loading at low SWCNT weight concentrations (1 wt %), until a peak value of J_{SC} = 2.34 mA cm^{-2} is achieved at 3 wt %. The open circuit voltage (V_{oc}) is dictated by the LUMO and HOMO band offset between the acceptor C_{60}@**COP-5** and donor SWCNT,[21] respectively. It agrees well with the band levels of the C_{60}@**COP-5** complex from the CV measurement. Neither the **COP-5**/SWCNT nor the C_{60}/SWCNT system shows promising photovoltaic performance, thus demonstrating the uniqueness and great importance of the C_{60}@**COP-5**/SWCNT nanohybrid system. The

experimental results also showed that the solar cell performance is highly dependent on the sequence of the three component mixing (**COP-5**, C_{60} and SWCNT) in solution, which is presumably due to the effect of SWCNTs on the **COP-5**/C_{60} complex binding: the initial π–π stacking between **COP-5** and SWCNTs may impede the further C_{60} binding. Only the preformed C_{60}@**COP-5** could provide a type-II heterojunction with the SWCNT component. Notably, for the best hybrid device with 1 wt % and 3 wt % SWCNT, we measured an equal AM1.5 power conversion efficiency (PCE) of 0.16%. Though showing a higher J_{sc}, high loading of SWCNT (3 wt %) does not guarantee higher PCE due to the decreased fill factor (FF). The decrease of FF results from the reduced shunt resistance or fast recombination from SWCNT bundling at relatively high 3 wt % loading, which is confirmed by non-uniformly distributed percolation morphology (Fig. 4.6b and c).

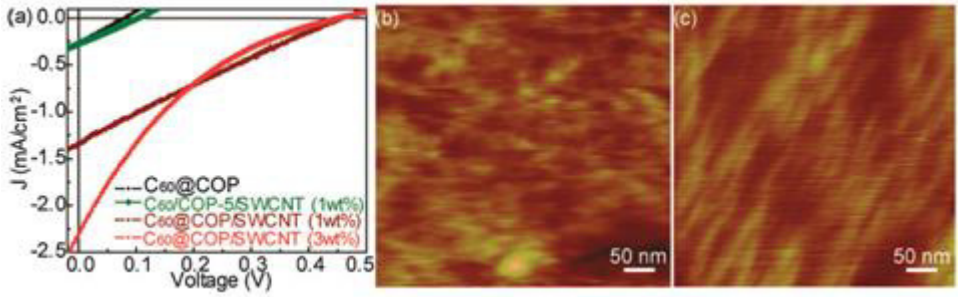

Figure 4.6. (a) The current–voltage characteristics of C_{60}@**COP-5**, C_{60}/**COP-5**/SWCNT (1 wt %), C_{60}@**COP-5**/SWCNT (1 wt %) and C_{60}@**COP-5**/SWCNT (3 wt %) solar cells under AM 1.5 sun illumination; (b) and (c) the solar cell surface morphology (AFM images) at 1 wt % and 3 wt % SWCNT loading, respectively.

Conclusions

By virtue of supramolecular π-π interactions, SWCNTs and C_{60}@COP complex form light-harvesting complexes en route to a novel type of versatile donor–acceptor nanohybrids,

C_{60}@**COP-5**/SWCNT. The porphyrin-containing COP-C_{60} complex (C_{60}@**COP-5**) binds to SWCNT in a "side-to-face" fashion through its two bicarbazolylacetylene side-arms, which represents a different binding mode from those conventional cases where porphyrin binds to SWCNT in a "face-to-face" fashion. The complementary use of electron microscopic and spectroscopic techniques confirmed the hierarchical integration of the electronically coupled constituents, namely C_{60}@**COP-5** complex and SWCNT. A thorough photophysical investigation (i.e., absorption and photoluminescence quenching measurements) sheds light on the formation of type-II heterojunction for the solution processed excitonic solar cells. To explore the feasibility of utilizing C_{60}@**COP-5**/SWCNT as an integrative component in solar cell devices, we studied the light harvesting performance of this novel nanohybrid as a photoactive layer. To this end, as a proof-of-concept experiment, we constructed a prototype solar cell comprised of a spun-cast photoactive thin film of C_{60}@**COP-5**/SWCNT. Under AM 1.5 conditions, a short circuit current of 1.4 mA/cm^2, an open circuit voltage of 0.47 V, a fill factor of 24%, and an efficiency of 0.16% were measured for this setup with 1 wt% SWCNT loading. We believe that the current results not only document the optoelectronic processes in the complex, but sketch a potent alternative for fabricating efficient photoactive molecular devices with this novel class of nanohybrid materials.

4.4 Experimental section

4.4.1 Materials and general methods

High purity semiconducting single-walled carbon nanotubes (s-SWCNTs) with nominal diameter in the range 1.2–1.7 nm and length in the range 300 nm – 5 μm (IsoNanotube-S from NanoIntegris, powder with 98% purity) were used in this study. The whole device structure consists of the following sequence of films and thicknesses: ITO/poly(3,4-ethylenedioxythiophene)-poly(styrenesulfonate) PEDOT-PSS) (30 nm)/ C_{60}@COP/SWCNT(120

nm) /Al (100 nm). PEDOT:PSS (Baytron PVP CH 8000) is spin cast onto a 0.5 × 0.5 in^2 glass substrate with pre-patterned ITO electrodes. The PEDOT: PSS is useful as a hole transport and the smoother of ITO. The blended C_{60}@COP/SWCNT (1 wt% or 3 wt%) solution is spun at 1000 rpm for 1 min, and allowed to solvent annealing overnight. The coated device was annealed at 140°C for 10 min, and then quickly cooled to room temperature. The 100 nm thick Al top contact layer was evaporated at a rate of 0.1 nm/s as the cathode, through a shadow mask to generate an array of patterned electrodes. The final device area was defined by the overlap between the top and bottom electrodes. The light illumination for solar cell device testing is provided from a 100 mW/cm^2 AM 1.5 solar simulator.

4.4.2 Electrochemical measurement

Cyclic voltammetry (CV) measurements were carried out under argon in anhydrous solvents with a BAS 100 Electrochemical Analyzer at a potential scan rate of 50 mV/s. The cell used three electrodes: a saturated silver chloride reference electrode (0.222 V vs. SHE), a glassy carbon working electrode, and a platinum counter electrode. The experiments were performed in a mixed solvent of toluene and dimethylformamide (2/1, v/v) with tetrabutyl ammonium hexafluorophosphate (0.1 M) as electrolyte. The concentrations of the analytes were at 0.50-1.0 mmol.

The onset potentials of the n-doping and p-doping can be used to determine the LUMO and HOMO energy levels of the analytes, and the potential difference can be used to estimate the energy gap of the analytes. E_{LUMO}= -(E_{red}+4.4) eV, E_{HOMO}= -(E_{ox}+4.4) eV, where E_{LUMO} is the LUMO energy level, E_{HOMO} is the HOMO energy level, and all electrode potential values are vs. SCE as the reference electrode.

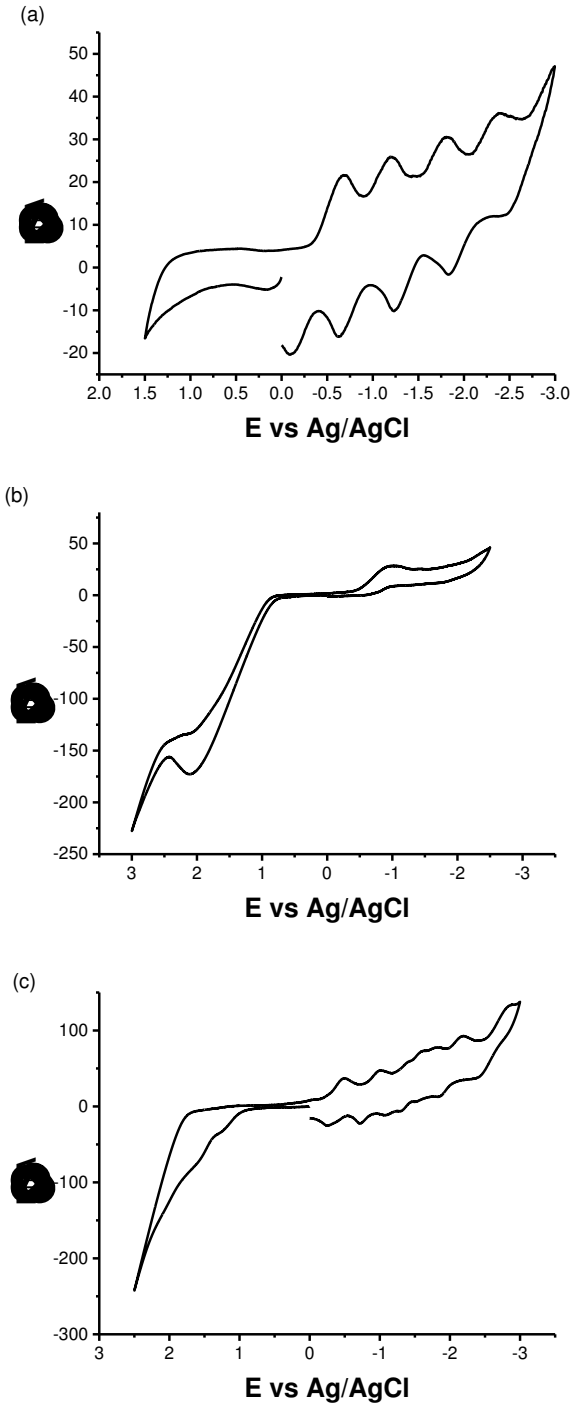

Figure 4.7. Cyclic Voltammetry of C_{60} (a), cage **COP-5** (b), and C_{60}@**COP-5** complex (c).

Table 4.2. Calculated HOMO and LUMO energy levels of the analytes.

	Oxidation potential (V vs. Ag/AgCl)/V	Reduction potential (V vs. Ag/AgCl)/V	Energy Level/eV		Band Gap/eV
			HOMO	LUMO	
Cage	0.88	-1.01	-5.26	-3.37	1.89
C_{60}	N/A	-0.35	N/A	-4.03	N/A
C_{60}@**COP-5**	0.94 (C_{60})	-0.26 (cage)	-5.32	-4.12	1.20

4.4.3 Modeling and structural characterization

The Amber 11.0 molecular dynamics program package was used to optimize the structure of the fullerene, the cage, the CNT, the cage/fullerene binding complexes, and the three-component binding complexes. The force field used was the general Amber force field (GAFF field) with the charge parameters computed by AM1-BCC method. For each structure optimization run, the molecule was first minimized for 1000 steps using the conjugate gradient method, and then it was further optimized by simulated annealing method for 150 picosecond with a time-step of 1 femtosecond. During the simulated annealing, the system temperature was first raised up to 1000 K for 50 picoseconds and then gradually cooled to 0 K for another 100 picoseconds. Finally, the annealed structure was minimized again for another 1000 conjugate gradient steps and the final energy was recorded. The non-bonded interactions during the simulation were computed directly with a cutoff distance of 25 Å. A dielectric constant of 4.8 was assumed during the simulation, which is a typical value for organic solvents.

A FEI Tecnai F20 XT FEG electron microscope operated at 200 kV was used for transmission electron microscopy (TEM). Surface morphology of the organic solar cell devices was investigated using Digital Instruments Dimension 3000 atomic force microscope (AFM)

operating in tapping mode. The C_{60}@**COP-5** binds to SWCNT surface through π-π interaction (Fig. 4.4a), which forms a type-II heterojunction for nanohybrid solar cells. By mixing the C_{60}, **COP-5** and SWCNT three components together, it is possible that the **COP-5** directly binds onto the SWCNT surface without the C_{60} bound inside (Fig. 4.4b), which makes the C_{60}/**COP-5**/SWCNT system is not efficient due to the lack of crucial C_{60}@**COP-5** complex.

4.4.4 J-V characterization of solar cell devices

The effect of porphyrin **COP-5** and C_{60} in combination with SWCNT on the photovoltaic properties of bulk heterojunction solar cells was demonstrated by the DC current density (J)–voltage (V) (Fig. 4.8). As shown in Fig. 4.8, the solar device shows a very small photoresponse from **COP-5**/SWCNT and C_{60}/SWCNT. This result further supports the tunable band level by the formation of **COP-5**/C_{60} complex, which makes a more effective photovoltaic system C_{60}@COP/SWCNT. By changing the mixing sequence among **COP-5**, C_{60} and SWCNT, we are able to identify better bonding of **COP-5** and SWCNT than that of **COP-5** and C_{60}. The photovoltaic performance further confirms that the **COP-5** preferentially binds with SWCNT to form a shell coating (Figure 4.4), which increase the fill factor of nanohybrid solar cell; however, the **COP-5** coated SWCNT and C_{60} leads to a low performance. By blending **COP-5** and C_{60} first, the preformed C_{60}/**COP-5** complex and SWCNT nanohybrids confirm a type-II heterojunction, as shown in the main text.

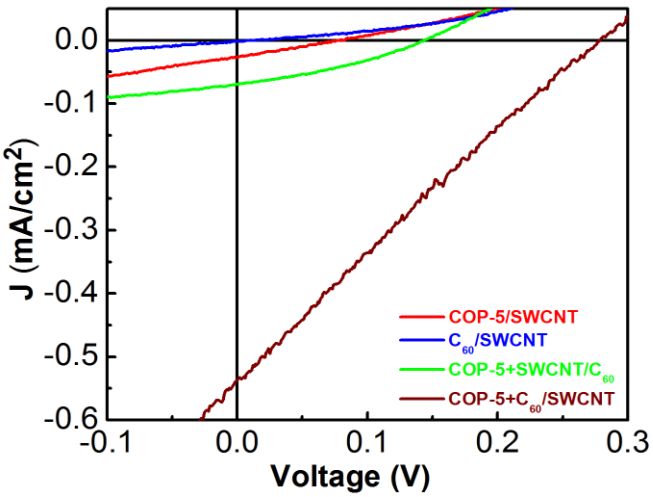

Figure 4.8. J-V characteristics of solar cells (Red: **COP-5**/SWCNT; Blue: C_{60}/SWCNT; Green: **COP-5** mixed with SWCNT (1 wt %) for 1 hour, followed by blending with C_{60} (1:1 weight ratio between **COP-5** and C_{60}); Brown: **COP-5** mixed with C_{60} for 1 hour (1:1 weight ratio between **COP-5** and C_{60}), followed by blending with 1wt % SWCNT) measured with incident light intensities from 100 mW/cm^2 AM 1.5 solar simulator.

4.5 References

1. Lohrman, J.; Zhang, C. X.; Zhang, W.; Ren, S. Q. *Chem. Commun.* **2012**, *48*, 8377.

2. Bernardi, M.; Giulianini, M.; Grossman, J. C. *ACS Nano.* **2010**, *4*, 6599.

3. Dang, X. N.; Yi, H. J.; Ham, M. H.; Qi, J. F.; Yun, D. S.; Ladewski, R.; Strano, M. S.; Hammond, P. T.; Belcher, A. M. *Nat. Nanotechnol*. **2011**, *6*, 377.

4. Ren, S. Q.; Bernardi, M.; Lunt, R. R.; Bulovic, V.; Grossman, J. C.; Gradecak, S. *Nano Lett.* **2011**, *11*, 5316.

5. D'Souza, F.; Das, S. K.; Zandler, M. E.; Sandanayaka, A. S. D.; Ito, O. *J. Am. Chem. Soc.* **2011**, *133*, 19922.

6. Sprafke, J. K.; Stranks, S. D.; Warner, J. H.; Nicholas, R. J.; Anderson, H. L. *Angew. Chem. Int. Ed.* **2011**, *50*, 2313.

7. Inokuma, Y.; Kawano, M.; Fujita, M. *Nat. Chem.* **2011**, *3*, 349.

8. Nam, Y. S.; Magyar, A. P.; Lee, D.; Kim, J. W.; Yun, D. S.; Park, H.; Pollom, T. S.; Weitz, D. A.; Belcher, A. M. *Nat. Nanotechnol.* **2010**, *5*, 340.

9. Olenyuk, B.; Whiteford, J. A.; Fechtenkotter, A.; Stang, P. J. *Nature* **1999**, *398*, 796.

10. Kay, A.; Gratzel, M. *J. Phys. Chem.* **1993**, *97*, 6272.

11. Tsuda, A.; Osuka, A. *Science* **2001**, *293*, 79.

12. Roquelet, C.; Garrot, D.; Lauret, J. S.; Voisin, C.; Alain-Rizzo, V.; Roussignol, P.; Delaire, J. A.; Deleporte, E. *Appl. Phys. Lett.* **2010**, *97*, 141918.

13. Lehn, J. M. *Science* **2002**, *295*, 2400.

14. Chichak, K. S.; Cantrill, S. J.; Pease, A. R.; Chiu, S. H.; Cave, G. W. V.; Atwood, J. L.; Stoddart, J. F. *Science* **2004**, *304*, 1308.

15. Jin, Y. H.; Voss, B. A.; Noble, R. D.; Zhang, W. *Angew. Chem. Int. Ed.* **2010**, *49*, 6348.

16. Jin, Y. H.; Zhang, A. B.; Huang, Y. S.; Zhang, W. *Chem. Commun.* **2010**, *46*, 8258.

17. Jyothish, K.; Zhang, W. *Angew. Chem. Int. Ed.* **2011**, *50*, 3435.

18. Stranks, S. D.; Sprafke, J. K.; Anderson, H. L.; Nicholas, R. J. *ACS Nano* **2011**, *5*, 2307.

19. Bindl, D. J.; Wu, M. Y.; Prehn, F. C.; Arnold, M. S. *Nano. Lett.* **2011**, *11*, 455.

20. Kanai, Y.; Grossman, J. C. *Nano Lett.* **2008**, *8*, 908.

21. Kymakis, E.; Amaratunga, G. A. J. *Appl. Phys. Lett.* **2002**, *80*, 112.

CHAPTER 5

Construction of Porphyrin-Based Macrocyclic Compound Using Alkyne Metathesis and the Study of Its Fullerene Binding Behavior[1]

5.1 Abstract

A bisporphyrin macrocycle was constructed from a porphyrin-based diyne monomer in one-step using alkyne metathesis. Fullerene binding studies (C_{60}, C_{70} and C_{84}) showed the highest binding affinity of the macrocycle for C_{84}, which is in great contrast to its bisporphyrin four-armed cage analogue that showed the strongest binding with C_{70}.

5.2 Introduction

Fullerenes have attracted enormous research interest due to their unique physical properties and important applications in photovoltaics, electronics and the biopharmaceutical industry, etc.[2-4] Despite the fascinating progress in fullerene chemistry, their practical applications have been hindered by the cost and energy intensive purification process as well as the poor solution processibility.[5,6] Synthetic host molecules capable of noncovalently interacting with fullerenes have been extensively used as the selective complexation agents to enhance the solubility of fullerenes or assist the purification of a particular fullerene from an organic solution of fullerene mixtures.[7-12] As a consequence, the search for fullerene receptors with high binding affinity and/or high selectivity has been an intensive research area.

Recently, we have synthesized a novel 3-D molecular cage (covalent organic polyhedron, **COP-5**) as a host molecule for fullerenes through alkyne metathesis, a highly efficient DC_vC approach, in one step from a readily accessible porphyrin-based precursor.[13] The shape-persistent **COP-5** showed strong binding interactions with fullerenes. It forms 1:1 complexes with C_{60} and C_{70} with the association constants of 1.4×10^5 M^{-1} (C_{60}) and 1.5×10^8 M^{-1} (C_{70}) in toluene, strongly favoring binding with C_{70} over C_{60} ($K_{C70}/K_{C60} > 1000$). Moreover, the binding between **COP-5** and fullerenes was fully reversible under the acid–base stimuli, thus allowing successful separation of C_{70}. Although the four-armed cage **COP-5** showed very interesting fullerene binding behavior, two important questions remain to be answered; What causes such a high binding selectivity for C_{70}? How important is the shape-persistency (rigidity) of the cage to the fullerene binding selectivity?

In this chapter, the synthesis of a series of bisporphyrin macrocycles was designed and pursued. After several failed synthetic routes, macrocycle **94** was synthesized and purified successfully. Similar to its structure analog **COP-5**, the macrocycle can act as a host for fullerenes. Its binding interactions with various fullerenes (C_{60}, C_{70} and C_{84}) were studied and compared to those of the bisporphyrin cage **COP-5**. It turned out that rigid **COP-5** binds most strongly with C_{70}, while macrocycle **94,** with conformational flexibility, exhibits the highest binding affinity for C_{84}, thus showing the feasibility of tailoring the fullerene binding selectivity of aromatic host molecules by fine tuning their chemical structures.

5.3 Results and discussion

A shape-persistent bisporphyrin macrocycle was designed as shown in Fig. 5.1. In which the R group could be tuned for different electronic property, and also be used for post-synthesis modification.

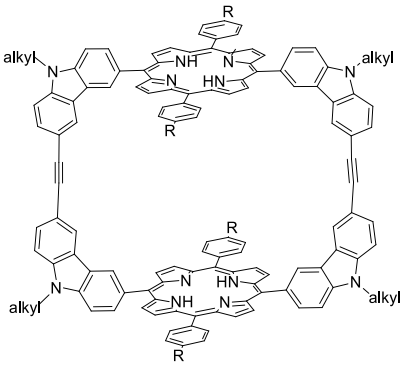

Figure 5.1. The structure of the designed bis-porphyrin macrocycle.

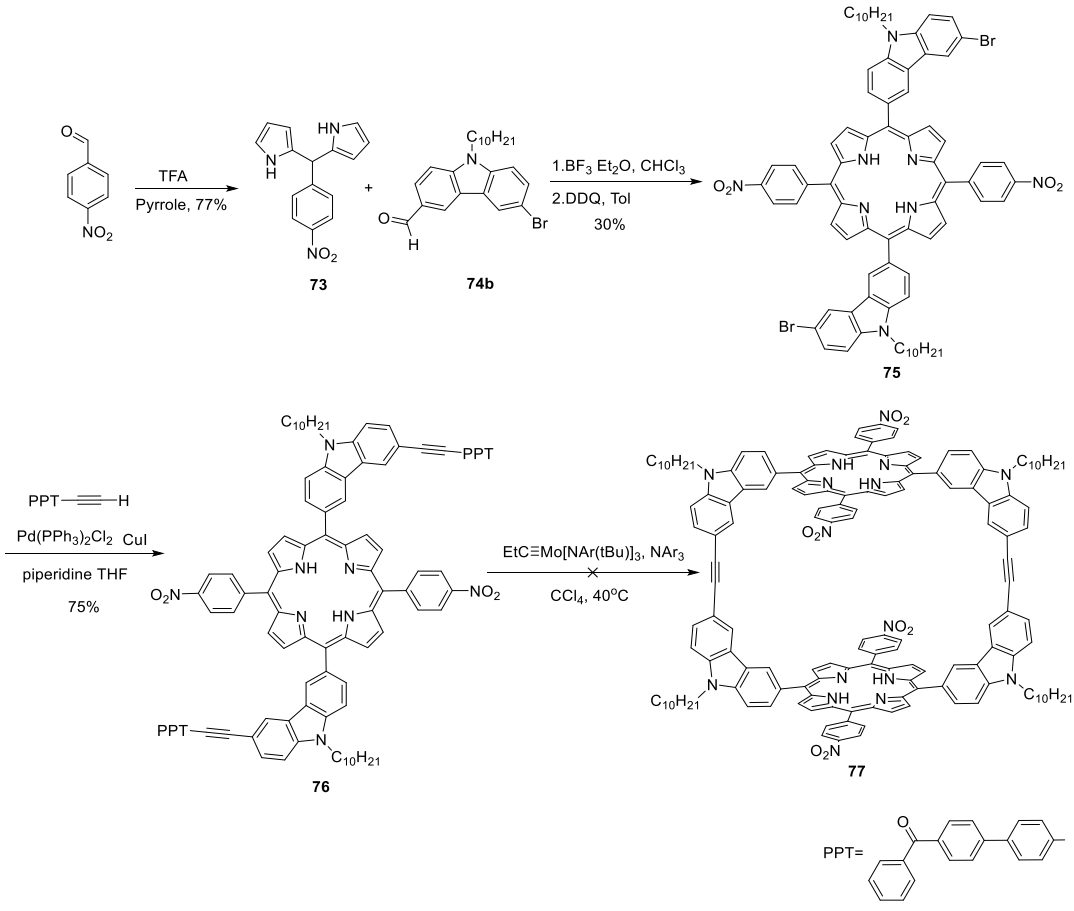

Scheme 5.1. Attempted synthesis toward the nitro-substituted macrocycle.

Nitro-substitution was pursued at the beginning for its great potential in post-synthesis modification (Scheme 5.1). Using azide chemistry, a nitro group could be converted to many other

functional groups efficiently. The monomer **76** was obtained through sonogashira coupling reaction on **75** to attach the end group for precipitation-driven alkyne metathesis. The porphyrin **75** was synthesized under BF_3 catalyzed typical porphyrin synthesis condition from aldehyde **74** and dipyrromathane **73**. Dipyrromathane **73** is obtained from the reaction between 4-nitrobenzaldehyde and excess amount of pyrrole. However, the synthesis toward macrocycle **77** was not successful under several alkyne metathesis conditions. A large amount of precipitates formed during the alkyne metathesis reaction while no desired product was observed by in either NMR or MS analysis. The failed macrocyclization was likely due to the poor solubility of the intermediate species formed along the reaction pathway.

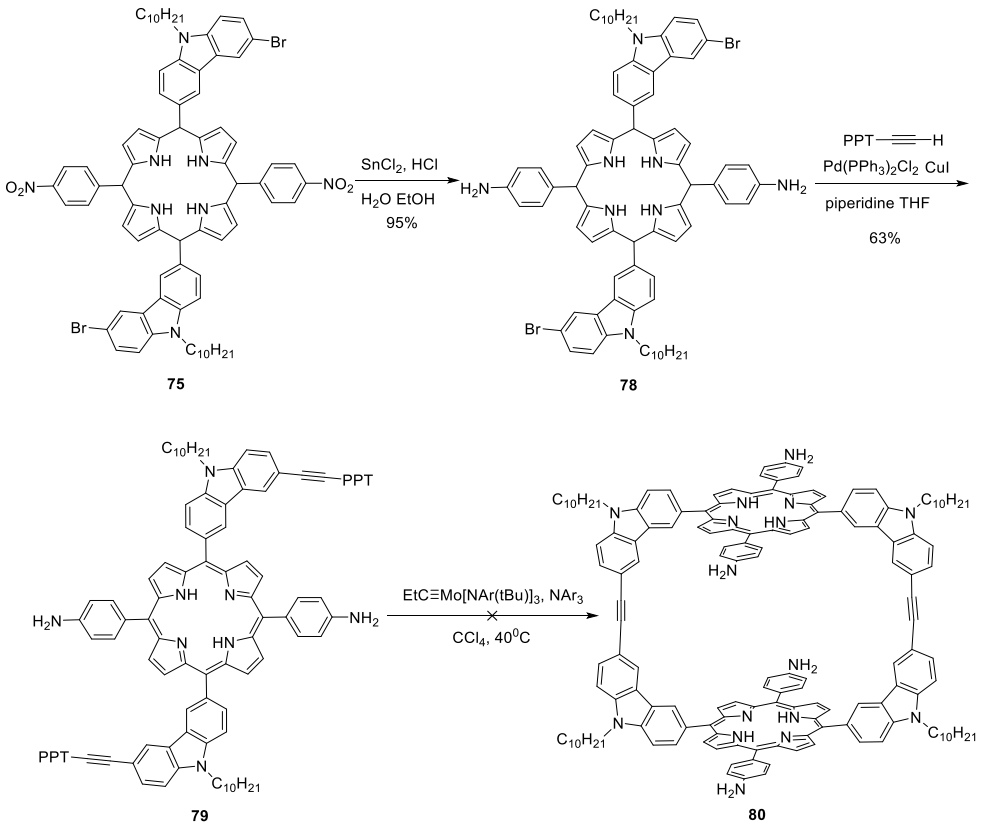

Scheme 5.2. Attempted synthesis toward the amino-substituted macrocycle.

Reduction of nitro groups to amino groups did not improve the macrocycle synthesis due to inhibition of the catalyst reactivity by amines (Scheme 5.2), which is confirmed by the model reaction where the alkyne metathesis of **81** would not proceed with the presence of 1 equiv. aniline. (Scheme 5.3)

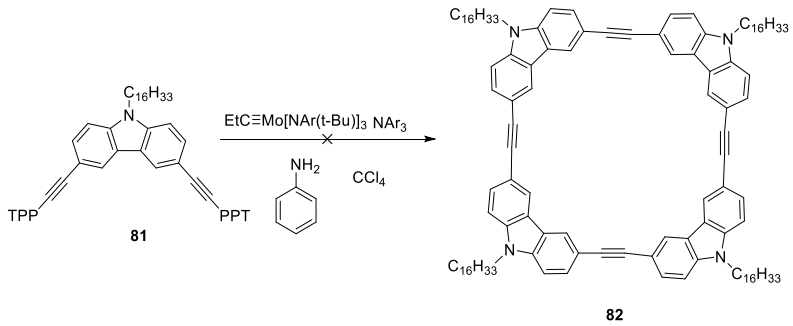

Scheme 5.3. Model reaction for the test of the compatibility of aniline with the alkyne metathesis reaction.

Protection of the amino group was then pursued in order to determine its inhibiting effect on the alkyne metathesis. Direct protection of di-amino compound **78** was not successful (Scheme 5.4). Under basic reaction conditions (TEA, DMAP), the NMR spectra of the crude reaction mixture showed that the center protons of porphyrin disappeared while the amine was not much affected. This result indicates that the porphyrin free base center will result in some side-reaction that inhibits the desired amine protection.

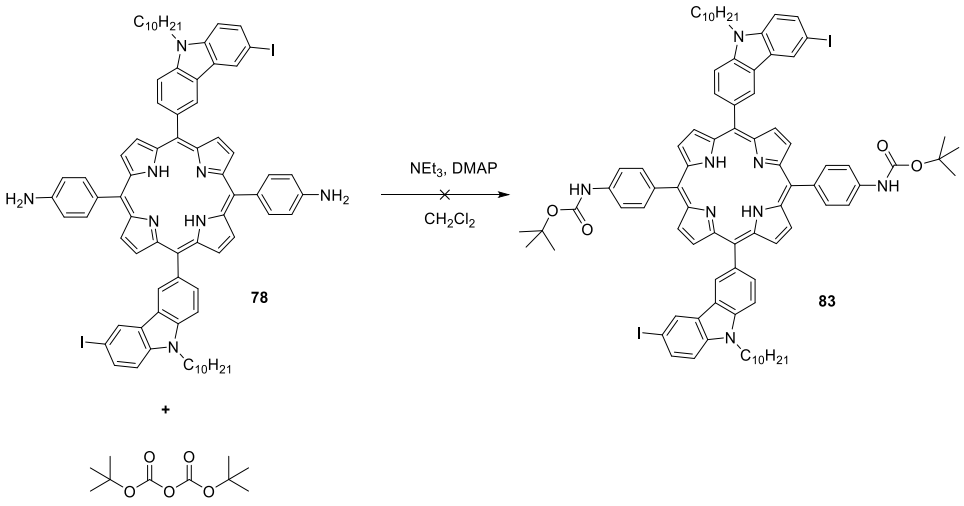

Scheme 5.4. Attempted *tert*-butyloxycarbonyl (BOC) protection of the amino groups.

Protection of the amino group prior to the porphyrin synthesis was then pursued in order to prevent the inhibition of porphyrin ring to the amine protection reaction. 3-Iodo-6-formyl-9-hexadecylcarbazole **(74)** was used instead of the previously used bromo-substitured carbazole aldehyde **74b** for two reasons: 1. The iodo-substituted carbazole is more reactive towards Sonogashira coupling than the bromo-substituted one. 2. The C_{10} alkyl chain was changed to a C_{16} linear chain in order to the further increase the solubility of the macrocycle, which was a potential problem in macrocycle synthesis.

However, with the protected amine group, the porphyrin formation step toward **85** was still unsuccessful. Deprotection of the acetyl group was observed as a side-reaction. More importantly, a large amount of the starting material **74** was recovered after the reaction, and lots of scrambled porphyrin side-product was detected. This result indicates that under such condition, scrambling side-reaction is highly preferred (Scheme 5.5). Similar results were also observed in later trials when the substituent is a strong electron-donating group.

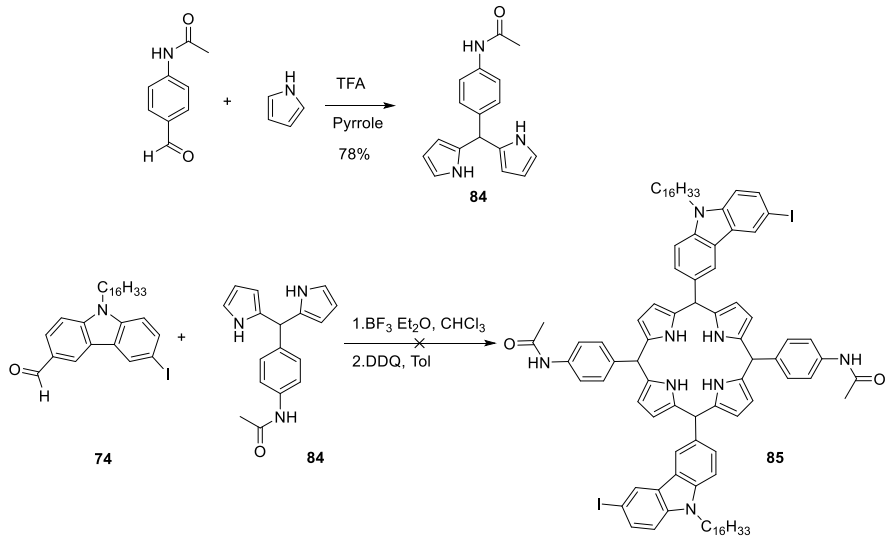

Scheme 5.5. Attempted synthesis of the porphyrin with protected amino groups.

Replacing the alkyl substituent with a more electron-rich alkoxyl chain ($C_{16}H_{33}O$-) was also pursued in hopes of improving the porphyrin formation (Scheme 5.6). Unfortunately, low conversion (<10%) was observed without any noticeable product formation. The only product isolated after reaction was meso-tetra(4-hexyldecyloxylphenyl)porphyrin, which indicates that the scrambling side-reaction dominates, thus leading to the formation of homo-sequenced porphyrin products (Scheme 5.6).[14] Similar to the previous case for the formation of **85**, such results indicate that the dipyrromethane piece bearing the strong electron-donating group may prefer the scrambling side-reaction.

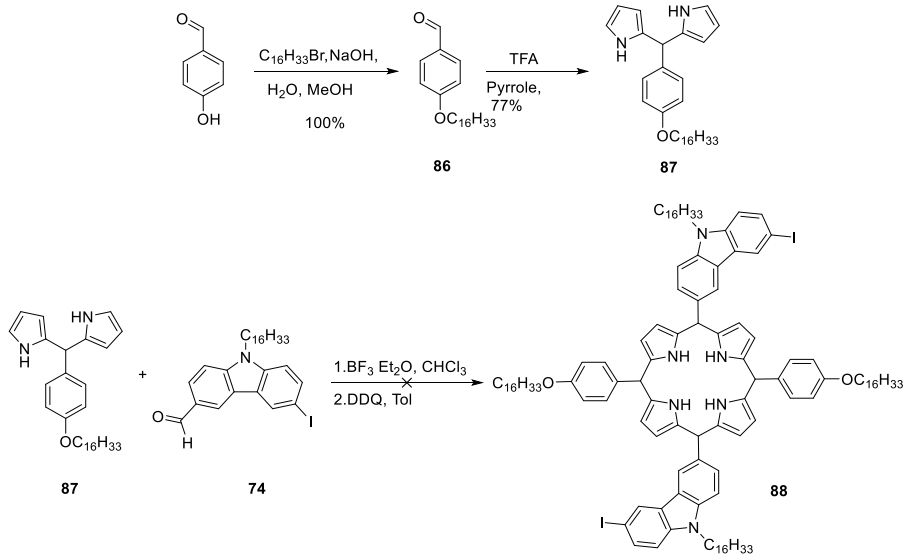

Scheme 5.6. Attempted synthesis of the macrocycle with alkoxyl substitution.

The porphyrin synthesis starting from the dipyrrole building block with a bromo-substituted phenyl group was also pursued. With the bromo-substituent, the porphyrin formation step yielded a mixture of different porphyrin products that are inseparable (Scheme 5.7). Further exploration with the *tert*-butyl substituent finally led to a successful synthetic route. The bisporphyrin macrocycle **94** was prepared from porphyrin-based diyne monomer **93** through one-step alkyne metathesis, catalyzed by the multidentate Mo(VI) alkylidyne catalyst.[15] Porphyrin diyne **83** was synthesized from carbazole 74 and 5-(4-*tert*-butyl-phenyl)-dipyrromethane (**91**) via ring cyclization under standard Lindsey conditions,[14,16] followed by Sonogashira coupling reaction to install the end-groups for precipitation-driven alkyne metathesis.[7] The metathesis reaction was conducted at 45 ^{o}C for 4 hours to give macrocycle **94** in 60% isolated yield.

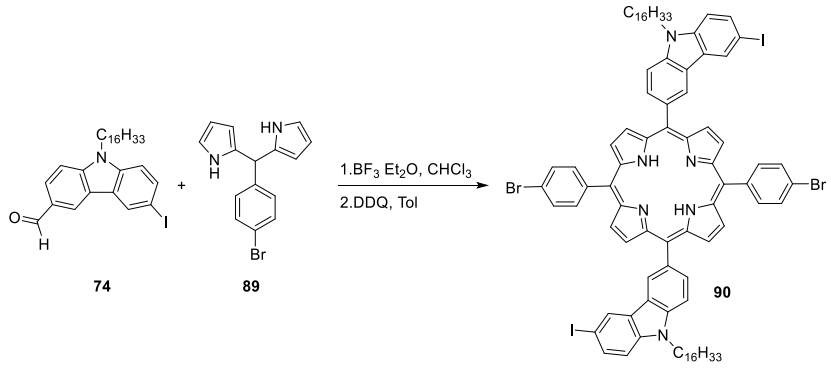

Scheme 5.7. Attempted synthesis of the bisporphyrin macrocycle with the bromophenyl-substituted dipyrrole building blocks.

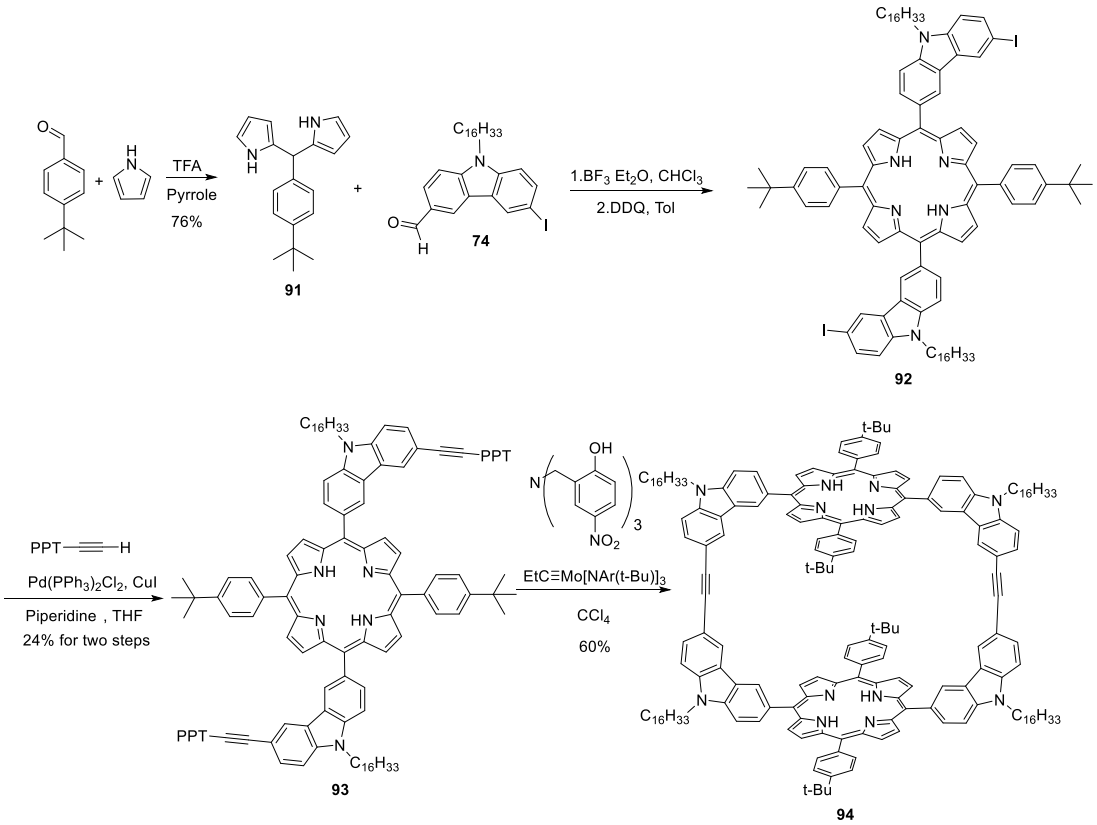

Scheme 5.8. The synthetic route for the bisporphyrin macrocycle containing *tert*-butyl substituted porphyrin moieties.

The gel permeation chromatography (GPC) trace of the crude reaction mixture showed the transformation of monomer **93** into the target macrocycle **94** without initial formation of a large

amount of oligomers or polymers along the reaction process (Fig. 5.2). Macrocycle **94** was purified by column chromatography, and characterized by ^{1}H and ^{13}C NMR, MALDI-MS and GPC.

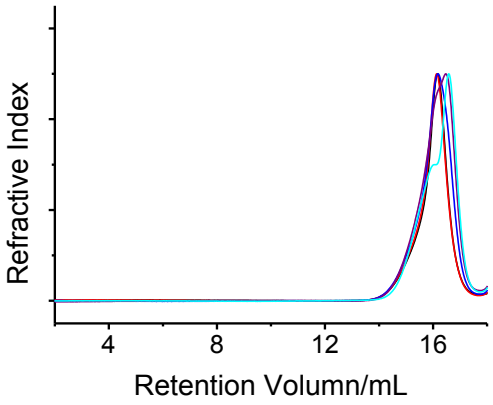

Figure 5.2. The GPC traces of the crude reaction mixture from the macrocycle **94** formation via alkyne metathesis. The reaction was conducted at 45 °C for 10 min (cyan), 30 min (purple), 1 h (blue), 2 h (red), and 4 h (black).

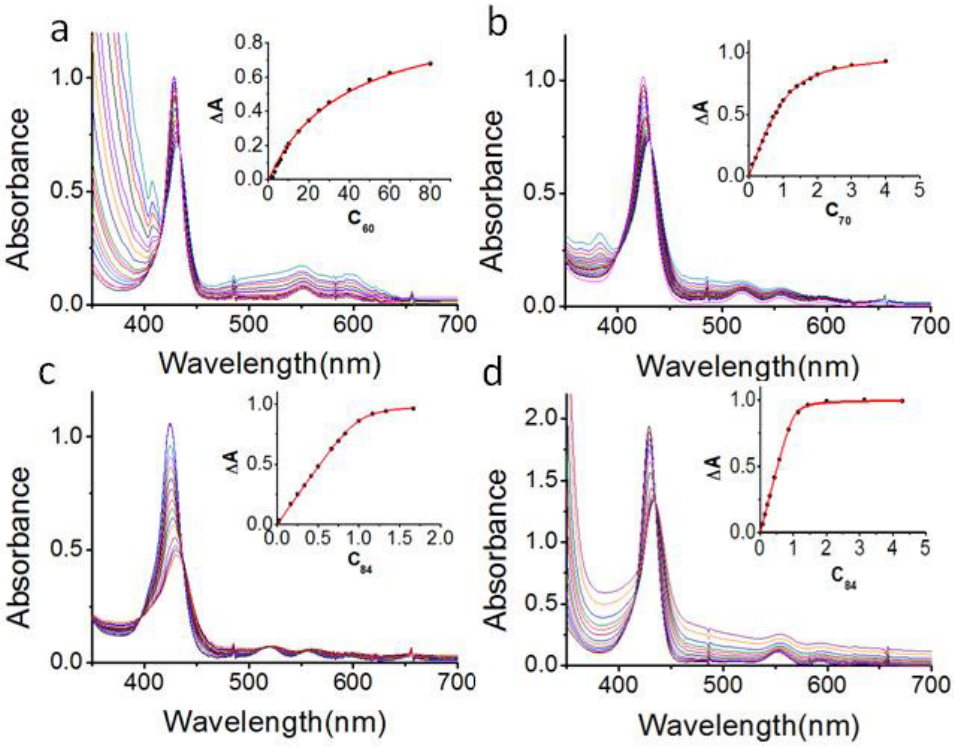

Figure 5.3. UV-vis titration of **94** with C_{60} (a), C_{70} (b), C_{84} (c), and **COP-5** with C_{84} (d). The titration was conducted in toluene, the concentration of **94** was 10^{-6} mol L^{-1}, and the concentration of **COP-5** was 2×10^{-6} mol L^{-1}. Inset: plot of normalized ΔA_{425nm} vs. equivalent of fullerene added. The absorbance at 425 nm was used for the titration of **94**. The absorbance at 428 nm was used for the titration of **COP-5**.

Given the successful bisporphyrin macrocycle synthesis, we next explored its fullerene binding behavior. Macrocycle **94** showed a strong binding interaction with fullerenes. The binding of **94** with C_{60}, C_{70}, and C_{84} was characterized by UV-vis titration experiments in toluene (Fig. 5.3). In all cases, we observed the decrease of the absorption peak at $\lambda_{max}\approx$ 425 nm, and the appearance of a new peak at $\lambda_{max}\approx$ 430 nm. Macrocycle **94** forms a 1:1 host–guest complex with C_{60}, C_{70} and C_{84}, respectively, based on the Job plot. (Fig. 5.4) We also observed the peaks corresponding to the complex C_{70}@**94**, and C_{84}@**94** on the MALDI-TOF MS spectrum of the cage-fullerene mixtures (Fig. 5.5). The association constants of C_{60}, C_{70} and C_{84} with macrocycle

94 were calculated based on the 1:1 binding mode and fitting of the UV-vis adsorption data at 425 nm at different fullerene concentrations. These results are summarized in Table 5.1. Macrocycle **94** forms the most stable complex with C_{84} with a binding constant of 2.2×10^7 M^{-1}, which is three orders of magnitude ($K_{C84}/K_{C60} > 1500$) higher than that of complex C_{60}@**94**.

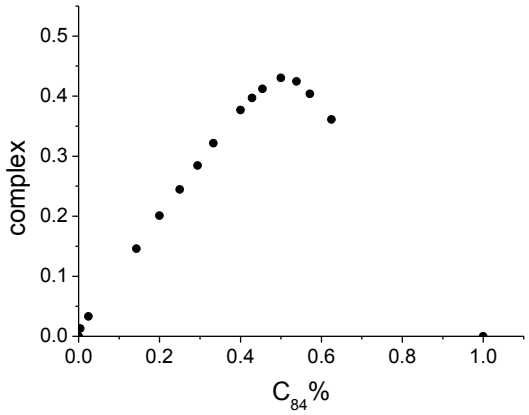

Figure 5.4. The Job plot from the titration of **94** with C_{84}. The highest point at 50% indicates 1:1 binding of **94** and C_{84}.

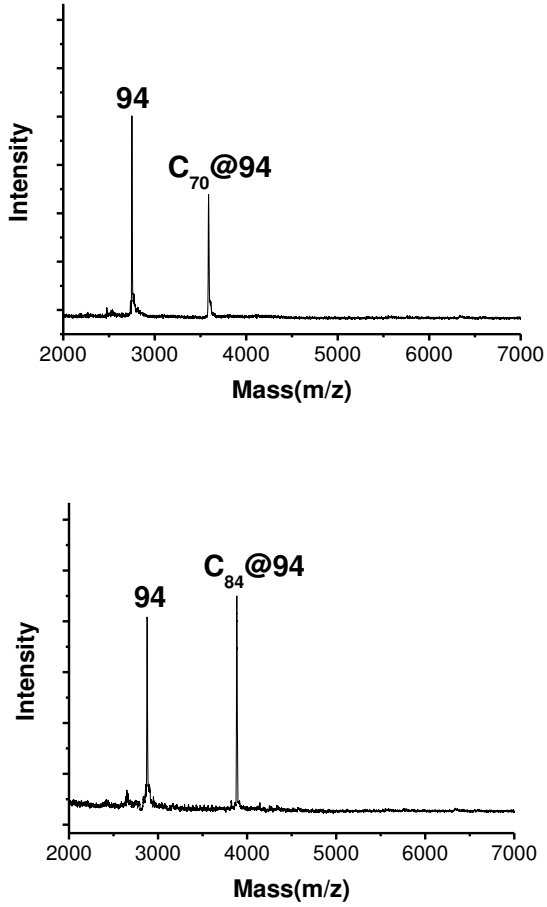

Figure 5.5. The MALDI-TOF Mass Spectra of 1:1 mixtures of **94** and C_{70} and C_{84}: C_{70}@**94** (left), C_{84}@**94** (right). The macrocycle peak was significant, presumably due to the premix of the complexes with acidic matrix solution (2,5-dihydroxybenzoic acid), which triggers the macrocycle-fullerene dissociation.

Table 5.1. Binding constants of **94** and **COP-5** with fullerenes

	K_{C60} (M^{-1})	K_{C70} (M^{-1})	K_{C84} (M^{-1})
94	1.3×10^4	2.0×10^6	2.2×10^7
COP-5	1.4×10^5	1.5×10^8	2.4×10^7

Previously, we reported that the four-armed bisporphyrin cage **COP-5** shows a much higher binding affinity for C_{70} over C_{60}.[13] For comparison purposes, we also measured the binding constant of **COP-5** with C_{84} (Fig. 5.3d), which is smaller than that of **COP-5** with C_{70} (K_{C70}/K_{C84} ~ 10). It is interesting to note that bisporphyrin macrocycle **94** forms the most stable complex with C_{84}, while the four-armed cage analog **COP-5** binds with C_{70} most strongly. Both macrocycle **94** and **COP-5** have two porphyrin moieties connected by the same type of rigid spacers. In order to gain some insight into this different binding preference of **COP-5** and **94**, we took a close look at the structural features of these two host molecules. The energy-minimized model reveals that macrocycle **94** is conformationally rather flexible although it consists of highly rigid aromatic building blocks. The free macrocycle **94** adopts a collapsed conformation with a minimal internal cavity. The ^{1}H NMR spectrum of **94** at 20 ^{o}C shows four sets of aromatic proton signals for the 4-*tert*-butylphenyl rings, which supports the conformation shown in Fig. 5.6.

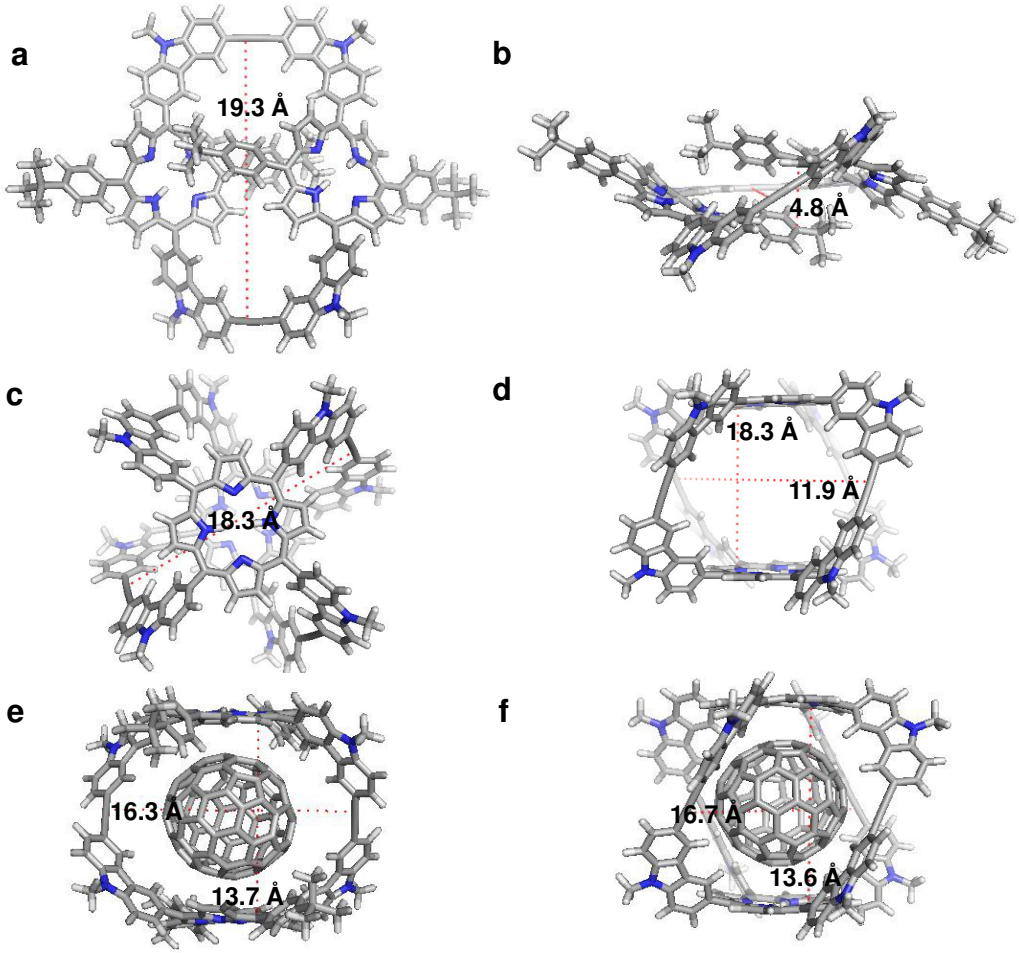

Figure 5.6. Energy-minimized models of **94** (a. top view; b. side view), **COP-5** (c. top view; d. side view), **C$_{84}$@94** (e), and **C$_{84}$@COP-5** (f). Methyl groups were used in the calculation instead of hexadecyl chains for simplification. The height of **94**, and **COP-5** was defined as the distance between the top and bottom porphyrin panels, and the diameters of the inside cavity of **94**, and **COP-5** were defined as the distance between the two ethynylene groups in the diagonal edges.

Upon addition of the fullerene guest, macrocycle **94** can adapt in size to accommodate the guest molecules, undergoing a remarkable geometry change, with an increase in the internal macrocyclic cavity size from 4.8 Å to 19.3 Å. However, cage **COP-5** is relatively rigid, and the size and geometry of the cage do not change much upon the fullerene encapsulation (Fig. 5.3c and d). Due to the high rigidity (shape-persistency) of **COP-5**, presumably C_{70} fits better inside of the

cage cavity, while C_{60} fits more loosely, and C_{84} fits a little bit too tight. Compared to the closed cage **COP-5**, macrocycle **94** has only two side arms, which allows the more bulky C_{84} to fit best in its more open cavity. Given the high binding selectivity of macrocycle **94** toward C_{84}, next we examined the feasibility of the pH-controlled release of C_{84} and regeneration of host macrocycle **94**. Previously, we reported the pH-driven reversible association and dissociation of **COP-5** and fullerene complexes, and successfully demonstrated the easy and efficient separation of C_{70} from a fullerene mixture.[13] Using a similar approach, we show here that C_{84}@**94** is also capable of undergoing the reversible association and dissociation process under acid–base stimuli. Addition of excess TFA (100 equiv.) to the solution of C_{84}@**94** in toluene protonates the porphyrin ring and weakens the porphyrin–fullerene interaction, thus leading to the dissociation of C_{84} and **94**. As a consequence, we observed the broadening and red shift of the adsorption band of C_{84}@**94** with the appearance of a new absorption band at 675 nm (Fig. 5.7). The absorbance of the acidified C_{84}@**22** complex is in good agreement with the acidified **94** itself, which indicates that C_{84} released from the cage. Subsequent addition of triethylamine (100 equiv.) to the abovementioned mixture neutralized the porphyrin ring and restored the binding interaction between **94** and C_{84}. Remarkably, the acid–base-mediated association–dissociation of the host–guest complex could be repeated many times without obvious change in the absorbance. The over 1500 times stronger binding interaction of macrocycle **94** with C_{84} over C_{60} and the reversible nature of this pH-triggered host–guest binding open up the possibility of using such a ‘‘Selective Complexation–Decomplexation’’ approach for purification of higher fullerenes (*e.g.,* C_{84}).

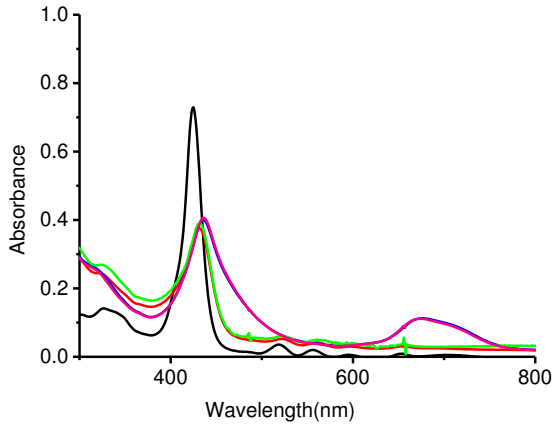

Figure 5.7. The UV-vis absorption spectra of C_{84}@**94** with the stimuli of acid and base. The absorbance of **94** (black); C_{84}@**94** (red); C_{84}@**94** with addition of 100 equiv. of TFA (blue); the C_{84}@**94** with 100 equiv. TFA then add 100 equiv. of TEA (green); **94** with addition of 100 equiv. of TFA (pink). The absorbance of the acidified C_{84}@**94** (blue curve) is in good agreement with the acidified **94** itself (pink curve) which indicates release of C_{84} from the cage under acidic conditions. The overlap of absorption curve of C_{84}@**94** (red) and that after successive treatment with TFA and TEA indicates the TFA-TEA triggered complexation-decomplexation process is reversible.

5.4 Conclusions

In conclusion, bisporphyrin macrocycle **94** with an adaptable cavity was synthesized via alkynemetathesis with high efficiency. The macrocycle showed a high binding selectivity for C_{84} over lower fullerenes, C_{70} and C_{60}, which is in great contrast to its four-armed more rigid cage analogue **COP-5** that shows the highest binding affinity for C_{70}. The significant difference in fullerene binding affinities and selectivity due to the relatively small structure variation of host molecules highlights the subtleness of such molecular recognition events involving fullerene guests. Our findings will contribute to the future design of novel 2-D or 3-D host-guest systems and composite materials, which would facilitate broad applications of fullerenes in various fields.

5.5 Experimental section

5.5.1 Materials and general synthetic methods

Reagents and solvents were purchased from commercial suppliers and used without further purification, unless otherwise indicated. Tetrahydrofuran (THF), toluene, CH_2Cl_2 and dimethylformamide (DMF) are purified by the MBRAUN solvent purification systems. 3-Formyl-*N*-hexadecyl-6-iodo-carbazole (**75**) and 4-benzoyl-4'-ethynylbiphenyl were synthesized following reported procedures.[13]

All reactions were conducted under dry nitrogen in oven-dried glassware, unless otherwise specified. Solvents were evaporated using a rotary evaporator after workup. Unless otherwise specified, the purity of the compounds was ≥95% based on ^{1}H NMR spectral integration.

Flash column chromatography was performed by using a 100-150 times weight excess of flash silica gel 32-63 μm from Dynamic Absorbants Inc. Fractions were analyzed by TLC using TLC silica gel F254 250 μm precoated-plates from Dynamic Absorbants Inc. Analytical gel permeation chromatography (GPC) was performed using a Viscotek GPCmaxTM, a Viscotek Model 3580 Differential Refractive Index (RI) Detector, a Viscotek Model 3210 UV/VIS Detector and a set of two Viscotek Viscogel columns (7.8 × 30 cm, l- MBLMW-3078, and l-MBMMW-3078 columns) with THF as the eluent at 30 °C. The analytical GPC was calibrated using monodisperse polystyrene standards. UV-vis absorption measurements were carried out with an Agilent 8453 spectrophotometer.

MALDI MS spectra were obtained using a Voyager-DE™ STR Biospectrometry Workstation using 2,5-dihydroxybenzoic acid (DHB) as the matrix. The high resolution Mass spectra were obtained on Waters SYNAPT G2 High Definition Mass Spectrometry System.

Analyte molecules were diluted into ESI solvents, either methanol or acetonitrile/water mixture, for final concentrations of 10 ppm or lower. The solution was injected into the electrospray ionization (ESI) source at a rate of 5 μL/min. Either the ESI^+ or ESI^- mode was used in reference to the molecular properties. Accurate mass analysis was performed by using the Lock Mass calibration feature with the instrument.

NMR spectra were taken using Inova 400 and Inova 500 spectrometers. $CHCl_3$ (7.27 ppm), toluene (2.09 ppm) were used as internal references in ^1H NMR, and $CHCl_3$ (77.23 ppm) for ^{13}C NMR. ^1H NMR data were reported in order: chemical shift, multiplicity (s, singlet; d, doublet; t, triplet; q, quartet; m, multiplet), coupling constants (*J*, Hz), number of protons.

The Amber 11.0 molecular dynamics program package was used to optimize the structure of the fullerene, the cage and the cage/fullerene binding complexes. The force field used was the general Amber force field (GAFF field) with the charge parameters computed by AM1-BCC method. For each structure optimization run, the molecule was first minimized for 1000 steps using the conjugate gradient method, and then it was further optimized by simulated annealing method for 150 picosecond with a time-step of 1 femtosecond. During the simulated annealing, the system temperature was first raised up to 1000 K for 50 picoseconds and then gradually cooled to 0 K for another 100 picoseconds. Finally, the annealed structure was minimized again for another 1000 conjugate gradient steps and the final energy was recorded. The non-bonded interactions during the simulation were computed directly with a cutoff distance of 25 Å. A dielectric constant of 4.8 was assumed during the simulation, which is a typical value for organic solvents.

5.5.2. Experimental procedures

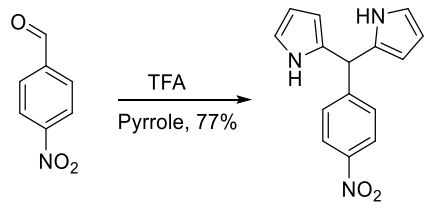

73

4-Nitrophenyl-dipyrrolemethane (**73**): To a solution of 4-nitrobenzaldehyde (0.756 g, 5.0 mmol) in pyrrole (15 mL) was added catalytic amount of TFA (0.57 g, 0.50 mmol). The mixture was stirred at rt for 15 min. Upon completion of the reaction, dilute NaOH solution (1 M, 15 mL) was added to quench the reaction. The product was extracted with CH_2Cl_2 (3 x 20 mL). After evaporating the solvent, purification by flash column chromatography using CH_2Cl_2 as the eluent, the product was obtained as a grey solid (1.026g, 77%). ^{1}H NMR ($CDCl_3$, 500 MHz): δ 8.16 (d, 2H, J =8.5 Hz), 7.99 (s, 2H), 7.39 (d, 2H, J =8.5Hz), 6.76 (dd, 2H, J_1 =4.1Hz, J_2=2.6Hz), 6.19 (dd, 2H, J_1 =5.9Hz, J_2 =2.9Hz), 5.88 (s, 2H), 5.60(s, 1H).

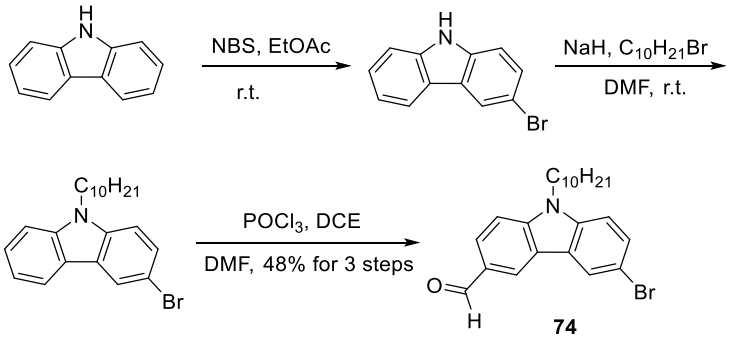

74

3-Formyl-N-decyl-6-bromo-carbazole (74b): To a solution of carbazole (5.00 g, 30 mmol) dispersed in ethyl acetate (150 mL), NBS (6.41 g, 36 mmol) in ethyl acetate (100 mL) was added slowl. The reaction was stirred at ambient temperature for 16 h. The reaction was quenched with aqueous Na_2SO_3. The mixture was extracted with CH_2Cl_2 (80 mL×3). The organic extracts were combined and the volatiles were removed. The crude product was collected as a white solid. (~60%

yield was determined by crude NMR integration.), and was used in the next step without further purification. The crude 3-bromocarbazole was dissolved in DMF (100 mL). NaH (1.80 g, 45 mmol, 60% dispersion in mineral oil) was added to the reaction mixture and stirred for 5 min at room temperature. Then 1-bromohexadecane (13.74 g, 45 mmol) was added and stirred for 4 h at room temperature. After completion of the reaction, the solvent was removed and the product was washed with HCl (1M, 100 mL). Extraction with CH_2Cl_2 (80 mL×3) followed by purification via flash column chromatography (CH_2Cl_2/hexane, 1/3, v/v) provided N-hexadecyl-3-iodo-carbazole as a white solid. To a mixture of DMF (47 mL, 600 mmol) and 1,2-dichloroethane (50 mL) was added $POCl_3$ (47.5 mL, 510 mmol) dropwise at 0 °C., The mixture was then heated to 35 °C and N-hexadecyl-3-bromo-carbazole was added. After stirring for 24 h at 90 °C, the mixture was cooled to room temperature, then poured to water (500 mL). The product was extracted with chloroform (150 mL×3), dried over $MgSO_4$ and purified via flash column chromatography (CH_2Cl_2/hexane, 1/1, v/v) to provide the pure product **75** as a white solid (7.85 g, Yield: 48 %.); ^{1}H NMR ($CDCl_3$, 500 MHz) δ 10.10 (s, 1H), 8.56 (d, *J* = 1.5 Hz, 1H), 8.27 (d, *J* = 1.9 Hz, 1H), 8.05 (dd, *J* = 8.5, 1.6 Hz, 1H), 7.62 (dd, *J* = 8.7, 1.9 Hz, 1H), 7.49 (d, *J* = 8.5 Hz, 1H), 7.34 (d, *J* = 8.6 Hz, 1H), 4.32 (t, *J* = 7.2 Hz, 2H), 1.88 (p, *J* = 7.3 Hz, 2H), 1.45 – 1.13 (m, 14H), 0.87 (t, *J* = 7.0 Hz, 3H).

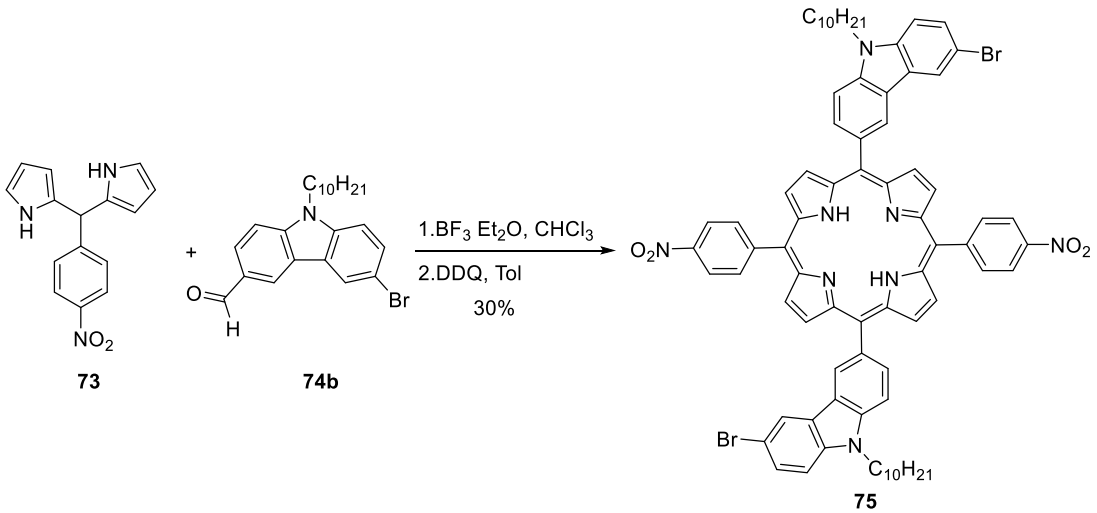

Compound 75: To a solution of compound **73** (1.07 g, 4.0 mmol) and **74b** (1.66 g, 4.0 mmol) in chloroform (200 mL) was added $BF_3 \cdot Et_2O$ (0.16 mL) dropwise at rt. The reaction mixture was stirred for 1 hour at r.t.. A solution of 2,3-dichloro-5,6-dicyanobenzoquinone (0.68 g, 3.0 mmol) in toluene (10 mL) was added slowly. After stirring 1 hour at ambient temperture, the reaction mixture was filtered through a silica gel pad. The volatiles were removed and the residue was purified by flash column chromatography (CH_2Cl_2/hexane, 1/1 v/v) to provide the product **75** as a purple solid (894 mg, 30%). ^{1}H NMR ($CDCl_3$, 500 MHz) δ 8.95 (d, *J* = 4.8 Hz, 4H), 8.88 – 8.85 (m, 2H), 8.76 (d, *J* = 4.8 Hz, 4H), 8.69 – 8.61 (m, 4H), 8.51 (d, *J* = 1.7 Hz, 2H), 8.43 (d, *J* = 8.6 Hz, 4H), 8.36 (dt, *J* = 8.3, 1.2 Hz, 2H), 7.83 (dd, *J* = 8.8, 1.7 Hz, 2H), 7.77 (d, *J* = 8.3 Hz, 2H), 7.39 (d, *J* = 8.8 Hz, 2H), 4.53 (t, *J* = 7.3 Hz, 4H), 2.10 (p, *J* = 7.4 Hz, 4H), 1.62 – 1.52 (m, 4H), 1.52 – 1.42 (m, 4H), 1.41 – 1.18 (m, 20H), 0.87 (t, *J* = 6.9 Hz, 6H).

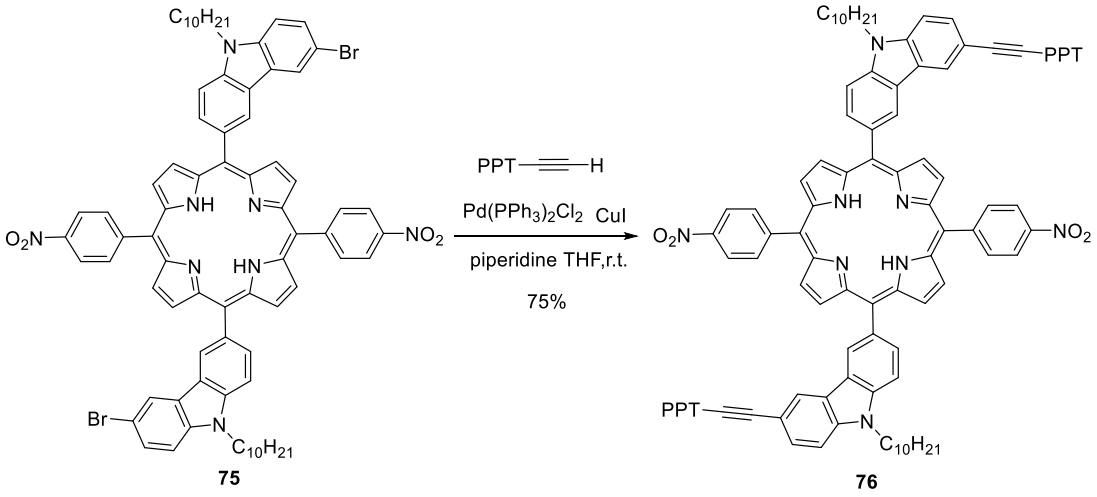

Compound 76: The general Sonogashira's procedure was followed. Using compound **75** (745 mg, 0.5 mmol), 4-benzoyl-4'-ethynyl-biphenyl (366 mg, 1.3 mmol), $Pd(PPh_3)_2Cl_2$ (21 mg, 0.03 mmol), CuI (1.0 mg, 0.005 mmol), piperidine (5 mL), and THF (25 mL). Flash column chromatography (CH_2Cl_2/hexane, 2/1, v/v) gives pure product as a yellowish solid (709 mg, 75%); ^{1}H NMR ($CDCl_3$,

500 MHz) δ 8.98 (d, *J* = 4.8 Hz, 4H), 8.94 (d, *J* = 1.7 Hz, 2H), 8.79 – 8.75 (m, 4H), 8.66 (dd, *J* = 8.8, 1.8 Hz, 4H), 8.46 – 8.42 (m, 6H), 8.39 (dd, *J* = 8.3, 1.7 Hz, 2H), 7.88 (d, *J* = 7.2 Hz, 2H), 7.84 – 7.78 (m, 8H), 7.72 – 7.68 (m, 4H), 7.64 – 7.57 (m, 12H), 7.50 (td, *J* = 7.7, 1.5 Hz, 4H), 4.59 (t, *J* = 7.3 Hz, 4H), 2.15 (p, *J* = 7.4 Hz, 4H), 1.61 (p, *J* = 7.5 Hz, 4H), 1.50 (p, *J* = 7.0 Hz, 4H), 1.44 – 1.16 (m, 44H), 0.86 (t, *J* = 6.9 Hz, 6H).

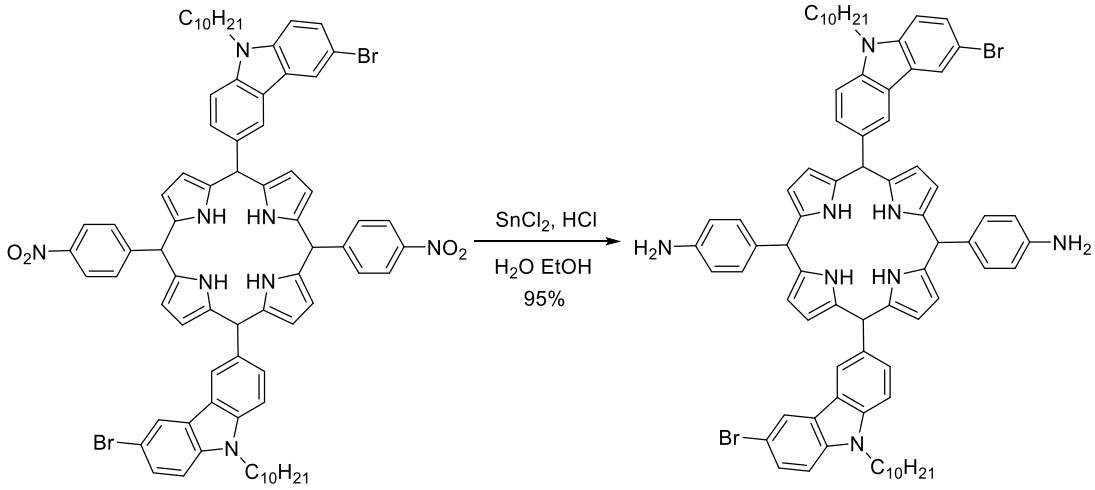

Compound 78: To a solution of **75** (745 mg, 0.5 mmol) in ethanol (50 mL) and hydrochloric acid (45 mL, 36% aq.), $SnCl_2$ (1.90 g, 10 mmol) was added and the reaction was stirred at 70 °C for 6 hours. After reaction completion, the reaction was cooled to ambient temperature and then neutralized with NH_4OH aqueous solution. Followed by extraction with CH_2Cl_2 and column chromatography (CH_2Cl_2/hexane/TEA, 50/50/1, v/v/v) to provide the product as purple solid. (682 mg, 95%); ^{1}H NMR ($CDCl_3$, 500 MHz) δ 8.93 (d, *J* = 4.8 Hz, 2H), 8.89 (s, 2H), 8.86 (d, *J* = 4.8 Hz, 2H), 8.50 (t, *J* = 1.4 Hz, 2H), 8.39 – 8.35 (m, 2H), 8.04 (d, *J* = 8.3 Hz, 4H), 7.82 (dd, *J* = 8.8, 1.7 Hz, 2H), 7.74 (d, *J* = 8.2 Hz, 2H), 7.38 (d, *J* = 8.8 Hz, 2H), 7.08 (d, *J* = 8.3 Hz, 4H), 4.53 (t, *J* = 7.3 Hz, 4H), 4.02 (s, 4H), 2.10 (p, *J* = 7.5 Hz, 4H), 1.64 – 1.18 (m, 48H), 0.90 – 0.85 (t, *J* = 6.9 Hz, 6H).

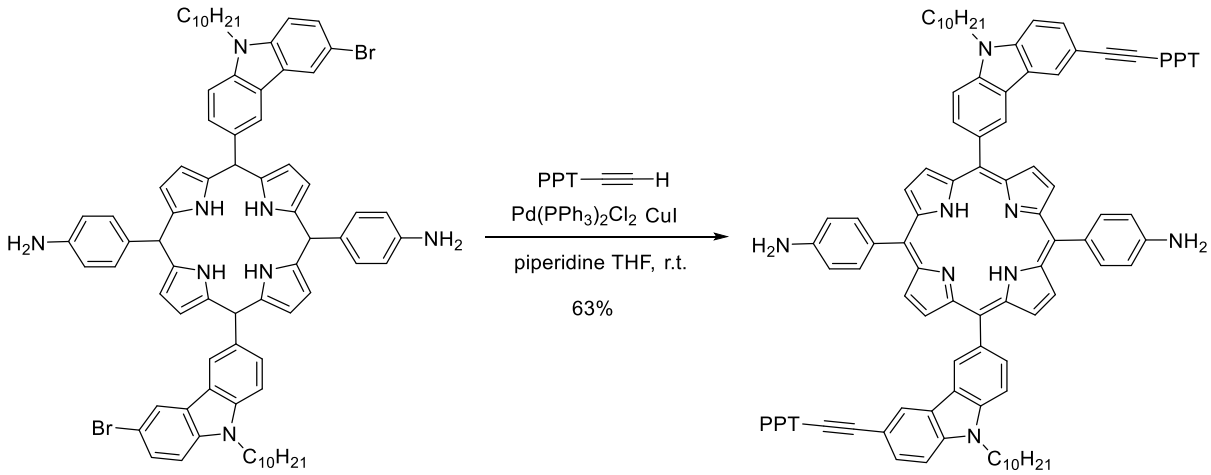

Compound 79: The general Sonogashira's procedure was followed. Using compound **78** (500 mg, 0.33 mmol), 4-benzoyl-4'-ethynyl-biphenyl (281 mg, 1 mmol), $Pd(PPh_3)_2Cl_2$ (28 mg, 0.04 mmol), CuI (0.6 mg, 0.003 mmol), piperidine (2 mL), and THF (20 mL). Flash column chromatography (CH_2Cl_2/TEA, 100/1, v/v) gives pure product as a yellowish solid (380 mg, 63%): ^{1}H NMR ($CDCl_3$, 500 MHz) δ 8.99 – 8.94 (m, 6H), 8.91 (d, *J* = 4.6 Hz, 4H), 8.44 (s, 2H), 8.40 (dd, *J* = 8.3, 1.7 Hz, 2H), 8.05 (d, *J* = 8.1 Hz, 4H), 7.88 (d, *J* = 8.4 Hz, 4H), 7.85 – 7.81 (m, 4H), 7.81 – 7.74 (m, 4H), 7.69 (d, *J* = 8.5 Hz, 4H), 7.65 – 7.55 (m, 14H), 7.50 (t, *J* = 7.6 Hz, 4H), 7.06 (d, *J* = 8.4 Hz, 4H), 4.56 (t, *J* = 7.3 Hz, 4H), 4.01 (s, 4H), 2.13 (p, *J* = 7.3 Hz, 4H), 1.66 – 1.17 (m, 48H), 0.88 (t, *J* = 6.9 Hz, 6H).

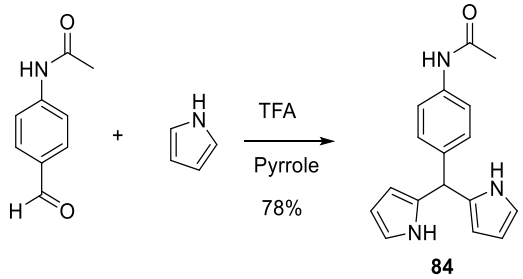

4-Acetylaminophenyl-dipyrrolemethane (**84**): To a solution of N-(4-formylphenyl)acetamide (0.816 g, 5.0 mmol) in pyrrole (15 mL) was added catalytic amount of TFA (0.57 g, 0.50 mmol). The mixture was stirred at r.t. for 15 min. Upon completion of the reaction, dilute NaOH solution (1 M, 15 mL) was added to quench the reaction. The product was extracted with CH_2Cl_2 (3 x 20 mL). After evaporating the solvent, purification by flash column chromatography using CH_2Cl_2 as the eluent, the product was obtained as a grey solid (1.09 g, 78%). ^{1}H NMR ($CDCl_3$, 500 MHz) δ 7.95 (s, 2H), 7.44 (d, *J* = 8.5 Hz, 2H), 7.18 (d, *J* = 8.5 Hz, 2H), 7.16 (s, 1H), 6.71 (td, *J* = 2.7, 1.6 Hz, 2H), 6.16 (q, *J* = 2.9 Hz, 2H), 5.92 (s, 2H), 5.46 (s, 1H), 2.18 (s, 3H).

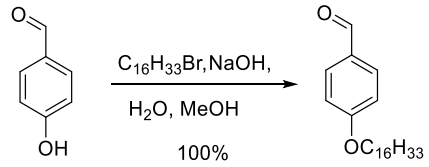

86

4-(hexyldecyloxy)benzaldehyde (86): To a solution of 4-hydroxylbenzaldehyde (2.45 g, 20 mmol) in 50 mL ethanol, 85 mL of 0.25 M NaOH was added and the mixture was stirred at ambient temperature for 15 min yield a clear deep red solution. The water was then removed by evaporation and the solid was dissolved in DMF (100 mL). The 1-bromohexadecane was then added and the solution was stirred at 70 ºC for 48 hours. After reaction, evaporate off the solvent followed by recrystallization from yields product as white crystals (6.93 g, 100%). ^{1}H NMR ($CDCl_3$, 500 MHz) δ 9.89 (s, 1H), 7.84 (d, *J* = 8.7 Hz, 2H), 7.00 (d, *J* = 8.7 Hz, 2H), 4.05 (t, *J* = 6.6 Hz, 2H), 1.82 (dt, *J* = 14.7, 6.7 Hz, 2H), 1.58 – 1.14 (m, 26H), 0.89 (t, *J* = 6.9 Hz, 3H).

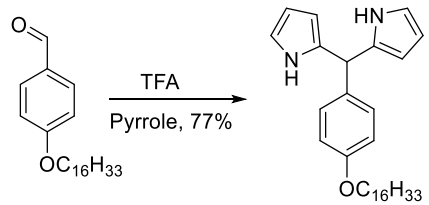

86 **87**

4-(Hexyldecyloxy)phenyl-dipyrrolemethane (87): Similar reaction condition as for compound **73** was followed. Using **86** (1.73 g, 5.0 mmol), pyrrole (15 mL), TFA (0.57 g, 0.50 mmol). Purification by flash column chromatography using CH_2Cl_2 as the eluent, the product was obtained as a white solid (1.78 g, 77%). ^{1}H NMR ($CDCl_3$, 500 MHz) δ 7.92 (s, 2H), 7.13 (d, *J* = 8.6 Hz, 2H), 6.85 (d, *J* = 8.8 Hz, 2H), 6.70 (td, *J* = 2.7, 1.6 Hz, 2H), 6.17 (q, *J* = 2.9 Hz, 2H), 5.96 – 5.87 (m, 1H), 5.44 (s, 1H), 3.94 (t, *J* = 6.6 Hz, 2H), 1.78 (td, *J* = 8.7, 6.7 Hz, 2H), 1.51 – 1.19 (m, 26H), 0.96 – 0.82 (m, 2H).

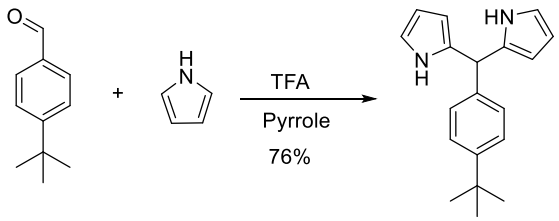

91

4-*tert*-butylphenyl-dipyrrolemethane (91): Similar reaction condition as for compound **73** was followed. Using 4-*tert*-butylbenzaldehyde (0.81 g, 5.0 mmol), pyrrole (15 mL), TFA (0.57 g, 0.50 mmol). Purification by flash column chromatography using CH_2Cl_2 as the eluent, the product was obtained as a white solid (1.06 g, 76 %): ^{1}H NMR (500 MHz, $CDCl_3$) δ 7.93 (s, 2H), 7.34 (d, *J* = 8.2 Hz, 3H), 7.15 (d, *J* = 8.2 Hz, 2H), 6.71 (m, 2H), 6.17 (m, 2H), 5.95 (m, 2H), 5.47 (s, 1H), 1.31 (s, 9H); ^{13}C NMR (100 MHz, $CDCl_3$) δ 31.4, 34.6, 43.6, 107.2, 108.5, 117.2, 125.7, 128.2, 132.9, 139.1, 149.9.

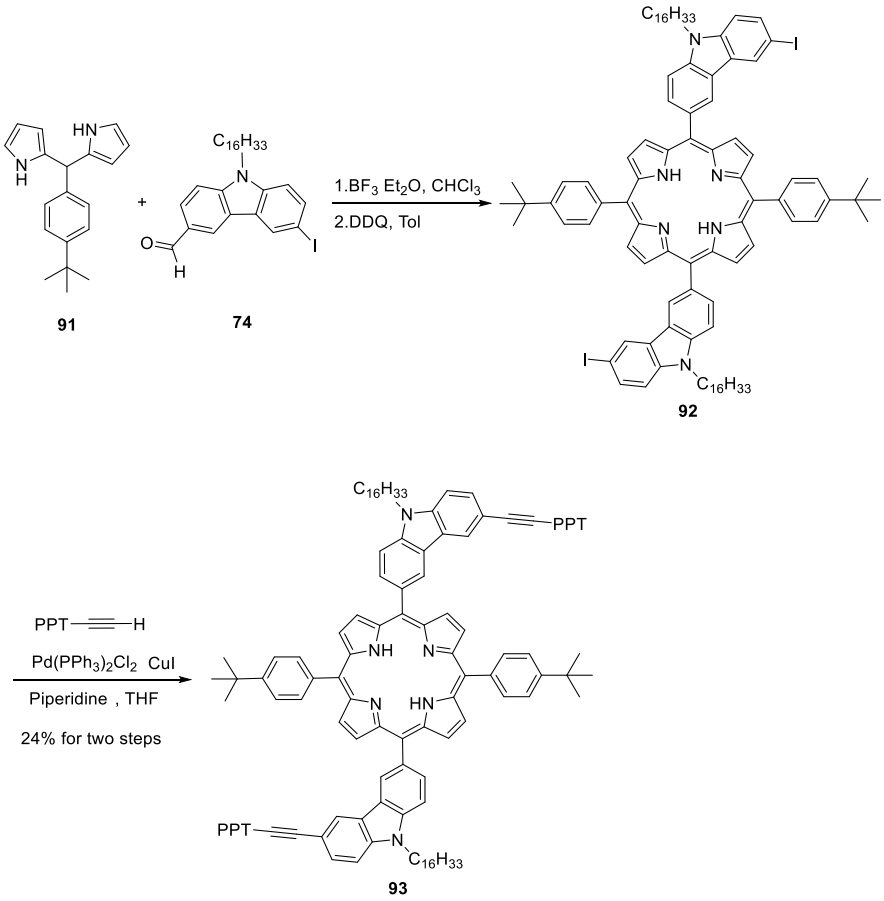

Compound 93: To a solution of dipyrrolemethane **91** (278 mg, 1.00 mmol) and aldehyde **74** (546 mg, 1.00 mmol) in chloroform (100 mL) was added $BF_3 \cdot OEt_2$ (40 μL) dropwise. The reaction mixture was stirred for 1 hour at r.t.. A solution of DDQ (0.17 g, 0.75 mmol) in toluene was added slowly. After stirring 1 hour at r.t., the reaction mixture was filtered through a silica gel pad. The volatiles were removed and the crude product was purified by flash column chromatography (CH_2Cl_2/hexane, 1/1, v/v). The resulting porphyrin mixture was subjected to the next step. The general procedure for Sonogashira coupling was followed. Using compound **92** (428 mg, 0.53 mmol), 4-benzoyl-4'-ethynylbiphenyl (367 mg, 1.3 mmol), $Pd(PPh_3)_2Cl_2$ (22 mg, 0.032 mmol), CuI (3 mg, 0.016 mmol), piperidine (10 mL), and THF (50 mL). The product **93** was obtained as a purple solid (230 mg, 24 %): ^{1}H NMR (400 MHz, $CDCl_3$) δ 8.98 (s, 2H), 8.92 (s, 8H), 8.46 –

8.37 (m, 4H), 8.20 (d, J = 8.2 Hz, 4H), 7.93 – 7.44 (m, 36H), 4.53 (t, J = 6.7 Hz, 4H), 2.14 (m, 4H), 1.61 (s, 18H), 1.51 – 1.12 (m, 52H), 0.95 – 0.78 (m, 6H), -2.55 (s, 2H); ^{13}C NMR (100 MHz, $CDCl_3$) δ 196.50, 150.67, 144.62, 141.26, 140.68, 139.50, 139.17, 137.91, 136.55, 134.78, 133.87, 133.54, 132.62, 132.19, 131.00, 130.22, 129.84, 128.59, 128.53, 127.33, 127.12, 126.97, 126.92, 124.74, 124.10, 123.87, 123.27, 121.44, 120.96, 120.84, 120.56, 120.44, 113.69, 109.33, 107.16, 92.48, 87.71, 43.93, 35.14, 32.17, 31.94, 29.96, 29.92, 29.88, 29.77, 29.61, 29.50, 27.75, 22.94, 14.39; MALDI-TOF(m/z): $[M+H]^+$ calcd. for $C_{138}H_{140}N_6O_2$, 1915.12; found: 1915.14.

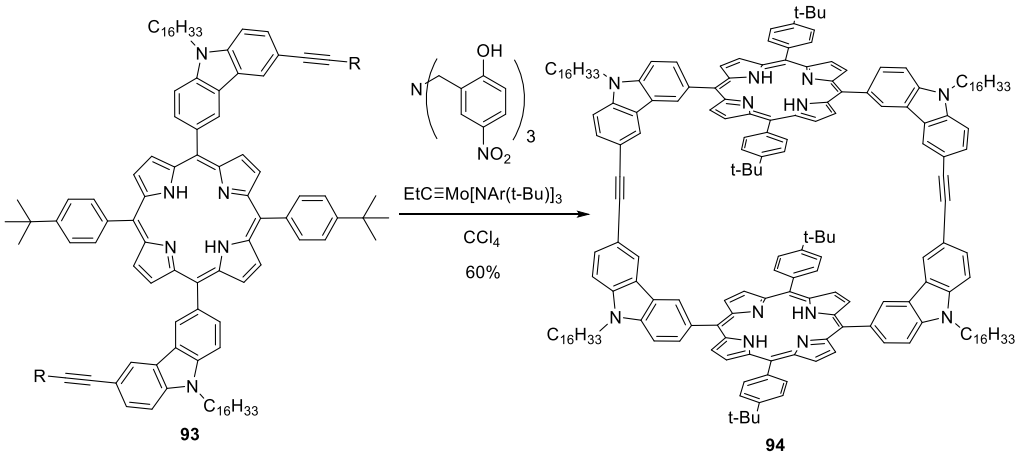

Compound 94: The target macrocycle compound **94** was obtained by following typical precipitation-driven alkyne metathesis procedures.[8] The multidentate ligand (1.5 mg, 0.0032 mmol) and the Mo(VI) carbyne precursor (2.0 mg, 0.0031 mmol) were premixed in dry carbon tetrachloride (3 mL) for 5 minutes to generate the catalyst in situ. Subsequently, the monomer **93** (77 mg, 0.040 mmol) was added and the stirring was continued at 45 °C overnight. The reaction was monitored by GPC. Upon completion of the reaction, the reaction mixture was filtered to remove the byproduct. The filtrate was concentrated and subjected to column chromatography over alumina adsorption (CH_2Cl_2/hexane, 1/2, v/v). The product **94** was obtained as a purple solid (33 mg, 60 %): ^{1}H NMR (400 MHz, $CDCl_3$) δ 8.78 (s, 4H), 8.75 (s, 16H), 8.35 – 8.28 (m, 8H),

8.04 (d, J = 7.9 Hz, 4H), 7.98 (d, J = 7.9 Hz, 4H), 7.79 (dd, J = 8.8, 1.4 Hz, 4H), 7.71-7.59 (m, 12H), 7.54 (d, J = 8.8 Hz, 4H), 4.53 (s, 8H), 2.19 – 1.99 (m, 8H), 1.69 – 1.55 (m, 8H), 1.54 (s, 36H), 1.45 (m, 8H), 1.41 – 1.16 (m, 88H), 0.87 (t, J = 6.8 Hz, 12H), -2.82 (s, 4H); ^{13}C NMR (100 MHz, $CDCl_3$) δ 150.41, 140.80, 140.57, 140.21, 139.37, 134.58, 134.49, 133.67, 132.81, 131.33, 129.44, 126.73, 124.26, 123.76, 123.60, 123.18, 121.26, 120.62, 120.32, 114.55, 109.15, 106.78, 89.21, 43.89, 35.12, 35.04, 32.15, 31.87, 29.95, 29.92, 29.91,29.90, 29.77, 29.70, 29.66, 29.60, 29.50, 27.76, 22.92, 14.37. MALDI-TOF (m/z): $[M+H]^+$ calcd. for $C_{196}H_{228}N_{12}$, 2752.84; found: 2752.53.

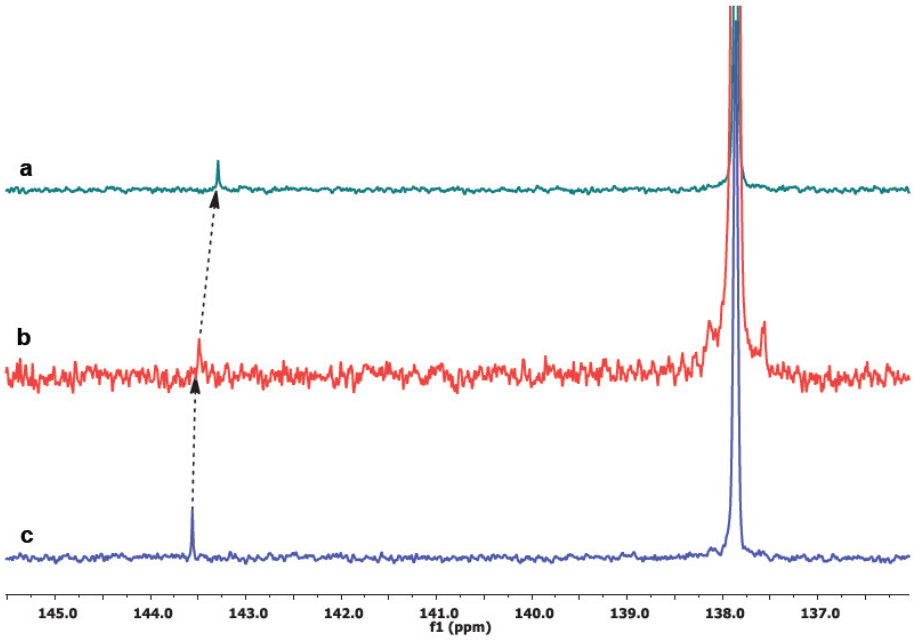

Figure 5.8. The ^{13}C NMR Spectra of (a) 2:1 mixture of C_{60}:**94**; (b) 1:1:1 mixture of C_{60}:C_{84}:**94**; (c) free C_{60} in toluene-d_8 at 20 °C. The C_{60} signal shifts to the higher field in (a) due to the shielding effect from macrocycle-fullerene binding interaction. However, in the presence of 1 equiv. of C_{84}, the binding between C_{60} and **94** is less favored due to their significantly lower binding affinity, thus leading to the C_{60} signal shifting back almost to the same position as in the free C_{60} case (c).

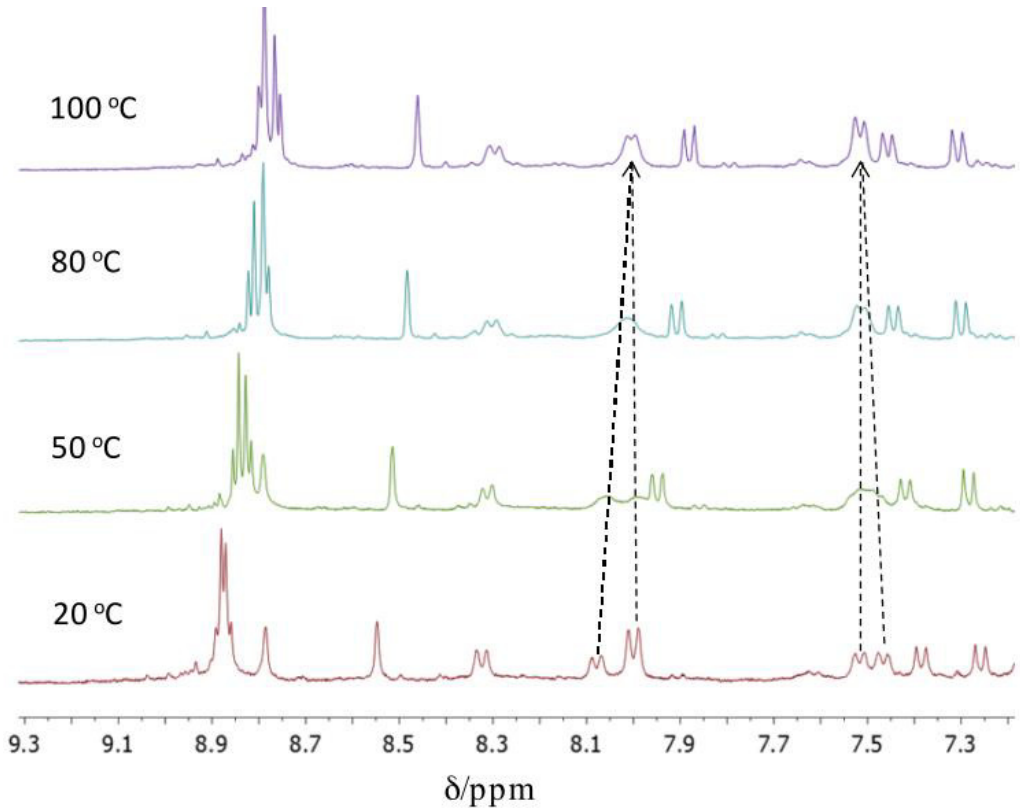

Figure 5.9. Variable temperature ^{1}H NMR spectra of the macrocycle **94** in toluene-d_8: 20 °C (red), 50 °C (green), 80 °C (blue), 100 °C (purple). The spectrum at 20 °C shows four sets of aromatic proton peaks for the *t*-butylphenyl groups. However, at elevated temperatures, those peaks coalesced into two sets. Such observation is consistent with the computer modeling study. At room temperature, two of those four phenyl groups are very close to porphyrin moieties due to the collapsed conformation of macrocycle **94**, thus showing different chemical shifts from the other two phenyl groups. However, at elevated temperatures, the rapid conformational interconversion leads to coalesce of their NMR signals.

5.6 References

1. Zhang, C. X.; Long, H.; Zhang, W. *Chem. Commun.* **2012**, *48*, 6172.

2. Babu, S. S.; Moehwald, H.; Nakanishi, T. *Chem. Soc. Rev.* **2010**, *39*, 4021.

3. Pivrikas, A.; Sariciftci, N. S.; Juska, G.; Osterbacka, R. *Prog. Photovolt: Res. Appl.* **2007**, *15*, 677.

4. Stephens, P. W.; Cox, D.; Lauher, J. W.; Mihaly, L.; Wiley, J. B.; Allemand, P. M.; Hirsch, A.; Holczer, K.; Li, Q.; Thompson, J. D.; Wudl, F. *Nature* **1992**, *355*, 331.

5. Nagata, K.; Dejima, E.; Kikuchi, Y.; Hashiguchi, M. *Chem. Lett.* **2005**, *34*, 178.

6. Bucsi, I.; Aniszfeld, R.; Shamma, T.; Prakash, G. K. S.; Olah, G. A. *Proc. Natl. Acad. Sci.* **1994**, *91*, 9019.

7. Gil-Ramirez, G.; Karlen, S. D.; Shundo, A.; Porfyrakis, K.; Ito, Y.; Briggs, G. A. D.; Morton, J. J. L.; Anderson, H. L. *Org. Lett.* **2010**, *12*, 3544.

8. Perez, E. M.; Martin, N. *Chem. Soc. Rev.* **2008**, *37*, 1512.

9. Komatsu, N. *J. Inclusion Phenom. Macrocycl. Chem.* **2008**, *61*, 195.

10. Tashiro, K.; Aida, T. *Chem. Soc. Rev.* **2007**, *36*, 189.

11. Bunz, U. H. F.; Rubin, Y.; Tobe, Y. *Chem. Soc. Rev.* **1999**, *28*, 107.

12. Atwood, J. L.; Koutsantonis, G. A.; Raston, C. L. *Nature* **1994**, *368*, 229.

13. Zhang, C. X.; Wang, Q.; Long, H.; Zhang, W. *J. Am. Chem. Soc.* **2011**, *133*, 20995.

14. Geier, G. R.; Littler, B. J.; Lindsey, J. S. *J. Chem. Soc. Perkin. Trans. 2* **2001**, 701.

15. Jyothish, K.; Zhang, W. *Angew. Chem. Int. Ed.* **2011**, *50*, 3435.

16. Geier, G. R.; Lindsey, J. S. *J. Chem. Soc. Perkin. Trans. 2* **2001**, 687.

CHAPTER 6

Conclusions and Future Work

6.1 Overview of objectives

The objectives of this thesis research were to construct various molecular architectures using dynamic covalent chemistry and study their properties, such as host-guest chemistry, self-aggregation and light harvesting. A series of shape-persistent phenylene vinylene macrocycles and rigid molecular cages are successfully constructed as described in previous chapters. Next, we would like to pursue the development of organic frameworks consisting of these well-defined molecular cage building blocks. The advantages of such design include precise structure/function control and modularity. Currently, there exist two large groups of organic frameworks: metal organic frameworks (MOFs) and covalent organic frameworks (COFs). MOFs consist of metal ions and organic ligands, and they have attracted massive amount of research interests, particularly in the past decade. Compared to the excessive study on MOFs, the research efforts devoted to COFs have lagged behind. The "*cage-to-framework*" strategy proposed herein would provide a powerful platform for developing a variety of organic porous materials (*organic cage frameworks*) targeting different applications.

6.2 Introduction

Metal organic frameworks (MOFs) have been intensely investigated, given their efficient synthesis[1-3] as well as wide applications in host-guest chemistry[4-6] and catalysis.[7,8] However, the frameworks constructed by purely organic building blocks (*e.g.*, COFs) have received much less

attention. The COF research was pioneered by Yaghi and coworkers. In 2005, they reported the synthesis of a two-dimensional (2-D) COF using dynamic boronic acid condensation reaction from a very simple precursor 1,4-benzenediboronic acid (BDBA) (Fig. 6.1).[9] This represents the first example of a porous and crystalline organic framework. The powder X-ray diffraction (PXRD) data confirmed the crystallinity of the COF and its pore size. The interlayer spacing was also calculated.

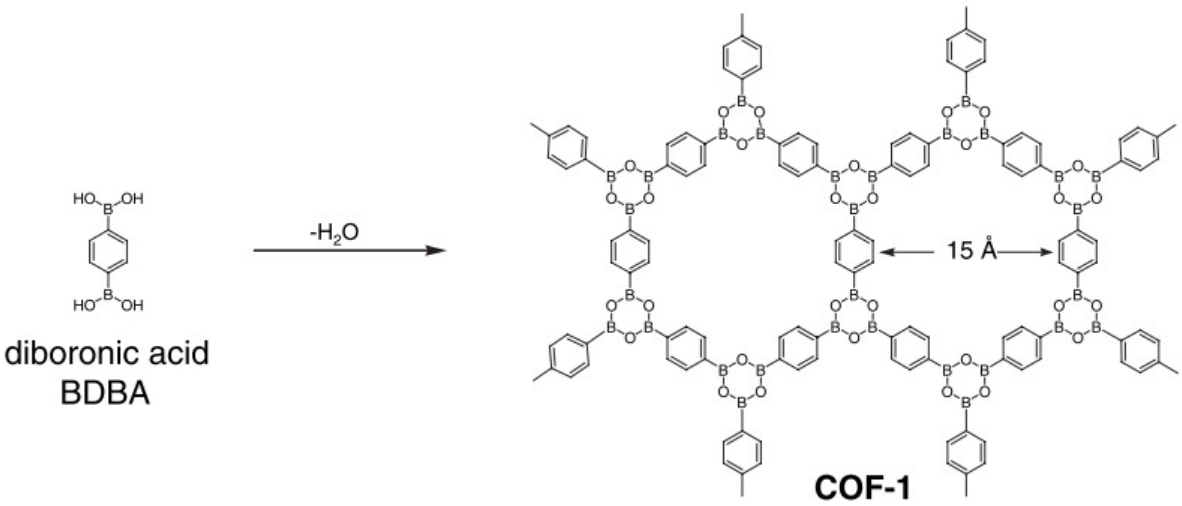

Figure 6.1. Synthesis of COF-1 through boronic acid condensation.

Three-dimensional (3-D) covalent organic frameworks were also reported by Yaghi and coworkers in 2007.[10] With rational design, the 3-D COFs were synthesized using boronic acid-diol condensation reaction. The obtained 3-D COFs exhibit high BET surface area (3472 and 4210 $m^2 g^{-1}$) as well as low density (as low as 0.17 g/cm^3). All these interesting properties enabled a very important application - gas molecule storage (*e.g.*, hydrogen storage).[11] The computation simulations showed a maximum excess H_2 uptake of 10 wt % at 77 K for **COF-105** and **COF-108**,

a total H_2 uptake of 18.9 wt % at 77 K for **COF-108** (Fig. 6.2). These excellent results suggest COFs are highly promising materials for H_2 storage.

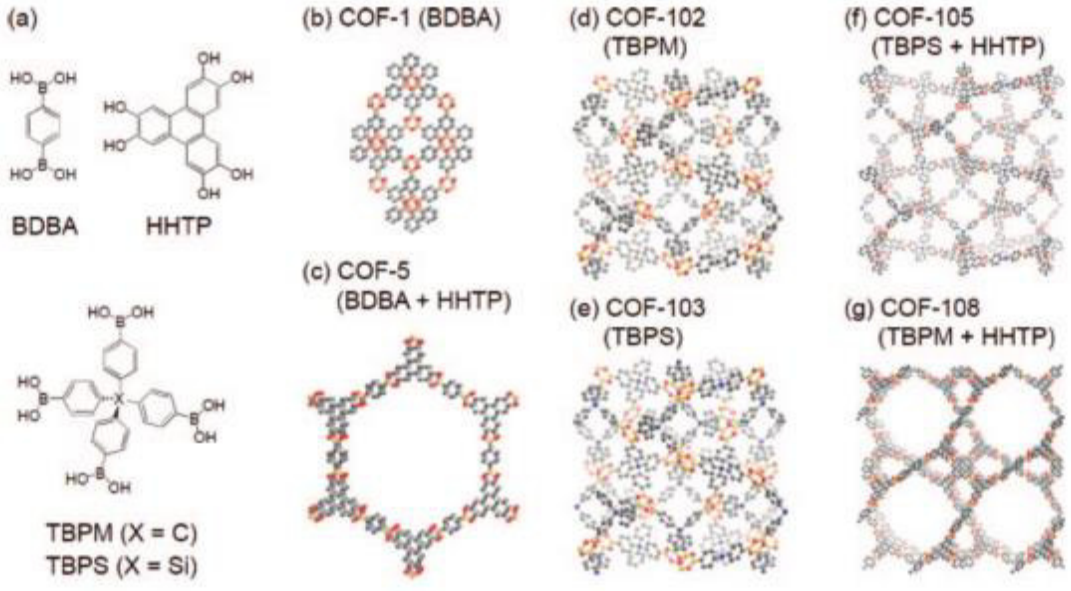

Figure 6.2. The COFs synthesized by Yaghi group and their building blocks. (Reproduced from reference 11.)

Further studies on COFs are mainly focused on their structural design and their applications in gas storage, heterogeneous catalysis and electron conducting materials.[12-18]

6.3 Research proposed toward organic cage frameworks (OCFs)

Our research goal is to integrate previously developed macrocycles[19,20] and molecular cages[21] into organic frameworks and study their properties in gas adsorption, molecular separation, and catalysis.

6.3.1. 2-D covalent organic frameworks

2-D organic frameworks can be constructed from shape-persistent macrocycle building blocks and molecular linkers. This part of work was performed by other group members and will not be covered in this thesis.

6.3.2. 3-D covalent organic frameworks

3-D organic cage frameworks were designed to be constructed from boronic acid substituted molecular cage building blocks (Scheme 6.1), which will be synthesized through highly efficient alkyne metathesis as demonstrated in previous chapters. Initial attempt of constructing cage **7** substituted with pinacol borate was unsuccessful. The alkyne metathesis reaction produced a large amount of precipitates within a few hours and the solution turned colorless. After removal of the precipitates, the NMR spectrum of the crude product showed no porphyrin starting materials in solution. GPC analysis of the crude product mixture showed no signal corresponding to the higher molecular species (MW > 1000). Such observation indicates that the reaction intermediates (*i.e.*, oligomers) are insoluble in the reaction solvent (toluene or $CHCl_3$/CCl_4 mixture). Longer reaction time (4 days) and higher temperature (70 ^oC) did not lead to any improvement.

Later we used another diol with long alkyl chains rather than pinacol to protect the boronic acid in order to improve the solubility of building blocks as well as oligomeric and polymeric intermediates (Scheme 6.2).

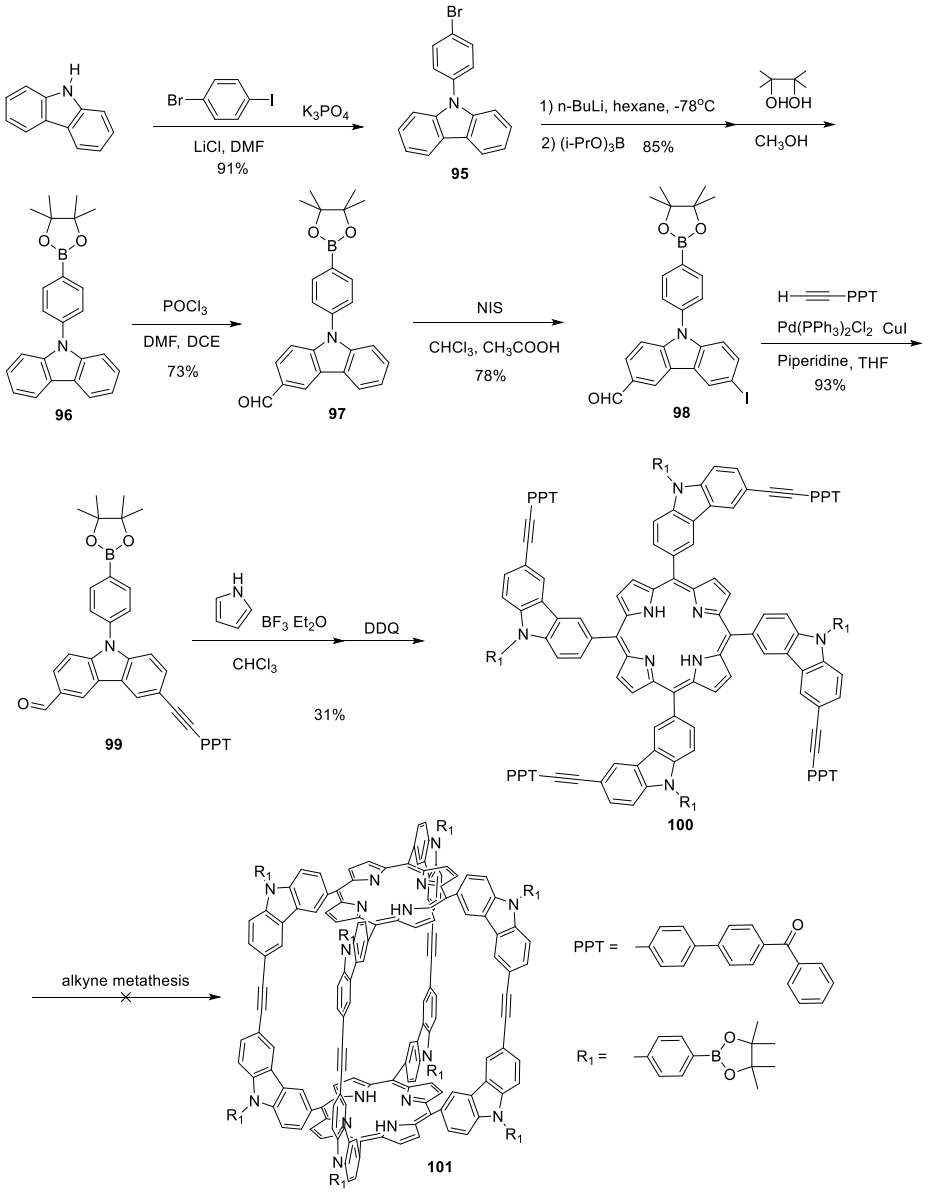

Scheme 6.1. Attempted synthesis of a molecular cage as the building block for COFs through the precipitation-driven alkyne metathesis.

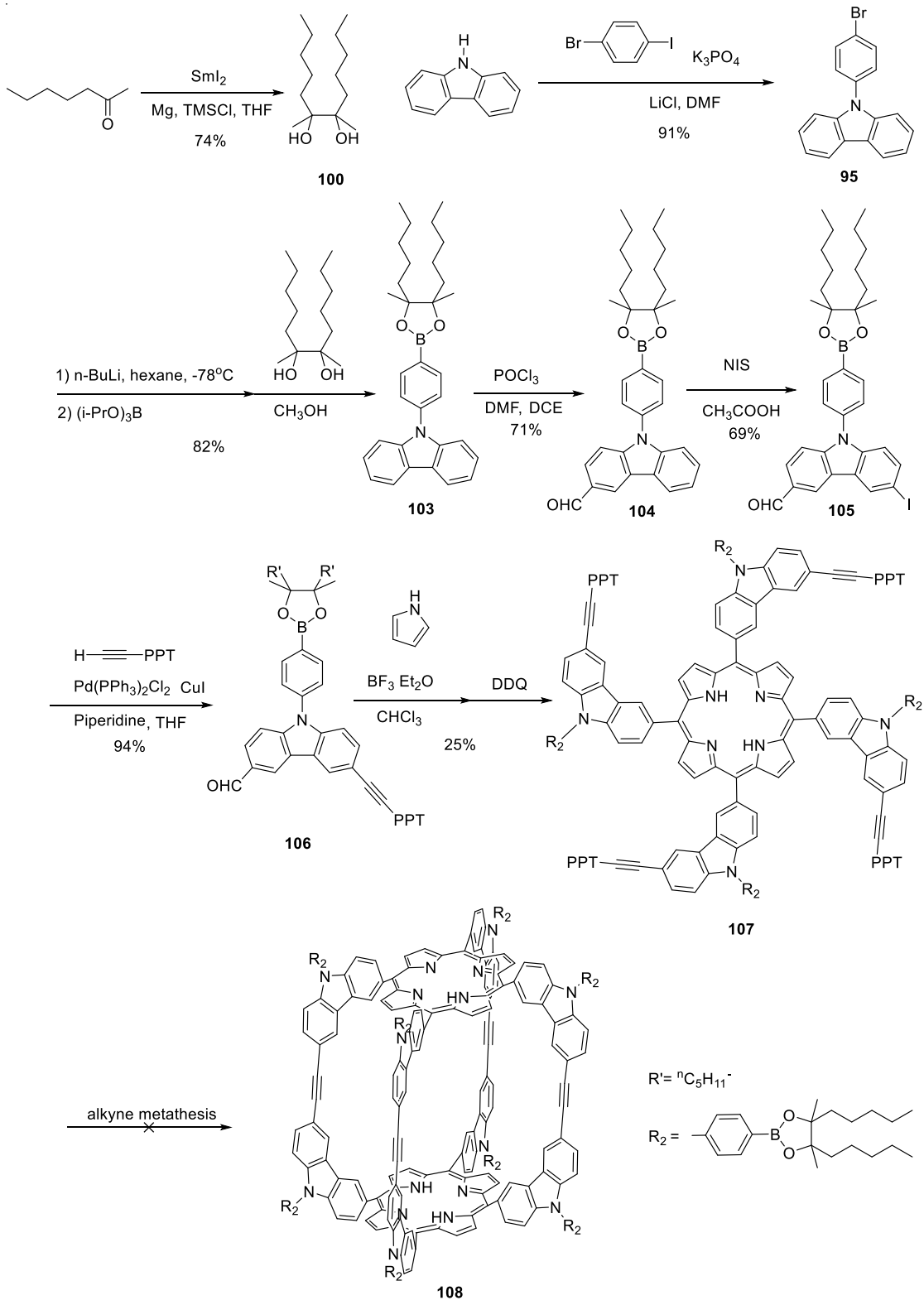

Scheme 6.2. Attempted synthesis of a molecular cage as the building block for COFs, through the precipitation-driven alkyne metathesis.

However, the alkyne metathesis of monomer **107** still produced a large amount of precipitates, similar to the previous case of cage **101** preparation. No signal corresponding to the desired cage was observed in MALDI-MS and crude NMR spectra. The large, rigid, aromatic PPT groups presumably contributed, at least partially, to the poor solubility.

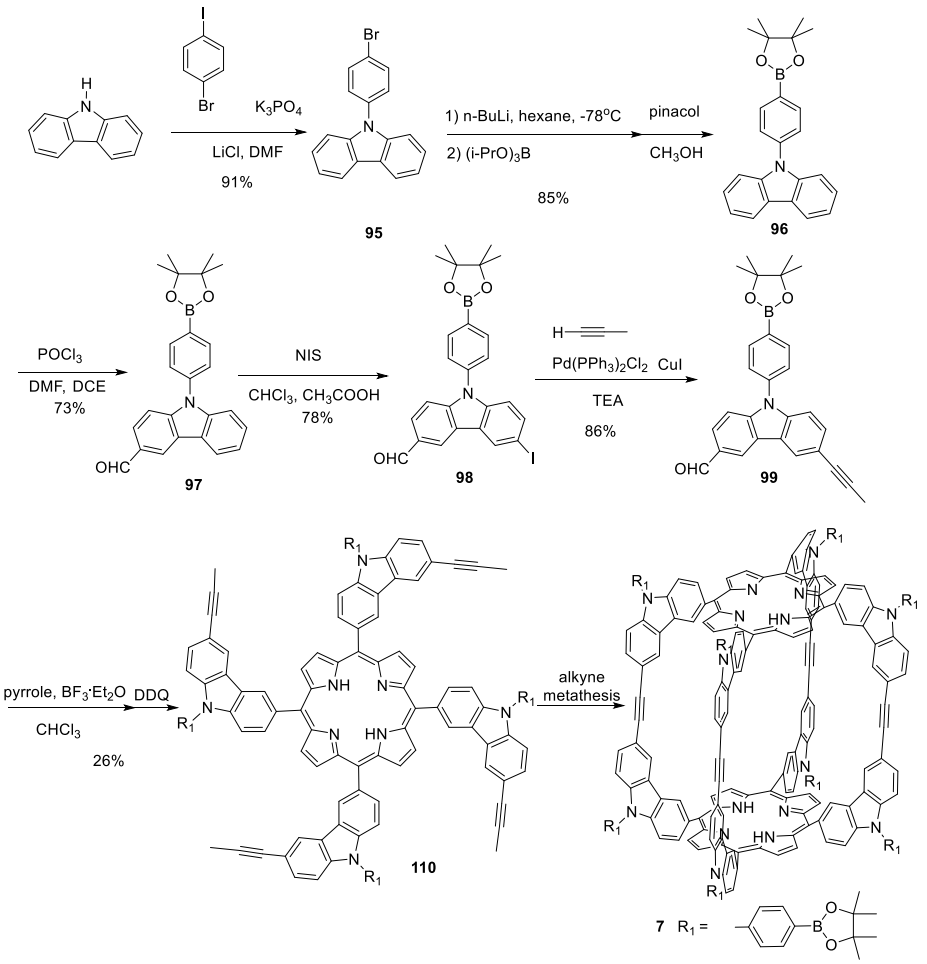

Scheme 6.3. Attempted synthesis of a molecular cage as the building block for COFs. Vacuum-driven alkyne metathesis was pursued.

To further optimize the solubility of the monomer as well as the oligomer intermediates formed along the reaction pathway, the vacuum-driven alkyne metathesis was also pursued for the

cage synthesis (Scheme 6.3). In the vacuum-driven alkyne metathesis, the low boiling point by-product (2-butyne) is removed under vacuum. With the replacement of four large aromatic PPT groups with four small propynyl group, the solubility of the monomer was indeed improved and the signal corresponding to the cage product was observed on the MALDI-MS of the reaction mixture after 16 hours at 55 ^{o}C. Further purification and study on this building block is still in progress.

6.3.3. Possible metal organic frameworks

3-D metal organic framework from macrocyclic tetra-acid building block **116** was proposed. The synthesis of ester-substituted macrocycle **115** is shown in Scheme 6.4. The tetra-ester substituted macrocycle **115** can be constructed from monomer **114** in one step through alkyne metathesis with high efficiency. Further study is still in progress.

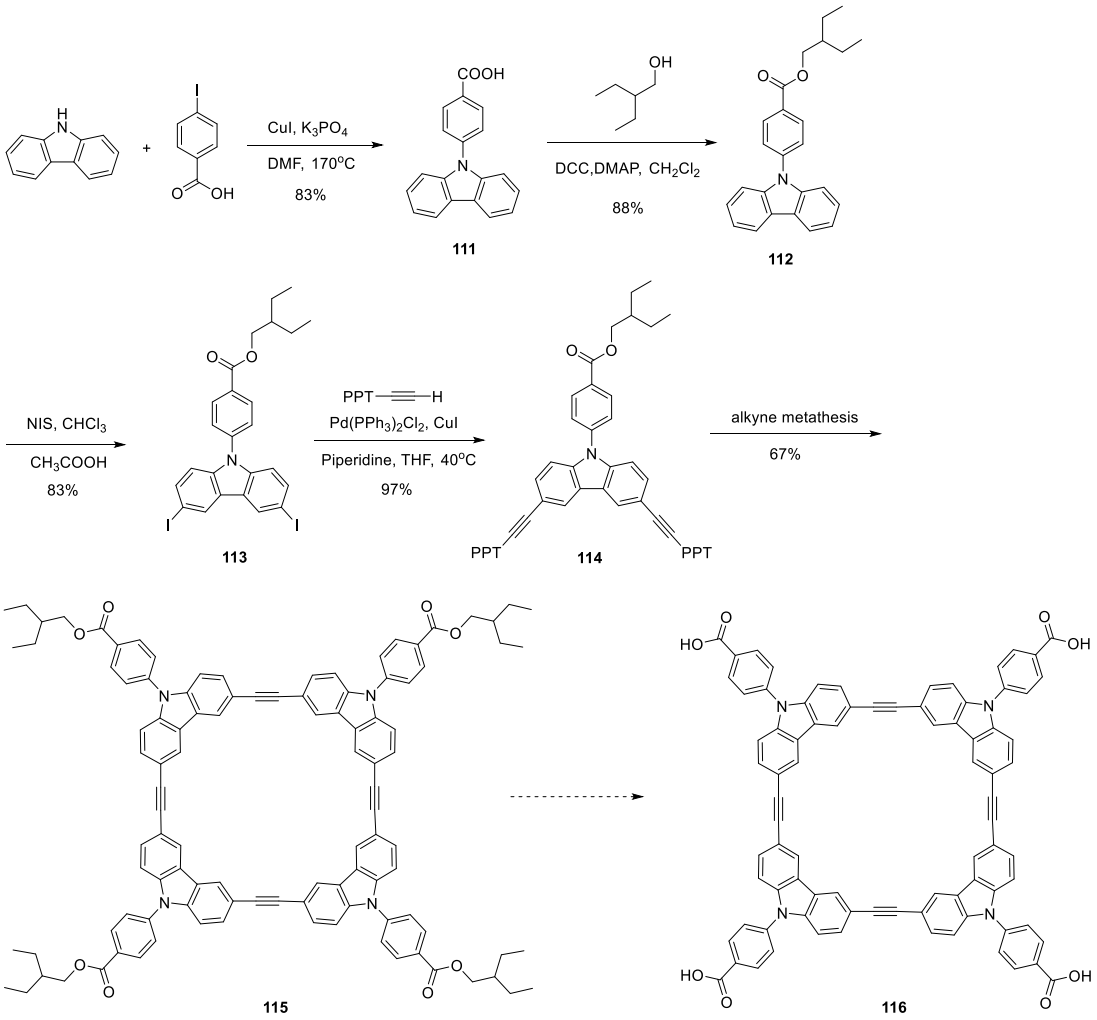

Scheme 6.4. The synthesis of a macrocycle as the building block for MOFs. Precipitation-driven alkyne metathesis was used.

With proper linkers, 3-D molecular cages can be used as building blocks toward constructing 3-D organic frameworks. The attempted synthesis of an ester-substituted organic cage building block **121** is shown in Scheme 6.5. The octa-ester will be converted to octa-aldehyde, which will be subjected to imine condensation reaction (with dialdehyde linker molecules) to form COFs.

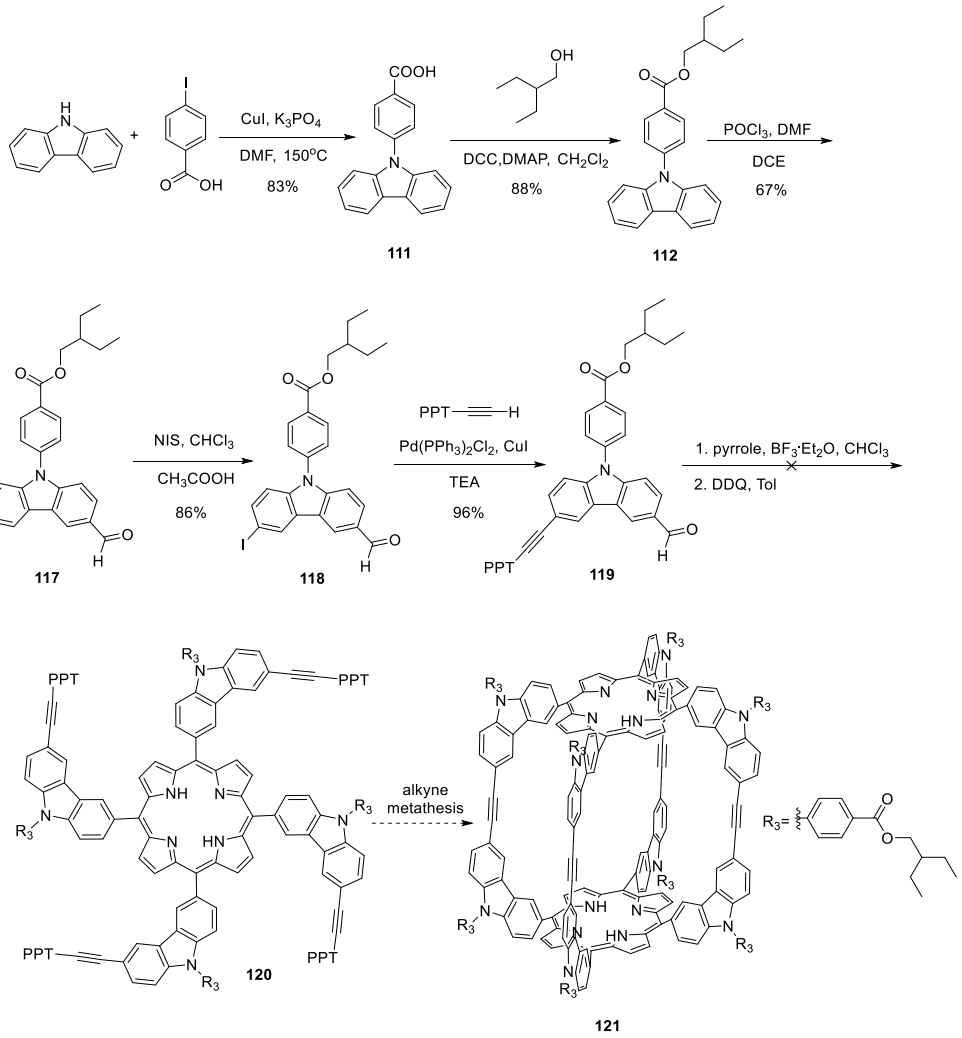

Scheme 6.5. The synthesis of a molecular cage as the building block for MOFs and COFs. Precipitation-driven alkyne metathesis was pursued.

Initially the molecular cage synthesis through the precipitation-driven alkyne metathesis was planned. However, monomer **120** containing four PPT groups cannot be successfully purified. The reaction side-products (some oligomers from pyrrole and aldehyde) are inseparable from the product. In the presence of a small amount of impurities, the cage **121** could not be successfully constructed. In order to lower the polarity of the monomer thus to improve the separation efficiency, vacuum-driven alkyne metathesis was pursued, in which the propyne groups with low polarity

were installed on the monomer instead of PPT. The synthetic route is shown in scheme 6.6. To our delight, cage **124** was successfully synthesized and purified. Preparation of **124** in larger scale and further MOF (using octa-acid cage) and COF (using octa-aldehyde cage) synthesis and study are still in progress.

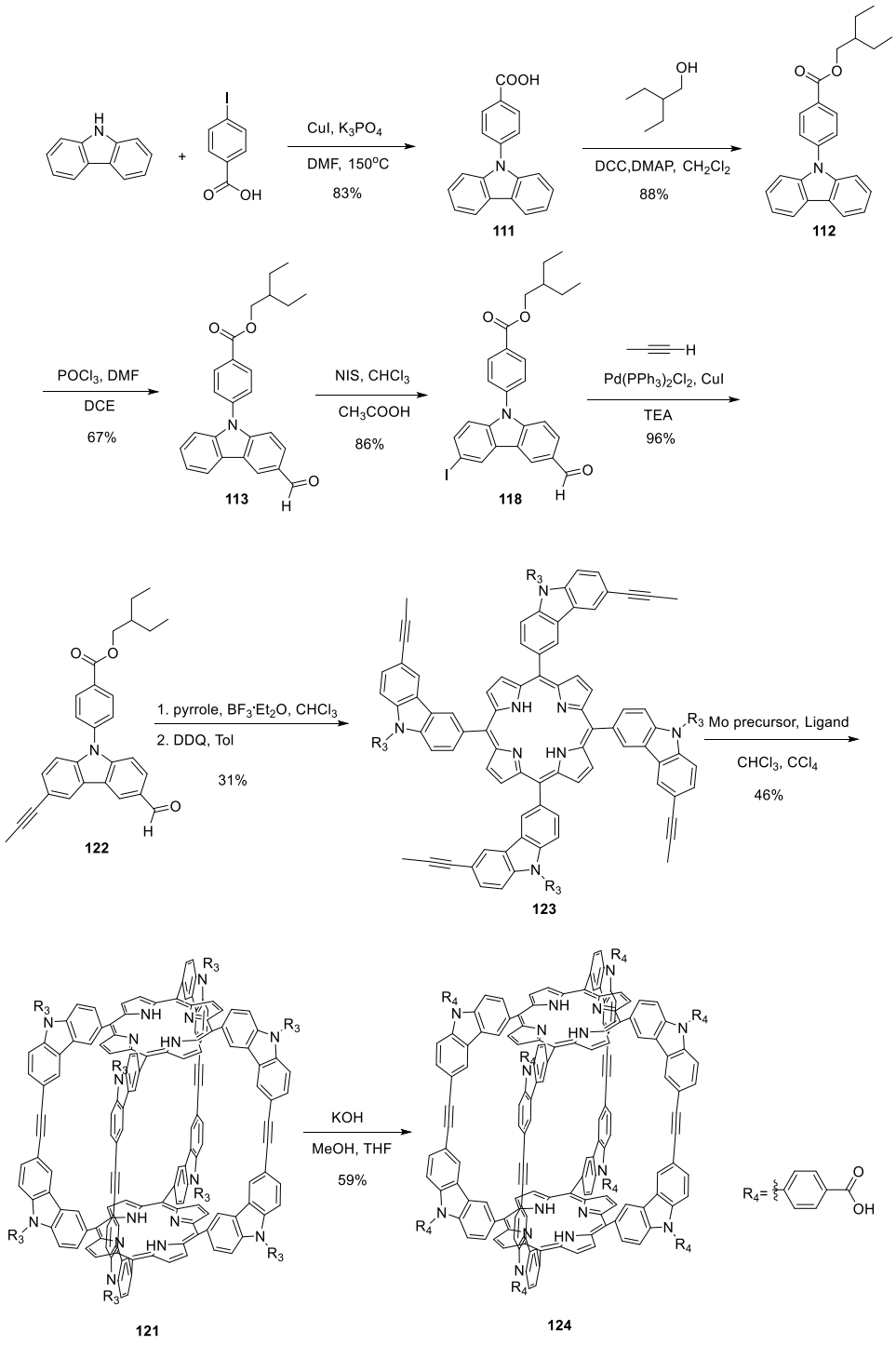

Scheme 6.6. The synthesis of a molecular cage as the building block for MOFs. Vacuum-driven alkyne metathesis was pursued.

Based on synthetic scheme 6.5, an alternative synthetic route was also designed and pursued. The synthetic sequence was altered to improve synthetic efficiency.

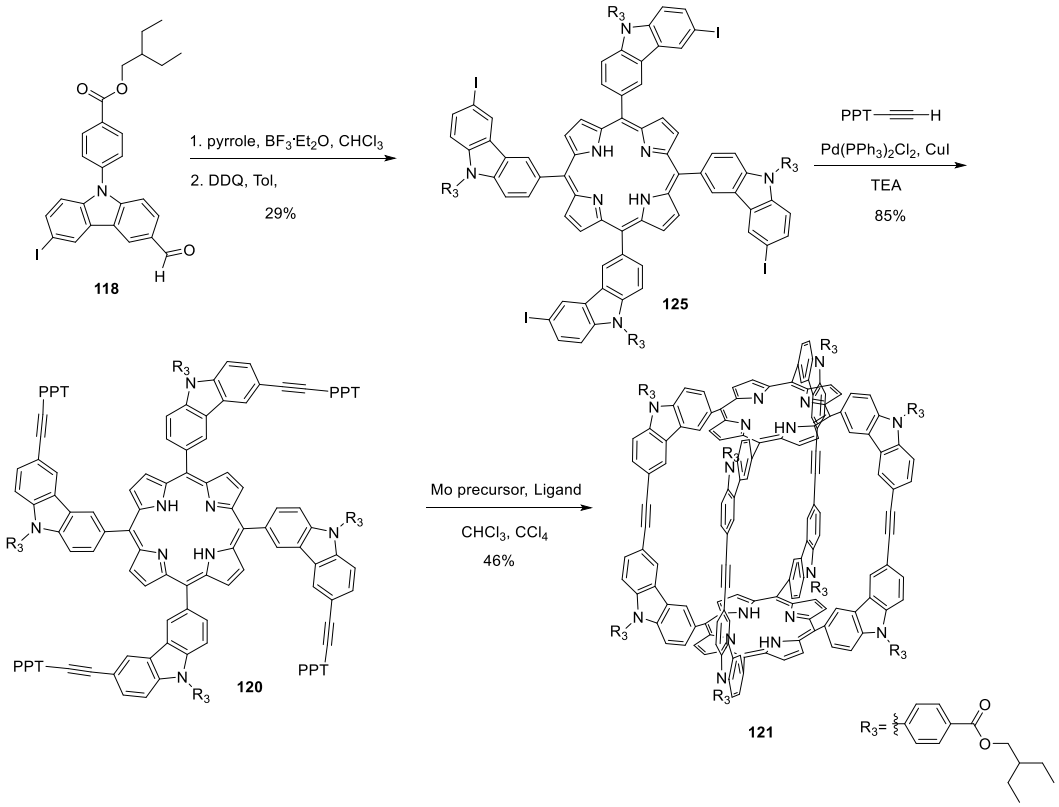

Scheme 6.7. An alternative synthetic route to the cage **121**.

6.4 Perspectives and future work

The synthesis of molecular cages with either boronic acid or carboxylic acid are. Given the fact that the boronic acid-diol condensation chemistry is widely used in constructing COFs, and acid-metal coordination interactions is one of the most commonly used methods for MOF construction, utilizing these cage building blocks to construct either COFs or MOFs is feasible. The construction of COFs with shape-persistent molecular cages as the building blocks and rigid organic linkers will generate isolated and tunable cavities. It will increase the porosity and the

host-guest binding selectivity as well as efficiency. Such by-design COFs are anticipated to be good candidates for gas adsorption/separation and catalysis applications.

In contrast to previously reported **COP-5**, cage compounds **121** and **124** do not have long solubilizing chains, which would lead to the increase in their BET surface area. After further metallation of the porphyrin moieties, the resulting cage frameworks could also be used for gas separation (e.g., O_2/N_2, or olefin/paraffin) and catalysis applications.

Cage **124**, containing eight carboxylic acid groups, is soluble in water. The cage itself preserves high binding affinity for fullerenes and other organic guests, thus could be useful for drug delivery applications.

In conclusion, the objective of this thesis research is to construct 2-D and 3-D COPs using a series of highly efficient synthetic tools, DC_vC. Multiple targets were designed and synthesized using olefin metathesis and alkyne metathesis. Further study involves synthesizing more cages with different functional groups or building blocks, and constructing frameworks from cage and macrocycle building blocks. Success here would open up many new possibilities for bottom-up design and synthesis of large, complex, molecular or polymeric architectures from readily accessible small building blocks.

6.5 Experimental section

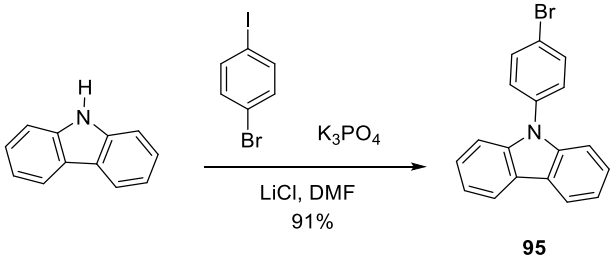

95

9-(4-Bromophenyl)-9H-carbazole (95): A Schlenk tube was charged with carbazole (3.00 g, 17.9 mmol), 1-bromo-4-iodobenzene (6.00 g, 21.2 mmol), K_3PO_4 (4.50 g, 21.2 mmol), LiCl (0.449 g, 10.6 mmol), CuI (0.468 g, 2.12 mmol), degassed and refilled with N_2 three times then anhydride DMF (30 mL) was added. The reaction was stirred at 160°C for 24h. Upon reaction completion, the solvent was washed with brine and then extracted with CH_2Cl_2 (4 x 20 mL), dried over Na_2SO_4, and concentrated to give the crude product. Further purification by flash column chromatography (ethyl acetate/hexane, 1/10, v/v) afforded product as a white solid. (5.25 g, 91%): ^{1}H NMR (500 MHz, $CDCl_3$) δ 8.15 (d, *J* = 7.8 Hz, 2H), 7.74 (d, *J* = 8.6 Hz, 2H), 7.52 – 7.37 (m, 6H), 7.31 (t, *J* = 8.0 Hz, 2H).

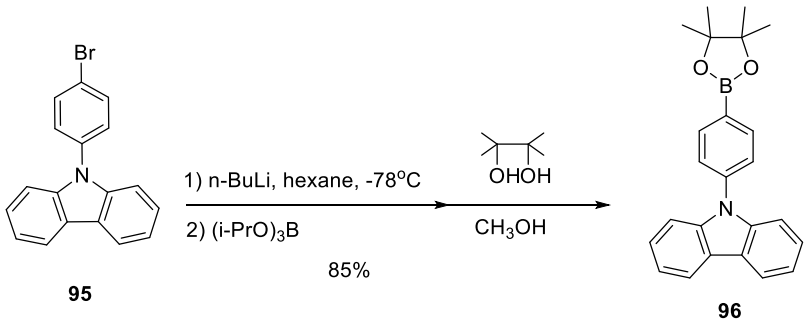

95 **96**

9-(4-Pinacolboratephenyl)-9H-carbazole (96): To a Schlenk tube was added compound **95** (3.22 g, 10.0 mmol), degassed and refilled with N_2 three times. 50 mL of dry THF was then added. The mixture was stirred and cooled to -78 °C under dry ice-acetone bath. *n*-Butyllithium (8.2 mL, 1.6M in hexane, 13.0 mmol) was added dropwise. And the reaction was stirred at -78°C for 1 hour. Triisopropyl borate (2.44 g, 13.0 mmol) was then added and the reaction was slowly warmed up to ambient temperature and then stirred for another 3 hours. The reaction was quenched by saturated NH_4Cl aqueous solution (50 mL) and then extracted with ethyl acetate (4 x 50 mL), dried over Na_2SO_4, and concentrated to give the crude product. The crude product was dissolved in methanol (100 mL) and pinacol (1.77 g, 15.0 mmol) was added. The reaction was stirred at ambient

temperature for 2 hours. Upon completion, the solvent was evaporated off and the crude mixture was subject to flash column chromatography (CH_2Cl_2/hexane, 1/1, v/v) gives product as a white solid. (3.13 g, 85%): ^{1}H NMR (500 MHz, $CDCl_3$) δ 8.17 (d, *J* = 7.8 Hz, 2H), 8.08 (d, *J* = 8.4 Hz, 2H), 7.63 (d, *J* = 8.3 Hz, 2H), 7.48 (d, *J* = 8.2 Hz, 2H), 7.43 (t, *J* = 8.2 Hz, 2H), 7.32 (t, *J* = 6.8 Hz, 2H), 1.43 (s, 12H).

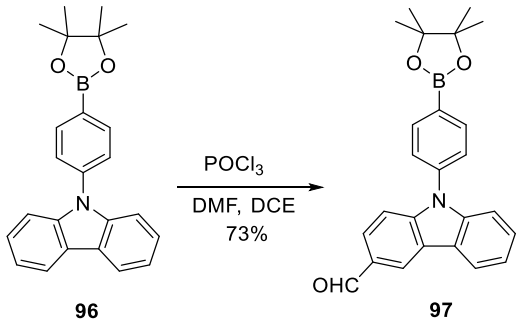

96 97

3-Formyl-9-(4-pinacolboratephenyl)-9H-carbazole (97): Typical Vilsmeier–Haack reaction condition were followed: To a mixture of DMF (12.6 mL, 160 mmol) and 1,2-dichloroethane (15 mL) was added $POCl_3$ (15.2 mL, 160 mmol) dropwise at 0 °C. The mixture was warmed up to 35 °C and **96** (3.00g, 8.10 mmol) was added. After heating at 90 °C for 24 h, the mixture was cooled to ambient temperature and poured into water (200 mL). The product was extracted with chloroform (50 mL × 4). The combined organic extracts were washed with water (100 mL), and brine (100 mL), dried over anhydrous $MgSO_4$ and concentrated. The residue was purified via flash column chromatography (ethyl acetate/$CHCl_3$/hexane, 1/20/20, v/v/v) to provide product **97** as a white solid (2.36 g, 73 %): ^{1}H NMR (500 MHz, $CDCl_3$) δ 10.13 (s, 1H), 8.68 (d, *J* = 1.5 Hz, 1H), 8.21 (d, *J* = 7.8 Hz, 1H), 8.10 (d, *J* = 8.1 Hz, 2H), 7.96 (dd, *J* = 8.6, 1.6 Hz, 1H), 7.58 (d, *J* = 8.2 Hz, 2H), 7.51 – 7.42 (m, 3H), 7.39 (t, *J* = 7.9 Hz, 1H), 1.42 (s, 12H); ^{13}C NMR (100 MHz, $CDCl_3$) δ 191.97, 144.43, 141.77, 139.43, 136.78, 129.70, 127.76, 127.24, 126.38, 123.98, 123.92, 123.53, 121.51, 120.89, 110.66, 110.37, 84.42, 53.65, 25.13.

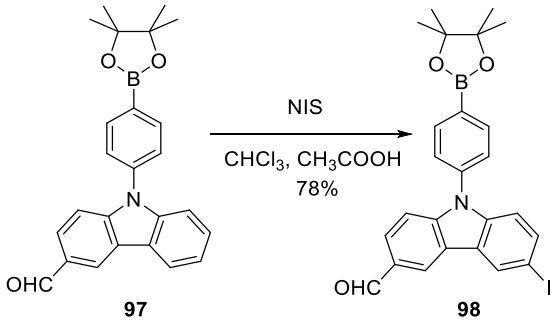

3-Formyl-6-iodo-9-(4-pinacolboratephenyl)-9H-carbazole (98): To a solution of **97** (1.99 g ,5 mmol), N-iodosuccinimide (1.24 g, 5.5 mmol) in $CHCl_3$ 100 mL, acetic acid (25 mL) was added and the reaction was stirred for 12 hours. Upon completion, the reaction was quenched with Na_2SO_3 aqueous solution (1 M, 20 mL) followed by wash with water (50 mL) then extracted with CD_2Cl_2 (50 mL × 4). After dried over anhydrous Na_2SO_4 and concentrated, the residue was purified via flash column chromatography (ethyl acetate/$CHCl_3$/hexane, 1/20/20, v/v/v) to provide product **98** as a white solid. (2.24 g, 78%): ^{1}H NMR (500 MHz, $CDCl_3$) δ 10.12 (s, 1H), 8.61 (d, *J* = 1.5 Hz, 1H), 8.52 (d, *J* = 1.6 Hz, 1H), 8.09 (d, *J* = 8.2 Hz, 2H), 7.98 (dd, *J* = 8.6, 1.6 Hz, 1H), 7.73 (dd, *J* = 8.6, 1.7 Hz, 1H), 7.54 (d, *J* = 8.2 Hz, 2H), 7.46 (d, *J* = 8.6 Hz, 1H), 7.20 (d, *J* = 8.6 Hz, 1H), 1.41 (s, 12H).

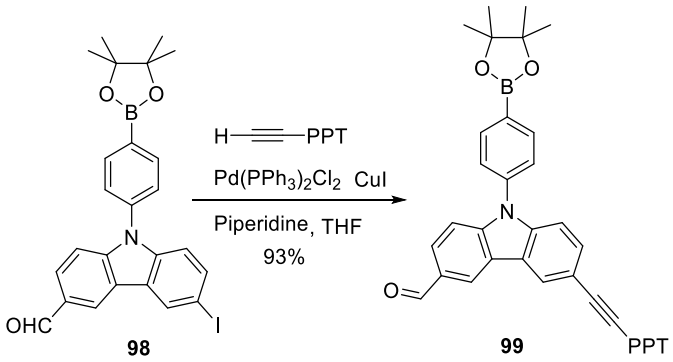

3-Formyl-6-(4'-benzoyl-[1,1'-biphenyl]-4-yl)ethynyl)-9-(4-pinacolboratephenyl)-9H-carbazole (99): The general Sonogashira procedure was followed.[22,23] Using **98** (2.09g, 4.0 mmol),

4-benzoyl-4'-ethynyl-biphenyl (1.69 g, 6.0 mmol), $Pd(PPh_3)_2Cl_2$ (0.112 g, 0.16 mmol), CuI (7.6 mg, 0.04 mmol), piperidine (30 mL), and THF (100 mL). Flash column chromatography ($MeOH/CH_2Cl_2$, 1/100, v/v) gave pure product as a yellowish solid (2.52 g, 93%): ^1H NMR (500 MHz, $CDCl_3$) δ 10.14 (s, 1H), 8.68 (d, *J* = 1.1 Hz, 1H), 8.43 (d, *J* = 1.4 Hz, 1H), 8.11 (d, *J* = 8.2 Hz, 2H), 7.99 (dd, *J* = 8.6, 1.6 Hz, 1H), 7.93 (d, *J* = 8.3 Hz, 2H), 7.86 (dd, *J* = 8.2, 1.3 Hz, 2H), 7.77 – 7.56 (m, 10H), 7.53 (t, *J* = 7.6 Hz, 2H), 7.49 (d, *J* = 8.6 Hz, 1H), 7.41 (dd, *J* = 8.4, 0.7 Hz, 1H), 1.42 (s, 12H).

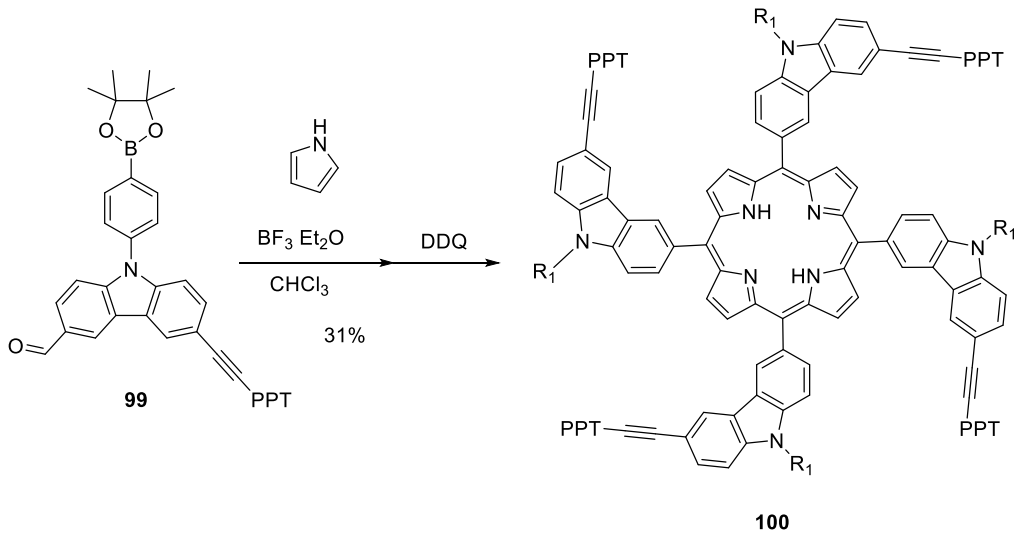

(100): To a solution of compound **99** (2.03 g, 3.0 mmol) and pyrrole (0.21 mL, 3.0 mmol) in chloroform (150 mL) was added $BF_3{\cdot}Et_2O$ (0.12 mL) drop wise at r.t.. The reaction mixture was stirred for 1 h at r.t.. A solution of 2,3-dichloro-5,6-dicyanobenzoquinone (0.50 g, 2.2 mmol) in toluene (80 mL) was then added slowly. After stirring 1 h at r.t., the reaction mixture was filtered through a silica gel pad. The volatiles were removed and the residue was purified by flash column chromatography ($MeOH/CH_2Cl_2$, 1/20, v/v) to provide the product **100** as a purple solid (0.67 g, 31 %): ^1H NMR (500 MHz, $CDCl_3$) δ 9.04 (t, *J* = 7.7 Hz, 4H), 8.96 (s, 8H), 8.49 (t, *J* = 9.4 Hz,

4H), 8.44 – 8.35 (m, 4H), 8.20 (d, *J* = 8.3 Hz, 8H), 7.98 – 7.40 (m, 64H), 7.22 – 7.15 (m, 8H), 1.44 (t, *J* = 3.5 Hz, 48H), -2.43 (s, 2H).

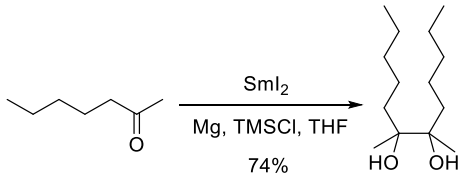

102

6,7-dimethyldodecane-6,7-diol (102): The procedure of similar reaction was followed.[24] Into a mixture of a 0.1 M solution of SmI_2 in THF (20 mL), TMSCl (2.53 mL, 20 mmol) and Mg (4.8 g, 200 mmol) which was activated by vigorous stirring for 1 hour, was added a mixture of 2-heptanone (2.8 mL, 20 mmol) and TMSCl (1.26 mL, 10 mmol). Upon reaction completion, filtration to remove excess of Mg then followed by flash column chromatography (ethyl acetate/hexane, 1/5, v/v). The product was obtained as colorless oil. (1.70 g, 74%): ^{1}H NMR (500 MHz, $CDCl_3$) δ 2.04 (s, 2H), 1.59 – 1.15 (m, 16H), 1.10 (d, *J* = 2.8 Hz, 6H), 0.86 (t, *J* = 7.1 Hz, 6H). ^{13}C NMR (100 MHz, $CDCl_3$) δ 77.32, 36.37, 36.02, 32.85, 23.64, 23.62, 22.94, 21.22, 20.81, 14.28.

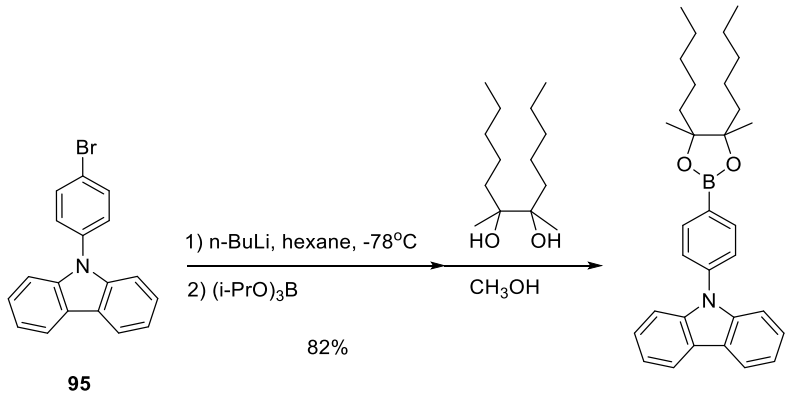

95 **103**

(103): Same reaction condition as for compound **96** was followed. Using **95** (3.22 g, 10.0 mmol), *n*-butyllithium (8.2 mL, 1.6M in hexane, 13.0 mmol), triisopropyl borate (2.44 g, 13.0 mmol) **102** (3.46 g, 15.0 mmol). Product was obtained as a white solid (3.95 g, 83%): ^{1}H NMR (500 MHz, $CDCl_3$) δ 8.16 (d, *J* = 7.8 Hz, 2H), 8.07 (d, *J* = 8.2 Hz, 2H), 7.61 (d, *J* = 8.1 Hz, 2H), 7.47 (d, *J* = 8.2 Hz, 2H), 7.42 (t, *J* = 7.0 Hz, 2H), 7.31 (t, *J* = 8.0 Hz, 2H), 1.83 – 1.72 (m, 2H), 1.68 – 1.33 (m, 20H), 0.94 (t, *J* = 6.8 Hz, 6H). ^{13}C NMR (100 MHz, $CDCl_3$) δ 140.77, 140.45, 136.59, 126.25, 126.16, 123.69, 120.50, 120.23, 110.06, 86.63, 37.65, 36.80, 32.77, 24.15, 22.88, 22.09, 14.34.

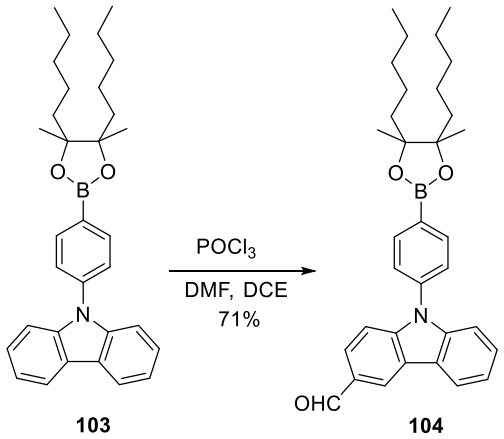

103 **104**

(104): Same reaction condition as for compound **97** was followed. Using DMF (12.6 mL, 160 mmol), 1,2-dichloroethane (15 mL), $POCl_3$ (15.2 mL, 160 mmol), **103** (3.85 g, 8.00 mmol). Purification including flash column chromatography (ethyl acetate/$CHCl_3$/hexane, 1/20/20, v/v/v) to provide product **104** as a white solid (2.89 g, 71%): ^{1}H NMR (500 MHz, $CDCl_3$) δ 10.13 (s, 1H), 8.68 (d, *J* = 1.5 Hz, 1H), 8.22 (d, *J* = 7.8 Hz, 1H), 8.09 (d, *J* = 8.1 Hz, 2H), 7.96 (dd, *J* = 8.5, 1.6 Hz, 1H), 7.58 (d, *J* = 8.2 Hz, 2H), 7.52 – 7.42 (m, 3H), 7.39 (ddd, *J* = 7.9, 6.9, 1.2 Hz, 1H), 1.82 – 1.73 (m, 2H), 1.66 – 1.20 (m, 20H), 0.94 (t, *J* = 6.9 Hz, 6H).

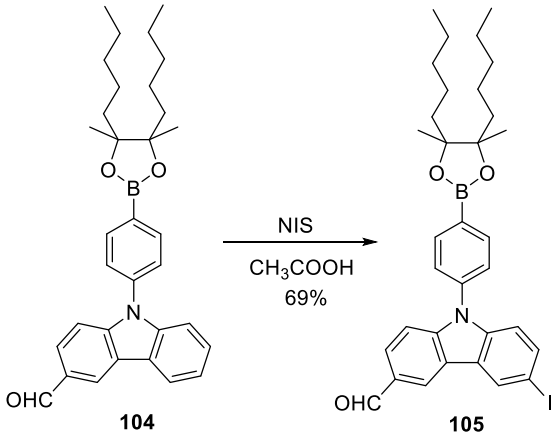

(105): Same reaction condition as for compound **98** was followed. Using **104** (2.55 g, 5.0 mmol), N-iodosuccinimide (1.24 g, 5.5 mmol). Purification including flash column chromatography (ethyl acetate/$CHCl_3$/hexane, 1/20/20, v/v/v) to provide product **105** as a white solid. (2.19 g, 69%): ^{1}H NMR (500 MHz, $CDCl_3$) δ 10.12 (s, 1H), 8.60 (d, *J* = 1.5 Hz, 1H), 8.51 (d, *J* = 1.5 Hz, 1H), 8.08 (d, *J* = 8.1 Hz, 2H), 7.98 (dd, *J* = 8.6, 1.6 Hz, 1H), 7.73 (dd, *J* = 8.6, 1.6 Hz, 1H), 7.54 (d, *J* = 8.2 Hz, 2H), 7.46 (d, *J* = 8.6 Hz, 1H), 7.20 (d, *J* = 8.6 Hz, 1H), 1.83 – 1.70 (m, 2H), 1.67 – 1.27 (m, 20H), 0.94 (t, *J* = 6.8 Hz, 6H).

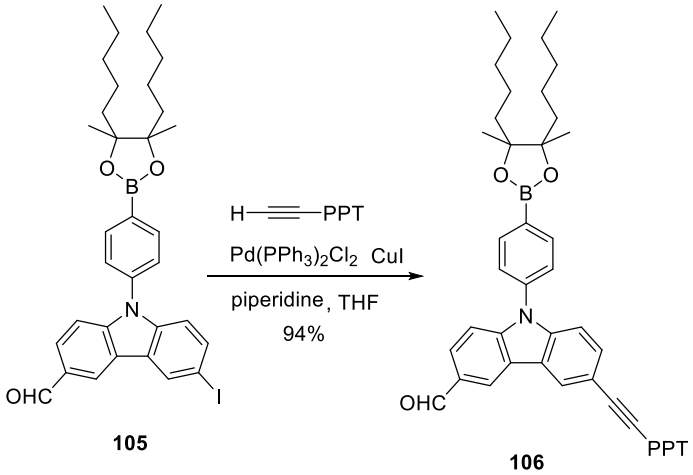

(**106**): The general Sonogashira's procedure was followed. Using **109** (1.91 g, 3.0 mmol), 4-benzoyl-4'-ethynyl-biphenyl (1.27 g, 4.5 mmol), $Pd(PPh_3)_2Cl_2$ (0.084 g, 0.12 mmol), CuI (5.7 mg,

0.03 mmol), piperidine (20 mL), and THF (80 mL). Flash column chromatography ($MeOH/CH_2Cl_2$, 1/100, v/v) gives pure product as a yellowish solid (2.23 g, 94%): ^1H NMR (500 MHz, $CDCl_3$) δ 10.14 (s, 1H), 8.67 (d, *J* = 1.1 Hz, 1H), 8.42 (d, *J* = 1.4 Hz, 1H), 8.11 (d, *J* = 8.2 Hz, 2H), 7.98 (dd, *J* = 8.5, 1.6 Hz, 1H), 7.92 (d, *J* = 8.4 Hz, 2H), 7.86 (dd, *J* = 8.2, 1.3 Hz, 2H), 7.79 – 7.56 (m, 10H), 7.53 (t, *J* = 7.5 Hz, 2H), 7.49 (d, *J* = 8.5 Hz, 1H), 7.41 (dd, *J* = 8.4, 0.7 Hz, 1H), 1.84 – 1.70 (m, 2H), 1.66 – 1.23 (m, 20H), 0.94 (t, *J* = 6.7 Hz, 6H).

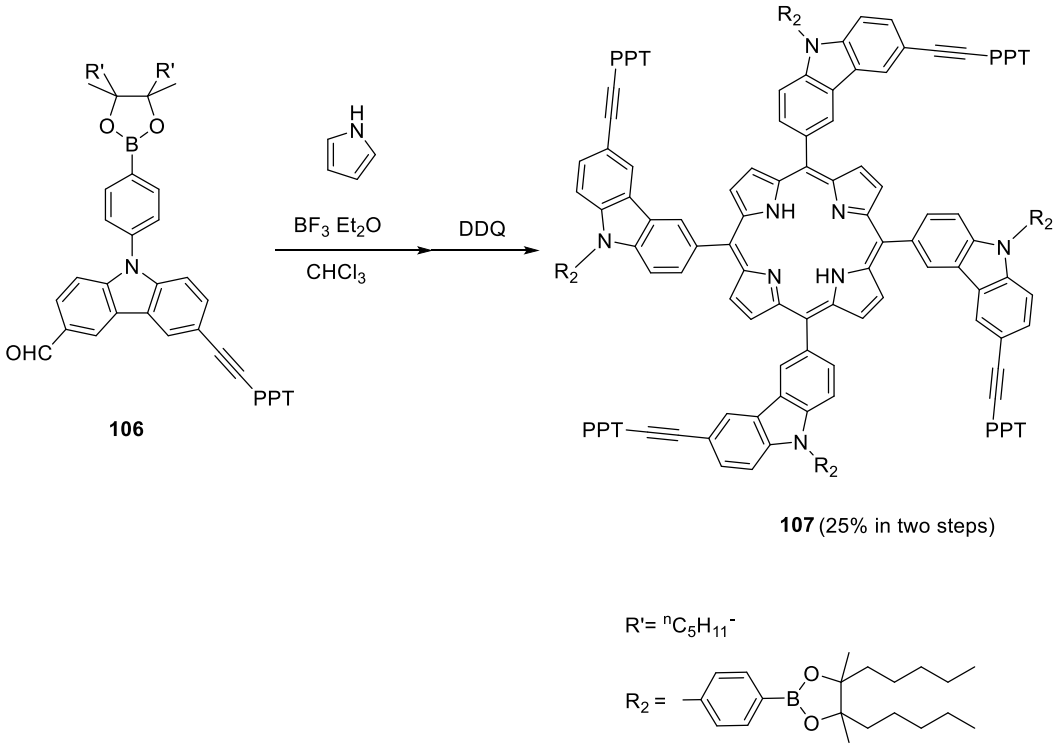

(107): The same reaction condition as for compound **100** was followed. Using **106** (1.58 g, 2.0 mmol), pyrrole (0.14 mL, 2.0 mmol) and $BF_3 \cdot Et_2O$ (0.08 mL) DDQ (0.37 g, 1.5 mmol). Flash column chromatography ($MeOH/CH_2Cl_2$, 1/100, v/v) gives pure product as a purple solid (0.419 g, 25 %): ^1H NMR (500 MHz, $CDCl_3$) δ 9.04 (t, *J* = 7.8 Hz, 4H), 8.96 (s, 8H), 8.49 (t, *J* = 9.3 Hz, 4H), 8.44 – 8.35 (m, 4H), 8.20 (d, *J* = 8.3 Hz, 8H), 8.00 – 7.39 (m, 64H), 7.22 – 7.15 (m, 8H), 1.84 – 1.71 (m, 2H), 1.68 – 1.24 (m, 20H), 0.94 (t, *J* = 6.8 Hz, 6H), -2.44 (s, 2H).

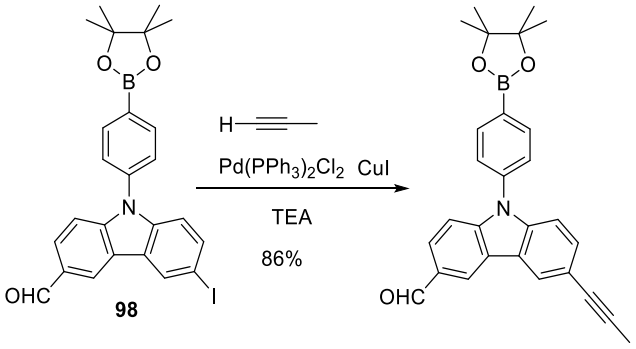

98 **109**

(**109**): The general Sonogashira's procedure was followed. Using **98** (2.09 g, 4.0 mmol), propyne (0.32 g, 8.0 mmol), $Pd(PPh_3)_2Cl_2$ (0.112 g, 0.16 mmol), CuI (7.6 mg, 0.04 mmol), TEA (100 mL). Propyne was added through syringe at -30 ^oC, the reaction then warmed up to 40 ^oC and stirred for 16 hours. Flash column chromatography (ethyl acetate/$CHCl_3$/hexane, 1/20/20, v/v/v) gives pure product as a yellowish solid (1.48 g, 86%): ^1H NMR (500 MHz, $CDCl_3$) δ 10.11 (s, 1H), 8.62 (d, J = 1.5 Hz, 1H), 8.24 (d, J = 1.6 Hz, 1H), 8.08 (d, J = 8.2 Hz, 2H), 7.96 (dd, J = 8.6, 1.6 Hz, 1H), 7.55 (d, J = 8.1 Hz, 2H), 7.52 – 7.42 (m, 2H), 7.33 (d, J = 8.5 Hz, 1H), 2.12 (s, 3H), 1.40 (s, 12H).

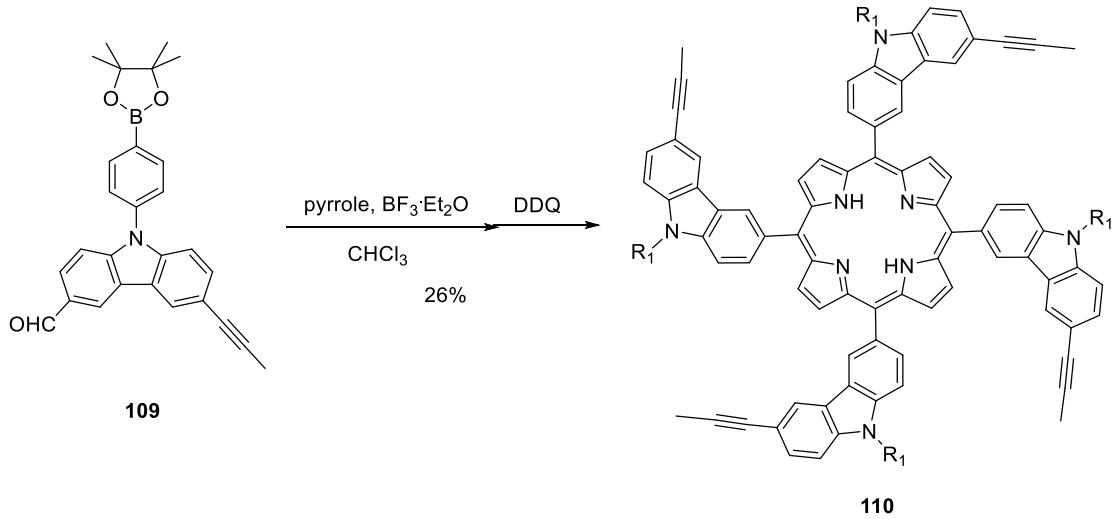

109 **110**

R_1 = 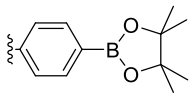

(110): Same reaction condition as for compound **100** was followed. Using **109** (1.31 g, 3.0 mmol), pyrrole (0.21 mL, 3.0 mmol) and $BF_3 \cdot Et_2O$ (0.12 mL) DDQ (0.50 g, 2.2 mmol). Flash column chromatography ($MeOH/CH_2Cl_2$, 1/100, v/v) gives the pure product as a purple solid (0.377 g, 26 %).

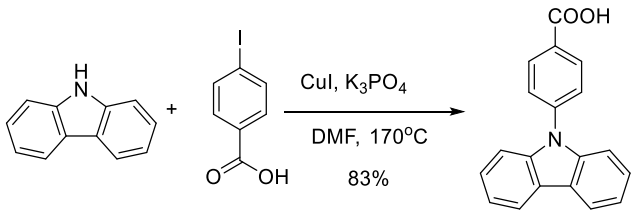

111

4-(9H-carbazol-9-yl)benzoic acid (**111**): Similar reaction condition as for compound **95** was followed. Using carbazole (3.00 g, 17.9 mmol), 4-iodo-benzoic acid (5.26 g, 21.2 mmol), K_3PO_4 (4.50 g, 21.2 mmol), LiCl (0.449 g, 10.6 mmol), CuI (0.468 g, 2.12 mmol). The reaction was stirred at 180°C for 48 hours. Further purification after reaction workup included washing with CH_2Cl_2 and recrystallization from acetone/CH_2Cl_2 solvent. The product was obtained as a white solid. (4.27 g, 83%): ^{1}H NMR (500 MHz, acetone-d_6) δ 8.37 (d, J = 8.2 Hz, 2H), 8.25 (d, J = 7.7 Hz, 2H), 7.84 (d, J = 8.3 Hz, 2H), 7.55 (d, J = 8.2 Hz, 2H), 7.48 (t, J = 8.3 Hz, 2H), 7.34 (t, J = 8.0 Hz, 2H).

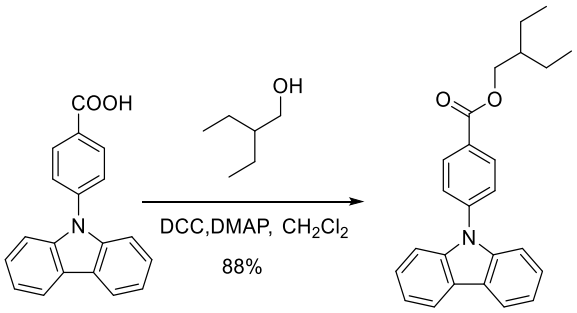

111 **112**

(112): To a suspension of **111** (2.87 g, 10 mmol) and 2-ethyl-butanol (1.12 g, 11 mmol) in dry

CH_2Cl_2, N,N'-dicyclohexylcarbodiimide (DCC) (2.06 g, 10 mmol) and 4-dimethylaminopyridine (DMAP) (0.122 g, 1.0 mmol) was added under N_2. The reaction mixture was stirred at ambient temperature for 12 hours. Upon completion of reaction, filtration to remove side product dicyclohexylurea and concentration to remove the solvent. Further flash column chromatography (CH_2Cl_2/hexane, 1/2, v/v) gives product as a colorless oil (3.27 g, 88%): ^{1}H NMR (500 MHz, $CDCl_3$) δ 8.31 (d, *J* = 8.5 Hz, 2H), 8.17 (dt, *J* = 7.7, 0.9 Hz, 2H), 7.70 (d, *J* = 8.5 Hz, 2H), 7.50 (dt, *J* = 8.3, 0.9 Hz, 2H), 7.44 (ddd, *J* = 8.2, 7.0, 1.2 Hz, 2H), 7.33 (ddd, *J* = 7.9, 7.1, 1.1 Hz, 2H), 4.35 (d, *J* = 5.7 Hz, 2H), 1.74 (hept, *J* = 6.2 Hz, 1H), 1.53 (p, *J* = 7.4 Hz, 4H), 1.01 (t, *J* = 7.5 Hz, 6H).

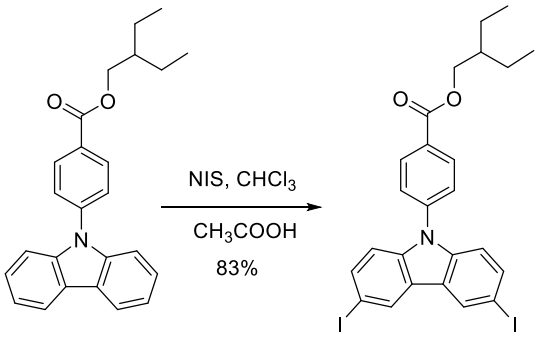

112 **113**

(113): Similar iodination condition as for compound **98** was followed. Using **112** (2.97 g ,8 mmol), N-iodosuccinimide (3.96 g, 17.6 mmol) acetic acid (40 mL) in $CHCl_3$ 160 mL. Further flash column chromatography (CH_2Cl_2/hexane, 1/2, v/v) gives product as a colorless oil (4.14 g, 83%): ^{1}H NMR (500 MHz, $CDCl_3$) δ 8.41 (d, *J* = 1.7 Hz, 2H), 8.30 (d, *J* = 8.5 Hz, 2H), 7.70 (dd, *J* = 8.7, 1.7 Hz, 2H), 7.61 (d, *J* = 8.5 Hz, 2H), 7.23 (d, *J* = 8.6 Hz, 2H), 4.34 (d, *J* = 5.7 Hz, 2H), 1.73 (hept, *J* = 6.3 Hz, 1H), 1.51 (p, *J* = 7.3 Hz, 4H), 1.00 (t, *J* = 7.5 Hz, 6H).

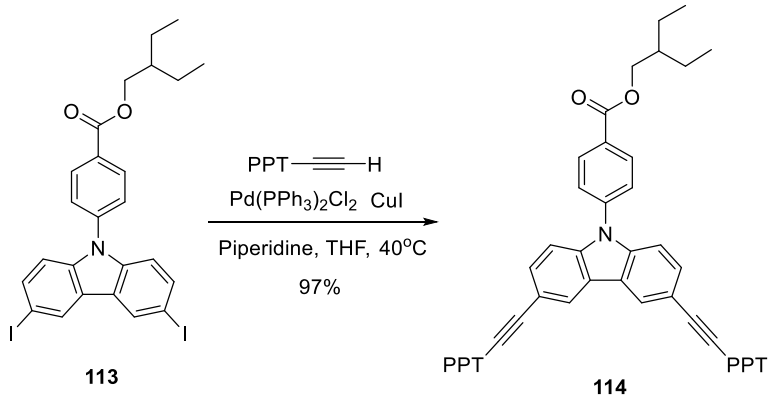

(114): The general Sonogashira's procedure was followed. Using **113** (3.74 g, 6.0 mmol), 4-benzoyl-4'-ethynyl-biphenyl (4.23 g, 15 mmol), $Pd(PPh_3)_2Cl_2$ (0.168 g, 0.24 mmol), CuI (11.4 mg, 0.06 mmol), piperidine (40 mL), and THF (160 mL). Flash column chromatography ($MeOH/CH_2Cl_2$, 1/100, v/v) gives pure product as a yellowish solid (5.42 g, 94%): ^1H NMR (500 MHz, $CDCl_3$) δ 8.38 (d, *J* = 1.6 Hz, 2H), 8.34 (d, *J* = 8.5 Hz, 2H), 7.93 (d, *J* = 8.4 Hz, 4H), 7.86 (dd, *J* = 7.9, 1.5 Hz, 4H), 7.76 (d, *J* = 8.3 Hz, 4H), 7.74 – 7.61 (m, 14H), 7.53 (t, *J* = 7.7 Hz, 4H), 7.46 (d, *J* = 8.5 Hz, 2H), 4.36 (d, *J* = 5.7 Hz, 2H), 1.75 (hept, *J* = 6.2 Hz, 1H), 1.53 (p, *J* = 7.3 Hz, 4H), 1.02 (t, *J* = 7.5 Hz, 6H).

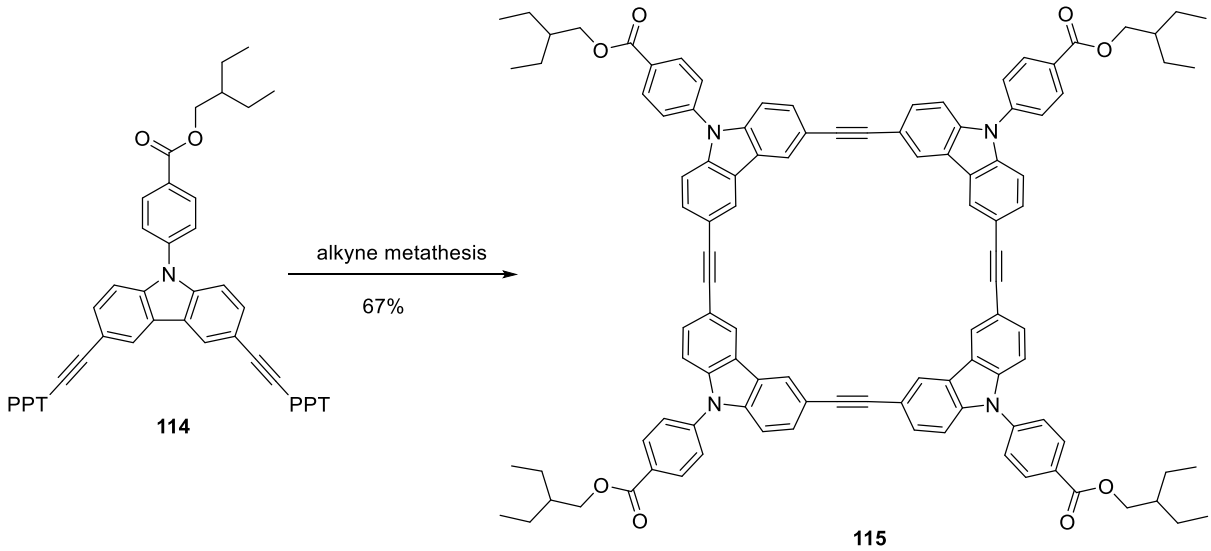

(115): Typical alkyne metathesis reaction condition was followed.[21,25] The multidentate ligand (8.1

mg, 0.02 mmol) and the Mo(VI) carbyne precursor (13.3 mg, 0.02 mmol) were premixed in dry carbon tetrachloride (20 mL) for 15 minutes to generate the catalyst in situ. Subsequently, the monomer **114** (931 mg, 1.0 mmol) was added and the stirring was continued for 16 h at 55 °C. Upon completion of the reaction, the reaction mixture was filtered to remove the byproduct and the filtrate was concentrated and subjected to flash column chromatography using CH_2Cl_2 as the eluent. The product **115** was obtained as a white solid (263 mg, 67%). ^{1}H NMR (500 MHz, $CDCl_3$) δ 8.46 (s, 8H), 8.33 (d, *J* = 8.5 Hz, 8H), 7.71 (d, *J* = 8.4 Hz, 8H), 7.67 (dd, *J* = 8.5, 1.6 Hz, 8H), 7.45 (d, *J* = 8.4 Hz, 8H), 4.37 (d, *J* = 5.7 Hz, 8H), 1.75 (hept, *J* = 6.2 Hz, 4H), 1.54 (p, *J* = 7.5 Hz, 16H), 1.02 (t, *J* = 7.5 Hz, 24H).

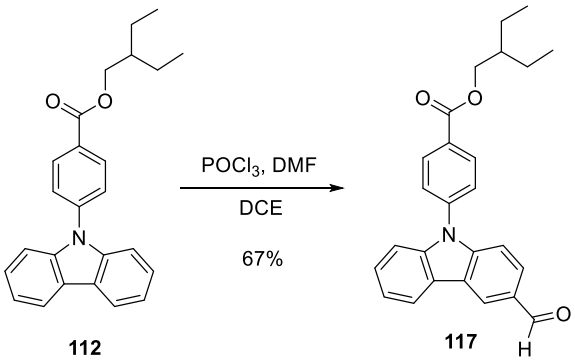

112 117

(117): Similar reaction condition as for compound **97** was followed. Using DMF (12.6 mL, 160 mmol), $POCl_3$ (15.2 mL, 160 mmol), **112** (3.00 g, 8.09 mmol). Flash column chromatography (CH_2Cl_2/hexane, 2/1, v/v) to provide product **97** as a white solid (2.16 g, 67 %): ^{1}H NMR (500 MHz, $CDCl_3$) δ 10.14 (s, 1H), 8.68 (d, *J* = 1.3 Hz, 1H), 8.33 (d, *J* = 8.5 Hz, 2H), 8.22 (dt, *J* = 7.8, 0.9 Hz, 1H), 7.98 (dd, *J* = 8.6, 1.6 Hz, 1H), 7.68 (d, *J* = 8.5 Hz, 2H), 7.54 – 7.45 (m, 3H), 7.41 (ddd, *J* = 8.0, 6.9, 1.2 Hz, 1H), 4.35 (d, *J* = 5.7 Hz, 2H), 1.73 (hept, *J* = 6.3 Hz, 1H), 1.52 (p, *J* = 7.3 Hz, 4H), 1.00 (t, *J* = 7.5 Hz, 6H). ^{13}C NMR (100 MHz, $CDCl_3$) δ 191.74, 165.90, 143.95, 141.33, 140.87, 131.62, 130.17, 129.94, 127.76, 127.34, 126.76, 124.06, 123.88, 123.62, 121.79, 120.93, 110.45, 110.17, 67.48, 40.65, 23.67, 11.32.

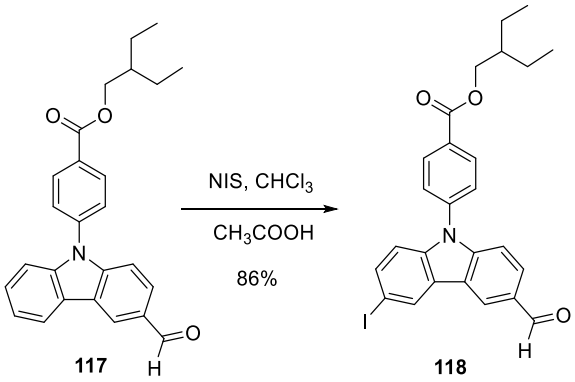

(118): Similar iodination condition as for compound **98** was followed. Using **117** (1.99 g, 5.0 mmol), N-iodosuccinimide (1.24 g, 5.5 mmol) acetic acid (10 mL) in $CHCl_3$ 40 mL. Further flash column chromatography (CH_2Cl_2/hexane, 2/1, v/v) gives product as colorless oil (2.26 g, 86%): ^{1}H NMR (500 MHz, $CDCl_3$) δ 10.12 (s, 1H), 8.60 (d, *J* = 1.4 Hz, 1H), 8.52 (d, *J* = 1.6 Hz, 1H), 8.33 (d, *J* = 8.4 Hz, 2H), 7.99 (dd, *J* = 8.6, 1.6 Hz, 1H), 7.74 (dd, *J* = 8.7, 1.7 Hz, 1H), 7.64 (d, *J* = 8.4 Hz, 2H), 7.49 (d, *J* = 8.6 Hz, 1H), 7.22 (d, *J* = 8.6 Hz, 1H), 4.35 (d, *J* = 5.7 Hz, 2H), 1.73 (hept, *J* = 6.2 Hz, 1H), 1.51 (p, *J* = 7.3 Hz, 4H), 1.00 (t, *J* = 7.5 Hz, 6H).

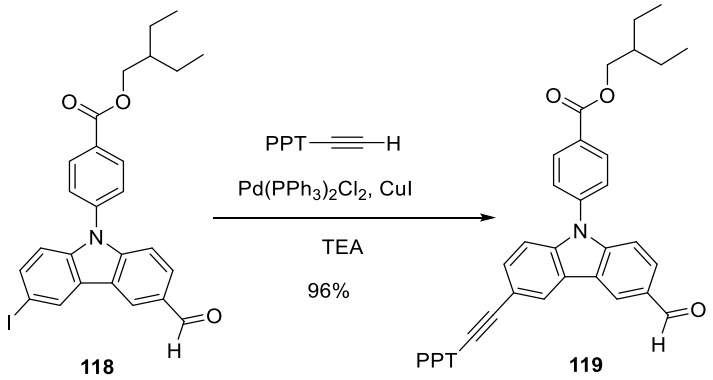

(119): The general Sonogashira's procedure was followed. Using **118** (2.10 g, 4.0 mmol), 4-benzoyl-4'-ethynyl-biphenyl (1.41 g, 5.0 mmol), $Pd(PPh_3)_2Cl_2$ (0.084 g, 0.12 mmol), CuI (5.7 mg, 0.03 mmol), TEA (25 mL), and THF (100 mL). Flash column chromatography (CH_2Cl_2/ethyl acetate, 20/1, v/v) gives pure product as a yellowish solid (2.61 g, 96%): ^{1}H NMR (500 MHz,

$CDCl_3$) δ 10.15 (s, 1H), 8.69 (d, *J* = 1.6 Hz, 1H), 8.33 (d, *J* = 8.4 Hz, 2H), 8.23 (d, *J* = 7.8 Hz, 1H), 7.98 (dd, *J* = 8.6, 1.6 Hz, 1H), 7.95 – 7.45 (m, 17H), 7.42 (ddd, *J* = 8.0, 6.9, 1.2 Hz, 1H), 4.35 (d, *J* = 5.7 Hz, 2H), 1.73 (hept, *J* = 6.2 Hz, 1H), 1.52 (p, *J* = 7.3 Hz, 4H), 1.00 (t, *J* = 7.5 Hz, 6H).

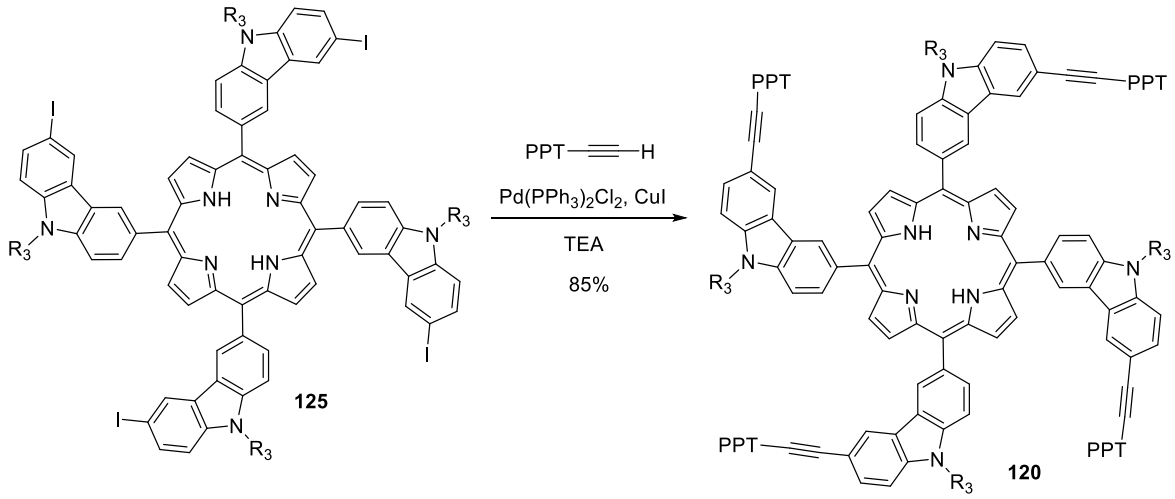

(120): The general Sonogashira's procedure was followed. Using **125** (2.51 g, 1.1 mmol), 4-benzoyl-4'-ethynyl-biphenyl (1.86 g, 6.6 mmol), $Pd(PPh_3)_2Cl_2$ (0.092 g, 0.13 mmol), CuI (8.0 mg, 0.044 mmol), TEA (20 mL), and THF (200 mL). Flash column chromatography (CH_2Cl_2/ethyl acetate, 20/1, v/v) gives pure product as a purple solid (2.72 g, 85%): ^{1}H NMR (500 MHz, $CDCl_3$) δ 9.07 (s, 4H), 8.99 (s, 8H), 8.50 (s, 4H), 8.44 (d, *J* = 8.9 Hz, 8H), 7.98 (d, *J* = 8.2 Hz, 8H), 7.92 – 7.37 (m, 68H), 4.38 (d, *J* = 5.9 Hz, 8H), 1.83 – 1.71 (m, 4H), 1.60 – 1.48 (m, 16H), 1.02 (t, *J* = 7.7 Hz, 24H), -2.41 (s, 2H). ^{13}C NMR (100 MHz, $CDCl_3$) δ 196.33, 166.14, 144.35, 141.67, 140.99, 140.59, 139.31, 137.78, 136.50, 135.40, 133.78, 132.58, 132.16, 131.80, 130.94, 130.90, 130.86, 130.17, 130.14, 129.88, 128.47, 127.29, 126.92, 126.86, 126.79, 124.66, 124.15, 123.70, 122.31, 120.68, 115.57, 110.42, 108.26, 91.87, 88.30, 67.54, 40.74, 23.76, 11.40. MALDI-TOF (m/z): $[M+H]^+$ calcd. for $C_{204}H_{154}N_8O_{12}$, 2910.18; found, 2911.40.

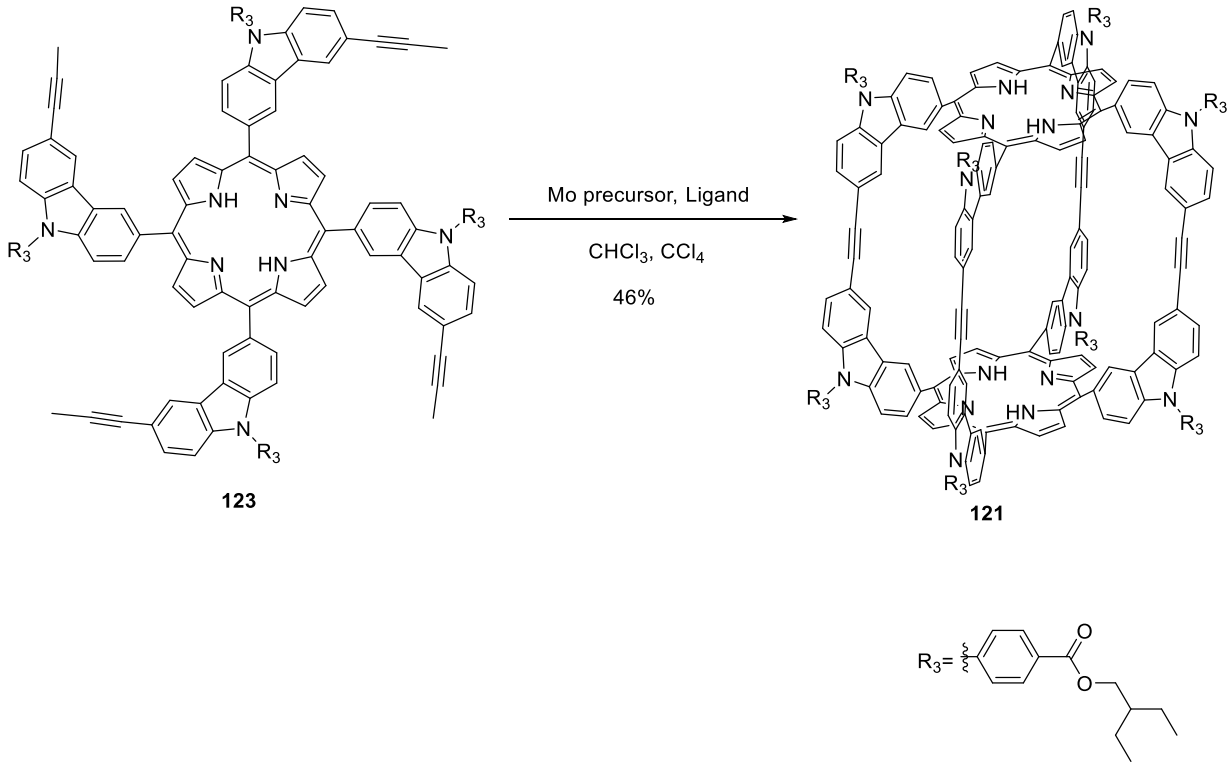

(121): Typical alkyne metathesis reaction condition was followed. The multidentate ligand (4.9 mg, 0.012 mmol) and the Mo(VI) carbyne precursor (8.0 mg, 0.012 mmol) were premixed in dry carbon tetrachloride (10 mL) for 15 minutes to generate the catalyst in situ. Subsequently, the monomer **123** (194 mg, 0.1 mmol) in $CHCl_3$ (10 mL) was added and the stirring was continued for 24 h at 70 ºC. Upon completion of the reaction, the reaction mixture was filtered to remove the byproduct and the filtrate was concentrated and subjected to flash column chromatography (ethyl acetate/$CHCl_3$, 1/5). The product **121** was obtained as a purple solid (84 mg, 46 %): ^{1}H NMR (500 MHz, $CDCl_3$) δ 8.86 (d, *J* = 1.7 Hz, 8H), 8.70 (s, 16H), 8.40 (d, *J* = 8.7 Hz, 16H), 8.35 (d, *J* = 1.0 Hz, 1H), 8.19 (dd, *J* = 8.2, 1.7 Hz, 8H), 7.93 (d, *J* = 8.6 Hz, 16H), 7.76 – 7.69 (m, 16H), 7.59 (d, *J* = 8.9 Hz, 8H), 4.36 (d, *J* = 5.7 Hz, 16H), 1.81 – 1.68 (m, 8H), 1.58 – 1.48 (m, 32H), 1.00 (t, *J* = 7.5 Hz, 48H), -2.76 (s, 4H).

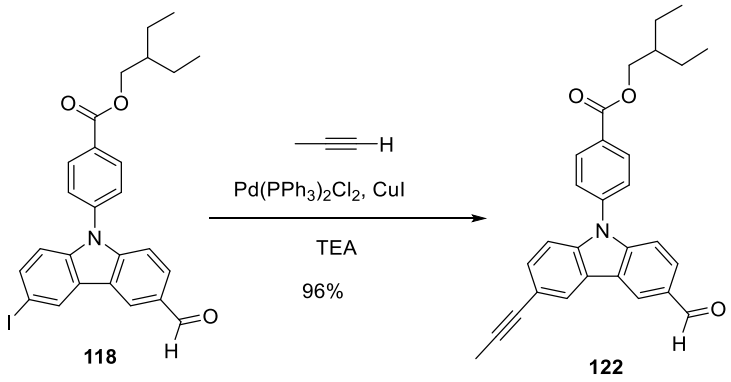

(122): The general Sonogashira's procedure was followed. Using **118** (2.10 g, 4.0 mmol), propyne (0.32 g, 8.0 mmol), $Pd(PPh_3)_2Cl_2$ (0.084 g, 0.12 mmol), CuI (5.7 mg, 0.03 mmol), TEA (100 mL). Flash column chromatography (CH_2Cl_2/hexane, 2/1, v/v) gives pure product as a colorless oil (1.68 g, 96%): ^{1}H NMR (500 MHz, $CDCl_3$) δ 10.13 (s, 1H), 8.63 (d, *J* = 1.2 Hz, 1H), 8.33 (d, *J* = 8.5 Hz, 2H), 8.25 (d, *J* = 1.1 Hz, 1H), 7.98 (dd, *J* = 8.6, 1.6 Hz, 1H), 7.66 (d, *J* = 8.4 Hz, 2H), 7.52 (dd, *J* = 8.5, 1.6 Hz, 1H), 7.50 (d, *J* = 8.5 Hz, 1H), 7.36 (d, *J* = 8.5 Hz, 1H), 4.35 (d, *J* = 5.7 Hz, 2H), 2.13 (s, 3H), 1.73 (hept, *J* = 6.2 Hz, 1H), 1.52 (p, *J* = 7.3 Hz, 4H), 1.00 (t, *J* = 7.5 Hz, 6H). ^{13}C NMR (100 MHz, $CDCl_3$) δ 191.76, 165.94, 144.42, 140.69, 140.54, 131.76, 130.87, 130.45, 130.28, 128.04, 126.85, 124.21, 124.16, 123.75, 123.69, 117.54, 110.47, 110.23, 85.22, 80.03, 67.61, 40.73, 23.75, 11.39, 4.67.

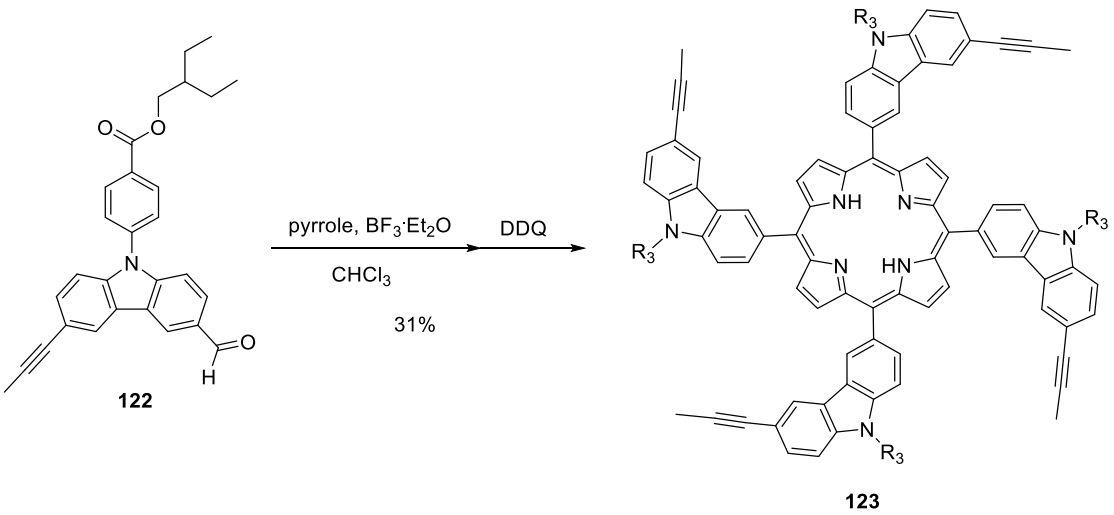

(123): Same reaction condition as for compound **100** was followed. Using **122** (0.875 g, 2.0 mmol), pyrrole (0.14 mL, 2.0 mmol) and $BF_3 \cdot Et_2O$ (0.08 mL) DDQ (0.37 g, 1.5 mmol). Flash column chromatography (ethyl acetate/CH_2Cl_2, 1/10, v/v) gives pure product as a purple solid (0.301 g, 31 %): ^{1}H NMR (500 MHz, $CDCl_3$) δ 8.98 (td, *J* = 6.9, 1.7 Hz, 4H), 8.93 (s, 8H), 8.42 (d, *J* = 8.0 Hz, 8H), 8.39 – 8.27 (m, 8H), 7.95 (d, *J* = 8.3 Hz, 8H), 7.84 (dt, *J* = 8.3, 4.1 Hz, 4H), 7.57 (s, 8H), 4.38 (d, *J* = 5.7 Hz, 8H), 2.10 – 2.03 (m, 12H), 1.76 (hept, *J* = 5.9 Hz, 4H), 1.55 (p, *J* = 7.1 Hz, 16H), 1.02 (t, *J* = 7.4 Hz, 24H), -2.46 (s, 2H).

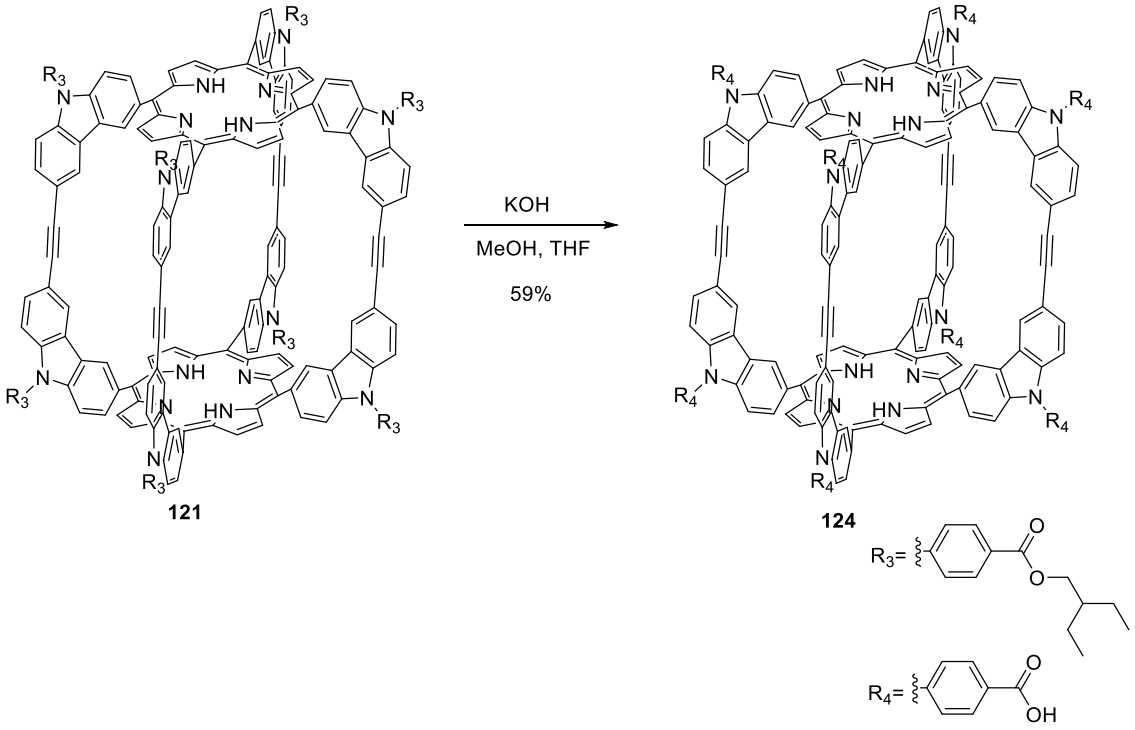

(124): To a solution of **121** (20.0 mg, 5.6 μmol) in methanol (2 mL) and THF (2 mL) co-solvent, KOH (24.4 mg, 0.44 mmol) was added, and the reaction was stirred at ambient temperature for 12 hours. Upon completion, the reaction was quenched by a drop of saturated aqueous NH_4Cl aqueous solution and removal of solvents. Further flash column chromatography using acetic acid as the eluent gives **124** as a purple solid. (9.6 mg, 59%). ^{1}H NMR (500 MHz, methanol-d_4) δ 8.88 (s, 8H), 8.56 (s, 16H), 8.37 (s, 8H), 8.34 (d, *J* = 8.2 Hz, 16H), 8.20 (d, *J* = 8.1 Hz, 8H), 7.84 (d, *J* = 8.2

Hz, 16H), 7.76 (d, *J* = 8.3 Hz, 8H), 7.70 (d, *J* = 8.9 Hz, 8H), 7.59 (d, *J* = 8.9 Hz, 8H), -3.64 (s, 4H).

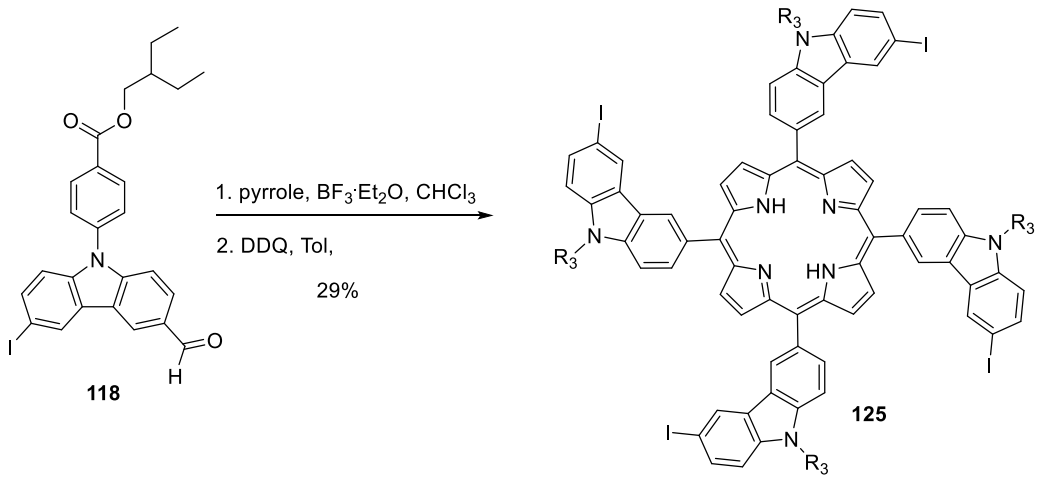

(125): Same reaction condition as for compound **100** was followed. Using **118** (1.05 g, 2.0 mmol), pyrrole (0.14 mL, 2.0 mmol) and $BF_3 \cdot Et_2O$ (0.08 mL) DDQ (0.37 g, 1.5 mmol). Flash column chromatography (ethyl acetate/CH_2Cl_2, 1/10, v/v) gives pure product as a purple solid (0.334 g, 29 %): ^{1}H NMR (500 MHz, $CDCl_3$) δ 8.96 (s, 4H), 8.91 (s, 8H), 8.57 (s, 4H), 8.43 (d, *J* = 8.3 Hz, 8H), 8.37 (t, *J* = 8.8 Hz, 4H), 7.93 (d, *J* = 8.3 Hz, 8H), 7.86 – 7.76 (m, 8H), 7.44 (d, *J* = 8.9 Hz, 4H), 4.38 (d, *J* = 5.7 Hz, 8H), 1.82 – 1.71 (m, 4H), 1.63 – 1.50 (m, 16H), 1.03 (t, *J* = 7.6 Hz, 24H), -2.49 (s, 2H).

6.6 References

1. Kitagawa, S.; Kitaura, R.; Noro, S. *Angew. Chem. Int. Ed.* **2004**, *43*, 2334.

2. Ferey, G. *Chem. Soc. Rev.* **2008**, *37*, 191.

3. Cook, T. R.; Zheng, Y. R.; Stang, P. J. *Chem. Rev.* **2013**, *113*, 734.

4. Chen, B. L.; Xiang, S. C.; Qian, G. D. *Acc. Chem. Res.* **2010**, *43*, 1115.

5. Sumida, K.; Rogow, D. L.; Mason, J. A.; McDonald, T. M.; Bloch, E. D.; Herm, Z. R.; Bae, T. H.; Long, J. R. *Chem. Rev.* **2012**, *112*, 724.

6. Li, J. R.; Kuppler, R. J.; Zhou, H. C. *Chem. Soc. Rev.* **2009**, *38*, 1477.

7. Lee, J.; Farha, O. K.; Roberts, J.; Scheidt, K. A.; Nguyen, S. T.; Hupp, J. T. *Chem. Soc. Rev.* **2009**, *38*, 1450.

8. Yoshizawa, M.; Tamura, M.; Fujita, M. *Science* **2006**, *312*, 251.

9. Cote, A. P.; Benin, A. I.; Ockwig, N. W.; O'Keeffe, M.; Matzger, A. J.; Yaghi, O. M. *Science* **2005**, *310*, 1166.

10. El-Kaderi, H. M.; Hunt, J. R.; Mendoza-Cortes, J. L.; Cote, A. P.; Taylor, R. E.; O'Keeffe, M.; Yaghi, O. M. *Science* **2007**, *316*, 268.

11. Han, S. S.; Furukawa, H.; Yaghi, O. M.; Goddard, W. A. *J. Am. Chem. Soc.* **2008**, *130*, 11580.

12. Furukawa, H.; Yaghi, O. M. *J. Am. Chem. Soc.* **2009**, *131*, 8875.

13. Feng, X.; Ding, X. S.; Jiang, D. L. *Chem. Soc. Rev.* **2012**, *41*, 6010.

14. Patel, H. A.; Je, S. H.; Park, J.; Chen, D. P.; Jung, Y.; Yavuz, C. T.; Coskun, A. *Nat. Commun.* **2013**, *4*.

15. Jin, Y. H.; Voss, B. A.; Jin, A.; Long, H.; Noble, R. D.; Zhang, W. *J. Am. Chem. Soc.* **2011**, *133*, 6650.

16. Jin, Y. H.; Voss, B. A.; McCaffrey, R.; Baggett, C. T.; Noble, R. D.; Zhang, W. *Chem. Sci.* **2012**, *3*, 874.

17. Wan, S.; Guo, J.; Kim, J.; Ihee, H.; Jiang, D. L. *Angew. Chem. Int. Ed.* **2008**, *47*, 8826.

18. Colson, J. W.; Woll, A. R.; Mukherjee, A.; Levendorf, M. P.; Spitler, E. L.; Shields, V. B.; Spencer, M. G.; Park, J.; Dichtel, W. R. *Science* **2011**, *332*, 228.

19. Zhang, W.; Moore, J. S. *J. Am. Chem. Soc.* **2005**, *127*, 11863.

20. Finke, A. D.; Gross, D. E.; Han, A.; Moore, J. S. *J. Am. Chem. Soc.* **2011**, *133*, 14063.

21. Zhang, C. X.; Wang, Q.; Long, H.; Zhang, W. *J. Am. Chem. Soc.* **2011**, *133*, 20995.

22. Sonogashira, K.; Tohda, Y.; Hagihara, N. *Tetrahedron Lett.* **1975**, 4467.

23. Sonogashira, K.; Yatake, T.; Tohda, Y.; Takahashi, S.; Hagihara, N. *Chem. Commun.* **1977**, 291.

24. Nomura, R.; Matsuno, T.; Endo, T. *J. Am. Chem. Soc.* **1996**, *118*, 11666.

25. Jyothish, K.; Zhang, W. *Angew. Chem. Int. Ed.* **2011**, *50*, 3435.

Bibliography

Ashton, P. R.; Girreser, U.; Giuffrida, D.; Kohnke, F. H.; Mathias, J. P.; Raymo, F. M.; Slawin, A. M. Z.; Stoddart, J. F.; Williams, D. J. *J. Am. Chem. Soc.* **1993**, *115*, 5422.

Ashton, P. R.; Isaacs, N. S.; Kohnke, F. H.; Dalcontres, G. S.; Stoddart, J. F. *Angew. Chem. Int. Ed.* **1989**, *28*, 1261.

Atwood, J. L.; Barbour, L. J.; Jerga, A. *Science* **2002**, *296*, 2367.

Atwood, J. L.; Koutsantonis, G. A.; Raston, C. L. *Nature* **1994**, *368*, 229.

Babu, S. S.; Moehwald, H.; Nakanishi, T. *Chem. Soc. Rev.* **2010**, *39*, 4021.

Baskaran, D.; Mays, J. W.; Zhang, X. P.; Bratcher, M. S. *J. Am. Chem. Soc.* **2005**, *127*, 6916.

Beer, S.; Hrib, C. G.; Jones, P. G.; Brandhorst, K.; Grunenberg, J.; Tamm, M. *Angew. Chem. Int. Ed.* **2007**, *46*, 8890.

Belowich, M. E.; Stoddart, J. F. *Chem. Soc. Rev.* **2012**, *41*, 2003.

Bernardi, M.; Giulianini, M.; Grossman, J. C. *ACS Nano* **2010**, *4*, 6599.

Bindl, D. J.; Wu, M. Y.; Prehn, F. C.; Arnold, M. S. *Nano Lett.* **2011**, *11*, 455.

Bisson, A. P.; Lynch, V. M.; Monahan, M.-K. C.; Anslyn, E. V. *Angew. Chem. Int. Ed.* **1997**, *36*, 2340.

Boyd, P. D. W.; Hodgson, M. C.; Rickard, C. E. F.; Oliver, A. G.; Chaker, L.; Brothers, P. J.; Bolskar, R. D.; Tham, F. S.; Reed, C. A. *J. Am. Chem. Soc.* **1999**, *121*, 10487.

Bucsi, I.; Aniszfeld, R.; Shamma, T.; Prakash, G. K. S.; Olah, G. A. *Proc. Natl. Acad. Sci.* **1994**, *91*, 9019.

Bunz, U. H. F.; Rubin, Y.; Tobe, Y. *Chem. Soc. Rev.* **1999**, *28*, 107.

Case, D. A. e. a. *AMBER 11*; University of California, San Francisco.

Chakrabarty, R.; Mukherjee, P. S.; Stang, P. J. *Chem. Rev.* **2011**, *111*, 6810.

Chen, B. L.; Xiang, S. C.; Qian, G. D. *Acc. Chem. Res.* **2010**, *43*, 1115.

Chichak, K. S.; Cantrill, S. J.; Pease, A. R.; Chiu, S. H.; Cave, G. W. V.; Atwood, J. L.; Stoddart, J. F. *Science* **2004**, *304*, 1308.

Christinat, N.; Scopelliti, R.; Severin, K. *Angew. Chem. Int. Ed.* **2008**, *47*, 1848.

Colson, J. W.; Woll, A. R.; Mukherjee, A.; Levendorf, M. P.; Spitler, E. L.; Shields, V. B.; Spencer, M. G.; Park, J.; Dichtel, W. R. *Science* **2011**, *332*, 228.

Cook, T. R.; Zheng, Y. R.; Stang, P. J. *Chem. Rev.* **2013**, *113*, 734.

Corbett, P. T.; Leclaire, J.; Vial, L.; West, K. R.; Wietor, J. L.; Sanders, J. K. M.; Otto, S. *Chem. Rev.* **2006**, *106*, 3652.

Cote, A. P.; Benin, A. I.; Ockwig, N. W.; O'Keeffe, M.; Matzger, A. J.; Yaghi, O. M. *Science* **2005**, *310*, 1166.

Coumans, R. G. E.; Elemans, J. A. A. W.; Rowan, A. E.; Nolte, R. J. M. *Chem. Eur. J.* **2013**, *19*, 7758.

D'Souza, F.; Das, S. K.; Zandler, M. E.; Sandanayaka, A. S. D.; Ito, O. *J. Am. Chem. Soc.* **2011**, *133*, 19922.

Dang, X. N.; Yi, H. J.; Ham, M. H.; Qi, J. F.; Yun, D. S.; Ladewski, R.; Strano, M. S.; Hammond, P. T.; Belcher, A. M. *Nat. Nanotechnol.* **2011**, *6*, 377.

Eaton, P. E.; Cole, T. W. *J. Am. Chem. Soc.* **1964**, *86*, 962.

Eickmeier, C.; Junga, H.; Matzger, A. J.; Scherhag, F.; Shim, M.; Vollhardt, K. P. C. *Angew. Chem. Int. Ed.* **1997**, *36*, 2103.

El-Kaderi, H. M.; Hunt, J. R.; Mendoza-Cortes, J. L.; Cote, A. P.; Taylor, R. E.; O'Keeffe, M.; Yaghi, O. M. *Science* **2007**, *316*, 268.

Escalante, A. M.; Orrillo, A. G.; Cabezudo, I.; Furlan, R. L. E. *Org. Lett.* **2012**, *14*, 5816.

Feng, X.; Ding, X. S.; Jiang, D. L. *Chem. Soc. Rev.* **2012**, *41*, 6010.

Ferey, G. *Chem. Soc. Rev.* **2008**, *37*, 191.

Ferrand, Y.; Crump, M. P.; Davis, A. P. *Science* **2007**, *318*, 619.

Finke, A. D.; Gross, D. E.; Han, A.; Moore, J. S. *J. Am. Chem. Soc.* **2011**, *133*, 14063.

Furstner, A. *Angew. Chem. Int. Ed.* **2013**, *52*, 2794.

Furstner, A.; Davies, P. W. *Chem. Commun.* **2005**, 2307.

Furukawa, H.; Yaghi, O. M. *J. Am. Chem. Soc.* **2009**, *131*, 8875.

Ge, P. H.; Fu, W.; Herrmann, W. A.; Herdtweck, E.; Campana, C.; Adams, R. D.; Bunz, U. H. F. *Angew. Chem. Int. Ed.* **2000**, *39*, 3607.

Geier, G. R.; Littler, B. J.; Lindsey, J. S. *J. Chem. Soc. Perkin. Trans. 2* **2001**, 701.

Gil-Ramirez, G.; Karlen, S. D.; Shundo, A.; Porfyrakis, K.; Ito, Y.; Briggs, G. A. D.; Morton, J. J. L.; Anderson, H. L. *Org. Lett.* **2010**, *12*, 3544.

Granzhan, A.; Schouwey, C.; Riis-Johannessen, T.; Scopelliti, R.; Severin, K. *J. Am. Chem. Soc.* **2011**, *133*, 7106.

Grimes, R. N.; Greene, P. T.; Bryan, R. F.; Rademake.Wj; Dennisto.Ml *J. Am. Chem. Soc.* **1972**, *94*, 1865.

Han, S. S.; Furukawa, H.; Yaghi, O. M.; Goddard, W. A. *J. Am. Chem. Soc.* **2008**, *130*, 11580.

Hasell, T.; Chong, S. Y.; Jelfs, K. E.; Adams, D. J.; Cooper, A. I. *J. Am. Chem. Soc.* **2012**, *134*, 588.

Hasell, T.; Wu, X. F.; Jones, J. T. A.; Bacsa, J.; Steiner, A.; Mitra, T.; Trewin, A.; Adams, D. J.; Cooper, A. I. *Nat. Chem.* **2010**, *2*, 750.

Hasell, T.; Zhang, H. F.; Cooper, A. I. *Adv. Mater.* **2012**, *24*, 5732.

Heppekausen, J.; Stade, R.; Goddard, R.; Furstner, A. *J. Am. Chem. Soc.* **2010**, *132*, 11045.

Horng, Y. C.; Lin, T. L.; Tu, C. Y.; Sung, T. J.; Hsieh, C. C.; Hu, C. H.; Lee, H. M.; Kuo, T. S. *Eur. J. Org. Chem.* **2009**, 1511.

Huerta, E.; Metselaar, G. A.; Fragoso, A.; Santos, E.; Bo, C.; de, M. J. *Angew. Chem. Int. Ed.* **2007**, *46*, 202.

Hutin, M.; Bernardinelli, G.; Nitschke, J. R. *Chem. Eur. J.* **2008**, *14*, 4585.

Inokuma, Y.; Kawano, M.; Fujita, M. *Nat. Chem.* **2011**, *3*, 349.

Ito, S.; Ono, K.; Iwasawa, N. *J. Am. Chem. Soc.* **2012**, *134*, 13962.

Iyer, K. S.; Norret, M.; Dalgarno, S. J.; Atwood, J. L.; Raston, C. L. *Angew. Chem. Int. Ed.* **2008**, *47*, 6362.

Jiang, S.; Bacsa, J.; Wu, X. F.; Jones, J. T. A.; Dawson, R.; Trewin, A.; Adams, D. J.; Cooper, A. I. *Chem. Commun.* **2011**, *47*, 8919.

Jiang, S.; Jones, J. T. A.; Hasell, T.; Blythe, C. E.; Adams, D. J.; Trewin, A.; Cooper, A. I. *Nat. Commun.* **2011**, *2*.

Jin, Y.; Yu, C.; Denman, R. J.; Zhang, W. *Chem. Soc. Rev.* **2013**, *42*, 6634.

Jin, Y. H.; Voss, B. A.; Jin, A.; Long, H.; Noble, R. D.; Zhang, W. *J. Am. Chem. Soc.* **2011**, *133*, 6650.

Jin, Y. H.; Voss, B. A.; McCaffrey, R.; Baggett, C. T.; Noble, R. D.; Zhang, W. *Chem. Sci.* **2012**, *3*, 874.

Jin, Y. H.; Voss, B. A.; Noble, R. D.; Zhang, W. *Angew. Chem. Int. Ed.* **2010**, *49*, 6348.

Jin, Y. H.; Zhang, A. B.; Huang, Y. S.; Zhang, W. *Chem. Commun.* **2010**, *46*, 8258.

Jin, Y. H.; Zhu, Y. L.; Zhang, W. *CrystEngComm* **2013**, *15*, 1484.

Jyothish, K.; Zhang, W. *Angew. Chem. Int. Ed.* **2011**, *50*, 3435.

Kanai, Y.; Grossman, J. C. *Nano Lett.* **2008**, *8*, 908.

Kay, A.; Gratzel, M. *J. Phys. Chem.* **1993**, *97*, 6272.

Kitagawa, S.; Kitaura, R.; Noro, S. *Angew. Chem. Int. Ed.* **2004**, *43*, 2334.

Klosterman, J. K.; Yamauchi, Y.; Fujita, M. *Chem. Soc. Rev.* **2009**, *38*, 1714.

Koblenz, T. S.; Wassenaar, J.; Reek, J. N. H. *Chem. Soc. Rev.* **2008**, *37*, 247.

Komatsu, N. *J. Inclusion Phenom. Macrocycl. Chem.* **2008**, *61*, 195.

Kymakis, E.; Amaratunga, G. A. J. *Appl. Phys. Lett.* **2002**, *80*, 112.

Lahiri, S.; Thompson, J. L.; Moore, J. S. *J. Am. Chem. Soc.* **2000**, *122*, 11315.

Lee, J.; Farha, O. K.; Roberts, J.; Scheidt, K. A.; Nguyen, S. T.; Hupp, J. T. *Chem. Soc. Rev.* **2009**, *38*, 1450.

Lehn, J. M. *Chem. Soc. Rev.* **2007**, *36*, 151.

Lehn, J. M. *Science* **2002**, *295*, 2400.

Li, H.; Eddaoudi, M.; O'Keeffe, M.; Yaghi, O. M. *Nature* **1999**, *402*, 276.

Li, J. R.; Kuppler, R. J.; Zhou, H. C. *Chem. Soc. Rev.* **2009**, *38*, 1477.

Lin, C. F.; Liu, Y. H.; Lai, C. C.; Peng, S. M.; Chiu, S. H. *Chem. Eur. J.* **2006**, *12*, 4594.

Lin, Z. H.; Sun, J. L.; Efremovska, B.; Warmuth, R. *Chem. Eur. J.* **2012**, *18*, 12864.

Liu, X.; Liu, Y.; Li, G.; Warmuth, R. *Angew. Chem. Int. Ed.* **2006**, *45*, 901.

Liu, Y.; Hu, C.; Comotti, A.; Ward, M. D. *Science* **2011**, *333*, 436.

MacGillivray, L. R.; Atwood, J. L. *Nature* **1997**, *389*, 469.

Martin, R. B. *Chem. Rev.* **1996**, *96*, 3043.

Mastalerz, M. *Chem. Commun.* **2008**, 4756.

Mastalerz, M. *Angew. Chem. Int. Ed.* **2010**, *49*, 5042.

Meissner, R. S.; Rebek, J., Jr.; Demendoza, J. *Science* **1995**, *270*, 1485.

Meyer, C. D.; Joiner, C. S.; Stoddart, J. F. *Chem. Soc. Rev.* **2007**, *36*, 1705.

Mitra, T.; Jelfs, K. E.; Schmidtmann, M.; Ahmed, A.; Chong, S. Y.; Adams, D. J.; Cooper, A. I. *Nat. Chem.* **2013**, *5*, 276.

Mortreux, A.; Coutelier, O. *J. Mol. Catal. A: Chem.* **2006**, *254*, 96.

Nagata, K.; Dejima, E.; Kikuchi, Y.; Hashiguchi, M. *Chem. Lett.* **2005**, *34*, 178.

Nam, Y. S.; Magyar, A. P.; Lee, D.; Kim, J. W.; Yun, D. S.; Park, H.; Pollom, T. S.; Weitz, D. A.; Belcher, A. M. *Nat. Nanotechnol.* **2010**, *5*, 340.

Neely, S. C.; Vanderhelm, D.; Marchand, A. P.; Hayes, B. R. *Acta. Cryst.* **1976**, *B32*, 561.

Nishiyabu, R.; Kubo, Y.; James, T. D.; Fossey, J. S. *Chem. Commun.* **2011**, *47*, 1124.

Nomura, R.; Matsuno, T.; Endo, T. *J. Am. Chem. Soc.* **1996**, *118*, 11666.

Novak, B. M.; Risse, W.; Grubbs, R. H. *Adv. Polym. Sci.* **1992**, *102*, 47.

Okochi, K. D.; Han, G. S.; Aldridge, I. M.; Liu, Y.; Zhang, W. *Org. Lett.* **2013**.

Okochi, K. D.; Jin, Y.; Zhang, W. *Chem. Commun.* **2013**, *49*, 4418.

Olenyuk, B.; Whiteford, J. A.; Fechtenkotter, A.; Stang, P. J. *Nature* **1999**, *398*, 796.

Patel, H. A.; Je, S. H.; Park, J.; Chen, D. P.; Jung, Y.; Yavuz, C. T.; Coskun, A. *Nat. Commun.* **2013**, *4*.

Pentecost, C. D.; Chichak, K. S.; Peters, A. J.; Cave, G. W. V.; Cantrill, S. J.; Stoddart, J. F. *Angew. Chem. Int. Ed.* **2007**, *46*, 218.

Perez, E. M.; Martin, N. *Chem. Soc. Rev.* **2008**, *37*, 1512.

Pivrikas, A.; Sariciftci, N. S.; Juska, G.; Osterbacka, R. *Prog. Photovolt: Res. Appl.* **2007**, *15*, 677.

Rebek, J., Jr. *Angew. Chem. Int. Ed.* **2005**, *44*, 2068.

Ren, S. Q.; Bernardi, M.; Lunt, R. R.; Bulovic, V.; Grossman, J. C.; Gradecak, S. *Nano Lett.* **2011**, *11*, 5316.

Roquelet, C.; Garrot, D.; Lauret, J. S.; Voisin, C.; Alain-Rizzo, V.; Roussignol, P.; Delaire, J. A.; Deleporte, E. *Appl. Phys. Lett.* **2010**, *97*, 141918.

Rowan, S. J.; Cantrill, S. J.; Cousins, G. R.; Sanders, J. K.; Stoddart, J. F. *Angew. Chem. Int. Ed.* **2002**, *41*, 898.

Sanchez-Molina, I.; Grimm, B.; Krick Calderon, R. M.; Claessens, C. G.; Guldi, D. M.; Torres, T. *J. Am. Chem. Soc.* **2013**, *135*, 10503.

Schneider, M. W.; Hauswald, H. J. S.; Stoll, R.; Mastalerz, M. *Chem. Commun.* **2012**, *48*, 9861.

Schneider, M. W.; Oppel, I. M.; Ott, H.; Lechner, L. G.; Hauswald, H. J. S.; Stoll, R.; Mastalerz, M. *Chem. Eur. J.* **2012**, *18*, 836.

Schrock, R. R. *Chem. Rev.* **2002**, *102*, 145.

Schrock, R. R. *Acc. Chem. Res.* **1990**, *23*, 158.

Schrock, R. R.; Czekelius, C. *Adv. Synth. Catal.* **2007**, *349*, 55.

Shetty, A. S.; Zhang, J. S.; Moore, J. S. *J. Am. Chem. Soc.* **1996**, *118*, 1019.

Sonogashira, K.; Tohda, Y.; Hagihara, N. *Tetra. Lett.* **1975**, 4467.

Sonogashira, K.; Yatake, T.; Tohda, Y.; Takahashi, S.; Hagihara, N. *Chem. Commun.* **1977**, 291.

Sprafke, J. K.; Stranks, S. D.; Warner, J. H.; Nicholas, R. J.; Anderson, H. L. *Angew. Chem. Int. Ed.* **2011**, *50*, 2313.

Stephens, P. W.; Cox, D.; Lauher, J. W.; Mihaly, L.; Wiley, J. B.; Allemand, P. M.; Hirsch, A.; Holczer, K.; Li, Q.; Thompson, J. D.; Wudl, F. *Nature* **1992**, *355*, 331.

Stranks, S. D.; Sprafke, J. K.; Anderson, H. L.; Nicholas, R. J. *ACS Nano* **2011**, *5*, 2307.

Sumida, K.; Rogow, D. L.; Mason, J. A.; McDonald, T. M.; Bloch, E. D.; Herm, Z. R.; Bae, T. H.; Long, J. R. *Chem. Rev.* **2012**, *112*, 724.

Taesch, J.; Heitz, V.; Topic, F.; Rissanen, K. *Chem. Commun.* **2012**, *48*, 5118.

Tashiro, K.; Aida, T. *Chem. Soc. Rev.* **2007**, *36*, 189.

Thomas, J. M.; Raja, R.; Sankar, G.; Bell, R. G. *Acc. Chem. Res.* **2001**, *34*, 191.

Tozawa, T.; Jones, J. T. A.; Swamy, S. I.; Jiang, S.; Adams, D. J.; Shakespeare, S.; Clowes, R.; Bradshaw, D.; Hasell, T.; Chong, S. Y.; Tang, C.; Thompson, S.; Parker, J.; Trewin, A.; Bacsa, J.; Slawin, A. M. Z.; Steiner, A.; Cooper, A. I. *Nat. Mater.* **2009**, *8*, 973.

Tsuda, A.; Osuka, A. *Science* **2001**, *293*, 79.

Umemoto, K.; Yamaguchi, K.; Fujita, M. *J. Am. Chem. Soc.* **2000**, *122*, 7150.

Umezawa, Y.; Tsuboyama, S.; Honda, K.; Uzawa, J.; Nishio, M. *Bull. Chem. Soc. Jpn.* **1998**, *71*, 1207.

Umezawa, Y.; Tsuboyama, S.; Takahashi, H.; Uzawa, J.; Nishio, M. *Tetrahedron* **1999**, *55*, 10047.

Vogtle, F.; Muller, W. M.; Werner, U.; Losensky, H. W. *Angew. Chem. Int. Ed.* **1987**, *26*, 901.

Vougioukalakis, G. C.; Grubbs, R. H. *Chem. Rev.* **2010**, *110*, 1746.

Wan, S.; Guo, J.; Kim, J.; Ihee, H.; Jiang, D. L. *Angew. Chem. Int. Ed.* **2008**, *47*, 8826.

Wang, J.; Wolf, R. M.; Caldwell, J. W.; Kollman, P. A.; Case, D. A. *J. Comput. Chem.* **2004**, *25*, 1157.

Weissman, H.; Plunkett, K. N.; Moore, J. S. *Angew. Chem. Int. Ed.* **2006**, *45*, 585.

Yanagisawa, M.; Tashiro, K.; Yamasaki, M.; Aida, T. *J. Am. Chem. Soc.* **2007**, *129*, 11912.

Yang, H. S.; Liu, Z. N.; Zhang, W. *Adv. Synth. Catal.* **2013**, *355*, 885.

Yoshizawa, M.; Tamura, M.; Fujita, M. *Science* **2006**, *312*, 251.

Zhang, C. X.; Wang, Q.; Long, H.; Zhang, W. *J. Am. Chem. Soc.* **2011**, *133*, 20995.

Zhang, J. S.; Moore, J. S. *J. Am. Chem. Soc.* **1992**, *114*, 9701.

Zhang, W.; Brombosz, S. M.; Mendoza, J. L.; Moore, J. S. *J. Org. Chem.* **2005**, *70*, 10198.

Zhang, W.; Moore, J. S. *Adv. Synth. Catal.* **2007**, *349*, 93.

Zhang, W.; Moore, J. S. *J. Am. Chem. Soc.* **2004**, *126*, 12796.

Zhang, W.; Moore, J. S. *J. Am. Chem. Soc.* **2005**, *127*, 11863.

Zhao, D. H.; Moore, J. S. *J. Org. Chem.* **2002**, *67*, 3548.

Vita

Chenxi Zhang was born on October, 5th, 1987 in Ezhou, Hubei, China. After his excellent work in junior high school in Ezhou No.1 Middle School, he was elected into National Science Class in The Experimental High School attached to Beijing Normal University. During the time as a high school student, his interest in chemistry was sprouting. After graduating, he then entered Peking University, majoring chemistry. As an undergraduate student, he joined Professor Yuguo Ma's lab as a research assistant, working on the design and synthesis of star-shaped polymers using atom-transfer radical polymerization and the study their applications in DNA separation. Graduated with a B.S. degree in chemistry in June 2009, he then enrolled in the doctoral program in University of Colorado at Boulder. Under the supervision of Professor Wei Zhang, he has been working on the construction of shape-persistent phenylene vinylene macrocycles and porphyrin-based molecular cages through dynamic covalent chemistry and their applications in fullerene separation. After completion of his doctoral studies, he will assume a postdoctoral position with Professor Sheng Dai at Oak Ridge National Laboratory.